AN INVESTIGATION OF ION PRODUCTION AND COMPLEMENTARY ELECTROSTATIC ION EXTRACTION AND FOCUSING SYSTEMS FOR HIGH SENSITIVITY MASS SPECTROMETER ION SOURCES

BY

MICHAEL JOHN WALLINGTON

A THESIS SUBMITTED FOR THE
DEGREE OF DOCTOR OF PHILOSOPHY
OF THE UNIVERSITY OF ASTON
IN BIRMINGHAM

DECEMBER, 1968

SUMMARY

Over the past six years, one of the major developments in the analytical applications of the mass spectrometer has been its use when connected directly to a gas chromatograph. However, the quantities of organic compound released from the chromatograph column are frequently too small to be analysed in the conventional mass spectrometer. It is therefore essential to increase sensitivity so that smaller sample quantities will give a useful spectrum. Hitherto, the sensitivity has been extremely small; typically for every million molecules entering the ion source only one ion eventually reaches the mass spectrometer collector. In the present study it is shown that the most significant limiting factor is the electron bombardment source. In spite of its importance, there has been little previous quantitative investigation.

In the first part of the thesis a mathematical treatment of the ion optics of the source is given. New computational techniques have been developed which enable the focal properties of the source to be computed rapidly and accurately. The theoretical predictions have been confirmed by experiments carried out on a commercial mass spectrometer.

In the mathematical analysis, the effects of electron space-charge were neglected. However, in the second part of the thesis it is shown experimentally that under certain circumstances, electron beam space-charge can cause the ion current emitted from the source to increase appreciably.

The experimental evidence, supported by a further theoretical analysis, suggests that this arises because the space-charge forces in the electron beam restrict the emergence of ions from the source to within a small angular wedge. When the pressure in the source is increased above a certain critical value, the ion current increases with pressure at a much reduced rate. It is shown that at this critical pressure, there is complete neutralisation of the electron space-charge by the ions produced. A new type of source is proposed which minimises this effect in organic mass spectrometry.

Acknowledgements

The author thanks Dr. J.D. Waldron, General Manager of the Scientific Apparatus Division and a Director of G.E.C.-A.E.I. (Electronics) Limited, for permission to submit this investigation for a higher degree. He would also like to express his gratitude to Mr. T. Mulvey, Supervisor, and Dr. J.S. Halliday, External Supervisor, for their advice and encouragement during the course of the study.

My thanks are also due to my wife for carefully checking through the manuscript and to Miss Susan Collins for her care and patience in typing the thesis.

CONTENTS

1 - INTRODUCTION

1.1 The Mass Spectrometer

A mass spectrometer consists of an ion source which produces ions characteristic of the sample being investigated, an analyser system which brings ions of a particular mass to a focal point, and a collecting system which detects and records the ion current at that mass. When the complete spectrum is recorded on a photographic plate the instrument is generally referred to as a mass spectrograph. In mass spectrometers, on the other hand, the ion beam is usually detected electrically and then amplified before recording. However, since many modern instruments incorporate both methods of detection, the division is of historical interest only. In this thesis therefore, any conclusions obtained for mass spectrometers will generally be valid also for mass spectrographs.

The history of the development of the mass spectrometer has been well-documented in the literature (see for example; Beynon, 1960; Farmer, 1963) and therefore in the following paragraphs only the important steps forward will be mentioned. The innovations of particular relevance to this work are those concerning improvements to the focussing of the ion beam and which result in greater instrumental resolution and sensitivity. The two types of focussing which are desirable in a mass spectrometer are: (a) angular focussing, in which ions of differing initial directions but of the same velocity are brought to a focus and (b) velocity focussing, for which a focus is achieved for ions of the same initial direction, but of different velocities.

The first mass spectra were produced by Wien (1898) and in the early experiments of J.J. Thomson. In a more refined mass spectrometer constructed by Thomson (1911), a collimated beam of positive ions was passed at right angles to parallel electrostatic and magnetic fields. However, it did not produce a focussed ion beam and the device suffered from inherently low resolving power and sensitivity.

The earliest instrument to incorporate focussing of the ion beam was the Aston (1919, 1920) mass spectrograph. In this arrangement, shown schematically in figure 1.1, successive electrostatic and magnetic fields enable velocity focussing to be achieved. A gas discharge tube was used to produce the ions and the spectrum was recorded on a photographic plate.

An alternative way of recording mass spectra was used by Dempster (1918). A schematic diagram of the arrangement is shown in figure 1.2 (a). Ions of different mass are brought successively to the same collector point by changing either the accelerating voltage or the magnetic field. It is easy to show that the equation relating the mass of the ion to the instrument parameters can be written in the form

$$\frac{M}{e} = \frac{B^2 r^2}{2V} \qquad \ldots\ldots \qquad (1.1)$$

where B is the magnetic flux density, r the radius of the ion path, M the mass of the ion, e its charge and V the energy of the ion.

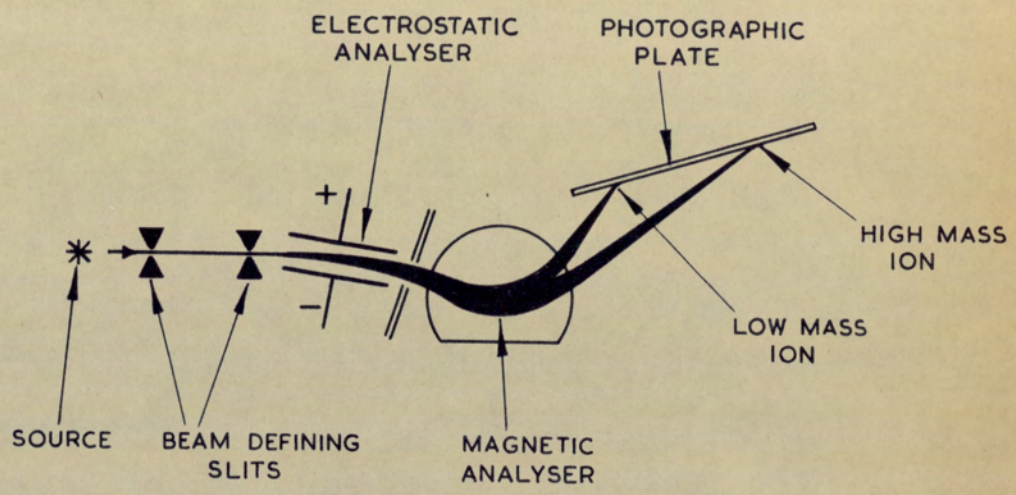

FIGURE 1.1. DIAGRAM OF ASTON'S (1919, 1920.) MASS SPECTROGRAPH.

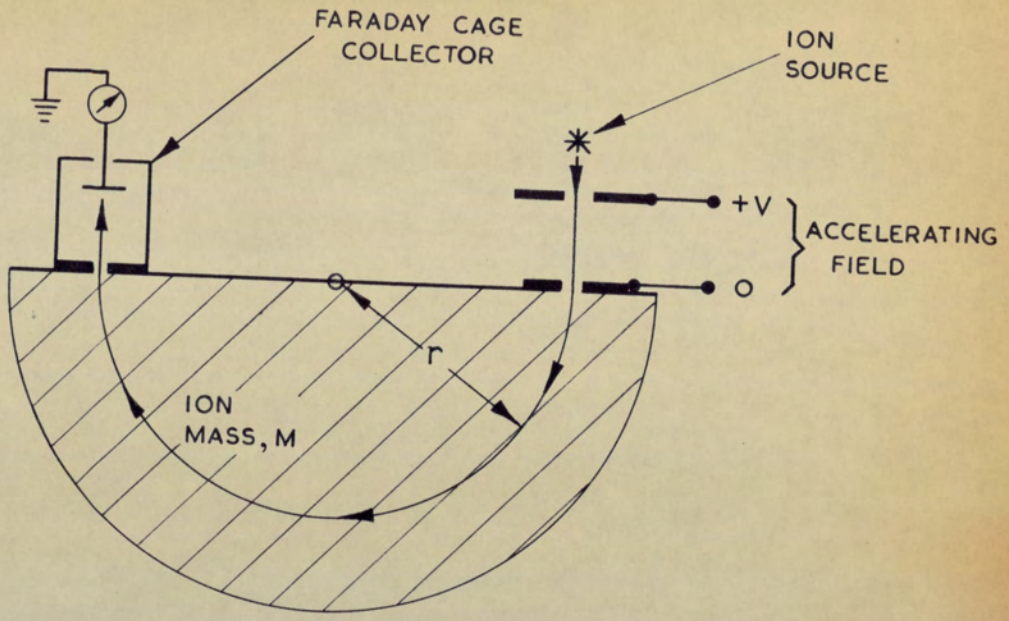

FIGURE 1.2 (a) SCHEMATIC DIAGRAM OF DEMPSTER'S (1918) MASS SPECTROMETER.

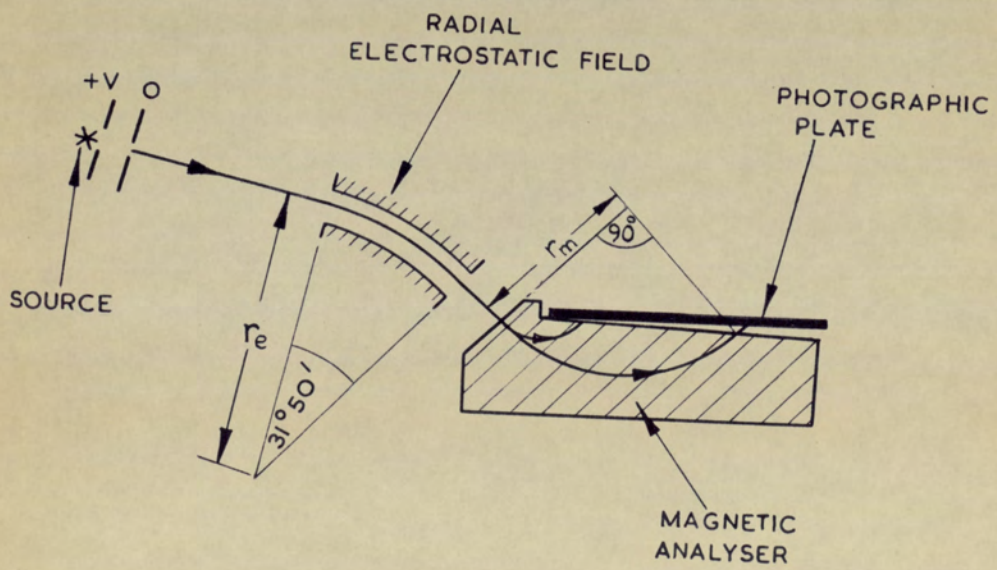

FIGURE 1.2 (b)

SCHEMATIC DIAGRAM OF A MATTAUCH–HERZOG (1934) TYPE MASS SPECTROGRAPH.

Reference to equation (1.1) shows that scanning from high mass to low mass ions can be achieved either by reducing the magnetic field strength or by increasing the accelerating voltage.

A significant advance in the design of early mass spectrographs was made by Mattauch and Herzog (1934) who proposed a spectrograph in which simultaneous angular and velocity focussing ('double-focussing') was obtained for all masses along the photographic plate (see figure 1.2 (b)). The innovation incorporated in this instrument was a pair of cylindrical shoes used to produce a radial electrostatic field. A mass spectrometer to this design was first built by Mattauch (1936).

The first double-focussing mass spectrometer to use the Dempster scanning technique was constructed by Nier and Roberts (1951); the theory used to determine the geometry and the relative positioning of the analysers, was given later by Johnson and Nier (1953). Figure 1.3a shows, in schematic form, the configuration of such a mass spectrometer. In addition to correcting first order angular and velocity aberrations, this design also eliminates the second order angular aberration.

Recently, several new methods of obtaining either higher resolution or sensitivity for given instrument size have been tried. Noteworthy is the stigmatic mass spectrograph of Ewald and Liebl (1959) employing

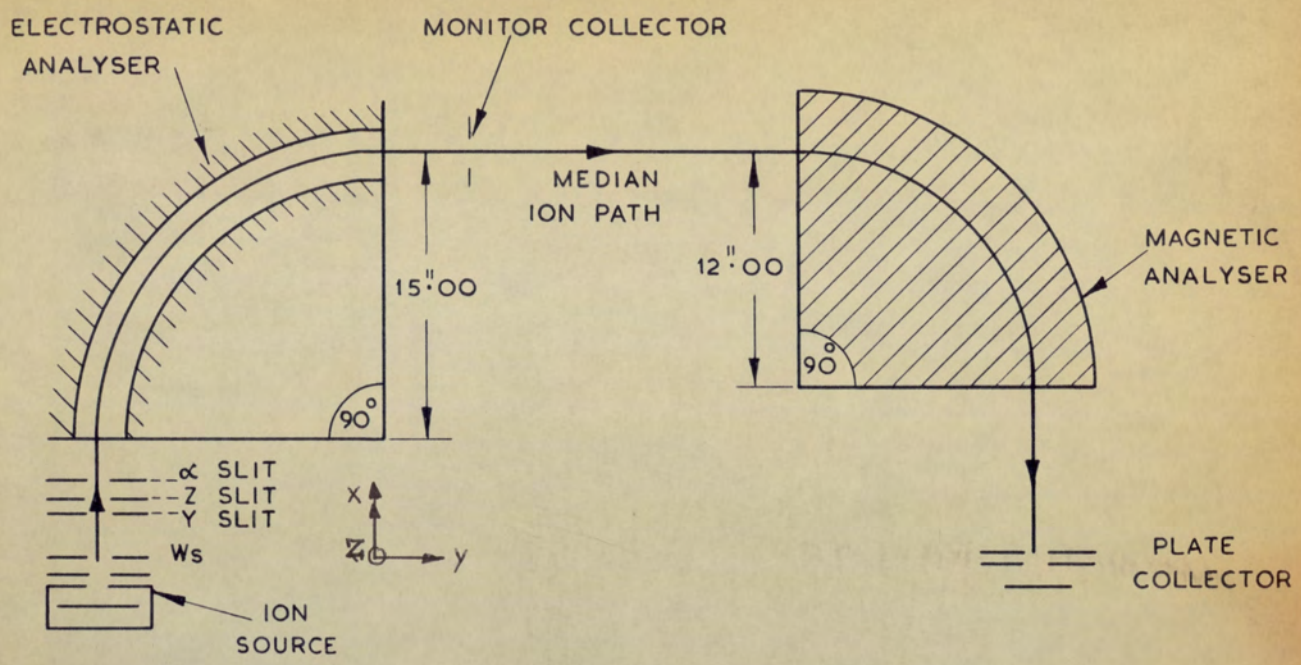

FIGURE 1.3 (a) SCHEMATIC LAYOUT OF A 12" DOUBLE-FOCUSSING MASS SPECTROMETER OF THE JOHNSON-NIER (1953) TYPE.

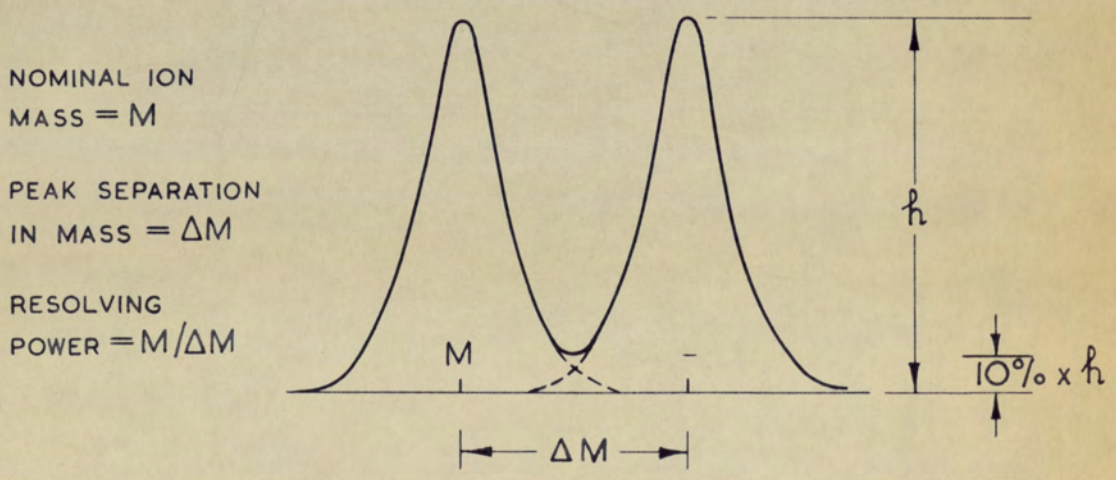

FIGURE 1.3 (b) DEFINITION OF 10% VALLEY RESOLVING POWER, M/ΔM.

a spherical electrostatic analyser to produce focussing in two planes. However, only small gains in sensitivity and resolution were reported by these authors. Perhaps a more promising development is the use of a non-uniform magnetic sector field with which the mass dispersion and resolving power can become much larger than for the case of a uniform magnetic field. A mass spectrograph incorporating a magnetic sector in which the field strength at a radius r varies as $1/r$, has given a resolving power of 500,000 (Matsuda and Fukumoto, 1966).

However, at present, the instruments most used by the chemist are the double-focussing designs of Mattauch and Herzog and that of Johnson and Nier. Over the past fifteen years, these mass spectrometers have been used increasingly by the organic chemist for the quantitative analysis of mixtures and the structural determination of organic compounds. Resolving powers of 70,000 are readily obtainably, although resolutions of between 10,000 and 20,000 are usually adequate for routine work. (Note: these resolutions are based on a 10% valley definition - see figure 1.3b). The accuracy of mass measurements is generally better than three parts per million and this is usually sufficient to enable the chemist to select one, two or perhaps three possible molecular formulae for an organic sample fragment ion containing hydrogen, carbon and several heteroatoms. Simple additional chemical information allows the chemist to specify uniquely the correct molecular formula. By an inspection of the

mass spectrum, fragmentation patterns can be established which give insight into the molecular structure of the compound. This process can be automated by analysing the spectrum with a digital computer, as has been done for peptide samples (Barber, Powers, Wallington and Wolstenholme, 1966).

Recently, it has become common practice to couple a gas chromatography column to the mass spectrometer source and to mass analyse time-spaced eluents, which can be as small as a fraction of a nanogram (10^{-9} gm). For such small sample amounts, the accuracy of measurement of peak intensity and mass are limited mainly by the ion statistics at the collector (Campbell and Halliday, 1965; Green, Merren and Murray, 1965). It is therefore essential that the sensitivity of the mass spectrometer should be increased so that smaller sample quantities will give a useful spectrum. Hitherto, sensitivity has been extremely small; typically for every million molecules entering the source, one thousand ions are produced, of which only one ion eventually reaches the mass spectrometer collector at 10,000 instrumental resolving power (see Chapter 5).

In the following sections, the factors limiting sensitivity will be determined. For convenience these will be divided into two groups, corresponding to the two principal functions of the mass spectrometer. The first will cover all those factors controlling ion production in the electron bombardment source. The second group embraces all those processes controlling ion transmission between the point of ion production and the mass spectrometer collector.

1.2 Factors limiting ion production

The number of ions produced in the source region by collisions of electrons with the gas molecules, may be calculated by using the following equation of Compton and Van Voorhis (1925, corrected 1926).

$$I^+ = NI^- Z p \quad \ldots\ldots \quad (1.2)$$

where I^+ amp is the ion current produced by an electron current I^- amp, travelling for a length Z cm, through a gas at pressure p torr. N, an experimentally determined coefficient, is the number of ionising collisions made per cm path, per torr pressure. For all gases the factor N is a function of electron energy, and a typical ionisation curve, obtained for nitrogen, is shown in figure 1.4. There is a threshold electron energy, the ionisation potential, after which N rises rapidly. Above 100eV electron energy there is little increase in N, and at still higher energies, N decreases. There is therefore little to be gained by increasing electron energy above the conventional value of 70eV, and any gains in source sensitivity must be obtained by increasing one of the other parameters of equation 1.2.

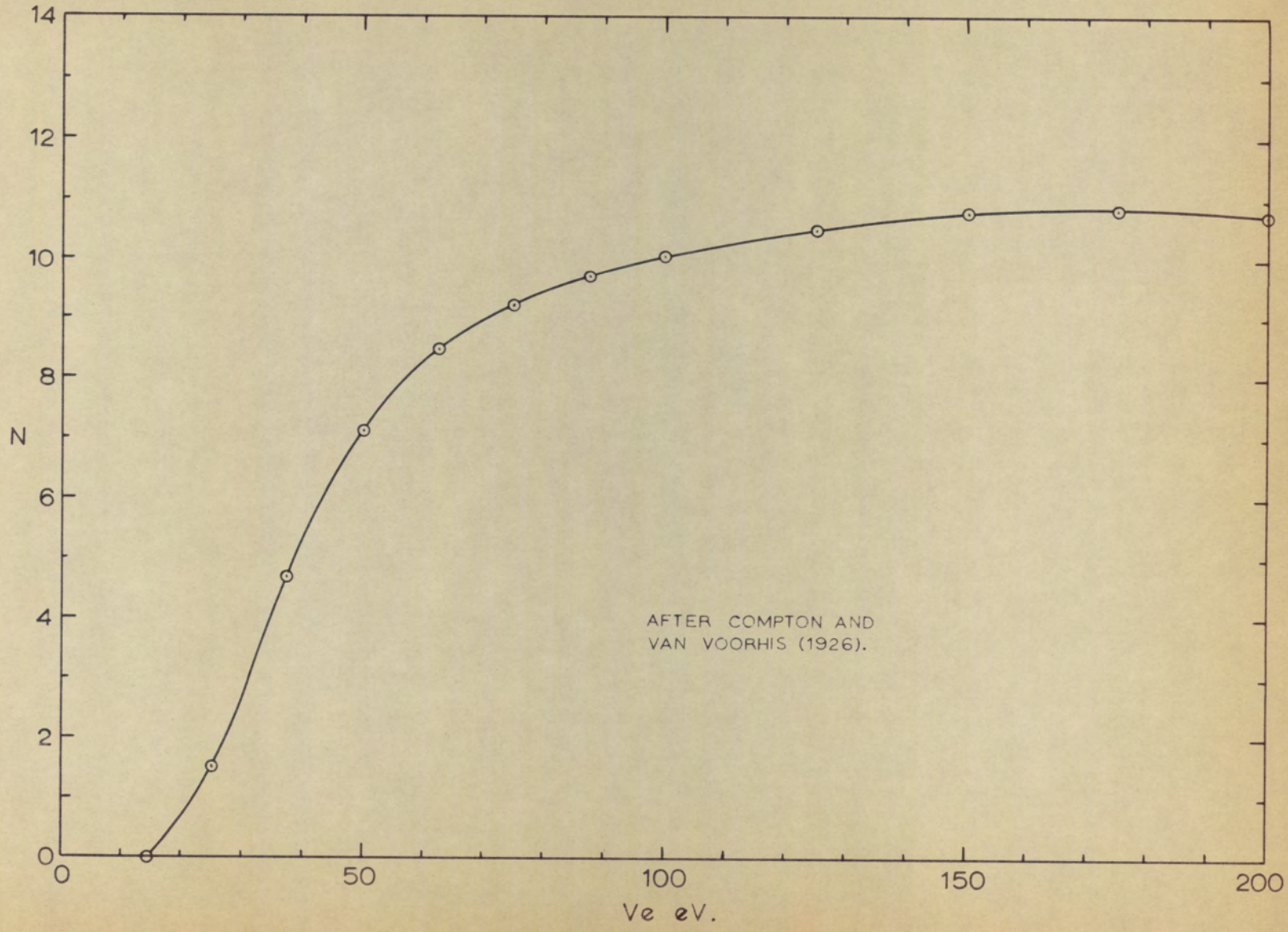

FIGURE 1.4. NUMBER OF IONISING COLLISIONS N, MADE PER cm. PATH THROUGH NITROGEN AT 1 Torr AS A FUNCTION OF ELECTRON ENERGY, Ve, eV.

The pressure p in the ionisation chamber is determined by the ratio of the quantity of gas per second Q, entering the chamber, to the volume per second S, flowing out.

That is: $p = Q/S$ ..... (1.3)

where typically, p is in torr, Q in litre-torr per second, and S in litre per second. For the situation where there is a given quantity of sample which is to be expended at a given rate, the pressure in the ionisation chamber can be increased only by restricting flow of gas out of the chamber.

By reference to equations (1.2) and (1.3), it is seen that an ideal source would have the following properties:

(i) Larger electron ionising current.

(ii) Longer electron path length.

(iii) Smaller flow rate of gas out of the ionisation chamber.

In addition, two other important characteristics are:-

(iv) Reproducibility of sensitivity.

(v) Linear increase in sensitivity with pressure.

1.3 Factors controlling ion transmission

The resolving power of a double focussing mass spectrometer is largely determined by the length and width of the slit apertures placed along the ion path, and in general, smaller apertures give a better resolution but reduced ion transmission. Slit sizes are therefore chosen to give the required resolution with the best ion transmission. The parameters limiting the performance of a double focussing mass spectrometer are detailed in the following analysis.

The theoretical 10% valley resolving power of a mass spectrometer may be derived from the following empirical equation (Duckworth and Ghoshal, 1963)

$$\frac{M}{\Delta M} = \frac{K}{mW_s + W_c + \Delta} \qquad \ldots\ldots \qquad (1.4)$$

where K is the mass dispersion, m the linear demagnification of the mass spectrometer, W_s the width of the source resolution-slit and W_c the collector slit width. The aberration and distortion of the image at the collector slit, are grouped together in the one term, Δ .

The image aberration is conventionally defined in terms of the deviation, y_b, of the aberrated ion path from the paraxial or median ion path, at the plane of the collector slit, where

$$y_b = r_m (B_1\alpha + B_2\beta + B_{11}\alpha^2 + B_{12}\alpha\beta + B_{22}\beta^2) \ldots\ldots \qquad (1.5)$$

r_m is the radius of the median ion path in the magnetic analyser, α is the initial angle between the aberrated ray and the median ray at the plane of the source slit, and β is the relative velocity deviation $\Delta v_o/v_o$ of the aberrated ray, where v_o is the velocity of the unaberrated median ray. B_1 and B_2 are termed respectively the first order angular and velocity aberration coefficients, and B_{11}, B_{12} and B_{22} are termed respectively the second order angular, second order angular and velocity, and second order velocity aberration coefficients.

The magnitude of the aberration coefficients is dependent on the choice of the geometry of the analysers and the relative positioning of the source, collector and the analysers. For a double-focussing mass spectrometer of the Johnson and Nier (1953) type, the coefficients B_1, B_2 and B_{11} are zero. Since β is usually smaller than α by a factor ten, the most significant of the remaining aberration terms is $B_{12}\alpha\beta$. Alpha is set by the α-slit which is placed between the ion source and the electrostatic analyser. Beta is determined by the energy spread superimposed on the ion beam by the ion source, and by the ripple on the accelerating voltage supply.

Image distortion mainly appears as curvature of the line image at the collector slit. This image curvature effect is attributable to the action of the magnet fringe fields on the ion beam. A theoretical analysis of the problem (Berry, 1956) shows that the effective image broadening Z_f, is approximately given by $Z_f = Z^2/r$, where Z is the half-length of the collector slit, and r is the radius of the magnetic analyser.

(Note: The coordinate system conventionally used in mass spectrometry is shown in figure 1.3a; at any given point of the ion path, the coordinate system is orientated in the x-y plane so that x is along the direction of travel of the ion beam. Z is mutually perpendicular to x and y).

Beam broadening can also occur if the plates of the electrostatic analyser are not parallel to each other. For a given set of plates, the effect is a linear function of the breadth of the beam in the Z-direction. The aberration term can be written as $K\,\Delta E/E$, where $\Delta E/E$ is the field non-uniformity across the beam and K is the mass dispersion.

Collecting together the above terms and inserting them in equation (1.4) gives the following equation for the theoretical resolving power of a double-focussing mass spectrometer with a magnetic analyser of twelve inches radius:

$$\frac{M}{\Delta M} = \frac{10.2}{0.66\ W_s + W_c + 0.95\alpha\beta + Z^2/r + 10.2\,\Delta E/E} \quad \ldots\ldots \quad (1.6)$$

in which the specific values of the constants K, m and B_{12} have been used.

It is seen that the factors playing a part in determining the resolution are the source and collector slit widths, the alpha slit width, the length of the beam in the non-focussing, Z direction, and the energy spread of the ion beam. In practice, the dimensions of the slit-apertures are set to obtain a particular resolution, and therefore any improvement in ion transmission must be obtained by changing the properties of the beam emitted from the source. An ideal source would therefore emit an ion beam with the following properties:

(vi) smaller angular spread in the focussing y-direction

(vii) smaller overall width at the resolution slit

(viii) smaller angular spread in the non-focussing z-direction

(ix) smaller energy spread ('beta' term in equation 1.4)

The conclusions reached in this section and the previous section show that the only way to improve the sensitivity of the mass spectrometer, for a given resolution, is to improve certain characteristics of the source. In the following section it is shown how previous attempts to improve source design are related to the desirable characteristics enumerated above.

1.4 Historical survey of the development of the electron bombardment source

Dempster (1916) was the first to use a mass spectrograph to study ions produced by electron bombardment of gas molecules. The design was a simple one in which an open source was placed in a vessel of the gas under study. The first significant advance on this design was made by Nier in 1940 (see Nier, 1947) who described a source with an enclosed ionisation region in which the sample gas was admitted to the ionisation chamber through a glass inlet line. Such a design impedes the movement of sample gas molecules out of the ionisation chamber, thereby achieving a greater gas pressure and a consequent increase in ion production (method (iii)).

The construction of the electron bombardment (e.b) sources, based on the Nier (1947) design, is shown diagrammatically in figure 1.5, while figure 1.6 is a photograph of a typical present-day source showing its construction on a flange demountable from the mass spectrometer. A rhenium wire or tungsten ribbon filament F, is heated to produce electrons which are accelerated to the filament plate FP, by a potential difference variable between 5V and 80V. The electrons then pass through a narrow slot in the filament plate and travel with approximately constant velocity across the ionisation chamber, through the trap plate TP, to the electron trap T, which is maintained at 6o volts positive with respect to TP to re-capture any secondary electrons produced. Gas molecules entering the ionisation chamber through the sample inlet ports are subjected to electron bombardment. Those molecules that are ionised are withdrawn from the ionising region by an electric field. Focussing and acceleration of the ions is achieved by connecting appropriate voltages to the repeller plate R, ion exit slit IES, beam-centring plates BC, and earth slit ES. The 'earth slit' is, in fact, the anode of the ion gun. This terminology is often used, because it is common practice to have the analysers of the mass spectrometer at earth potential, and to maintain the source ionisation chamber at a high potential with respect to earth.

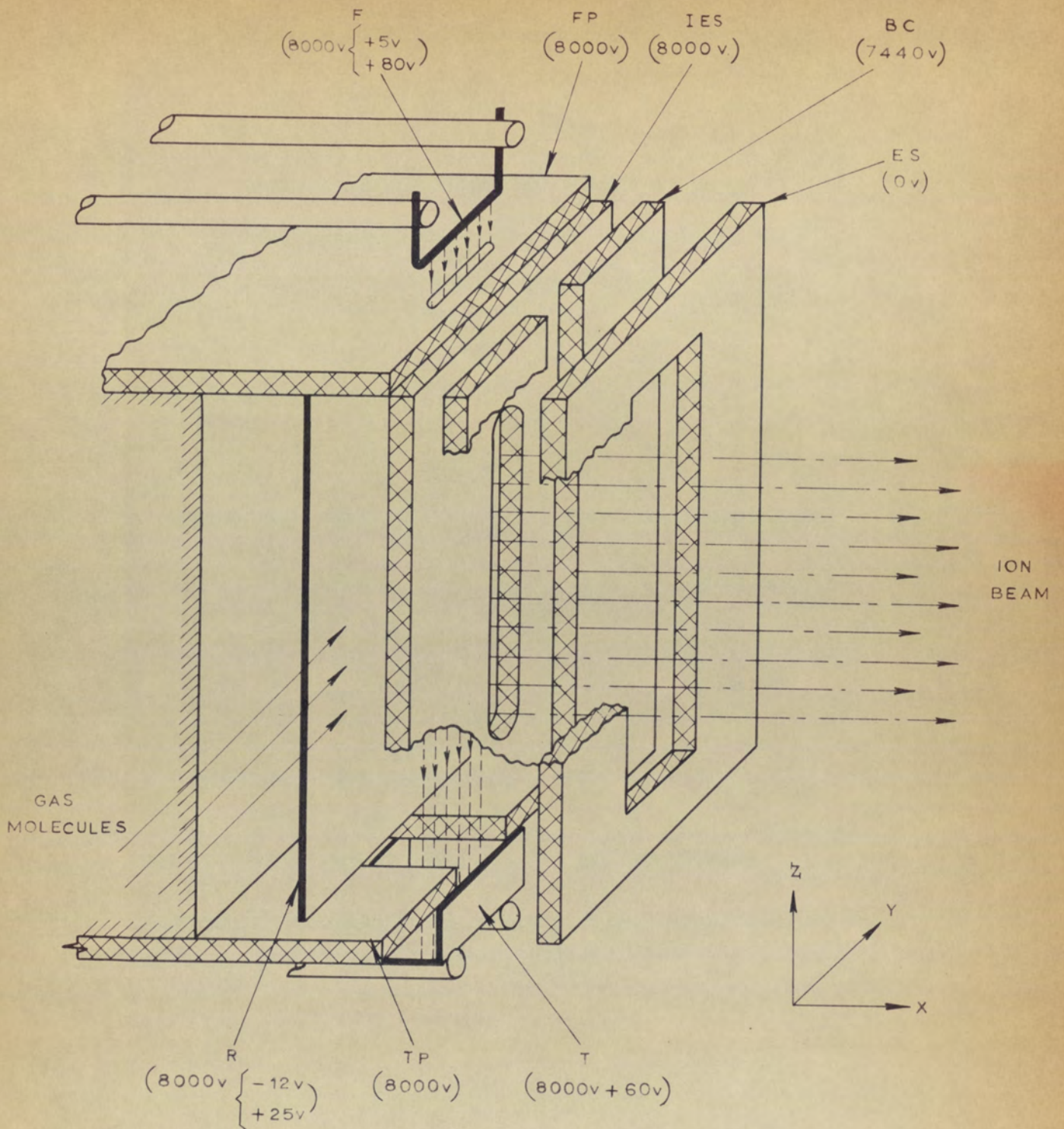

FIGURE 1.5 CUT-AWAY SKETCH SHOWING THE DISPOSITION OF THE COMPONENTS OF AN ELECTRON BOMBARDMENT (E.B.) ION SOURCE.

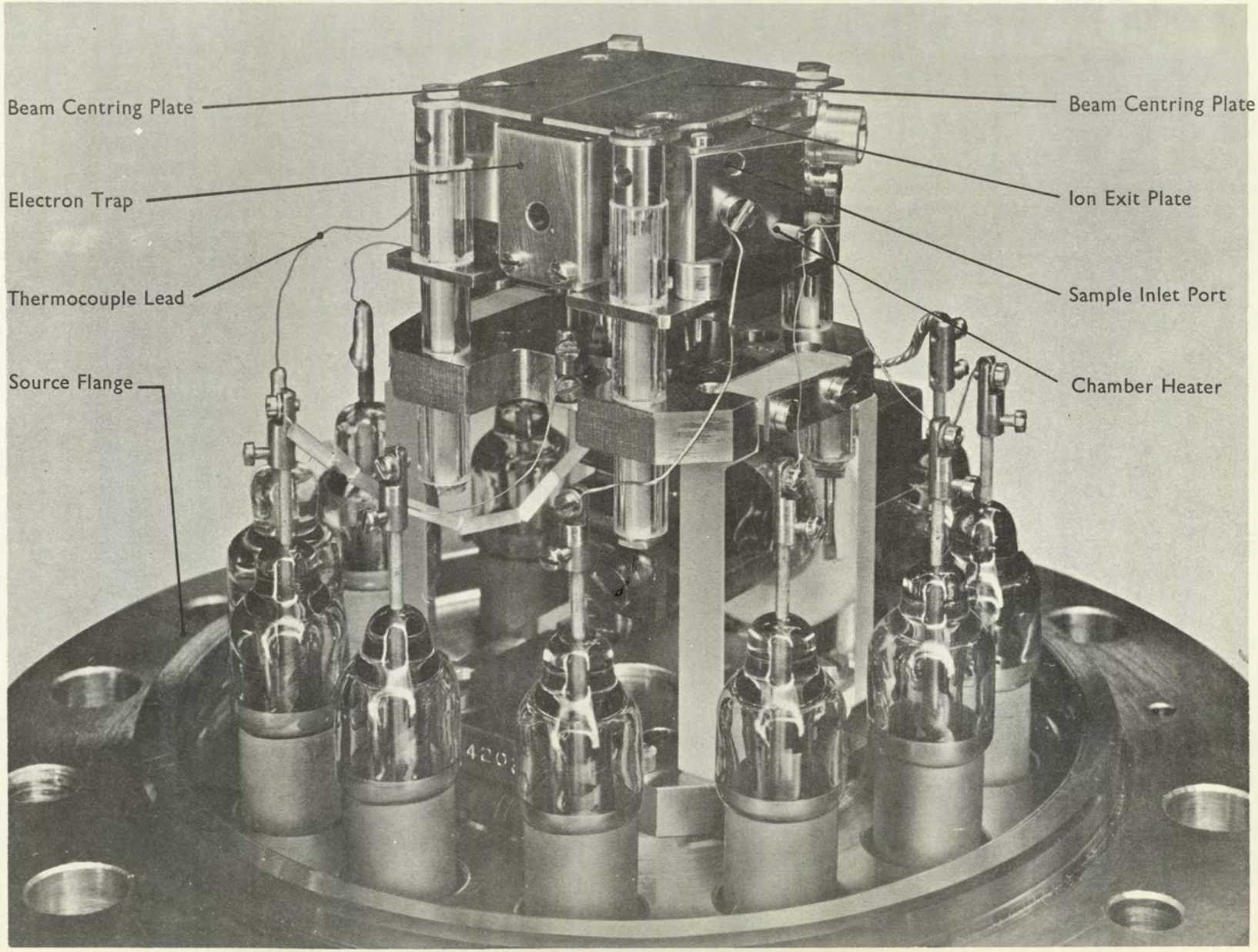

Fig. 1.6 MS902 E.B. Ion Source

For a typical mass spectrometer, the repeller voltage would be variable between -12V and 25V, and the mean beam-centring voltage set to a fixed proportion of the accelerating voltage. A potential difference may be applied between the beam-centring plates to correct for any electrode misalignment. A magnetic field, parallel to the direction of travel of the electrons, is used to confine the electron beam, and to minimise shift of the electron beam by the action of the electrostatic field accelerating the ions. The field strength, of between three and five hundred gauss, is usually provided by two permanent magnets, known as the source magnets, placed at either end of the source ionisation chamber. (For the MS902 mass spectrometer the earth slit and source magnets are mounted on the source housing and therefore they do not appear in figure 1.6).

Hitherto, large improvements to the performance of the standard Nier design have been achieved by altering the shape and path of the electron beam. Several authors have built sources in which the electron beam is fired into the ion chamber in the direction of the ion beam. After travelling about half-way across the chamber, the electrons are reflected by the ion extraction-field, and attracted towards a trap plate encircling the filament aperture. Such a design was first proposed by Finkelstein and Smith (1940), and recently, designs suitable for organic mass spectrometry have been reported to be ten times more sensitive than the conventional Nier source (Dotoroff and Grossel, 1962;

Tsuyama, Hirose and Nakajima, 1966). An explanation of the increased performance has not yet been given in the literature but it is probably due to processes which are similar to those occuring in the improved Nier design to be described in this report. However, the coaxial electron/ion beam source has the serious limitation that the ion beam has an energy spread of between two and thirty volts, compared with a half a volt or less, for the Nier source (Tsuyama, Hirose and Nakajima, 1966). Therefore, the use of a coaxial electron/ion beam source would reduce the resolving power of the mass spectrometer.

An alternative way of directing the electron beam was proposed by Barnard (1949, 1956). The electron beam was passed through crossed electric and magnetic fields, so that the electrons followed curtate trochoidal paths. (See sketch opposite). In this way many revolutions of the electron beam can occur within a small volume. As a consequence of this increased path-length, increased ion current is produced (method ii). However the gain in sensitivity obtained was much less than a factor of ten, and since the energy spread of the emerging beam is increased to several volts, this design has little advantage over the conventional Nier design.

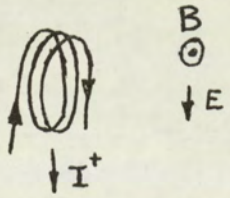

Perhaps the only published work describing improvement to the Nier source by means other than by changing the electron beam, is that by Okamoto and Mitani(xvi). For a gas inlet line, they used a long, narrow pipe which entered the ionisation chamber through a round aperture in the repeller plate. Such an arrangement enables the gas molecules to enter the ionisation chamber in a well-defined molecular beam. On the first pass of the gas molecules through the electron beam, the majority of ions formed will be moving towards the earth slit. Thereby, the angular spread of the ions, in the y and z directions, is reduced (methods vi and viii). The sensitivity was claimed to be ten times that of a conventional source, but similar experiments in the present investigation showed only a 20% increase in sensitivity. It is probable that the ten-fold increase observed was, in fact, due to the effects of electron space-charge, to be described in later chapters.

Recent work on ion sources has, in general, focused attention on the properties and effects of the electron beam within the ionization chamber, but emphasis has been given to multiply-charged ion production, rather than to producing a more sensitive source for the organic mass spectroscopist. However, some of the concepts developed and the experimental results obtained are particularly useful in determining some of the properties of ion sources, and for this reason the relevant literature is now described.

Multiply-charged ions may be produced by trapping the primary ions in the electron beam so that they may undergo further ionising collisions. Redhead (1966, 1967) described a slightly modified conventional Nier source for producing large currents of multiply-charged ions. He noted that the primary ion current had also increased, but gave no explanation of the phenomenon. Baker and Hasted (1966) gave detailed explanations of the sensitivity-pressure relationships obtained experimentally with their trapped-ion source. However, the present investigation shows that the sensitivity-pressure variation for singly-charged ions has a much simpler explanation than that conceived by Baker and Hasted. Correct interpretation of this relationship is essential for determining the limitations of the present source for organic mass spectrometry.

1.5 Scope of the Present Investigation

It is apparent from the above review that the literature contains descriptions of several source designs which have improved performance, but in no case is the source analysed to discover from whence the increased ion current was derived. In addition, there is no adequate description of the ion extraction and focusing properties of ion sources. Therefore, the following investigation commences with a detailed theoretical analysis of electron bombardment sources (sections 2, 3 and 4). The results are in good agreement with the experimental results obtained for sources operating with low electron currents. However, by itself, this study did not lead to an explanation of the characteristics

of electron bombardment sources operating with high electron currents. Elucidation of this problem followed from a detailed experimental analysis, supported by a further theoretical study (sections 5 and 6). It is shown that the phenomena occurring at high electron current result from the presence of electron space-charge within the electron beam.

Section 2 describes the way in which the axial potential distribution in the source was derived by using the Method of Conformal Transformation. The method is particularly suitable for analysing ion sources used for mass spectrometers, since these sources usually consist of plane electrodes, some of which have a slit-aperture. For the mathematical analysis, an electrode of finite thickness is replaced by two infinitely-thin electrodes, and for most source geometries, it is adequate to consider a system comprising six infinitely-thin planes, five of which contain a slit-aperture. It was necessary to develop new iterative procedures to obtain a solution from transformation equations, which hitherto were unsolved. For a typical source geometry, potentials can be computed at least ten times faster than is possible with the method of numerical relaxation. It is shown that the computed axial potential distribution never deviates by more than 3% from the true curve. This accuracy is quite adequate for determining the focal properties of practical slit systems, where dimensions usually have a tolerance of ± 10%.

Section 3 details the Liebmann (1949) ray-tracing procedure, as modified by Archard (1954) for systems of two dimensional symmetry. In the present study, because initial ion energies were small, fine interval sizes were used at the beginning of each trajectory. Thereby, it was possible to obtain an accuracy of better than one percent for paraxial rays. It is shown how linear and angular demagnification, source efficiency and time-of-flight of the ions may be determined from the computed trajectories. The results of the paraxial analysis are shown to be approximately valid for an ion object which has a height equal to the width of the aperture in the ion exit slit; for example, the true demagnification of an object of this size is no more than 15% larger than that calculated by paraxial theory.

The results of the theoretical analysis are collected together in section 4. It is shown how relatively small changes in repeller voltage can cause large changes in the overall linear and angular demagnification of the source, the ion residence time and the source efficiency. An approximate analysis yields a theoretical curve of sensitivity as a function of repeller voltage, displaying the main characteristics of the well-known two-maxima experimental curve. Further ray-tracing demonstrates that the source efficiency for any geomtry or object-plane position , but with a carefully chosen set of voltages on the electrodes, is approximately the same. There is therefore, no clearly defined 'optimum' geometry, which gives higher efficiency than any other geometry. A similar situation

exists for electron guns, as has been shown in an experimental investigation by Haine and Einstein (1952).

Section 5 gives a detailed experimental analysis of the AEI MS902 electron bombardment source, although the conclusions obtained are valid for all electron bombardment sources. For low electron ionising currents ($\lesssim$ 20μA) the loss occuring at each of the beam-defining apertures is determined, and it is shown that a theoretical estimate of ion transmission is in agreement with the experimentally obtained value. For electron currents above 500μA, the experimental evidence, supported by a further theoretical analysis, suggests that the space-charge forces in the electron beam restrict the emergence of ions from the antinodes of the electron beam to within a small angular wedge. The effect is such, that above 4000 volts accelerating voltage all ions pass through the alpha and Z angular apertures of the mass spectrometer. The ion object size is reduced, and in addition, collected ions emerge from three of the electron beam antinodes. However as only one-tenth of the total number of ions produced is trapped in this way, the overall sensitivity increase is limited to a factor of twelve. This agrees with the experimentally observed increase. It is shown that these features of the source only hold good when the sample pressure in the source is below 5×10^{-6} torr (a gauge pressure of 5×10^{-7} torr). Above this pressure, analysis indicates that neutralisation of the electron space-charge by the ions, prevents further ions from being produced. It is this phenomenon which causes "suppression" of sample fragment ions by reference compound ions, thereby effectively reducing the sensitivity of the source to the sample.

The first part of section 6 considers ways of obtaining, and maintaining high sensitivity. It was found that the optimum sensitivity was obtained only when a particular source geometry was used. The optimum dimensions, together with the tolerances required on these dimensions, are experimentally determined. To maintain optimum performance, several constructional changes were required on the source used by the author. The second part of section 6 considers possible ways of obtaining even better source sensitivities. Increase of electron current to 2 m.a. is shown to be feasible, giving such a source a sensitivity of forty times greater than that of a conventional Nier design. It is shown that the suppression of sample peaks can be avoided by using a partitioned source design; some preliminary experimental results obtained with this type of source are included.

2 - COMPUTATION OF THE POTENTIAL DISTRIBUTION

Calculation of the focal properties of an ion source requires the use of two distinct procedures, that of solving Laplace's equation to determine the potential distribution and that of plotting trajectories through this potential field. This section deals with the first procedure in which Laplace's equation for the region is solved.

In general, previous analyses of ion sources have required lengthy experiments or elaborate computer studies to determine the potential distribution, allowing perhaps only one source geometry to be investigated. Consequently, the present study has concentrated on establishing an elegant method which would quickly yield the paraxial properties of a particular source geometry for, typically, ten sets of different voltages on the electrodes. The result is a computer program which will complete the above task in six minutes on an IBM 360/40 computer, entailing a cost of about £5. A full analysis of the effect of geometry changes can be completed for less than £50. If the conventional method of numerical relaxation were to be used to calculate the potential distribution, it is estimated that the total cost would be at least ten times this amount.

2.1 Introduction

Analytical expressions for the potential distribution in round-aperture lenses have been given in a few simple cases only; in particular Brüche and Scherzer (1934), (see Zworykin et al, p. 282, 1945), derived an expression for the potential distribution in the neighbourhood of a round-aperture in a single, plane electrode, by using a coordinate system consisting of confocal hyperboloids and conjugate confocal ellipsoids. For slit-aperture lenses however, many configurations can be treated by an application of the Schwarz-Christoffel transformation, together with use of one or two simple conformal transforms; such mathematical treatments are described in text books by Gibbs (1958), Green (1962), Binns and Lawrenson (1963), Morse and Feshback (p. 443, 1953) and Walker (1933).

The equipotentials in slit-aperture and circular-aperture lenses have been given by Henneberg (1935), while Glaser and Henneberg (1935) considered the case of a thin lens with a constant field on each side of the lens plane. For slit-aperture lenses, the equipotentials were measured using an electrolytic plotting tank, while those for circular-aperture lenses were calculated using the Brüche and Scherzer formulae. Straschkewitch (1940) gave an approximate formula for the potential distribution along the axis of a lens consisting of three plane and parallel electrodes, the central electrode having a slit-aperture; the formula is valid only for the case where the width of the aperture is much less than the separation of adjacent electrodes.

The need to obtain potential distributions for the more complex systems used in practice led Moch, Roth and Salmon (1950) to a study of a practical ion source, for which potentials were measured with an electrolytic plotting-tank analogue; trajectories through the lenses were calculated using an approximate formula derived from the general ray equation. An alternative analogue technique, the resistor network, has been used by Liebmann (1950) for magnetic electron lenses of cylindrical symmetry, but the method can easily be adapted to systems of planar symmetry. Dietz (1959) used the resistance paper analogue to analyse thermal ion sources.

The potential distributions in systems consisting of three electrodes, each with a slit-aperture, were calculated simultaneously by Laudet (1953) and Archard (1954), using the Method of Conformal Transformation. However, in both treatments, certain conditions were made regarding the symmetry of the system so that the transformation constants could be derived without too much difficulty. This work was extended by Boerboom (1957). In part I of a series of articles (Boerboom, 1959), an iterative procedure has been developed for solving the five non-linear simultaneous equations resulting from the conformal transformation of a system with three electrodes; the method is valid only for cases where the separation of adjacent electrodes is greater than the width of the apertures. In part II (Boerboom, 1960a), this restriction is relaxed, but an added

restriction is that the central electrode must be a plane of symmetry. The methods given to solve the equations are lengthy, and since they involve graphical techniques they are not suited for computer solution. Part III (Boerboom, 1960b) gives the transformation equations relevant to a system of many electrodes, together with the solution for a system of special symmetry.

Recently, numerical relaxation on a digital computer has become a common method for calculating the potentials in electrostatic lenses (Kirstein and Hornsby, 1964, and Hamza, 1966) and magnetic lenses of cylindrical symmetry (Bullough, Heath and Vine, 1963). However, at the present time such calculations entail large computer costs, making an extensive study of ion sources prohibitively expensive.

Consequently it was decided to re-examine the work of Boerboom, and to develop a new iterative procedure, for obtaining the transformation constants from the set of ten non-linear simultaneous equations, for a system comprising five planes, each with a slit-aperture, and an apertureless plane.

2.2 Preliminaries

In the experiments to be detailed in section 5, use was made of the AEI MS902 mass spectrometer, and so that the experimental and theoretical results may be compared, the theoretical analysis described in the following sections will be modelled on the MS902 electron bombardment source. Nevertheless, all the computer programs have been written so that any source geometry (within the limits to be defined later), together with any set of electrode voltages may be used.

Figure 2.1 is a scale drawing (x10) of a cross-sectional plane of the MS902 electron bombardment source showing the relative positions and sizes of the electrodes. The dispositions of the electron gun, electron trap and the collimating magnets are shown in figure 2.2. For the following study, the co-ordinate system shown on these figures has been used, since it has been conventional in transformation theory to adopt y as the axis of symmetry of the cross-sectional plane. This co-ordinate system should not be confused with that conventionally used in mass spectrometry, where x is along the direction of motion of the ions and y is the axis along which the major focusing action occurs.

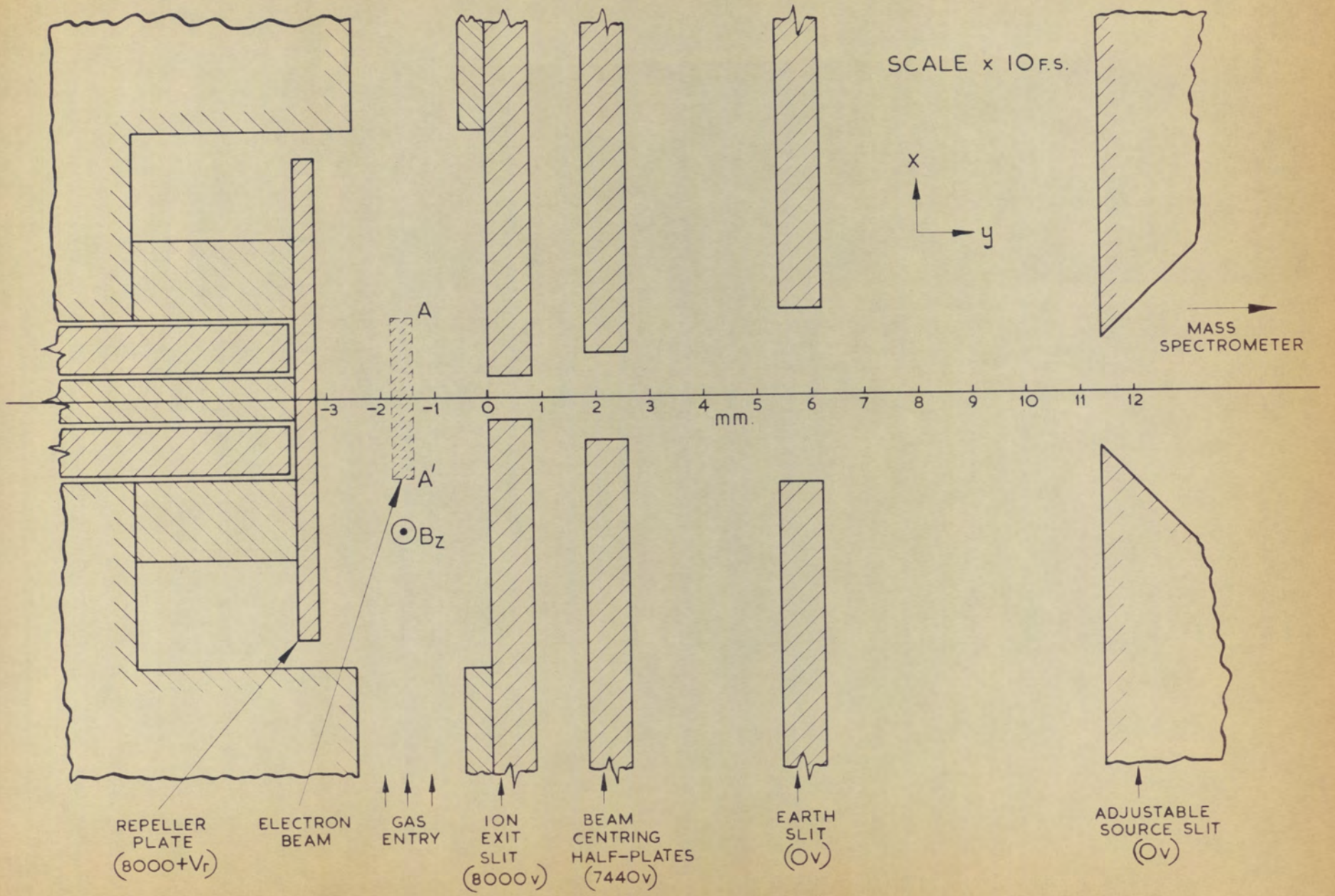

FIGURE 2.1. X-Y CROSS SECTION OF THE AEI MS902 ELECTRON BOMBARDMENT

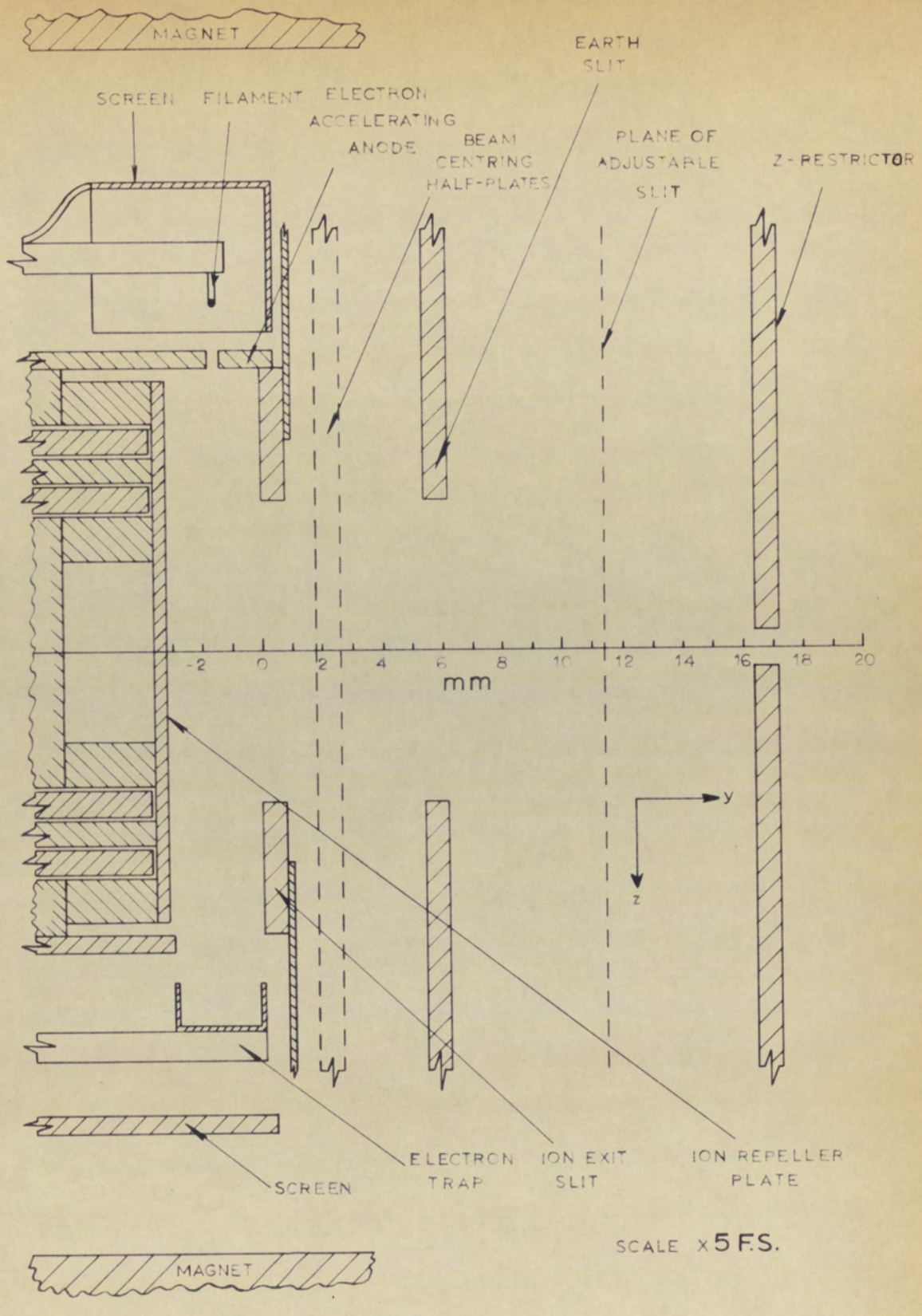

FIGURE. 22 Z-Y CROSS SECTION OF THE AEI MS902 E.B. ION SOURCE SHOWING ELECTRON GUN ASSEMBLY.

Figure 2.4 shows a proposed thin-electrode equivalent of the MS902 electron bombardment source, using five planes, each with a slit-aperture, and an apertureless plane. The repeller plate is represented by a thin plane at its right hand edge; the ion exit slit, and the beam-centring slit each by two apertured planes; and the earth slit by a single apertured plane at its left-hand edge. Where a thick electrode is replaced, for the mathematical analysis,by two thin electrodes, each of the thin electrodes is at the same potential as the thick electrode. There will be a small error in the theoretical treatment since no account is taken of the potential boundary along the line joining the ends of the two bounding planes (i to g, for example, in figure 2.4). The magnitude of this error will be given in section 2.7.

The Liebmann ray-tracing method requires that the optic axis is straight and along the axis of symmetry of the cross-section plane. This corresponds to the case where there are no net cross-fields or 'beam-deflecting voltages'. In practice, the beam deflecting voltages are used to straighten the optic axis along the above-defined symmetry axis, thereby compensating for cross-fields resulting from mechanical misalignments of the source electrodes. Therefore, this ray-tracing method can be used for the analysis of real sources.

* * *

The computer program has been written to solve a system consisting of five apertured planes and an apertureless plane. However, since an explanation of the transformation method and the iterative procedure required for such a system would be extremely cumbersome, it has been preferred to give in the next section, and in Appendices I and II, a theoretical discussion in terms of a system with two apertured planes and an apertureless plane. The equations and techniques are easily extended to the case of any specified number of apertured planes.

2.3 Voltage equations for a system of two apertured planes and an apertureless plane

The cross-sectional plane of this system is shown in figure 2.3. The separation between the plane and the nearest apertured electrodes is d_2, and between the two apertured electrodes is a gap of d_1. The apertures have widths $2s_2$ and $2s_1$. The voltages on the electrodes are, from left to right, V_3, V_2 and V_1, respectively ($V_2' = V_2$, and $V_1' = V_1$ since there are to be no cross-fields).

The voltage V, along the y-axis as a function of y is given by the following pair of parametric equations:-

$$V = \frac{2}{\pi}(V_1 - V_2)\arctan\frac{v}{b} + \frac{2}{\pi}(V_2 - V_3)\arctan\frac{v}{d} + V_3 \ldots \qquad (2.1)$$

$$y = v - \frac{2d_1}{\pi}\arctan\frac{b}{v} - \frac{2d_2}{\pi}\arctan\frac{d}{v} + d_1 \qquad \ldots\ldots \qquad (2.2)$$

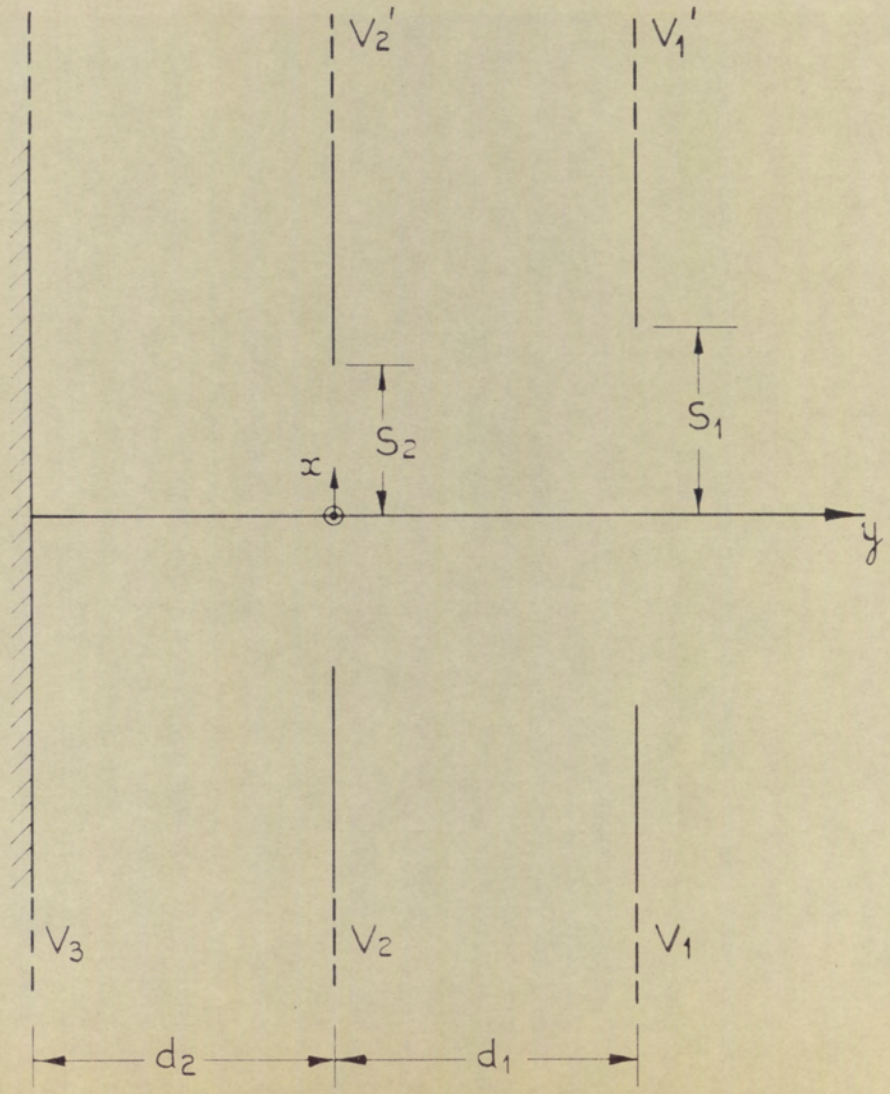

FIGURE 2.3. —CROSS SECTION OF A 1—PLANE, 2—SLIT APERTURE SYSTEM.

These equations, and ones for the first two derivatives of V, are derived in Appendix I using the Schwarz-Christoffel transformation. The parameters V_1, V_2, V_3, d_1 and d_2 have been defined above, and are known parameters for this system. The variable v is the auxilliary parameter which links the voltage equation (2.1) to the distance equation (2.2). The letters b and d in equations (2.1) and (2.2), together with the letters a and c,are termed the transformation constants of the system, and are determined from a set of simultaneous equations derived from the transformation equation and a knowledge of the boundary conditions. As shown in Appendix I, the set of equations for the system comprising two apertured planes and an apertureless plane is:-

$$s_1 = a + r_1 \ln \frac{a+b}{a-b} + r_2 \ln \frac{a+d}{a-d} \quad \ldots\ldots \quad (2.3)$$

$$s_2 = c + r_1 \ln \frac{b+c}{b-c} + r_2 \ln \frac{c+d}{c-d} \quad \ldots\ldots \quad (2.4)$$

$$r_1 = \frac{(a^2 - b^2)(b^2 - c^2)}{2b(b^2 - d^2)} = \frac{d_1}{\pi} \quad \ldots\ldots \quad (2.5)$$

$$r_2 = \frac{(a^2 - d^2)(c^2 - d^2)}{2d(b^2 - d^2)} = \frac{d_2}{\pi} \quad \ldots\ldots \quad (2.6)$$

In Appendix II details are given of a new iterative scheme suitable for the solution of these equations.

2.4 Extension to a system of an apertureless plane and five apertured planes

The transformation equations for a system comprising an apertureless plane and five planes, each with a slit-aperture may be derived in exactly the same way as for the system described above. The nomenclature for this larger system is given in Figure 2.4. The width of the slit-apertures are, respectively, $2s_1$ to $2s_5$, the electrode separations d_1 to d_5, and the transformation constants a to j. The relevant voltage equations are given in Figure 2.5, while the ten non-linear simultaneous equations required for the derivation of a to j are given in Figure 2.6. The iterative scheme developed in Appendix II may easily be extended to solve these equations, and for each of a large variety of geometries it has been found that the ten constants may be derived, to within a prescribed accuracy, after 30-40 successive iterations. The criterion for accuracy has been chosen so that the absolute error in 'a' will be less than $\pm$ 1 x 10^{-8}. For a geometry where the linear dimensions are of the order of unity, 'a' will also be of the order of unity. Although any system of units may be used, each linear dimension must be in the same unit.

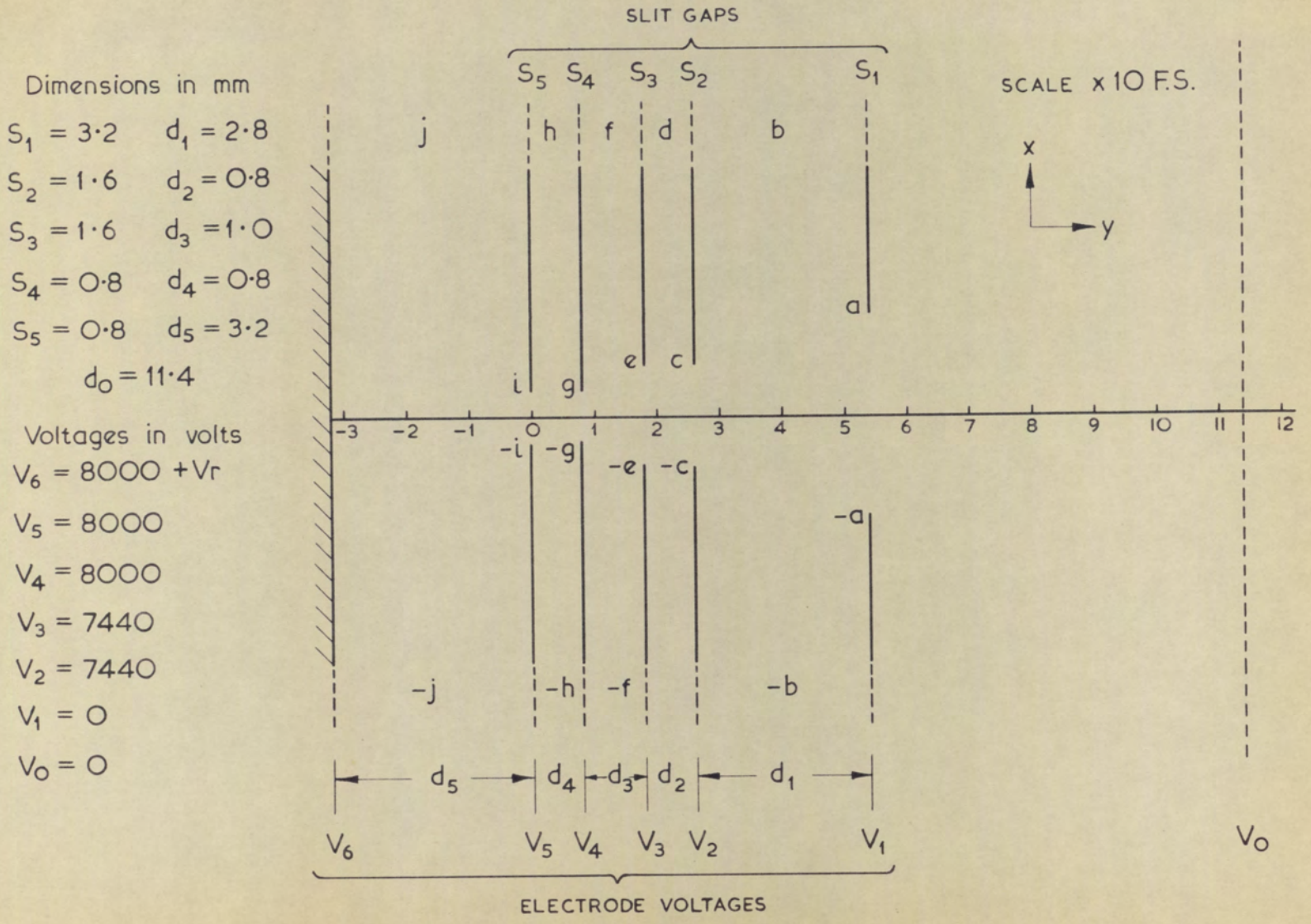

FIGURE 2.4. CROSS SECTION OF A 1-PLANE, 5-SLIT APERTURE SYSTEM TO SIMULATE THE AEI MS902 E.B. ION SOURCE.

$$y = v - \frac{2d_1}{\pi}\tan^{-1}\frac{b}{v} - \frac{2d_2}{\pi}\tan^{-1}\frac{d}{v} - \frac{2d_3}{\pi}\tan^{-1}\frac{f}{v} - \frac{2d_4}{\pi}\tan^{-1}\frac{h}{v} - \frac{2d_5}{\pi}\tan^{-1}\frac{j}{v}$$
$$+ d_1 + d_2 + d_3 + d_4$$

$$V = \frac{2}{\pi}(V_1 - V_2)\tan^{-1}\frac{v}{b} + \frac{2}{\pi}(V_2 - V_3)\tan^{-1}\frac{v}{a} + \frac{2}{\pi}(V_3 - V_4)\tan^{-1}\frac{v}{f}$$
$$+ \frac{2}{\pi}(V_4 - V_5)\tan^{-1}\frac{v}{h} + \frac{2}{\pi}(V_5 - V_6)\tan^{-1}\frac{v}{j} + V_6$$

$$V' = \frac{2}{\pi}\cdot\frac{\partial v}{\partial y}\cdot\left\{\frac{b(V_1 - V_2)}{b^2 + v^2} + \frac{d(V_2 - V_3)}{d^2 + v^2} + \frac{f(V_3 - V_4)}{f^2 + v^2} + \frac{h(V_4 - V_5)}{h^2 + v^2} + \frac{j(V_5 - V_6)}{j^2 + v^2}\right\}$$

$$V'' = \left(\frac{\partial v}{\partial y}\right)^2 \left\{\frac{\partial^2 V}{\partial v^2} - \frac{\partial^2 y}{\partial v^2}\cdot V'\right\}$$

where $$\frac{\partial v}{\partial y} = \frac{(v^2+b^2)}{(v^2+a^2)}\frac{(v^2+d^2)}{(v^2+c^2)}\frac{(v^2+f^2)}{(v^2+e^2)}\frac{(v^2+h^2)}{(v^2+g^2)}\frac{(v^2+j^2)}{(v^2+i^2)}$$

$$\frac{\partial^2 V}{\partial v^2} = -\frac{4v}{\pi}\left\{\frac{b(V_1 - V_2)}{(b^2+v^2)^2} + \frac{d(V_2 - V_3)}{(d^2+v^2)^2} + \frac{f(V_3 - V_4)}{(f^2+v^2)^2} + \frac{h(V_4 - V_5)}{(h^2+v^2)^2} + \frac{j(V_5 - V_6)}{(j^2+v^2)^2}\right\}$$

$$\frac{\partial^2 y}{\partial v^2} = -\frac{4v}{\pi}\left\{\frac{bd_1}{(b^2+v^2)^2} + \frac{dd_2}{(d^2+v^2)^2} + \frac{fd_3}{(f^2+v^2)^2} + \frac{hd_4}{(h+v^2)^2} + \frac{jd_5}{(j^2+v^2)^2}\right\}$$

FIG. 2.5. PARAMETRIC EQUATIONS FOR AXIAL VOLTAGE AND ITS DERIVATIVES FOR A 1PLANE, 5 APERTURE SLIT SYSTEM.

$$S_1 = a + r_1 \ln \frac{a+b}{a-b} + r_2 \ln \frac{a+d}{a-d} + r_3 \ln \frac{a+f}{a-f} + r_4 \ln \frac{a+h}{a-h} + r_5 \ln \frac{a+j}{a-j}$$

$$S_2 = c + r_1 \ln \frac{b+c}{b-c} + r_2 \ln \frac{c+d}{c-d} + r_3 \ln \frac{c+f}{c-f} + r_4 \ln \frac{c+h}{c-h} + r_5 \ln \frac{c+j}{c-j}$$

$$S_3 = e + r_1 \ln \frac{b+e}{b-e} + r_2 \ln \frac{d+e}{d-e} + r_3 \ln \frac{e+f}{e-f} + r_4 \ln \frac{e+h}{e-h} + r_5 \ln \frac{e+j}{e-j}$$

$$S_4 = g + r_1 \ln \frac{b+g}{b-g} + r_2 \ln \frac{d+g}{d-g} + r_3 \ln \frac{f+g}{f-g} + r_4 \ln \frac{g+h}{g-h} + r_5 \ln \frac{g+j}{g-j}$$

$$S_5 = i + r_1 \ln \frac{b+i}{b-i} + r_2 \ln \frac{d+i}{d-i} + r_3 \ln \frac{f+i}{f-i} + r_4 \ln \frac{h+i}{h-i} + r_5 \ln \frac{i+j}{i-j}$$

$$r_1 = \frac{(a^2-b^2)(b^2-c^2)(b^2-e^2)(b^2-g^2)(b^2-i^2)}{2b\ (b^2-f^2)(b^2-d^2)(b^2-h^2)(b^2-j^2)} = \frac{d_1}{\pi}$$

$$r_2 = \frac{(a^2-d^2)(c^2-d^2)(d^2-e^2)(d^2-g^2)(d^2-i^2)}{2d\ (d^2-f^2)(b^2-d^2)(d^2-h^2)(d^2-j^2)} = \frac{d_2}{\pi}$$

$$r_3 = \frac{(a^2-f^2)(c^2-f^2)(e^2-f^2)(f^2-g^2)(f^2-i^2)}{2f\ (b^2-f^2)(d^2-f^2)(f^2-h^2)(f^2-j^2)} = \frac{d_3}{\pi}$$

$$r_4 = \frac{(a^2-h^2)(c^2-h^2)(e^2-h^2)(g^2-h^2)(h^2-i^2)}{2h\ (b^2-h^2)(d^2-h^2)(f^2-h^2)(h^2-j^2)} = \frac{d_4}{\pi}$$

$$r_5 = \frac{(a^2-j^2)(c^2-j^2)(e^2-j^2)(g^2-j^2)(i^2-j^2)}{2j\ (b^2-j^2)(d^2-j^2)(f^2-j^2)(h^2-j^2)} = \frac{d_5}{\pi}$$

FIG. 2.6. TRANSFORMATION EQUATIONS FOR A SLIT SYSTEM OF 5 APERTURES AND 1 PLANE.

2.5 Presentation of results

The complete program performs four distinct functions before arriving at a figure for the source sensitivity under given operating conditions; therefore it has been convenient to print out some of the intermediate working as an indication that the calculations have progressed as expected.

After the iteration process has been carried out, a set of results is printed. As an example, Figure 2.7 shows a set for the MS902 electron bombardment ion source. The first line under the title gives the number of iterations required to obtain the transformation constants to the afore-mentioned accuracy. As a check that the values of a to j obtained are the correct ones, they are substituted back into the equations shown in Figure 2.6 to yield 'calculated' values of the geometry constants, S_1 to S_5 and d_1 to d_5. These are presented together with the actual values as shown in Figure 2.7. It can be seen that the calculated values are correct to within several parts in 10^7, which is quite adequate for the study of practical sources, where the machining tolerances amount to several parts in 10^3, for a dimension in the order of several millimetres. The given slit-aperture widths are the full widths, that is:-

$$S_1 = 2s_1; \ldots\ldots; S_5 = 2s_5$$

TRAJECTORIES IN SLIT LENS SYSTEMS USING POTENTIAL DISTRIBUTIONS

DERIVED BY CONFORMAL TRANSFORMATION

SOLUTION USING KNOWN LENS GEOMETRY - 36 ITERATIONS REQUIRED

S1	= 3.200000	D1	= 2.800000	A= 8.42328291, -1
S1(CALC)=	3.200000	D1(CALC)=	2.800000	B= 3.27148536, -1
S2	= 1.600000	D2	= 0.800000	C= 6.52562339, -2
S2(CALC)=	1.599998	D2(CALC)=	0.800000	D= 3.26727544, -2
S3	= 1.600000	D3	= 1.000000	E= 1.71559947, -2
S3(CALC)=	1.600002	D3(CALC)=	1.000000	F= 8.94960127, -3
S4	= 0.800000	D4	= 0.800000	G= 2.15327162, -3
S4(CALC)=	0.799999	D4(CALC)=	0.800000	H= 7.09109134, -4
S5	= 0.800000	D5	= 3.200000	I= 2.31282884, -4
S5(CALC)=	0.800000	D5(CALC)=	3.200000	J= 2.33122552, -5

FIGURE 2.7 SPECIMEN PRINT-OUT OF THE TRANSFORMATION CONSTANTS FOR THE SIMULATED MS902 e.b. ION SOURCE

In the right-hand column the values of a to j appear in the computer floating-point format. The equivalent in conventional notation, for f for example, is $2.15327162 \times 10^{-3}$. It is to be noted that a>b>c>d>e>f>g>h>i>j as stipulated by the theory.

Figure 2.8 shows the next set of results, which commences with a print-out of the voltages connected to the electrodes. Then follows a table in which values of y (the distance along the axis) and the corresponding values of the axial potential V, and its derivatives V' and V" are given as a function of V (extreme left-hand column), which is the auxiallary parameter v (the computer typewriter will only print letters in the upper case). v is tabulated between the absolute values of 10^{-6} and 100, where each step of 10 is subdivided into 25 equally spaced logarithmic intervals, making 200 intervals in all. (For example, $1.585 = \text{antilog}_{10} 0.2$). To avoid a lengthy results sheets, every fifth set of parameters is printed. The advantage of using a logarithmic scale in v is that the corresponding values of y are in the range of interest for a wide range of geometries. The potential and the derivatives given here are plotted in Figure 2.9. Figure 2.10 shows the left-hand portion of each curve on an enlarged scale.

VOLTAGES ON ELECTRODES - DO= 11.40

V6	V5	V4	V3	V2	V1	V0
7997.00	8000	8000	7440	7440	0	0

V	Y	V	V'	V''
1.000, -6	-3.112	7997.03	0.31	-0.03
1.585, -6	-3.060	7997.04	0.31	-0.04
2.512, -6	-2.979	7997.07	0.31	-0.07
3.981, -6	-2.852	7997.11	0.30	-0.11
6.310, -6	-2.656	7997.16	0.27	-0.17
1.000, -5	-2.366	7997.23	0.20	-0.30
1.585, -5	-1.971	7997.28	0.03	-0.59
2.512, -5	-1.504	7997.21	-0.40	-1.36
3.981, -5	-1.047	7996.83	-1.44	-3.72
6.310, -5	-0.670	7995.90	-3.93	-11.17
1.000, -4	-0.386	7994.13	-9.45	-31.66
1.585, -4	-0.171	7991.11	-20.00	-70.49
2.512, -4	0.008	7986.18	-36.26	-109.70
3.981, -4	0.178	7978.28	-57.54	-142.03
6.310, -4	0.354	7965.70	-88.13	-219.81
1.000, -3	0.531	7945.81	-141.50	-401.86
1.585, -3	0.702	7914.54	-231.13	-640.54
2.512, -3	0.870	7866.06	-346.28	-672.88
3.981, -3	1.052	7793.14	-449.10	-443.64
6.310, -3	1.264	7689.73	-519.08	-245.09
1.000, -2	1.510	7555.52	-570.56	-200.12
1.585, -2	1.779	7393.98	-635.61	-309.50
2.512, -2	2.061	7199.06	-759.04	-593.06
3.981, -2	2.355	6945.27	-991.45	-989.40
6.310, -2	2.663	6587.81	-1333.75	-1145.95
1.000, -1	3.007	6066.74	-1675.26	-779.19
1.585, -1	3.421	5323.33	-1884.11	-264.37
2.512, -1	3.928	4351.25	-1914.52	111.84
3.981, -1	4.515	3266.07	-1753.77	430.42
6.310, -1	5.142	2270.66	-1390.73	700.71
1.000, +0	5.814	1500.73	-905.39	679.89
1.585, +0	6.608	966.15	-481.39	383.94
2.512, +0	7.672	614.69	-221.10	144.51
3.981, +0	9.229	389.15	-93.75	43.42
6.310, +0	11.614	245.87	-38.32	11.75
1.000, +1	15.339	155.22	-15.42	3.04
1.585, +1	21.211	97.96	-6.16	0.77
2.512, +1	30.495	61.81	-2.46	0.20
3.981, +1	45.195	39.00	-0.98	0.05
6.310, +1	68.486	24.61	-0.39	0.01

FIGURE 2.8 SPECIMEN PRINT-OUT OF THE AXIAL VOLTAGE DISTRIBUTION AND ITS DERIVATIVES FOR THE MS902 e.b. ION SOURCE

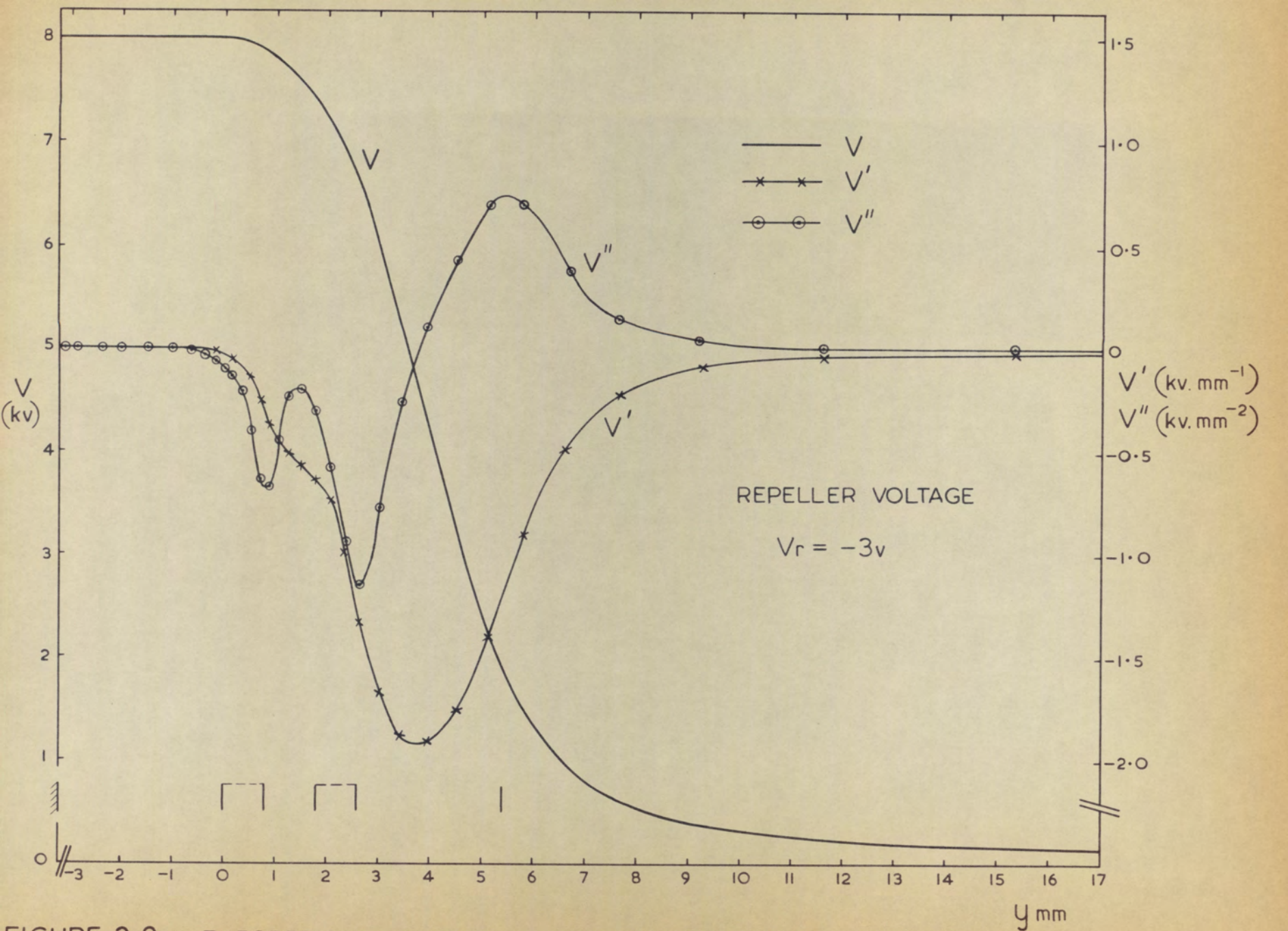

FIGURE 2.9. THEORETICAL POTENTIAL DISTRIBUTION AND ITS DERIVATIVES FOR MS902 E.B. ION SOURCE.

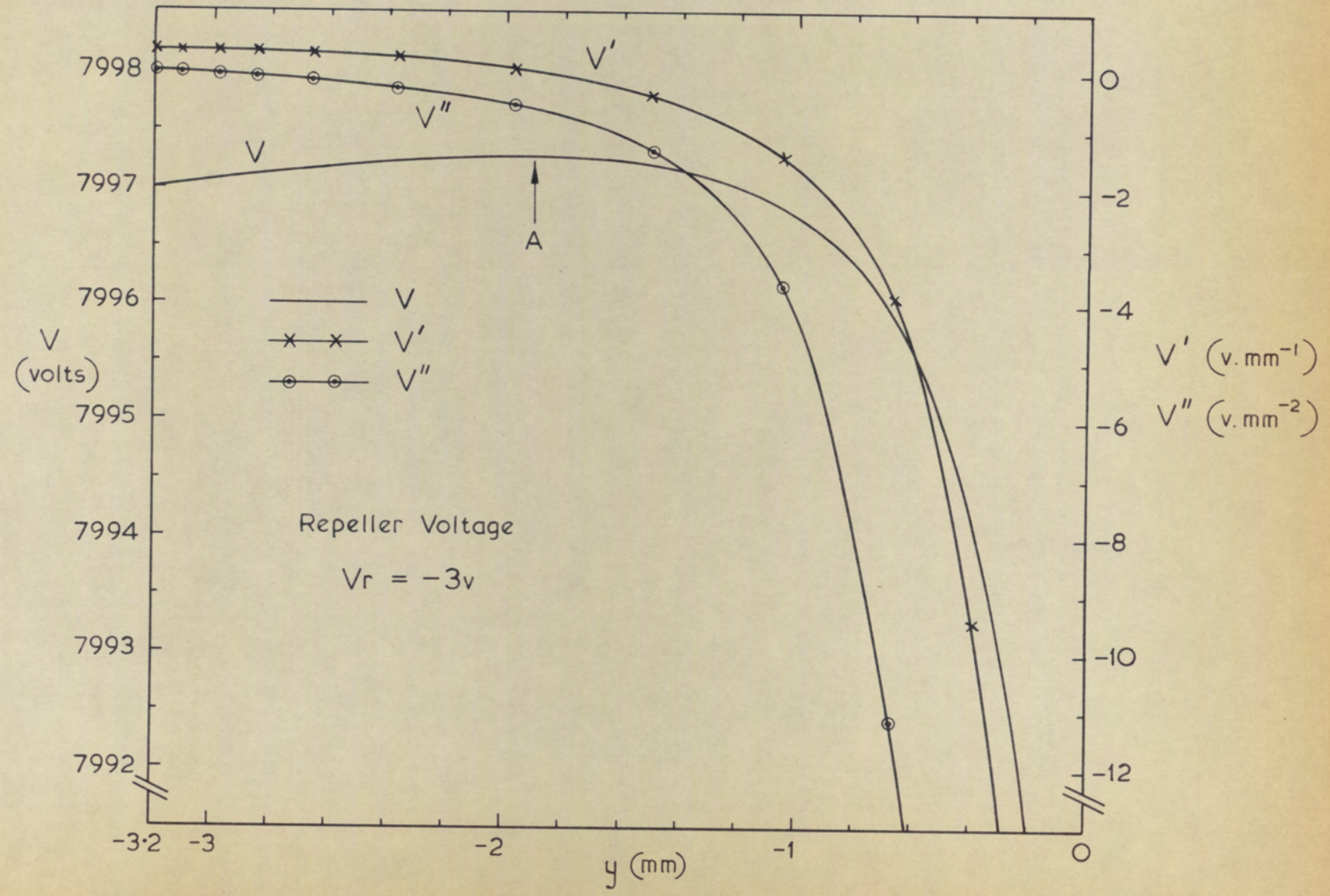

FIGURE 2.10. ENLARGED PORTION OF FIGURE.

2.6 Equipotentials in the ionisation chamber

Sketches of some equipotential lines in the ionisation chamber for repeller voltages of -3.12V and 17.4V are given in figures 2.11 and 2.12 respectively. The potential values on the axis are those derived by the computer calculation, while the approximate positions of the potentials V(x) close to the axis ($|x| \ll 1$) have been derived by using the following Taylor series expansion.

$$V(x) = V(o) + \left(\frac{\partial V}{\partial x}\right)_o . x + \frac{1}{2} \left(\frac{\partial^2 V}{\partial x^2}\right)_o x^2 + \text{------}$$

Since the potential distribution is symmetrical about the y-axis, the odd derivatives are zero. Also, Laplace's equation may be written in the form

$$\frac{\partial^2 V}{\partial x^2} = -\frac{\partial^2 V}{\partial y^2}$$

Therefore, $V(x) = V(o) - \frac{1}{2} V''(o) . x^2 + O(x^4)$

where the approximate potential V(x), is expressed in terms of the axial potential and its second derivative. For large off-axis distances ($|x| \gg 1$), the equipotentials tend to the equipotentials of a uniform repeller field. The intermediate segments of equipotential lines have been sketched in.

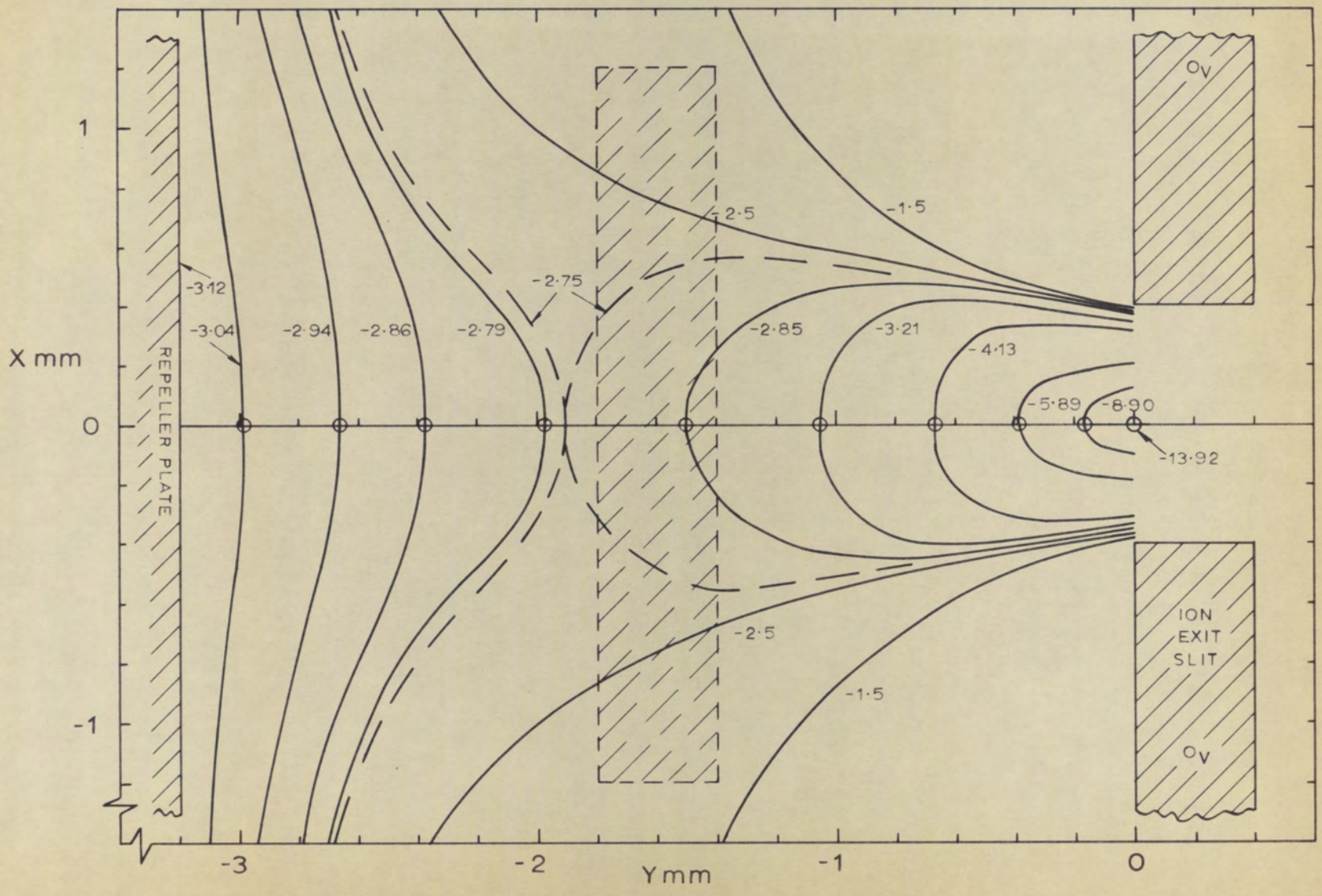

FIGURE 2.11 EQUIPOTENTIAL PLOT IN THE ION CHAMBER OF THE MS 902 E.B. ION SOURCE. ION REPELLER VOLTAGE = -3.12v.

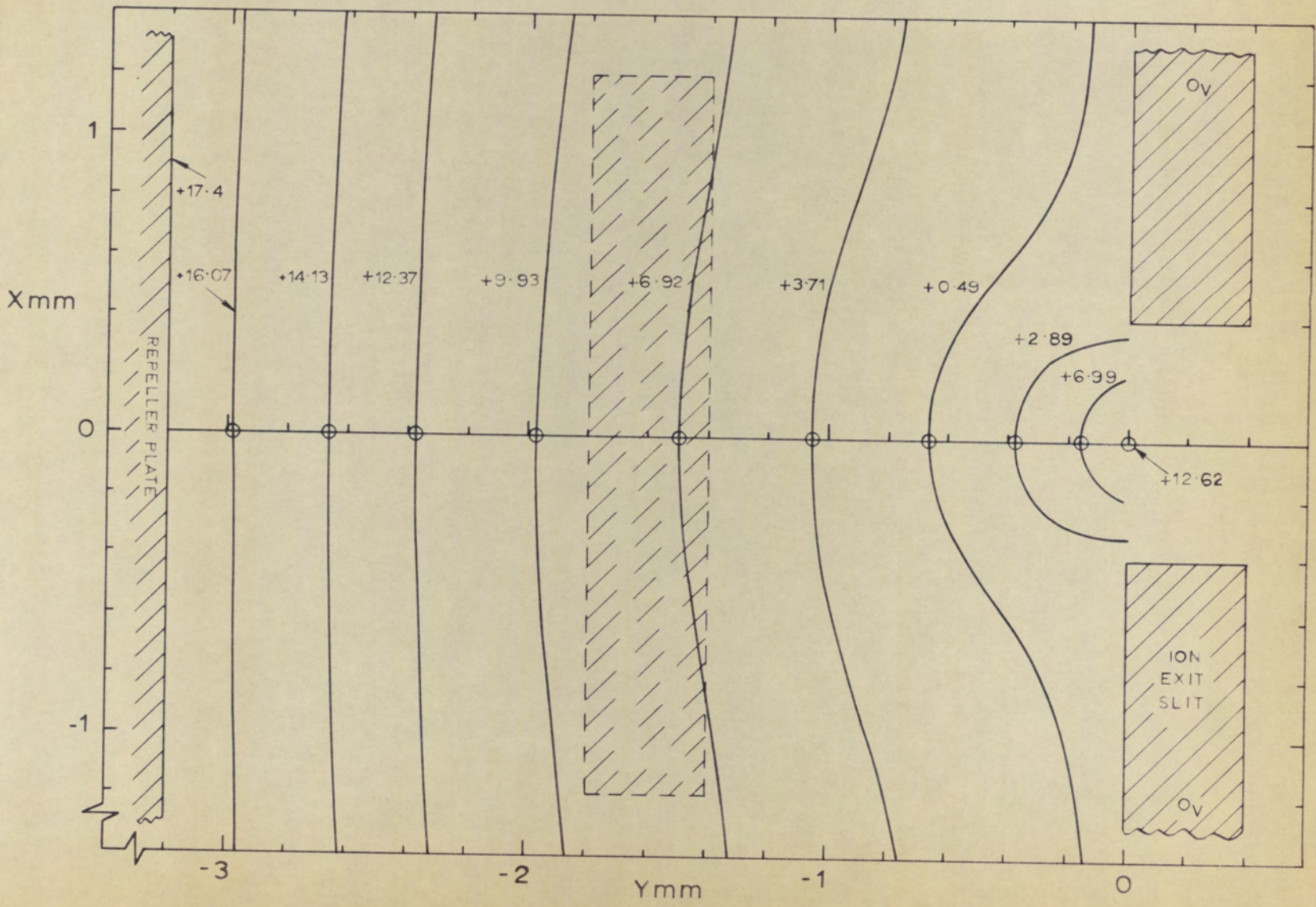

FIGURE 2.12 EQUIPOTENTIAL PLOT IN THE ION CHAMBER OF THE MS902 E.B. ION SOURCE. ION REPELLER VOLTAGE = +17·4V.

Study of such equipotential plots can give information on the energy spread given to the ions by the source. For a repeller voltage of -3.12V (figure 2.11), the positive extraction field at the centre of the ionisation chamber, caused by leakage from the main accelerating field, is almost cancelled by the negative repeller field. The potential difference across the electron beam (shown by the broken line rectangle) is small and hence the energy spread of the ions will also be small (~0.1 volt). When the repeller voltage is 17.4 volts (figure 2.12), the repeller field dominates and the energy spread of the ions will be much larger, at approximately 3 volts.

2.7 Accuracy of Computed Potentials

The results produced by the focal property part of the program can be checked very easily by a method detailed in later sections, but it implicitly assumes that the potential distribution has been computed correctly. The latter can only be checked by comparing the results produced by independent methods.

One such method is resistor network analysis, and fortunately, the results obtained by Liebmann (1954, unpublished) for an ion source, still exist; he determined the axial potential distribution in the AEI MS2 electron bombardment source, the geometry of which is shown in the inset of figure 2.13. It differs from the MS902 source only in the thickness and separation of the beam-centring and earth slits.

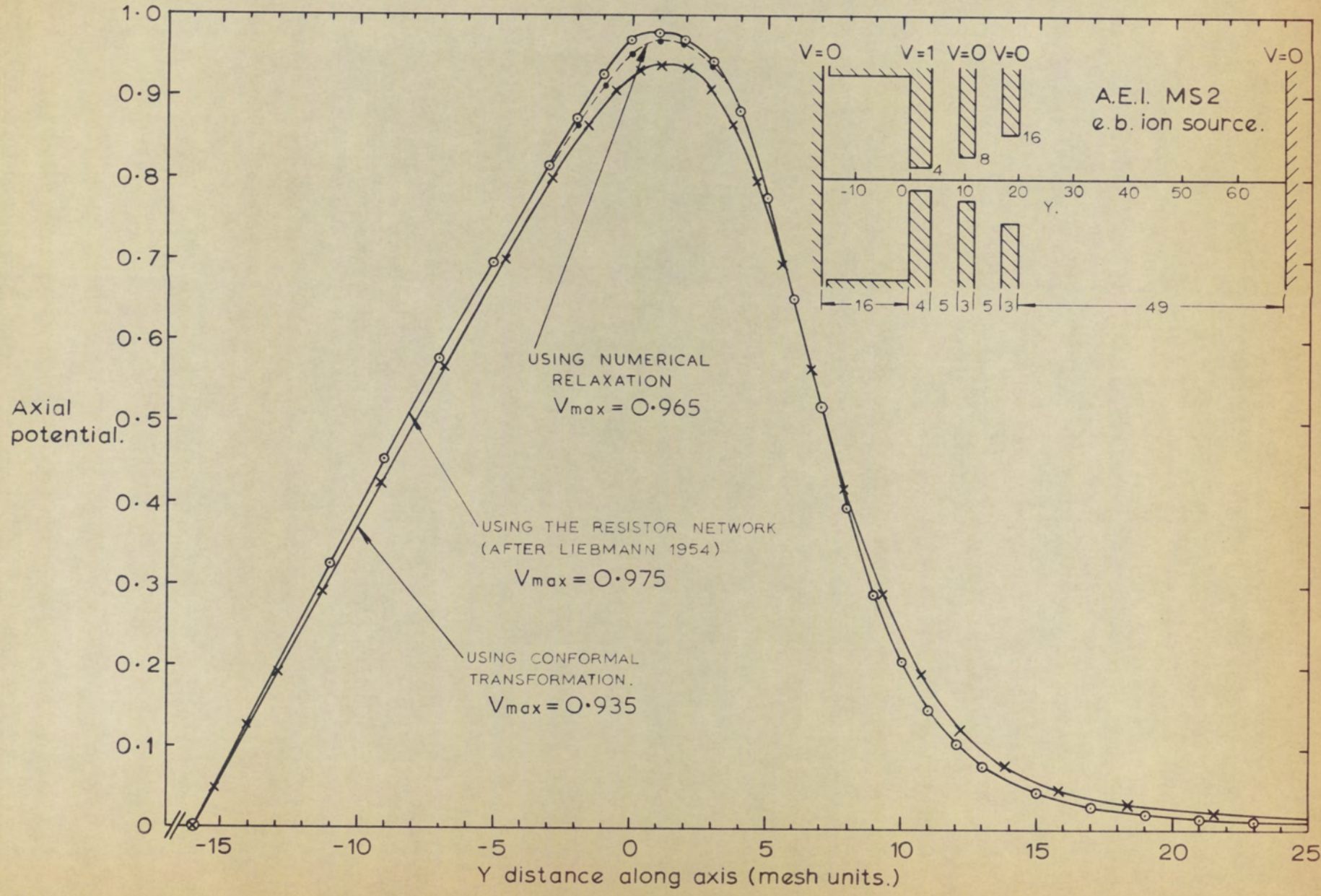

FIGURE 2.13 ELEMENTARY POTENTIAL DISTRIBUTION DETERMINED ON A RESISTOR NETWORK COMPARED WITH THE CONFORMAL TRANSFORMATION SOLUTION.

Alternatively, the potentials may be checked by a numerical relaxation method by using the computer program of Hamza (1966).

The axial potential distributions for the MS2 source, determined by each of the three independent methods, is shown in figure 2.13. The results for the numerical relaxation, and the resistor network analyses differ by 1% at the maximum potential, but by much less away from the edge of the ion exit slit. However, conformal transformation gives a potential at maximum which is 3% lower than the numerical relaxation result. Such a depression results from treating a thick electrode as two thin electrodes (see section 2.2). The high values of potential obtained by conformal transformation at large y values is also to be expected, since the conformal transformation analysis assumes that the right-hand side plane at V = 0 is at plus infinity, compared with y = +69 for the resistor network and numerical relaxation analyses.

The above comparison demonstrates that the potential determination part of the computer program is functioning correctly, and shows that the absolute accuracy of the potentials in the main focussing region is better than 3%. The relative accuracy of the potential values, one to the other, is limited only by computer word length, and would be better than 1 part in 10^5. The same relative accuracies would hold good for the derivatives of the potential, since these are derived from analytical expressions.

2.8 Range of Validity of iteration process

As demonstrated by the results shown in figure 2.7 the iteration process is valid for geometries such as that employed in the MS902 source, where the ratio between the width of the aperture of a given electrode and the distance between this electrode and the adjacent electrode, is as great as 4 to 1. Larger asymmetry ratios have been tried with success and figures 2.14 (a) and 2.14 (b) show two such geometries, embodying 20:1 and 50:1 asymmetry ratios respectively, which are soluble with the new iterative scheme.

Other geometries which might be used, are those where there is a large asymmetry ratio between every aperture width and every electrode separation. This is a more stringent test of the iteration procedure and overall asymmetries of up to about 5:1 may be considered. Figures 2.14 (c) and 2.14 (d) show the two 5:1 asymmetry cases, both of which compute satisfactorily. Larger overall asymmetry ratios (10 to 1 for example) will fail for oneof two reasons. For cases where the width of each aperture is much narrower than each electrode separation, the values of a^2 to j^2 may range from 1 to 10^{-35} respectively. This value for j^2 is beyond the range of the computer and the calculation fails. For cases where each aperture is much wider than each electrode separation, the iteration proceeds slowly and many more than fifty iterations are required to obtain a solution with the desired accuracy.

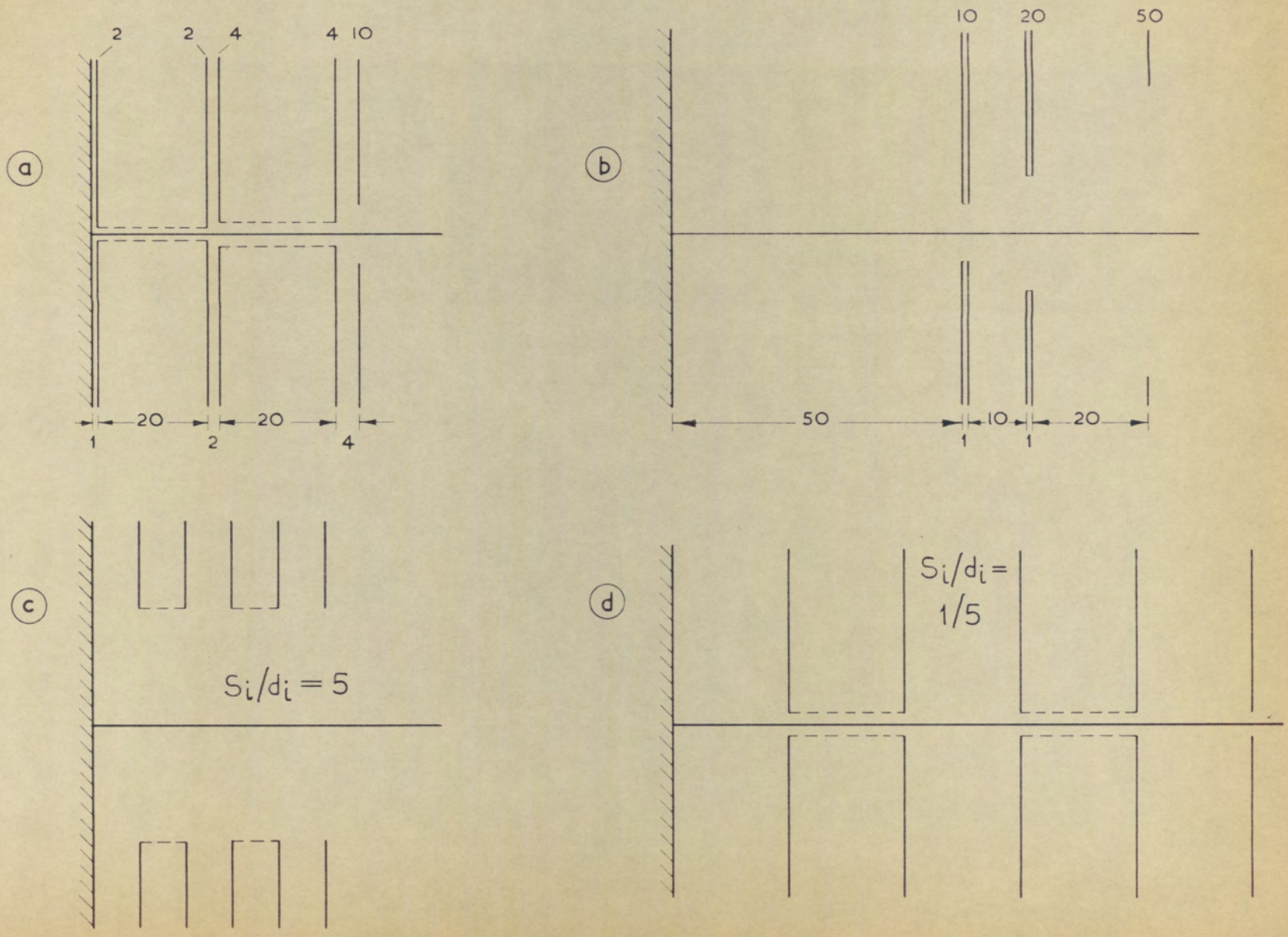

FIGURE 2.14. GEOMETRY EXTREMES FOR WHICH THE ITERATION IS APPLICABLE.

The iteration procedure is, therefore, applicable to geometries of widely differing symmetries, including those commonly used in practical mass spectrometer ion sources.

2.9 Summary and Conclusions

Axial potential distributions in electrostatic extraction lenses, computed by a conformal transformation, are shown to be obtained quickly and accurately. The constants of transformation of the set of ten non-linear simultaneous equations, for a system comprised of five planes, each with a slit-aperture, and an apertureless plane, are derived by using a new iterative procedure. For the mathematical analysis a thick electrode is replaced by two thin electrodes, but no account is taken of the uniform potential boundary joining the ends of the two bounding planes. However, comparison with results obtained by numerical relaxation and resistor network analysis, shows that the absolute accuracy of the potentials in the main focussing region is better than 3%, while the relative accuracy of the potential values, one to another, is better than 1 part in 10^5. The iterative process is valid for slit systems with gap-to-separation ratios of between 1:5 and 5:1, which is quite adequate for practical slit systems.

3 - CALCULATION OF THE PARAXIAL FOCAL PROPERTIES

The previous section has described a relatively quick way to calculate the potential distribution generated by a slit-aperture electrostatic lens system of the required geometry, and having the required electrode voltage configuration. This section details the ray-tracing procedure used, together with the way in which the various first order paraxial focal properties of an ion source may be derived from two characteristic trajectories plotted through the lens.

3.1 Introduction

The first published theoretical study concerning the order of magnitude of the focal properties and aberrations of electrostatic lenses used in ion sources was by Bertein (1950, a,b,c), while Vauthier (1950 a,b, 1955 a,b), has studied these properties in more detail. Potential distributions were obtained using the approximate formula of Straschkewitch (1940), and trajectories plotted through the lens using Gans' (1937) method; for a typical trajectory thirty steps were required in the calculation. Effects upon trajectory paths of different voltages on the electrodes, and finite electron beam width, were considered, together with an estimation of source efficiency. The effect of a non-zero repeller field was not considered in detail, and no explanation was given for the characteristic changes observed in collected ion current when the repeller voltage is varied.

Detailed theoretical investigation of the focusing properties of mass spectrometer ion sources was undertaken at the University of British Columbia. Initially, Allard and Russell (1963) considered the case of a single electrode, in which there was a slit aperture, and gaves rules for the quick construction of equipotentials in the system. An iterative procedure was developed to solve the equations giving the exact potential at any point. Later Naidu and Westphal (1966) investigated the properties of the repeller field in a mass spectrometer ion source. It was assumed however, that the width of each aperture was much smaller than the separation of the electrodes. Potentials were derived using conformal transformation, and the ray equation solved using the Runge-Kutta method of order four. Their calculations showed very well the effect of the repeller field on the ion withdrawal space, but the slit system considered was so unlike a practical slit configuration that the results obtained are of little use to the source designer.

In these theoretical analyses of simple extraction systems no author determines source efficiency, so that for example, one source design may be compared with another. Therefore in the following sections, it is shown in detail how source efficiency may be derived from the properties of the paraxial ray equation. Before this can be developed it is relevant to consider the ray-tracing method used.

3.2 Ray Tracing Recurrence Relations

The motion of an ion in a planar-symmetrical electrostatic field is specified by the equations of motion along two mutually perpendicular axes, x and y. These equations may be written in the form:-

$$\left.\begin{aligned} m\frac{d^2y}{dt^2} &= -eE_y \\ \text{and}\quad m\frac{d^2x}{dt^2} &= -eE_x \end{aligned}\right\} \qquad \ldots\ldots \quad (3.1)$$

where e and m are respectively the charge and mass of the ion; E_x ($= \partial V/\partial x$) and E_y ($= \partial V/\partial y$) are the components of electrostatic field acting on the ion in the x and y directions respectively; and t is time. The electrostatic fields may be derived from the potential distribution in the region, which in turn is derived from Laplace's equation. From the solution of equations (3.1), it is possible to determine the (x, y) position of the ion at any given instant of time, t, and thence to determine the ion trajectory in the potential system. In practice, values of potential are usually tabulated at a finite number of points along the symmetry axis of the system, which therefore requires the ray-tracing to be carried out by a step-by-step procedure. A number of such ray-tracing methods have been proposed and these may be divided into two groups.

The first group use equations (3.1) as a basis for the ray trace. A set of recurrence relations is derived by using Taylor series expansions of x and y in ascending powers of the time interval, Δt (Maloff and Epstein, 1938 p86; Reinders, Zilverschoon and Kistemaker, 1952; Vine, 1959; Hechtel 1962). To a second order of approximation these may be written:-

$$\left.\begin{aligned} x_{n+1} &= x_n + \dot{x}_n \Delta t + (1/2)\ddot{x}_n \Delta t^2 \quad ; \quad y_{n+1} = y_n + \dot{y}_n \Delta t + (1/2)\ddot{y}_n \Delta t^2 \\ \dot{x}_{n+1} &= \dot{x}_n + \ddot{x}_n \Delta t \quad ; \quad \dot{y}_{n+1} = \dot{y}_n + \ddot{y}_n \Delta t \\ \ddot{x}_{n+1} &= -(e/m)(\partial V/\partial x)_n \quad ; \quad \ddot{y}_{n+1} = -(e/m)(\partial V/\partial y)_n \end{aligned}\right\} \quad (3.2)$$

where the superscripted dots indicate successive differentiations of x and y with respect to time, t.

The equations give the values of x and y, and their respective derivatives, at the (n + 1)th. tabular point, given their values at the n th. tabular point; Δt is the time separation of these two tabular points. The terms $(\partial V/\partial x)_n$ and $(\partial V/\partial y)_n$ are the x and y components of the electrostatic field at the n th. tabular point. The ray-tracing procedure is to set the second derivatives (acceleration) equal to zero, and to specify the initial velocities, $\dot{x}$ and $\dot{y}$, and initial positions, x and y. The new values of x, y, $\dot{x}$, $\dot{y}$, $\ddot{x}$, $\ddot{y}$ at the next point, Δt away, are then calculated from equation (3.2) These are then used to calculate the values at the next point and the process is repeated up to the required point along the axis.

This method, commonly called the time-of-flight method, is of particular use when the optic axis is not known, since the spatial parameters x and y are referred to a fixed set of rectilinear co-ordinates, rather than to the optic axis.

An alternative approach is to start from the general ray equation given as follows:

$$\frac{2V\,x''}{1+(x')^2} + \frac{\partial V}{\partial y} \cdot x' - \frac{\partial V}{\partial x} = 0 \qquad \ldots\ldots \qquad (3.3)$$

This is derived from equations (3.1) by eliminating the time variable. (See Appendix III, section 1, for a derivation). In this equation, V is the volt energy of the ion and the primes denote successive differentiations of x with respect to y, that is:-

$$x' = dx/dy \quad ; \quad x'' = d^2x/dy^2$$

Many iterative procedures have been given to solve equation (3.3), or approximations to it (See for example, Zworykin et al, 1945, p.400; Maloff and Epstein, 1938, p.80; Grivet, 1966; p. 74).

A widely used method is that due to Liebmann (1949), which has been given in form relevant to electrostatic slit lenses by Archard (1954). The iteration is carried out with the following pair of recurrence relations, which are applied in exactly the same way as the previous method:

$$\left.\begin{aligned} x_{n+1} &= Q_1 x_n + Q_2 x_n' \\ x_{n+1}' &= Q_3 x_n' + Q_4 x_n \end{aligned}\right\} \qquad (3.4)$$

where

$$Q_1 = 1 - (1/4)(V''/V)\Delta y^2 + (1/24)(V'V''/V^2)\Delta y^3$$

$$Q_2 = \Delta y - (1/4)(V'/V)\Delta y^2 + (1/24)[(V'/V)^2 - 2(V''/V)]\Delta y^3$$

$$Q_3 = 1 - (1/2)(V'/V)\Delta y + (1/8)[(V'/V)^2 - 2(V''/V)]\Delta y^2$$

$$Q_4 = -(1/2)(V''/V)\Delta y + (1/8)[V'V''/V^2]\Delta y^2$$

These are derived (see Appendix III, section 2) by writing down the Taylor Series for x and x' in ascending powers of Δy, where Δy is the distance between the n th. and (n + 1) th. step along the y axis. The potential and its derivatives are the arithmetic mean of their respective values at the n th. and (n + 1) th. points.

In the previous sections, it has been shown that it is possible to generate the axial potential distribution, V, and its derivatives $V' = \partial V/\partial y$ and $V'' = \partial^2 V/\partial y^2$ in the form of a table, in which V, V' and V" are tabulated at closely spaced points along the y symmetry axis

of the lens system. To avoid the extra work of interpolation, it is convenient if the tabular points for the ray trace coincide with the tabular points for the potential distribution and its derivatives. It can be seen from equation (3.4) that this is easily arranged for the spatial recurrence relations, requiring adjustment of Δy only. However, this is not so for the time-of-flight recurrence relations (3.2), where the spatial tabular points are defined successively, by way of the time interval, as the iteration proceeds. Further, for different starting conditions (initial energy, for example), the spatial recurrence relations require the same set of tabular points, whereas the time-of-flight method requires potentials at a completely new set of points.

It is for these reasons that the Liebmann/Archard method has been chosen for the present investigation of electrostatic lens systems.

To enable the path of a trajectory to be plotted manually, the computer output for the source design program includes the first three pairs of trajectories computed. A 'pair' consists of a paraxial ray and an off-axis ray (see section 3.3). Figure 3.1 shows such a print-out. As before, the result at every fifth step is given. In the extreme left-hand margin is Y, the distance along the y axis, and this is followed, from left to right, by the off-axis distance of each pair of rays, each in units of y. The caption to the sheet gives the initial energy and

E(INT)- -0.040
Y(OBJ)- -1.50 , -1.60 , -1.70

Y	1ST.PAIR X(P)	1ST.PAIR X(OA)	2ND.PAIR X(P)	2ND.PAIR X(OA)	3RD.PAIR X(P)	3RD.PAIR X(OA)
-3.112	0.000	0.000	0.000	0.000	ION REFLECTED	
-3.060	0.000	0.000	0.000	0.000		
-2.979	0.000	0.000	0.000	0.000		
-2.852	0.000	0.000	0.000	0.000		
-2.656	0.000	0.000	0.000	0.000		
-2.366	0.000	0.000	0.000	0.000		
-1.971	0.000	0.000	0.000	0.000		
-1.504	0.000	0.600	0.108	0.545		
-1.047	0.188	-0.088	0.072	-0.425		
-0.670	0.058	-0.343	-0.085	-0.331		
-0.386	-0.024	-0.298	-0.112	-0.139		
-0.171	-0.058	-0.196	-0.095	-0.006		
0.008	-0.068	-0.098	-0.068	0.075		
0.178	-0.065	-0.016	-0.039	0.121		
0.354	-0.057	0.051	-0.012	0.145		
0.531	-0.044	0.098	0.010	0.150		
0.702	-0.030	0.123	0.026	0.138		
0.870	-0.016	0.131	0.036	0.115		
1.052	-0.003	0.129	0.042	0.087		
1.264	0.009	0.121	0.045	0.058		
1.510	0.021	0.111	0.048	0.028		
1.779	0.031	0.100	0.050	-0.000		
2.061	0.040	0.089	0.050	-0.026		
2.355	0.047	0.075	0.050	-0.048		
2.663	0.052	0.060	0.047	-0.066		
3.007	0.054	0.043	0.042	-0.081		
3.421	0.055	0.025	0.036	-0.094		
3.928	0.055	0.005	0.030	-0.106		
4.515	0.055	-0.015	0.023	-0.120		
5.142	0.056	-0.034	0.018	-0.134		
5.814	0.059	-0.054	0.012	-0.152		
6.608	0.064	-0.077	0.007	-0.176		
7.672	0.071	-0.110	-0.000	-0.212		
9.229	0.084	-0.159	-0.011	-0.267		
11.614	0.104	-0.236	-0.026	-0.355		
15.339	0.135	-0.357	-0.050	-0.494		
21.211	0.186	-0.548	-0.089	-0.715		
30.495	0.266	-0.852	-0.149	-1.066		
45.195	0.394	-1.334	-0.245	-1.622		
68.486	0.596	-2.098	-0.398	-2.505		

FIGURE 3.1 SPECIMEN PRINT-OUT OF TRAJECTORY PAIRS FOR THE SIMULATED MS902 e.b. ION SOURCE

starting position for each pair (Note: although three pairs of trajectories are printed out, it is possible to compute up to seven pairs of trajectories. In the case shown, three pairs are computed).

3.3 Lagrange-Helmholtz Relation

The Liebmann/Archard ray tracing equations detailed above are true for a paraxial approximation, in which rays are assumed to be close to the axis. The computed rays will therefore satisfy an approximate form of the general ray equation, known as the 'paraxial ray equation'. In this section it is shown how a number of properties of the paraxial system may be derived from the paraxial equation, while section 3.4 uses the formulae derived as a means for determining an approximate value for the source efficiency.

To derive the paraxial ray equation a Taylor series expansion of $V(x,y)$ is used, that is

$$V(x,y) = V(y) - \frac{x^2}{2!} V'' + O(x^4) \qquad \ldots\ldots \quad (3.5)$$

Hence, to a first approximation, the following expressions are true

$$V(x,y) = V(y)$$

$$\partial V(x,y)/\partial x = - x.V''(y)$$

$$\partial V(x,y)/\partial y = + V'(y)$$

Also for rays close to the axis the ray slope x' will be much smaller than unity.

Substituting these conditions in equation (3.3) gives the paraxial form

$$2Vx'' + V'x' + V''x = o \qquad \ldots\ldots \qquad (3.6)$$

where the primes denote successive differentiations with respect to y.

Equation (3.6) is a linear differential equation, and as such has a general solution comprised of two linearly-independent solutions. Therefore, it follows that to determine the complete first order focusing properties of an electrostatic slit lens system, it is necessary and sufficient to calculate two linearly independent trajectories through the system. Every other trajectory is a linear combination of these two. These characteristic rays may be compared with the principal rays used in the investigation of light optical systems.

Following the method of Maloff and Epstein (1938, p.90), it is possible to determine a relationship between the two characteristic trajectories, and hence to the relationship between one of the characteristic trajectories and another trajectory.

Dividing each term of equation (3.6) by $2\sqrt{V}$ and re-arranging, gives the equation

$$\frac{d}{dy}\left(\sqrt{V}.x'\right) + \frac{V''}{2\sqrt{V}}.x = 0 \qquad \ldots\ldots \qquad (3.7)$$

If x_1 (y) and x_2 (y) are two independent solutions of equation (3.6) representing the trajectories of two ions, then the relevent forms of equation (3.7) are:-

$$\frac{d}{dy}\left(\sqrt{V}.x'_1\right) + \frac{V''}{2\sqrt{V}}.x_1 = o \qquad \ldots\ldots \qquad (3.8)$$

$$\frac{d}{dy}\left(\sqrt{V}.x'_2\right) + \frac{V''}{2\sqrt{V}}.x_2 = o \qquad \ldots\ldots \qquad (3.9)$$

Multiplying equation (3.8) by x_2 (y), and subtracting equation (3.9) multiplied by x_1 (y), and noting that $x_1' \cdot d/dy\ (x_2) = x_2' \cdot d/dy\ (x_1)$, leads to the equation $\frac{d}{dy}\left[\sqrt{V} \cdot (x_2x_1' - x_1x_2')\right] = 0$

Integrating between the limits a and b gives the equation:

$$\sqrt{V(b)}\left[x_2(b)x_1'(b) - x_1(b)x_2'(b)\right] = \sqrt{V(a)}\left[x_2(a)x_1'(a) - x_1(a)x_2'(a)\right] \qquad \ldots\ldots (3.10)$$

Equation (3.10) is a relationship expressing a correspondence between the values of ion volt-energy, trajectory slope and off-axis distance of two trajectories (1 and 2) at a point 'a' in the system, to the values of these variables at another point 'b'.

In the following work, two particular characteristic trajectories have been used. These are termed the 'paraxial ray' and 'off-axis ray', though it should be noted that they are both paraxial rays in the sense that they both obey the paraxial ray equation (3.6). The 'paraxial ray' is defined to be that ray which starts on, but at a non-zero angle α_1, to the axis in the plane y = a (the object plane). The 'off-axis ray' is defined to be that ray which starts off parallel to the axis from the off-axis point x = h($\neq$0) in the object plane at y = a. Figure 3.2 shows the pair of characteristic trajectories for the MS902 electron bombardment source under the specified conditions, and which are plotted from the values tabulated under the '2ND PAIR' column in Figure 3.1. The image plane is at the point where the paraxial ray crosses the axis. In general there may be more than one image plane, there being one image plane to each cross-over of the paraxial ray. The image size at each of such points is the distance of the off-axis ray from the axis.

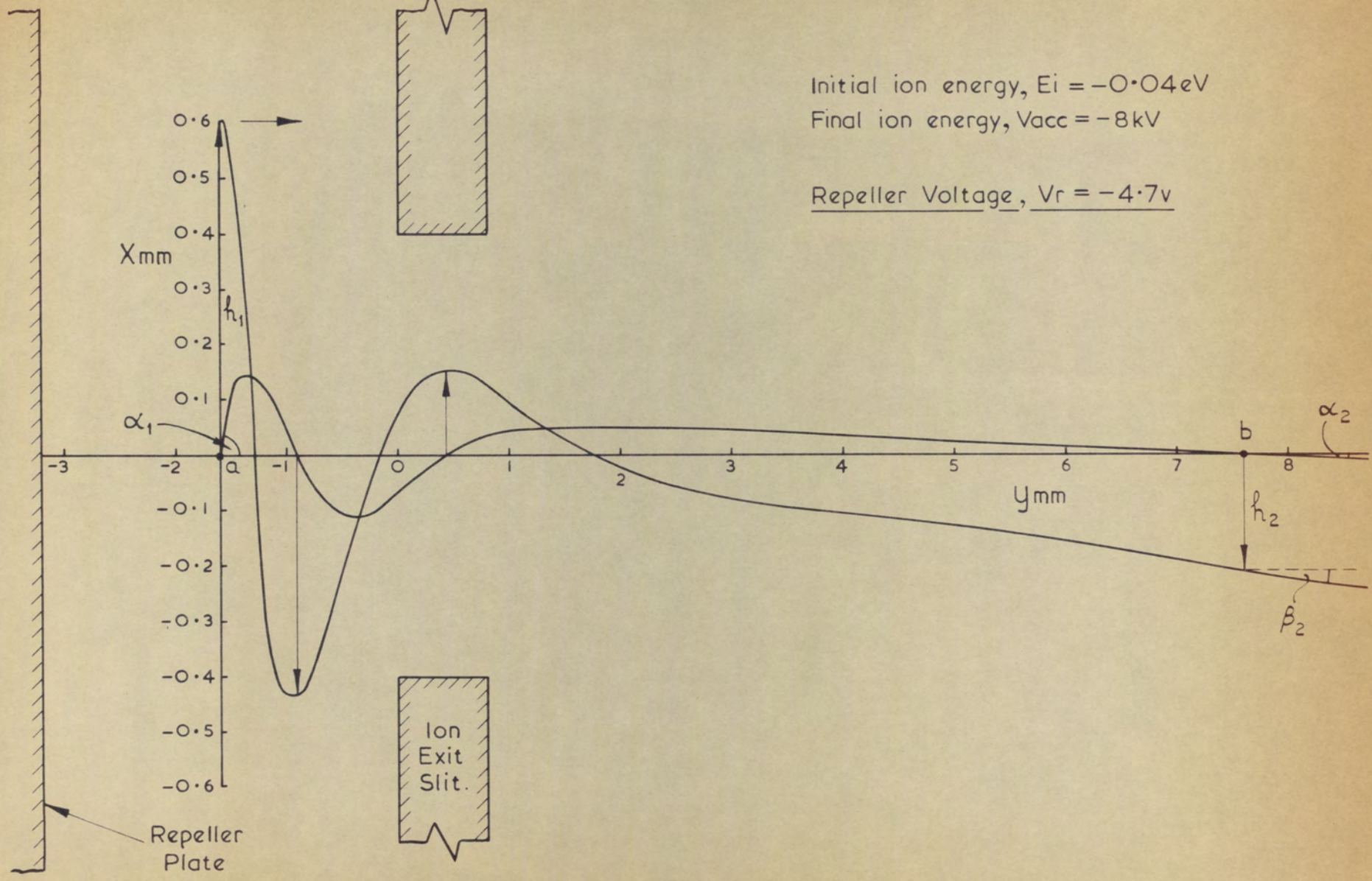

FIGURE 3.2. EXAMPLE OF TRAJECTORY PAIRS AND IMAGE FORMATION FOR THE MS902 E.B. ION SOURCE.

Suppose the plane at $y = b$ is an image plane at which the slope of the paraxial ray is α_2 and the off-axis distance and slope of the off-axis ray are h_2 and β_2 respectively (see figure 3.2); then for these two rays the boundary conditions relevant to equation (3.10) are

off-axis trajectory	paraxial trajectory
$x_1(a) = h_1$	$x_2(a) = 0$
$x_1'(a) = 0$	$x_2'(a) = \tan \alpha_1$
$x_1(b) = h_2$	$x_2(b) = 0$
$x_1'(b) = \tan \beta_2$	$x_2'(b) = \tan \alpha_2$

with which equation (3.10) reduces to

$$\sqrt{V(b)}\ h_2\ \tan\alpha_2 = \sqrt{V(a)}\ h_1\ \tan\alpha_1 \qquad \ldots\ldots \qquad (3.11)$$

This is one form of the Lagrange - Helmholtz relation for electron and ion optics. Equation 3.11 may be re-written in the form

$$\epsilon M = (E_i/V_{acc})^{1/2} \qquad \ldots\ldots \qquad (3.12)$$

where $\epsilon (= \tan\alpha_2/\tan\alpha_1)$ is the angular magnification; $M (= h_2/h_1)$ the linear magnification; E_i, the initial ion energy and V_{acc}, the accelerating voltage or final energy of the ion.

Digression

Although the Lagrange-Helmoltz formula appears in several forms, and under several different names in the literature, it is in each case an expression of the 'Law of invariance of Brightness' which is valid for electro-magnetic radiations and charged particle systems.

According to historical notes written by Lord Rayleigh (1886), the law was first enunciated for light optics by Smith (1738), but later re-discovered by Lagrange (1803) and Helmholtz (1874). It is for this reason that the law is attributed mainly to the latter two authors, although Smith was the originator. The validity of the law to thermodynamic problems was demonstrated by Kirchhoff (1860) and Clausius (1864), whose names also appear in connection with this law.

The mathematical form of the law apparently varies according to the method used for its derivation. A number of electron optics textbooks refer to the treatise of Maloff and Epstein (1938, p.91), in which the tangent law is directly derived from the paraxial ray equation, a Gaussian approximation of the true equation. Thus Jacob (1951, p.47), refers to the 'Lagrange Law'; Grivet (1965, p.67) to the 'Lagrange-Helmholtz Relation' and Hanszen and Lauer (Septier, 1967, p.257) to the 'Helmholtz-Lagrange formula'. The validity of the tangent law in a Gaussian approximation is further shown by the light-optical proof given in Born and Wolf (1959). The tangent law derived is called the 'Smith-Helmholtz formula'.

However Zworykin et al. (1945, p.354) give the derivation of the theorem, originated by Clausius (1864), in which consideration of radiating black bodies gives rise to a sine law. No approximations or assumptions are made, other than that the system obeys the Lambert cosine law and Snell's law. An analogous derivation for electron-optical systems is given by Pierce (1949, p.122), in which the result is termed the 'Abbe sine law'.

It is concluded therefore that, subject to the correctness of Lambert's cosine law and Snell's law for electron and ion optical systems, the sine law is the exact mathematical form of the 'Law of invariance of Brightness'. Although the tangent law is an approximation of it, it should be regarded as the correct form to use when Gaussian optics are considered, as it can be derived from the paraxial ray equation without further approximation. For this reason the tangent law has been used in the present study.

3.4 Calculation of Source Efficiency

In an ion source, it is required to extract as many ions as possible within the wedge defined by the α-slit of the mass spectrometer. Qualitatively, best efficiency will be obtained when both ϵ and M, the angular and linear demagnifications are each as small as possible, and from equation (3.12) it is seen that this may be fulfilled, for rays very close to the axis, when the ratio of the final energy to the

initial energy is as large as possible. For a mass spectrometer however, the source of ions is an extended source, and although equation (3.12) will be valid for those ions starting out near the axis, it will not be true for the majority of ions formed. Therefore, it is to be expected that the efficiency of the ion source will depend on factors other than initial and final energies. Experimentally it is found that such a factor is the repeller voltage, a change of which will alter the extraction field at the region of ion production. For electron guns, a similar relationship exists between brightness and bias voltage, as has been shown experimentally by Haine and Einstein (1952), Haine (1961).

It is important to note that the efficiency is very dependent on the initial energy of the ion, and it is certainly not valid to ignore it in comparison with the final energy, as has been done by Naidu and Westphal (1966). It is because of the non-inclusion of initial energy, that their star-shaped extraction regions extend to infinity in an off-axis direction.

In an ion source, each molecule undergoes many collisions with the source chamber walls before it is ionized. The ions that are produced will take on the energy and direction of the gas molecules, and can therefore be moving in any direction, with a distribution of energies corresponding to the Maxwell-Boltzmann distribution.

Therefore, the mathematical problem is to find the range of initial directions δ_+ to δ_-, in which an ion may start off so that it emerges from the ion source within the wedge $+\alpha$ to $-\alpha$, defined by the α-slit. Delta may be found by a second application of equation (3.10). The off-axis trajectory starting-off from the object plane, at height h_1 from the axis, and at an angle δ to the y-axis, is compared with the computed off-axis trajectory starting off from the same point, but parallel to the axis. Thus, the boundary conditions are:-

Reference off-axis trajectory	Unknown trajectory
$x_1(a) = h_1$	$x_2(a) = h_1$
$x_1'(a) = 0$	$x_2'(a) = \tan\delta$
$x_1(b) = h_2$	$x_2(b) = h_2$
$x_1'(b) = \tan\beta_2$	$x_2'(b) = \tan\alpha$

The boundary conditions for the reference off-axis trajectory are the same as those given in section 3.3. Since both off-axis trajectories start at the same point in the object plane (a), they also meet at the same off-axis point h_2, in the apparent image plane (b). Substituting the above conditions into equation (3.10), gives the following relationship:

$$\sqrt{V(b)} \cdot (h_2 \cdot \tan\beta_2 - h_2 \cdot \tan\alpha) = \sqrt{V(a)} \cdot (-h_1 \cdot \tan\delta)$$

$$\therefore \quad \delta = -\tan^{-1}\frac{1}{\epsilon}(\tan\beta_2 - \tan\alpha) \qquad \ldots\ldots \qquad (3.13)$$

where $-\pi/2 \leq \delta \leq \pi/2$

where ϵ is defined by equation (3.12). δ is the initial angle required for the ray to emerge at an angle $+\alpha$ to the axis. This will be termed δ_+; δ_-, defined in the same way, but for an emergent angle of $-\alpha$, is given by equation (3.13) with $(-\alpha)$ substituted for α. It is therefore possible to define the 'ion withdrawal wedge', $|\delta_+ - \delta_-|$ such that ions starting off within this angle will emerge from the source system within the angle $+\alpha$ to $-\alpha$.

The source efficiency will also be a function of the apparent linear demagnification M; if M is increased, fewer ions will pass through the source resolution-slit (of gap width up to 0.2 mm). An overall measure of the extraction efficiency can therefore be expressed as:-

$$\text{Efficiency} = \frac{|\delta_+ - \delta_-|}{2.\alpha.M} \qquad \ldots\ldots \qquad (3.14)$$

DIGRESSION

It is of interest to compare equation (3.14) with the equation measuring the efficiency of a point source

$$1/\epsilon M$$

Using the forms of equation (3.13) for δ_+ and δ_- gives

$$\tan \delta_+ - \tan \delta_- = \frac{2}{\epsilon} \tan\alpha$$

$$\therefore \quad \frac{1}{\epsilon M} = \frac{\tan \delta_+ - \tan \delta_-}{2M \tan\alpha} \qquad \ldots\ldots \qquad (3.15)$$

Now since α is small, $\tan\alpha$ approximately equals α, which leads to a simple expression for the ratio of the off-axis efficiency, equation (3.14), to the point-source efficiency, equation (3.15). Thus:-

$$\frac{\text{Off-axis efficiency}}{\text{Point source efficiency}} = \frac{|\delta_+ - \delta_-|}{\tan\delta_+ - \tan\delta_-} \qquad \ldots\ldots \qquad (3.16)$$

The point source efficiency is a constant, subject to constant initial and final energies (Lagrange - Helmholtz Law), and it is easy to show that $|\delta_+ - \delta_-|$ has a maximum when $\delta_+ = -\delta_-$ (see Appendix III, section 3). The implication of this will be considered in section 4.1.4.

3.5 Integration Over the Object Plane

Equation (3.13) is applicable only for rays which leave a point in the object plane, distance h_1 from the y-axis. For other points in this plane it is necessary to scale the term $\tan\beta_2$ (the emergent slope of the reference off-axis ray), which appears in equation (3.13). However, since the Liebmann-Archard ray tracing equations (3.4) are linear in x and x', linear scaling of $\tan\beta_2$ is all that is required. For example, for an off-axis starting point of $h_1/2$, the angle δ_+ is given by the equation

$$\delta_+ = -\tan^{-1}\left[\frac{1}{\epsilon}\ (0.5\ \tan\beta_2\ - \tan\alpha)\right]$$

with the source efficiency defined as before.

To determine the overall source efficiency it has been assumed that ions are produced with equal probability at all points across the breadth (x) of the electron beam. For the integration, the source efficiency is determined at forty, equally spaced points across the x-breadth of the electron beam, and the overall efficiency set equal to the arithmetic mean of the values thus obtained.

To account for finite width of the electron beam in the y-direction, it is necessary to compute additional rays. The computer program has been written so that this is easily achieved, but details of this are deferred until section 4.

3.6 Accuracy of Computations

The Lagrange-Helmholtz relationship provides the potential of a rigorous check of a large part of the program. The computed linear and angular demagnifications will obey equation (3.11), provided that the derivatives of the potential, and the two characteristic rays have been computed correctly. To check that the computations are correct, it is necessary and sufficient to consider the initial and final properties of the two rays. In practice, the method is to compare $\sqrt{V_{acc}/E_i}$ with $(h_1/h_2)\ \tan\alpha_1/\tan\alpha_2$. Any small deviation will give an estimate of the error incurred in the ray tracing operation. For every result

calculated, the deviation from equation (3.6) is found and printed out. In this way it is possible to be confident of any results obtained. It is important to note however, that it will not check the potential distribution itself, and there is therefore a small gap in the internal checking system after the determination of the transformation constants, but before the determination of the derivatives. The validity of the computed potentials has already been discussed in section 2.7.

To improve the accuracy of the ray-trace to within a few per cent, it has been found necessary to incorporate a fine interval size at the beginning of the trajectory. The need for this arises because the initial energy of the ion (~ -0.04eV) is similar in magnitude to the change in energy from one tabular point to the next. Subdividing each of the first six intervals into twenty equally spaced intervals has been found adequate. Intermediate values of V, V' and V" were found by linear interpolation.

3.7 Validity of the Paraxial Approximation

To determine the errors incurred by using the paraxial ray equation for computing off-axis rays, use has been made of a modified version of the computer program written by Hamza (1966). This calculates the potentials over the whole region by using numerical relaxation, and ray traces by direct use of the equations of motion (3.1). The only errors in the results from this program will be due to the finite size of the mesh.

A comparison of the trajectories obtained by each method for the MS902 electron bombardment source is shown in figures 3.3 (a) and (b). To match the potential distributions obtained by the two methods, an ion exit slit gap of 0.5 mm was used for the conformal transformation computations. For each method, the paraxial ray starts off at an angle of +0.1 radians to the axis, while the off-axis ray is fired at an angle of -0.1 radians to the axis. Initial ion energy is -0.16eV. Figure 3.3 (c) shows the demagnifications $|M|$, of the real images plotted as a function of the off-axis starting point X(O.A.), of the off-axis trajectory. Since the paraxial ray equation is linear in r, the appropriate value of $|M|$ is constant with increasing X(O.A.) (broken curves). However, when the general ray equation is used (full curves), the object demagnification increases for increasing object size, but is still only 15% larger than that predicted from paraxial theory, at the point where the object height is the same as the ion exit slit width. This is a relatively small error, and therefore the conclusions obtained by a paraxial analysis can be accepted with confidence. For an object size just under twice the ion exit slit width, the paraxial theory error is 40%, and for any further increase, the demagnification increases rapidly until finally at X(O.A.) = 0.9 mm ions strike the ion exit slit.

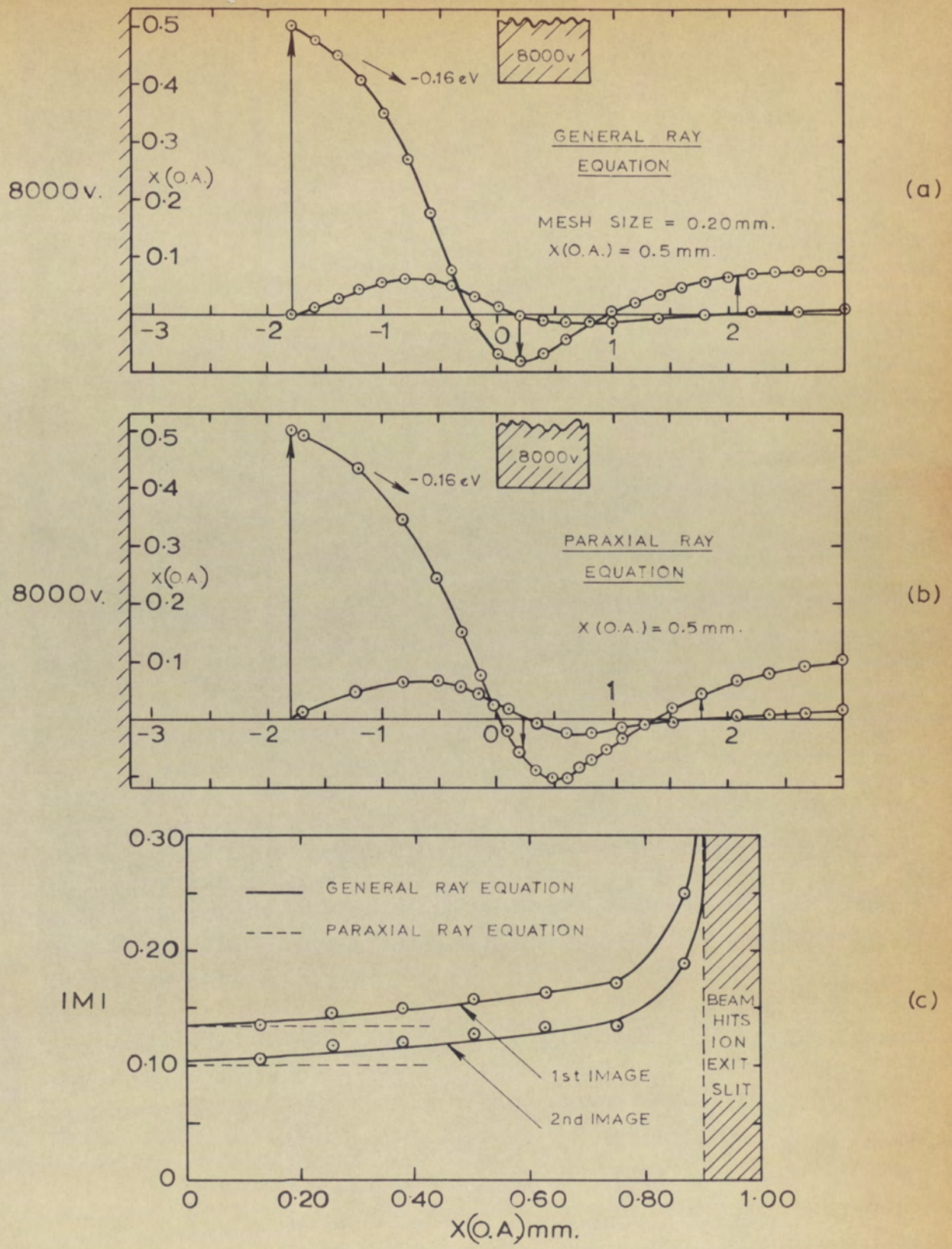

FIGURE 3.3 COMPARISON OF GENERAL AND PARAXIAL RAY EQUATIONS APPLIED TO THE MS902 e.b. ION SOURCE.

These conclusions are supported by those of Naidu and Westphal (1966) who carried out a similar analysis for a single slit-aperture. From their results they were able to define a 'paraxial region' (see figure 3.4) within which the paraxial theory is not 'grossly invalid'. However, they do not specify the accuracy of the results obtained with this region.

3.8 Ion Residence-time in Source

A factor of interest to the chemist studying metastable transitions* is the time taken for an ion to travel from the point of ion production to the source resolution-slit, at which it will have reached its final energy. Since this transit time varies with the extraction field, its value is calculated for each paraxial trajectory computed.

The method is to compute the time Δt, taken by the ion to travel over each incremental step of the x-axis, Δx, and then to sum the results between the starting point and the source slit. This time interval is given by

$$\Delta t = \frac{\Delta x}{v} \sqrt{1 + r'^2}$$

---

*Metastable transitions are those caused by ions decaying into fragment parts after leaving the region of ion production. The characteristic spectra obtained give additional chemical information for the analysis of the compound.

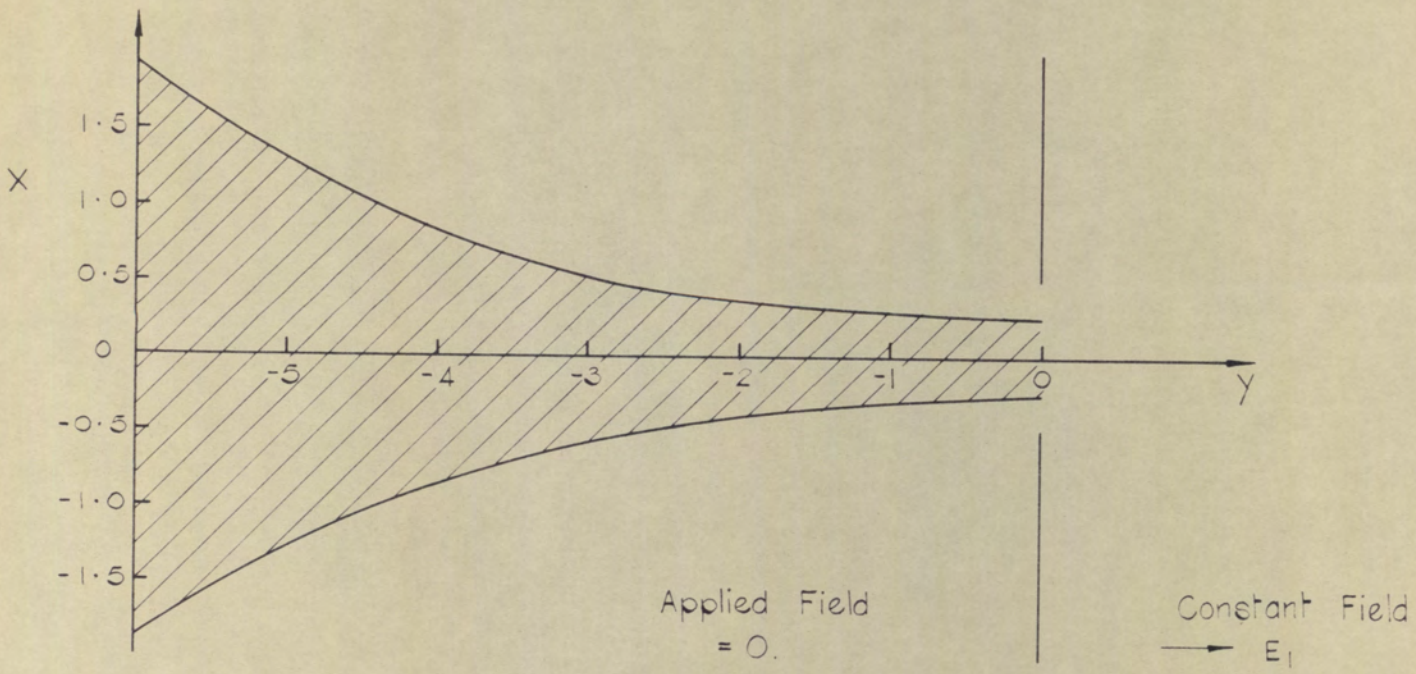

FIG. 3.4. THE PARAXIAL REGION [AFTER NAIDU AND WESTPHAL, 1966 a].

where r' is the slope of the trajectory over interval, Δx. The ion velocity v, is determined from the volt energy V, by way of the energy equation.

Therefore, for an ion of 1 a.m.u., the time interval Δt is given by:-

$$\Delta t = 0.072009 \cdot \Delta x \sqrt{\frac{1 + r'^2}{-V}} \ \mu s \qquad \ldots\ldots \qquad (3.17)$$

where Δx is in mm. and V is in volts. The ion residence-times printed in the computer output are those for an ion of mass 1 a.m.u. To obtain the corresponding transit time for an ion of mass M, the computer result is multiplied by $\sqrt{M}$.

3.9 Computer Output

Figure 3.5 shows a typical output sheet obtained from the focal property, check and residence-time part of the program. Reading from left to right, the first two columns give respectively the potential difference V(REP), between the repeller plate and the ion exit slit, and V(FOC)/V(ACC), the ratio of the potential difference between the centre slit (focusing plates) and the final accelerating slit, to the overall accelerating voltage.

FIGURE 3.5 SPECIMEN OUTPUT FOR THE FOCAL PROPERTY, CHECK AND TRANSIT TIME

TABLE FOR THE MS902 e.b. ION SOURCE

V(REP)	V(FOC) V(ACC)	E(INT)	Y(OBJ)	Y (1,3)	M	Y (2,4)	M		TIME (US)
-4.700	0.930	-0.040	-1.50	-0.482	-0.547	1.105	0.212		0.33
		-0.040	-1.60	-0.914	-0.728	0.445	0.250	2	0.47
				7.615	-0.350				
		-0.040	-1.70	ION REFLECTED					
-3.000	0.930	-0.040	-1.50	0.024	-0.294	2.593	0.219		0.23
		-0.040	-1.60	-0.039	-0.303	2.264	0.204		0.25
		-0.040	-1.70	-0.115	-0.321	1.967	0.188		0.28
-1.300	0.930	-0.040	-1.50	0.223	-0.233	4.254	0.201		0.19
		-0.040	-1.60	0.201	-0.224	4.037	0.190		0.20
		-0.040	-1.70	0.179	-0.217	3.842	0.181		0.22
0.400	0.930	-0.040	-1.50	0.353	-0.210	5.929	0.222		0.17
		-0.040	-1.60	0.343	-0.198	5.792	0.205		0.17
		-0.040	-1.70	0.336	-0.188	5.687	0.191		0.19
2.100	0.930	-0.040	-1.50	0.453	-0.197	8.159	0.300		0.15
		-0.040	-1.60	0.450	-0.185	8.088	0.279		0.16
		-0.040	-1.70	0.449	-0.174	8.062	0.261		0.17
3.800	0.930	-0.040	-1.50	0.537	-0.189	12.267	0.480		0.14
		-0.040	-1.60	0.538	-0.177	12.388	0.455		0.15
		-0.040	-1.70	0.540	-0.166	12.615	0.437		0.15
5.500	0.930	-0.040	-1.50	0.609	-0.182	24.581	1.056		0.13
		-0.040	-1.60	0.613	-0.170	26.241	1.064		0.14
		-0.040	-1.70	0.618	-0.160	28.688	1.103		0.14
7.200	0.930	-0.040	-1.50	0.673	-0.176	-381.249	-18.300	A	0.13
		-0.040	-1.60	0.678	-0.164	-138.585	-6.315	A	0.13
		-0.040	-1.70	0.685	-0.154	-79.560	-3.460	A	0.13

The next pair of columns headed E(INT) and Y(OBJ) give the initial ion energy, in electron volts, and the position of the object plane along the y-axis, referred to the ion exit slit. All the output in the first four columns is information supplied to the computer in the form of data. The following two pairs of columns headed Y, M (1,3) and Y, M (2,4), give y-positions and magnifications of the images. The Y, M parameters for the first image occur in the first pair of columns, those for the second image in the second pair of columns, and if there is a third and perhaps a fourth image the respective parameters will appear on a new line immediately under the parameters for the first and second image. (See the entry for V(REP) = -4.7V and Y(OBJ) = -1.60 in figure 3.5). If there is only one real image, the position and magnification of the apparent image (as seen from $y = +\infty$) is given in the second pair of columns and the M value is followed by a letter 'A' (See the entries for V(REP) = 7.20V in figure 3.5).

These results are followed by a single column of numbers which give the percentage deviation of the focal properties from the Lagrange-Helmholtz law. A space indicates less than 0.5%, while an asterisk (*) indicates greater than 9.5%.

The last column, headed TIME (μS) gives the residence time in μs of an ion of mass 1 a.m.u. travelling between the object plane and the source resolution-slit.

The results are given in vertical blocks of one or up to seven lines, where each line corresponds to a different ion initial energy or to a different object plane position (option specified in data - See Appendix IV for details). Each block corresponds to a different electrode voltage or set of electrode voltages. In the output shown in figure 3.5, it is the repeller voltage which has been varied. In this way it is possible to investigate the variation of the focal properties and residence times, as a function of any of a number of parameters.

If an ion has insufficient energy to surmount any potential barrier it may come across, it will be reflected. Since there is no practical interest in ions which are reflected back to the repeller plate, the program detects such an ion and prints out the caption 'ION REFLECTED' (See entry for V(REP) = -4.7V and Y(OBJ) =-1.70 in figure 3.5).

Figure 3.6 shows a typical output in which the source efficiency is detailed under the heading 'ION WITHDRAWAL-WEDGE TABLE'. This table is a horizontal continuation of the focal property, check, and residence-time table (figure 3.5), and the results are therefore blocked in a corresponding manner.

FIGURE 3.6

SPECIMEN OUTPUT FOR THE SOURCE EFFICIENCY TABLE FOR THE MS902

e.b. ION SOURCE

ION WITHDRAWAL-WEDGE TABLE

XI(C.A.)= 0.600 ALPHA = 0.00625 I.W.W. =DELTA/2M.ALPHA

EPS.	TAN(B2)	SAMPLE AT X= 0.015	0.285	0.585	SUM TO X= 0.150	0.300	0.450	0.600
8.66, -3	-0.0328	386.7	115.4	31.8	338.3	253.4	193.8	155.3
-6.54, -3	-0.0378	358.3	58.1	14.2	287.2	192.0	139.8	109.3
ION REFLECTED								
1.70, -2	0.0092	426.7	405.1	346.6	424.7	418.7	409.1	396.8
1.79, -2	0.0028	428.9	427.0	420.8	428.8	428.2	427.3	426.1
1.81, -2	-0.0039	431.3	427.6	416.0	431.0	430.0	428.3	425.9
1.46, -2	0.0268	419.0	258.1	108.9	399.1	351.5	300.9	258.0
1.60, -2	0.0242	423.2	295.6	143.5	408.6	371.4	327.8	287.5
1.72, -2	0.0218	427.9	327.9	181.2	417.2	388.3	351.7	315.2
1.11, -2	0.0336	402.4	152.7	46.8	361.5	284.6	224.3	182.7
1.21, -2	0.0320	408.3	180.1	59.5	373.9	304.4	245.0	202.0
1.30, -2	0.0307	414.5	205.7	73.0	385.1	322.0	264.2	220.3
7.71, -3	0.0352	370.3	84.9	21.9	312.3	222.1	165.8	131.3
8.31, -3	0.0338	378.3	102.1	27.3	326.4	239.6	181.5	144.7
8.83, -3	0.0326	386.0	118.9	33.1	339.0	255.5	196.1	157.4
4.74, -3	0.0342	307.6	39.4	9.0	245.5	158.1	113.2	87.7
5.00, -3	0.0326	315.6	47.7	11.1	258.4	170.9	123.4	96.1
5.18, -3	0.0312	322.4	55.8	13.0	269.4	182.5	132.8	103.7
2.14, -3	0.0317	187.3	10.5	2.2	148.0	85.3	58.8	44.8
2.12, -3	0.0299	186.4	11.9	2.5	152.6	89.4	61.8	47.2
2.04, -3	0.0281	181.6	12.7	2.6	153.5	91.3	63.2	48.2
-1.24, -4	0.0284	13.6	0.0	0.0	11.4	5.8	3.9	2.9
-3.58, -4	0.0262	38.3	0.5	0.1	36.0	18.8	12.6	9.5
-6.50, -4	0.0242	67.8	2.0	0.4	64.3	36.0	24.4	18.4

The initial conditions are given below the heading; these are: the half-breadth (x) of the electron beam XI(O.A.), the half-angle, α radians, of the alpha-slit and the definition of the source efficiency (I.W.W.).

For the purposes of comparison, it is necessary to know the source efficiency at the source resolution-slit, rather than at the real image, the position of which varies with repeller voltage. It is for this reason that the angular magnification, ϵ, used in the source efficiency calculation, is the angular magnification of the apparent image. The values of the apparent angular magnification appear in the first column headed EPS. The second column contains the values of TAN (B2) computed for rays starting in the object plane and at the off-axis distance XI(O.A.). Its value for other off-axis starting points is obtained by linear interpolution as discussed in section 3.5.

The remaining columns are grouped in a set of three and a set of four. The first set give the source efficiency for particular points in the object plane, at the off-axis position given in the heading to each column. The second set of columns give the mean values of the source efficiency derived by integration up to the off-axis point specified by the heading to each column. There are no results for a reflected ion and an appropriate caption is printed out.

3.10 Summary and Conclusions

Ray tracing of characteristic trajectories was carried out be means of the Liebmann (1949) recurrence relations, in the modified form given by Archard (1954) for systems of two dimensional symmetry. Because initial ion energies were small, fine interval sizes were used at the beginning of each trajectory, with the result that for most geometry and voltage configurations a paraxial ray-tracing accuracy of better than one percent was obtained. The result of the paraxial analysis are shown to be approximately valid for an ion object which has a height equal to the width of the aperture in the ion exit slit; for example, the true demagnification of an object of this size is no more than 15% larger than that calculated by paraxial theory.

By using the Lagrange-Helmholtz relation it is shown how source efficiency may be defined in terms of the properties of two characteristic rays. For completeness the computer calculations, for each ray trace, include the time taken for an ion to travel from the point of production to the source resolution-slit of the mass spectrometer.

4 - RESULTS OF THE THEORETICAL ANALYSIS

This section collects together the results of the theoretical analysis of an electron bombardment ion source. It is shown how relatively small changes in repeller voltage can cause large changes in the overall linear and angular demagnifications of the source, the ion residence time and the source efficiency. Further computations reveal how changes of source efficiency occur with changes in object (or electron beam) position, initial ion energy, ion accelerating voltage, mean beam-centring voltage and source geometry. The section concludes with a brief study to determine the possible effect, on the results obtained, of some parameters not included in the analysis.

The effect of electron beam space-charge, and the correlation between source efficiency and mass spectrometer sensitivity in amps. per torr, are deferred until the next section.

4.1 REPELLER VOLTAGE

With conventional electron bombardment sources it is well-known that large changes of sensitivity occur when the repeller voltage is changed, and all other voltages kept constant. Therefore, in the following sections the effects of repeller voltage change on the properties of the computer analogue of the MS9 source are examined.

4.1.1 Paraxial Imagery

The electric field acting on an ion in the ionisation chamber, is the resultant of that part of the main accelerating field which penetrates into this region, and the repeller field, generated between the ion exit slit and repeller plate. When the repeller voltage is changed, the field distribution in the ionisation chamber will alter, resulting in a change of focal properties of the source. One focal property which can be easily computed is the position of the paraxial image formed by the ions.

Figure 4.1 shows the theoretical values for the position, in mms from the ion exit slit, of the image as a function of the repeller voltage. It is seen that the image closest to the object (labelled '1st Image') stays in substantially the same position when the repeller voltage, Vr, is varied between -5V and +25V. The position of this image in relation to the slits can be seen by reference to figure 2.1.

As the repeller voltage is reduced, resulting in a reduction of the resultant ion-extraction field at the electron beam, a second image, initially formed at plus infinity, gradually moves towards the ion source, so that when Vr = +3V, this image is situated near the source resolution-slit.

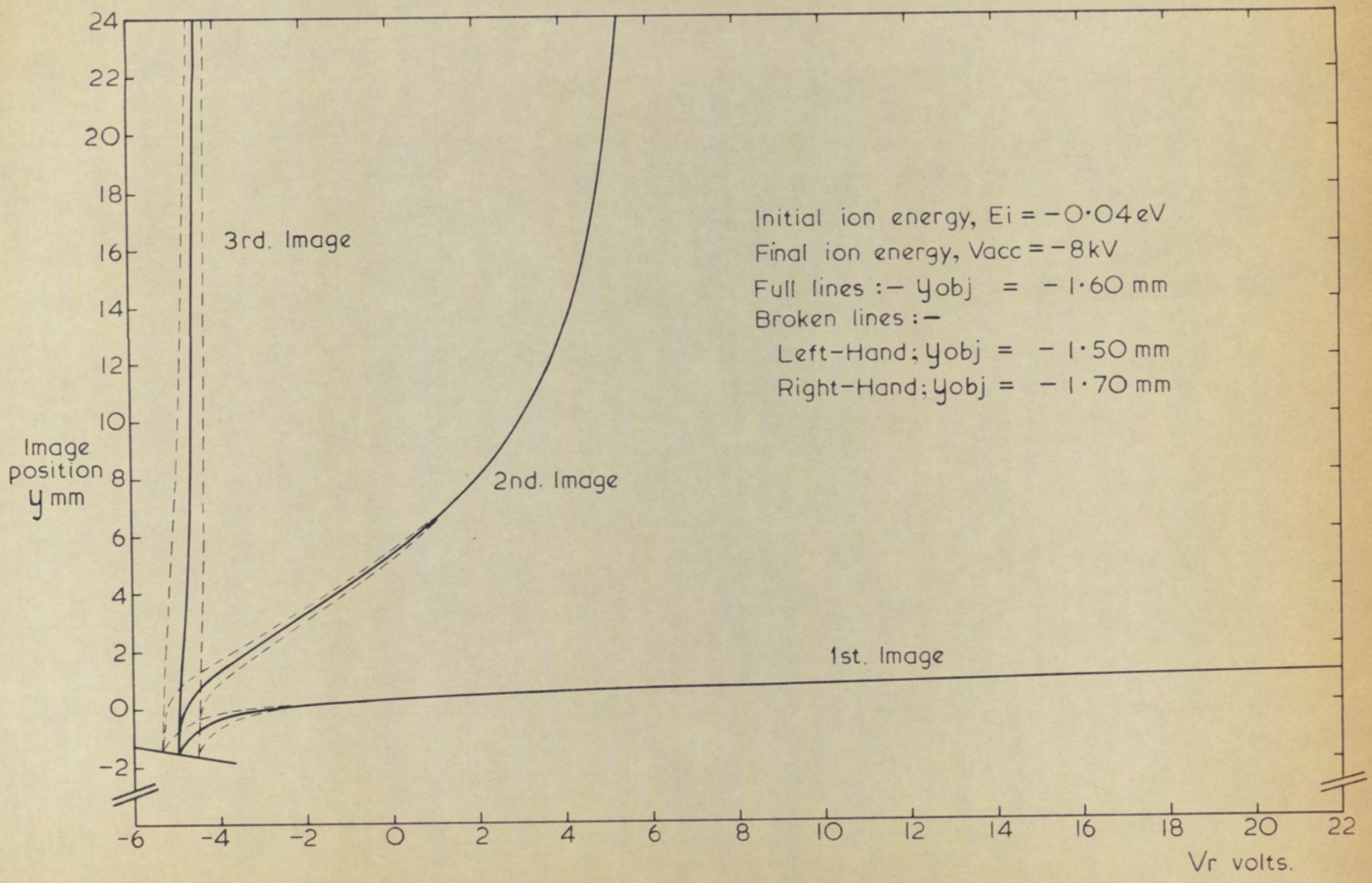

FIGURE 4.1. PARAXIAL IMAGERY OF THE MS902 E.B. ION SOURCE AS A FUNCTION OF ION REPELLER VOLTAGE, Vr.

When the repeller voltage is reduced to about -4.5 volts, so that the repeller field opposes the accelerating field, a third image is formed. Under these conditions the ion starts-off in a retarding field, and it has just sufficient energy to surmount the potential barrier. For repeller voltages a few tenths of a volt more negative, all ions of -0.04eV initial energy which start from y = 1.6 mm are attracted to the repeller plate.

The broken-line curves on figure 4.1 are the image position curves for different object planes. The electron beam is usually confined between the planes y = -1.40 and y = -1.80 mm, and therefore the object planes at y = -1.50, -1.60 and -1.70 mm have been chosen as a representative sample of planes; the region with the bounding broken lines represents a band within which the image is most likely to be present.

Figures 4.2 and 4.3 show, respectively, the apparent linear demagnification and the corresponding angular demagnification as a function of repeller voltage. The angular demagnification curve shows a striking resemblance to an experimental repeller curve (see figure 4.7). The linear demagnification never becomes smaller than 0.13.

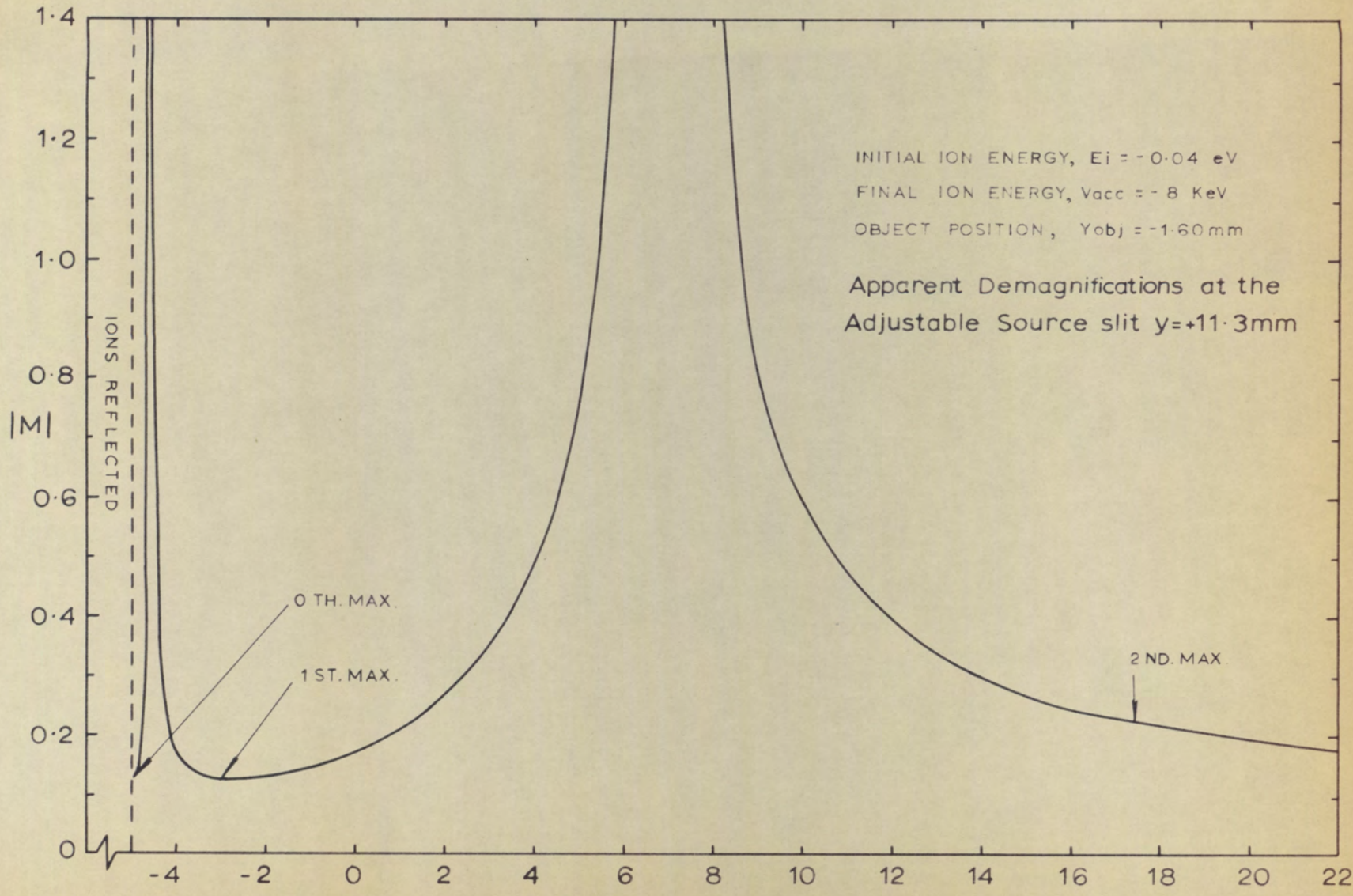

FIGURE 4.2 APPARENT LINEAR DEMAGNIFICATION |M| OF THE MS902 E.B. ION SOURCE AS A FUNCTION OF THE REPELLER VOLTAGE, Vr.

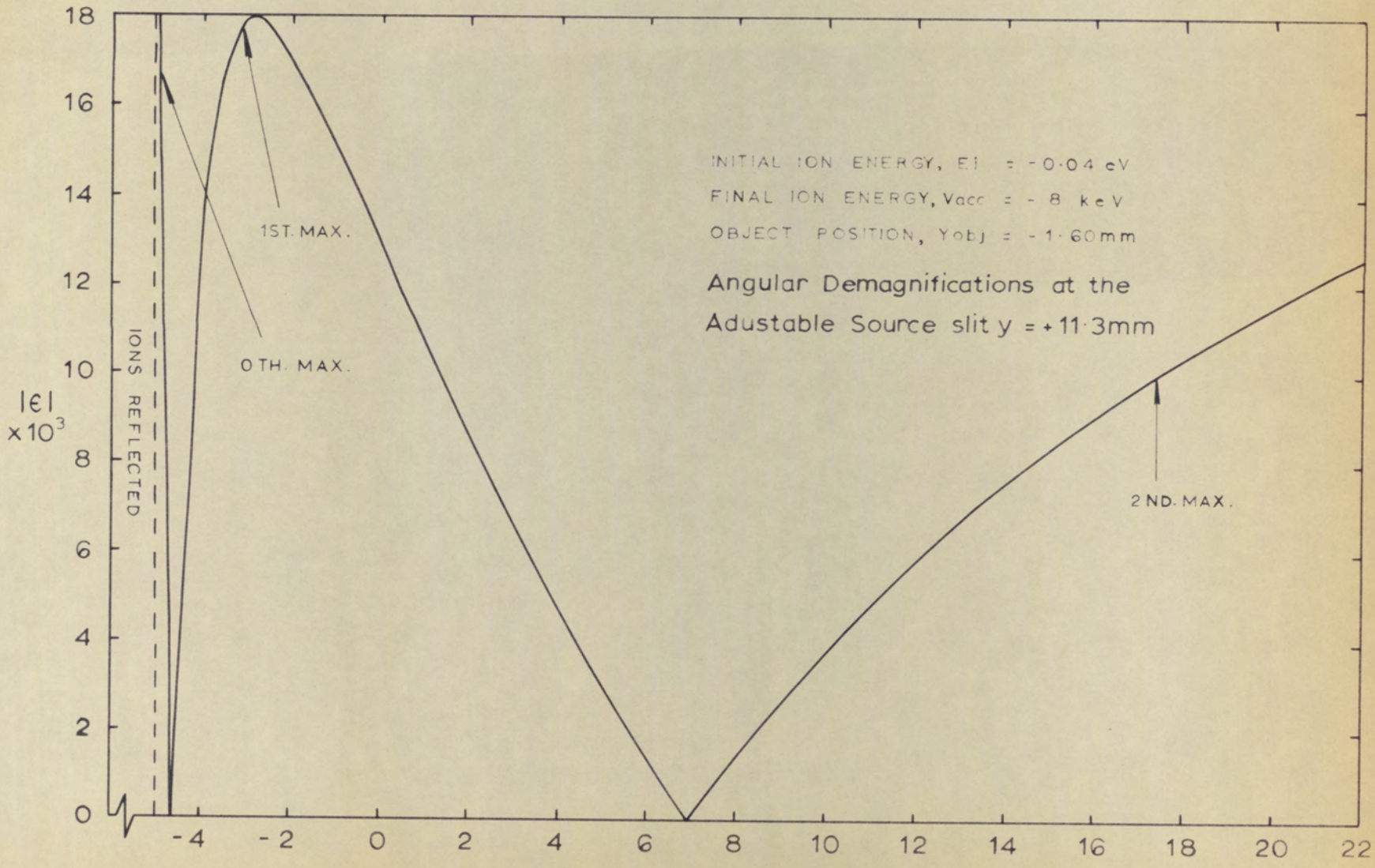

FIGURE 4.3 ANGULAR DEMAGNIFICATION |ε| OF THE MS902 E.B. ION SOURCE AS A FUNCTION OF THE REPELLER VOLTAGE, Vr.

4.1.2 Ion Residence-time

The variation of the ion residence-time in microseconds (μs) as a function of ion repeller voltage for the MS902 electron bombardment ion source is shown in figure 4.4. A feature of this curve is that for positive repeller voltages, the time remains substantially constant at values of between 0.1 and 0.2 μs (times for a mass of 1 a.m.u.). When the repeller voltage is negative and approaches the condition of zero resultant extraction field, ions take longer to attain a given energy. Below the critical voltage (a value depending on the object plane position) the ions are attracted towards the repeller plate, and the residence-time is not defined.

The residence-times given are the times taken for the ions to travel to the source resolution-slit. The time taken for an 8kV ion to travel from the source resolution-slit to the collector of the mass spectrometer (a distance of about 80 inches), is

$$\frac{80 \times 2.54}{(2 \times 8000 \times 1.6 \times 10^{-12} \times 6.02 \times 10^{23})^{\frac{1}{2}}} = 1.6 \text{ μs (for M = 1 a.m.u.)}$$

An ion therefore spends approximately 10% of its life in the source region of the mass spectrometer.

For ions of mass M, all residence-times are increased by a factor of $M^{\frac{1}{2}}$.

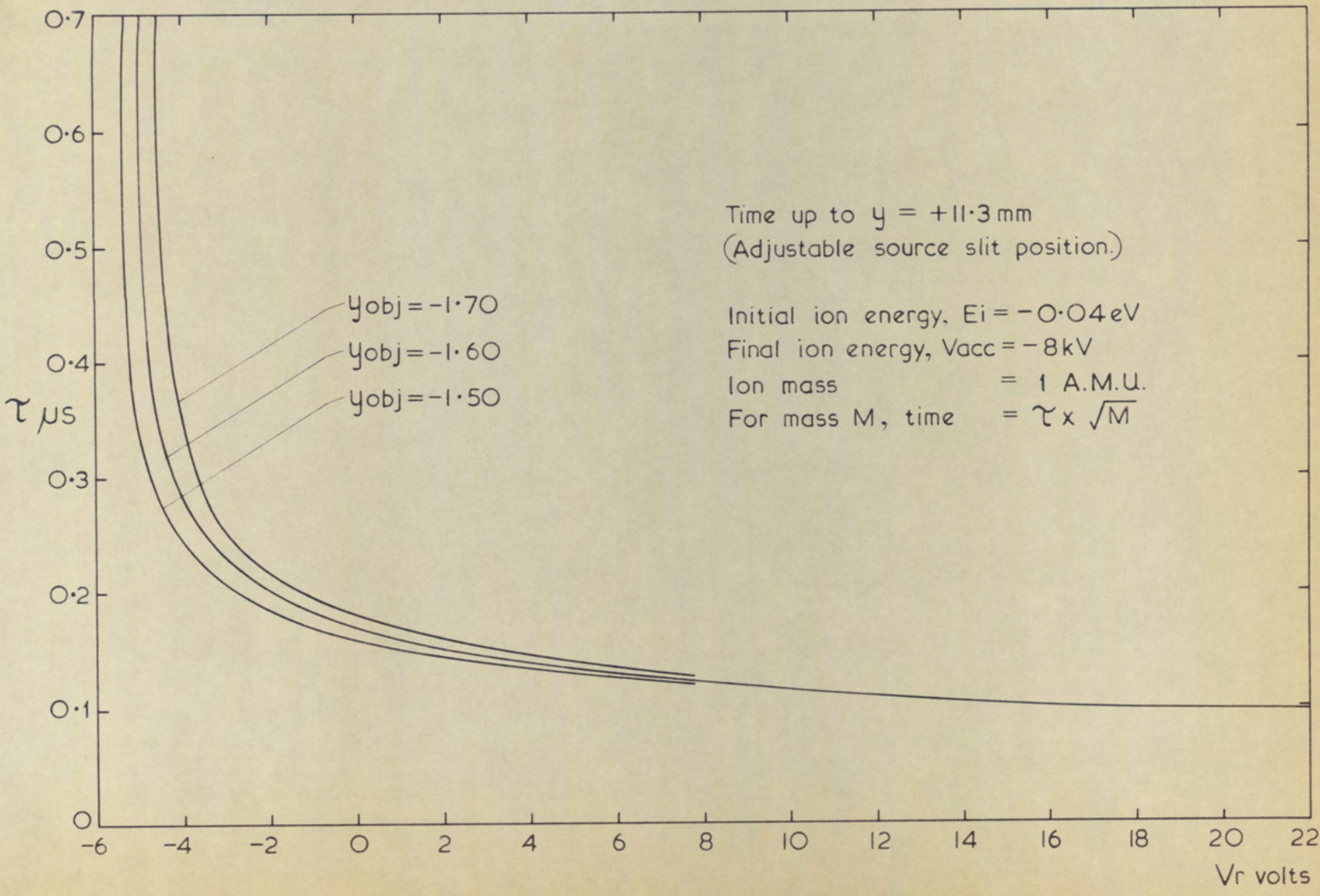

FIGURE 4.4. ION RESIDENCE TIME, $\tau\mu s$, IN THE MS902 E.B. ION SOURCE AS A FUNCTION OF ION REPELLER VOLTAGE, Vr.

4.1.3 Source Efficiency

It was explained in section 3.4 that it is necessary to integrate from the y-axis to the edge of the electron beam to obtain a representative source efficiency value. Figure 4.5 shows the ion extraction efficiency values as a function of repeller voltage for ions starting at the given off-axis points. It is seen that for a starting point near the axis (X = 0.03 mm), the source efficiency remains substantially constant to repeller voltage changes. Thus for the case of a 'point source' the source efficiency is almost independent of the ~~exact~~ value of the extraction field, provided this field is greater than the field at cut-off.

For ions starting out some distance from the axis, the source efficiency attains its maximum at three sharply defined repeller voltages. Away from these maxima, the source efficiency falls-off rapidly. (Note: to avoid confusion the left-most branch of the curves has been included in one case only).

Figure 4.6 shows the integrated source efficiency curves. Thus the curve labelled 'sum to x = 0.3 mm' is the repeller curve to be expected for an ion source with an electron beam 0.6 mm broad. The integrated curves are substantially the same for different electron beam breadths, but have the characteristic that the broader the electron beam, the sharper the efficiency maxima.

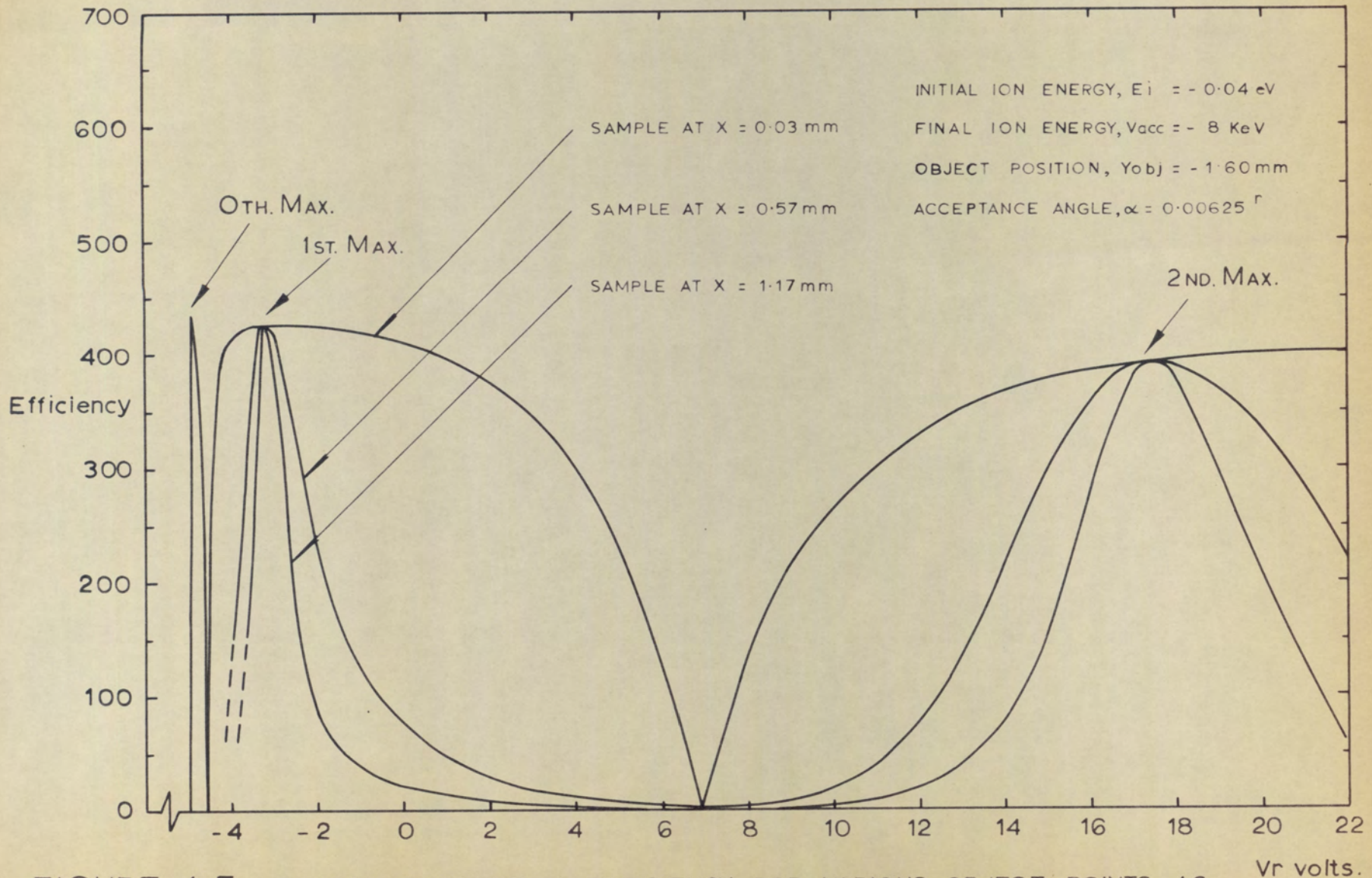

FIGURE 4.5 SOURCE EXTRACTION EFFICIENCY FOR VARIOUS OBJECT POINTS AS A FUNCTION OF REPELLER VOLTAGE, Vr.

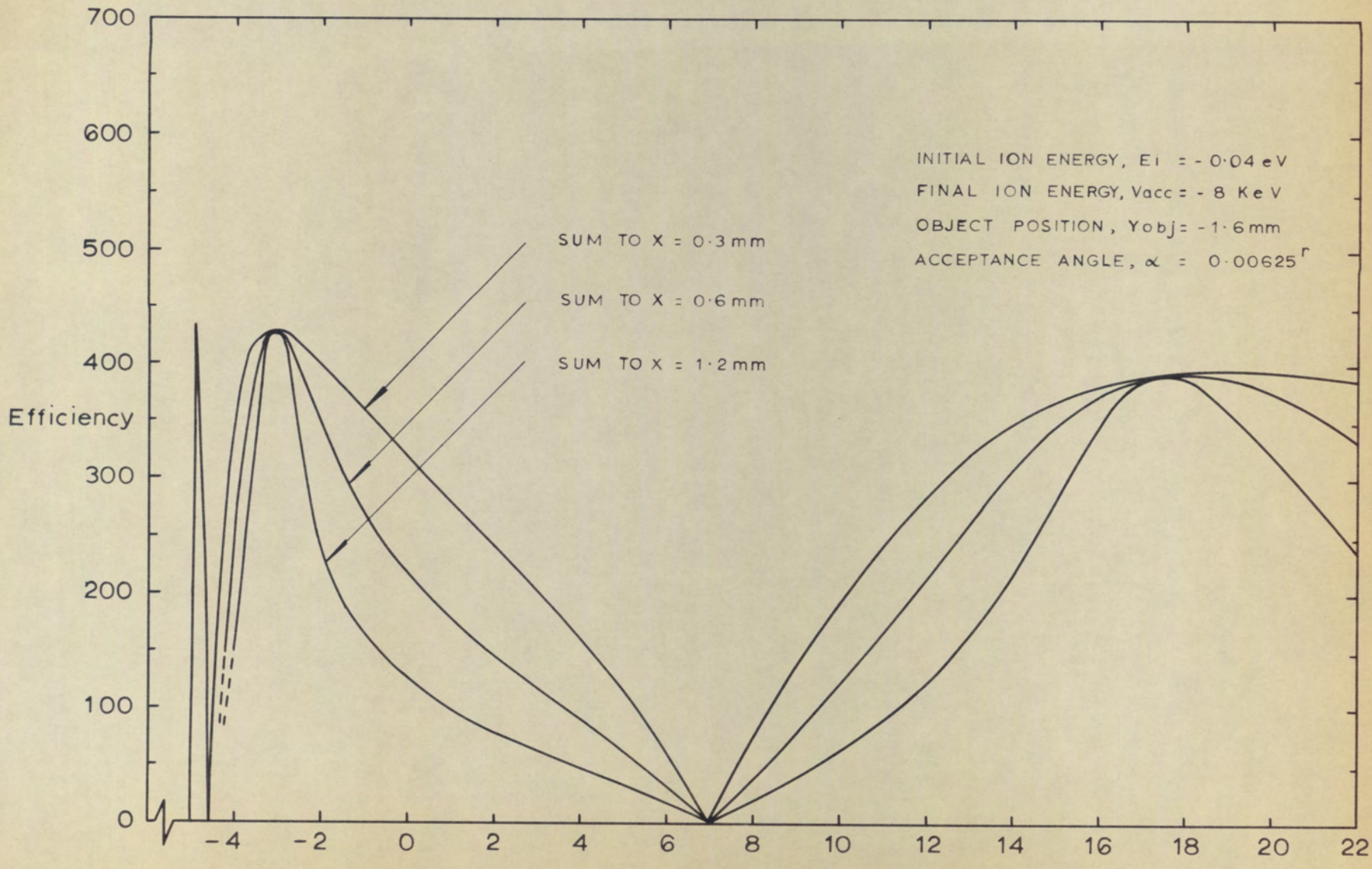

FIGURE 4.6 SOURCE EXTRACTION EFFICIENCY FOR VARIOUS OBJECT PORTIONS AS A FUNCTION OF REPELLER VOLTAGE, Vr.

The repeller curves obtained on the computer analogue have exactly the same characteristics as practical ion repeller curves obtained on a mass spectrometer. Figure 4.7 shows a selection of such curves obtained on different MS902 mass spectrometers. The curve (A) displays the basic characteristics predicted by theory. These are:-

(a) a 'cut-off' in ion current at a repeller voltage between -5V and -10V.

(b) A maximum of ion current at about -3V (termed the 'first maximum').

(c) A second maximum of ion current at about +17V (termed the 'second maximum').

However, the narrow 'Zeroth' maximum occurring just before the cut-off on the theoretical curves, is not displayed on the experimental curve; it is probably superimposed on the first maximum.

Curves (B), (C) and (D) are different in that the second maximum occurs at voltages in excess of 30V. The presence of non-conducting deposits (condensed, decomposed sample) on the electrode surfaces probably has little effect on the shape of the repeller curve, as is exemplified by

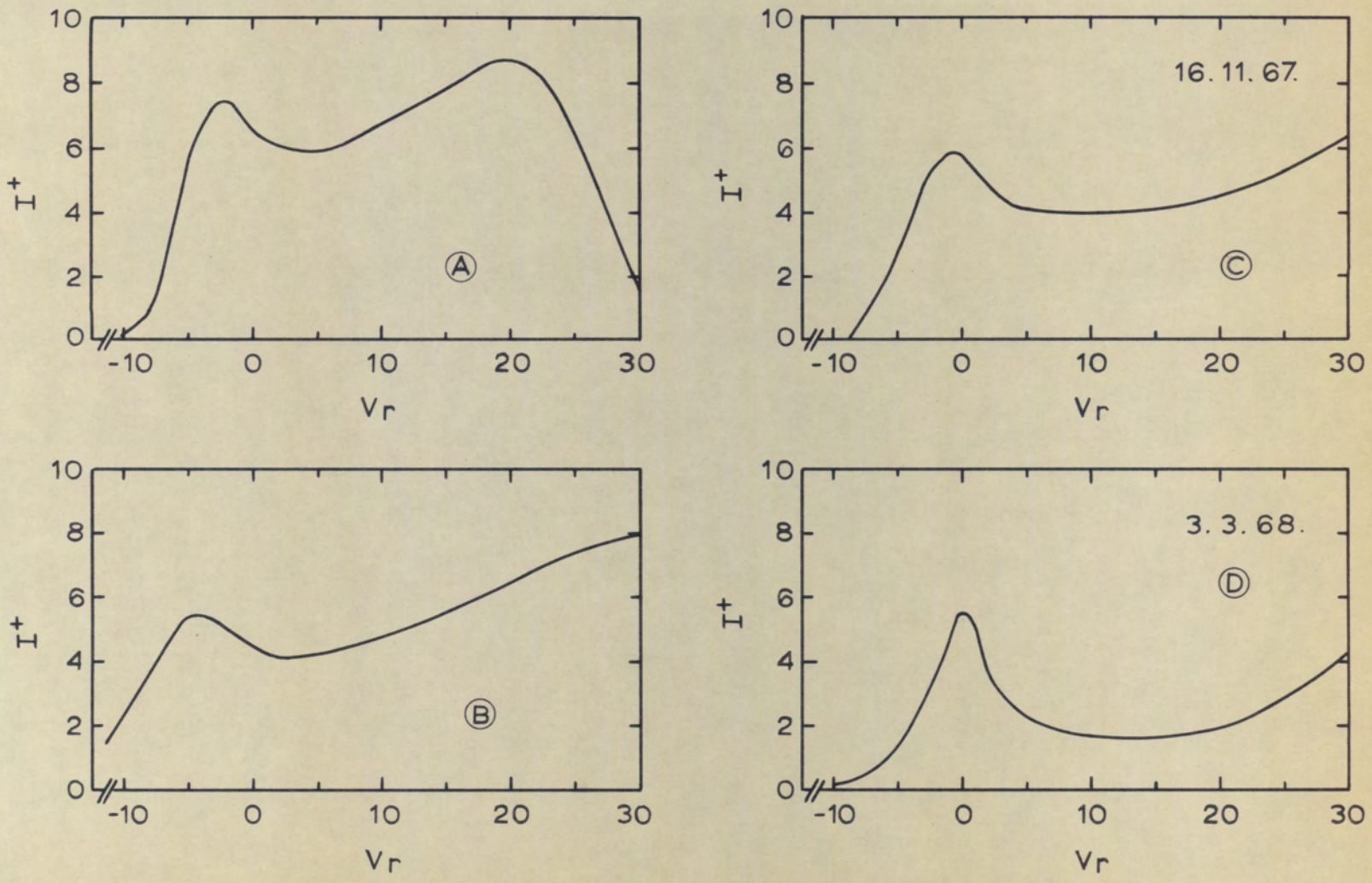

ELECTRON TRAP CURRENT, I_T, = 20μA
ACCELERATING VOLTAGE, Vacc, = 8 kV

ABSCISSAE: REPELLER VOLTAGE, Vr, VOLT
ORDINATES: ION CURRENT $I^+ \times 10^{13}$ AMP

FIGURE 4.7 EXPERIMENTAL ION REPELLER CURVES TAKEN ON DIFFERENT M.S.902 E.B. ION SOURCES.

curves (C) and (D). Curve (C) was taken on a clean source, after it had been baked for 24 hours at 150°C, while curve (D) was taken on the same source after it had been used for five months (same filament). It will be shown in section 4.2 that different repeller curves are caused by different source geometry and electron beam position.

4.1.4 Physical Explanation of the Repeller Curve

Figure 4.6 shows that efficiency maxima of 390 and 430 occur at repeller voltages of +17.4V and -3.12V respectively. For a point source, the efficiency would be constant at $1/\epsilon_M = (V_{acc}/E_i)^{\frac{1}{2}}$, provided that the ion was not reflected (See section 3.4). For the case under consideration, the ion accelerating voltage V_{acc}, is equal to -8kV and the ion initial energy, E_i, is equal to -0.04eV. Thus, the point source efficiency is 466. It is apparent from figure 4.6 that a minimum in efficiency occurs for a repeller voltage of about 7V.

To investigate the nature of the repeller curve, a set of trajectories has been computed for the simulated MS902 electron bombardment source; repeller voltages, Vr, of +17.4V, 0V and -3.12V were chosen. The trajectories are plotted in figures 4.8, 4.9 and 4.10 respectively.

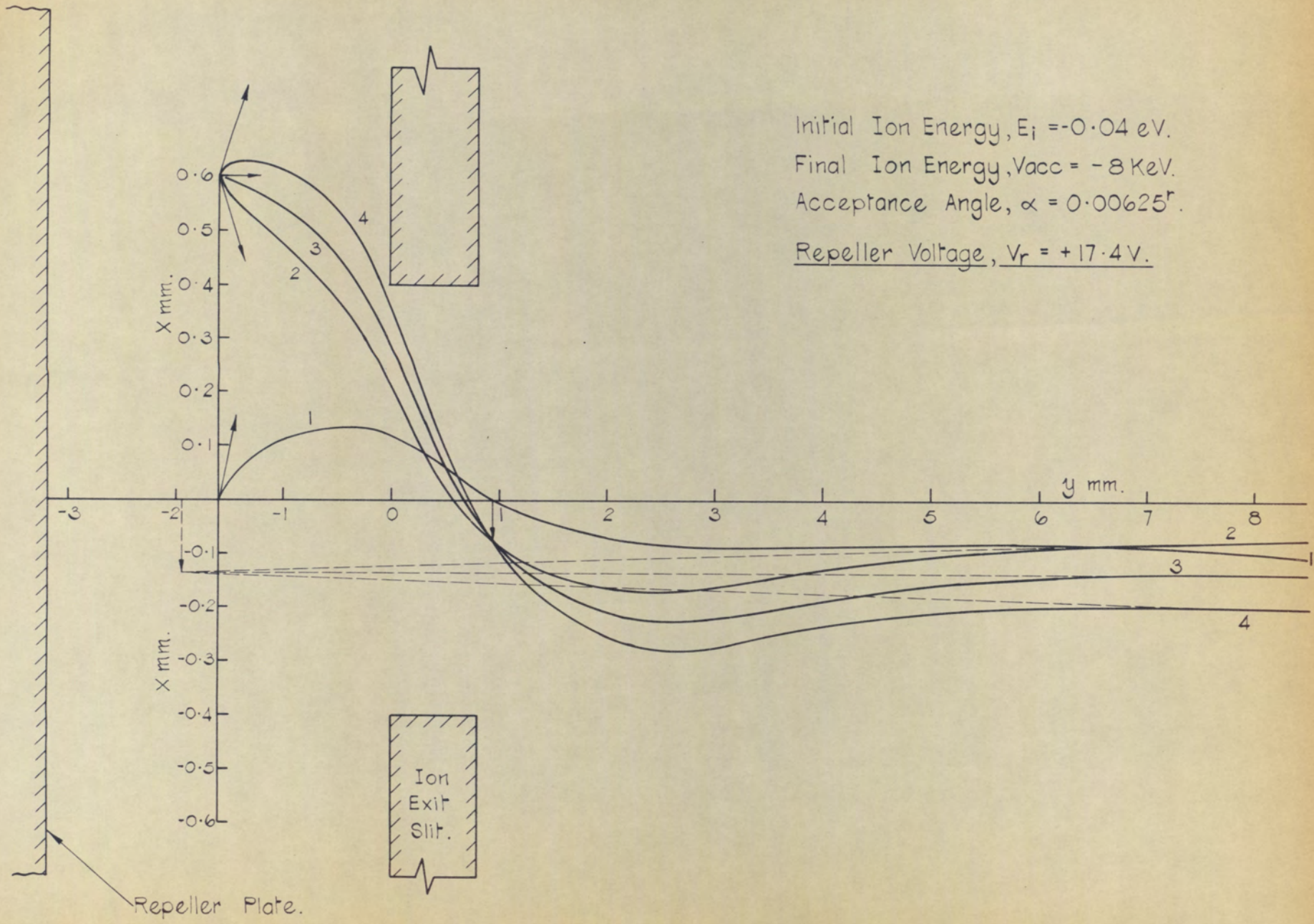

FIG. 4.8. FOUR TRAJECTORIES FOR THE A.E.I. M.S.902 E.B. ION SOURCE WITH A REPELLER VOLTAGE V_r = +17·4 V.

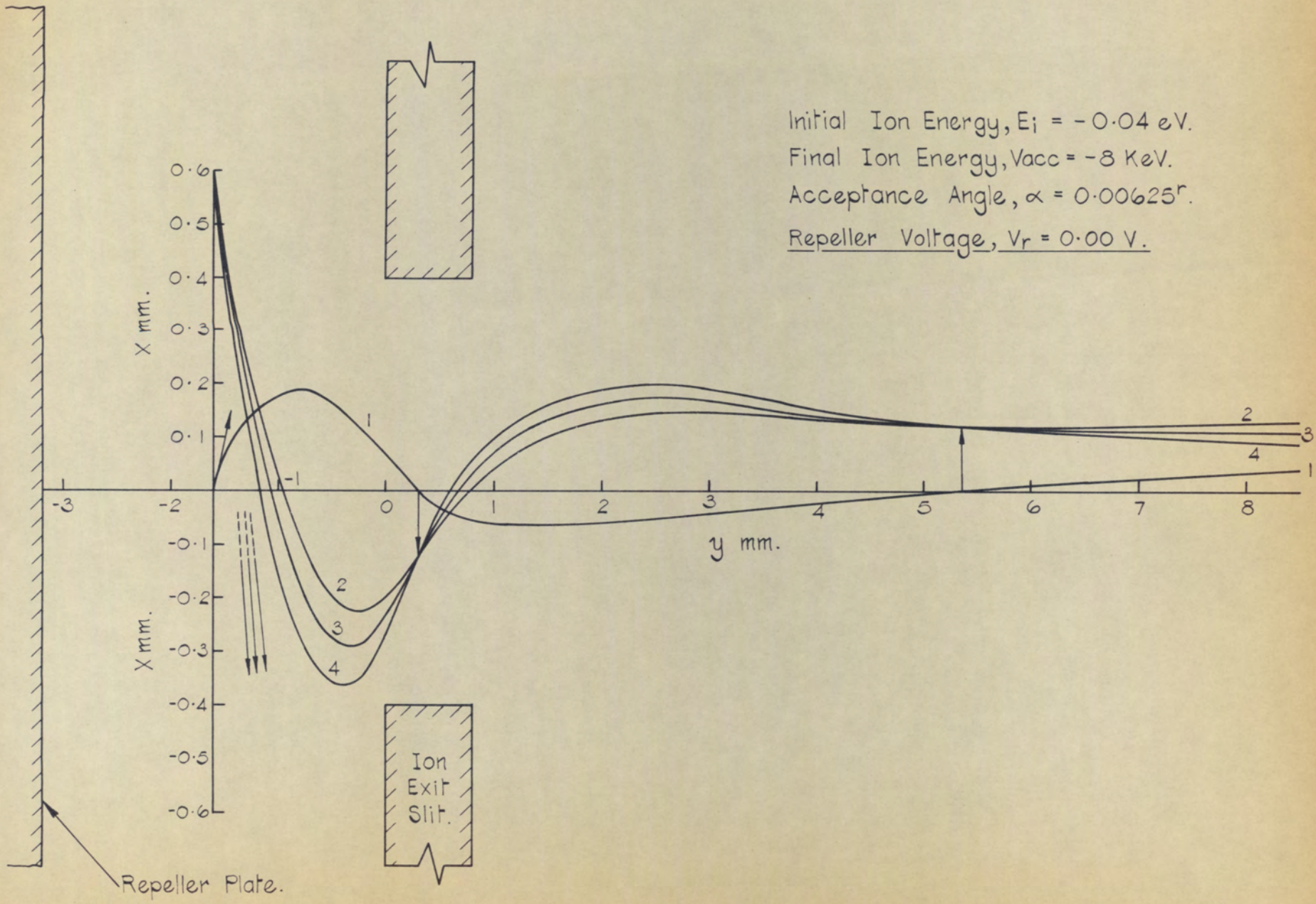

FIG. 4.9. FOUR TRAJECTORIES FOR THE A.E.I. M.S. 902 E.B. ION SOURCE WITH A REPELLER VOLTAGE, $V_r = 0.00$ V.

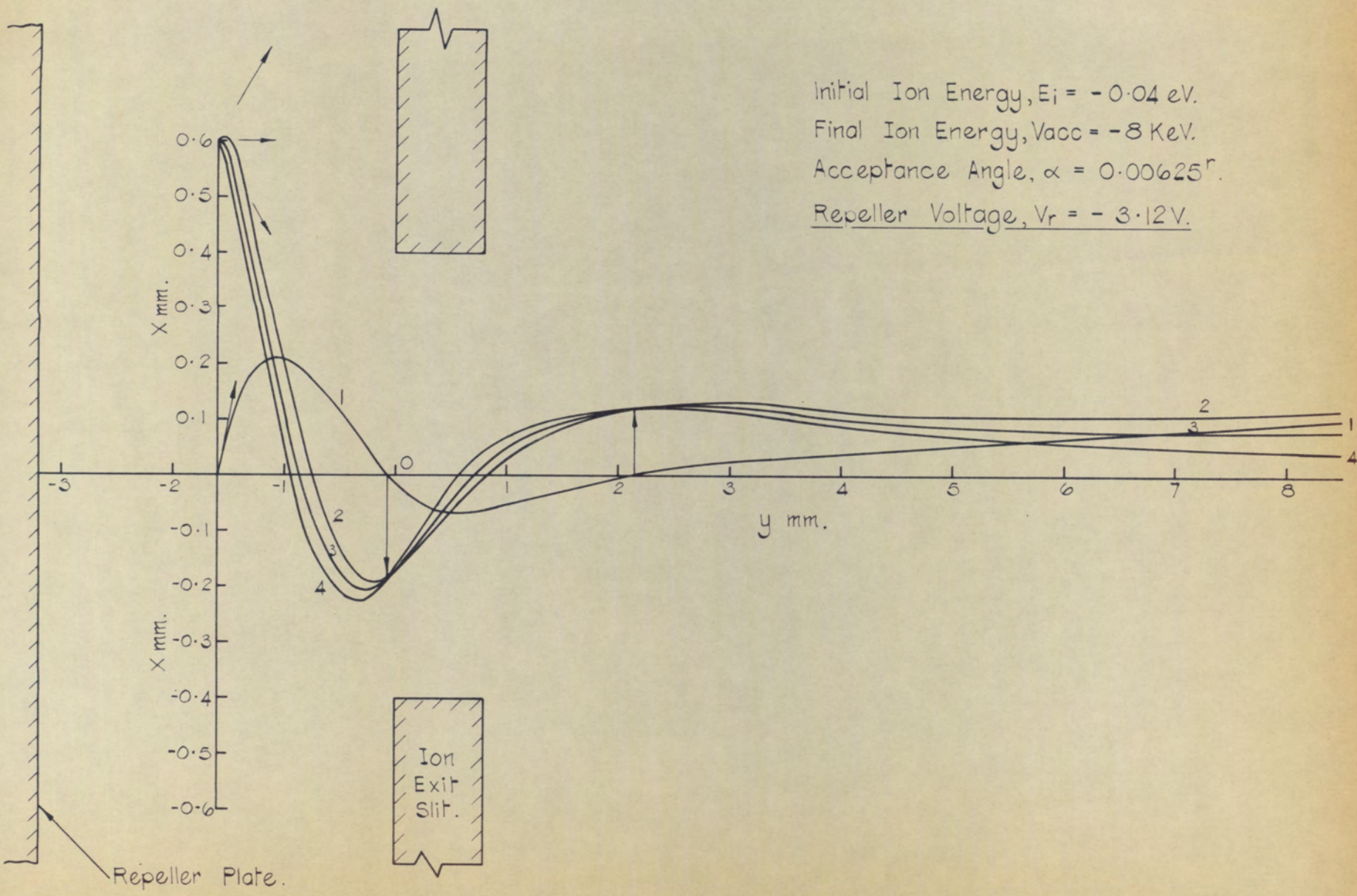

FIG. 4.10. FOUR TRAJECTORIES FOR THE A.E.I. MS 902 E.B ION SOURCE WITH A REPELLER VOLTAGE, V_r = - 3·12 V.

The first (1), is the paraxial trajectory which can be used to determine the position of the images. The other three are trajectories which emerge from the slit system at angles $+\alpha$ (no. 2), 0 (no. 3) and $-\alpha$ (no. 4) to the axis, where α is the half-angle of acceptance of the α- slit of the mass spectrometer (α = 0.00625, for the MS902 mass spectrometer). In each case, the parameters of interest are the initial angles of the trajectories, the linear demagnification, and the source efficiency. These parameters, for each set of three off-axis trajectories, are given in the table below. The initial angles of the trajectories are in degrees.

Vr	INITIAL ANGLE OF TRAJECTORY, δ°			$\lvert\Delta\delta\rvert$ (2,4)	Ma	$\frac{\lvert\Delta\delta\rvert}{2\alpha M}$
	(2)	(3)	(4)			
+17.40V	-32	0	32	64	0.228	390
0.00V	-62.1	-67.2	-70.7	8.6	0.175	68.5
-3.12V	19.45	0	-19.45	38.9	0.126	430

The ion withdrawal wedge $\Delta\delta$, is the difference between the initial angles of trajectories (2) and (4). The source efficiency ($\Delta\delta/2\alpha M$), has been defined in section 3.

From this table, it is seen that the drop in source efficiency which occurs when the repeller voltage is changed from -3.12V to 0V, results from a large reduction in the ion withdrawal wedge $\Delta\delta$, together with a small increase in the linear demagnification. Further, it is seen that the two cases of greatest off-axis efficiency (Vr = +17.4V and Vr = -3.12V) are those for which the initial bounding trajectories are on either side of the horizontal (see figures 4.8 and 4.10 respectively). That is, $\delta_+ = -\delta_-$, as was predicted from the Lagrange-Helmholtz law (see section 3.4 and Appendix 3.3). For such cases, the ray (3) which emerges parallel to the axis, starts off parallel to the axis. It is now clear why the repeller curve has a number of maxima; the 'second' maximum occurs when there is one real image between the object plane and the source resolution-slit, while the 'first' maximum occurs when there are two real images between these two planes. The theoretically predicted 'zeroth' maximum occurs when there are three real images formed. Although there is every reason to suppose that more than three images could be formed, each new maximum in the repeller curve would be closer to and narrower than the previous one; identification of such maxima would therefore be difficult.

The off-axis efficiency is a minimum when $|\delta_+|$ and $|\delta_-|$ each tend to $\pi/2$ (ray starts-off perpendicular to the axis) and with reference to equation (3.13), it is seen that this occurs when ϵ tends to zero. For the MS902 source this condition is reached when the repeller voltage is about 7 volts (see figures 4.5 and 4.6). However, theoretically the minimum source efficiency is zero, whereas the experimental minimum is not usually less than a factor of four smaller than the maximum efficiency. The discrepancy arises because at a repeller voltage of 7V, ions start off almost at right angles to the axis; the paraxial theory is grossly invalid for such trajectories. At a repeller voltage which gives a maximum in source efficiency, the initial angles of the trajectories are small, and trajectories calculated by the paraxial theory are good approximations to the true trajectories. From a practical point of view, it is the properties of the source at the maxima in source efficiency which are important. Therefore, the paraxial theory may be used with confidence to determine, for example, whether or not there is an optimum source geometry which gives higher sensitivity than any other source.

4.2 CHANGES OF VOLTAGES AND OF GEOMETRY

In this and the following sections the effects of geometrical and voltage changes on a 'standard' ion repeller curve are considered. The 'standard' curve is the one obtained theoretically under the following conditions:-

(a) MS902 electron bombardment ion source geometry.

(b) Ion accelerating voltage of +8kV.

(c) Focusing half-plate voltage of +7.44kV.

(d) Initial ion energy of -0.04eV (= 190°C).

(e) Object plane position, Y_{obj} = -1.60 mm.

(f) Efficiency values integrated up to x = $\pm$ 0.6 mm.

4.2.1 Change of Object Position

The object plane is coincident with the plane of the electron beam. However, in practice, the electron beam is about 0.4 mm wide (y) and may be located anywhere between y = -1.6 and y = -0.8 mm. This imprecision results mainly from the lack of precision in the positioning of the source magnets. Figure 4.11 shows the repeller curves obtained when the object plane is sited at y = -1.6, -1.05 and -0.85 mm. It is seen that it is possible for the position of the second efficiency maxima to vary by

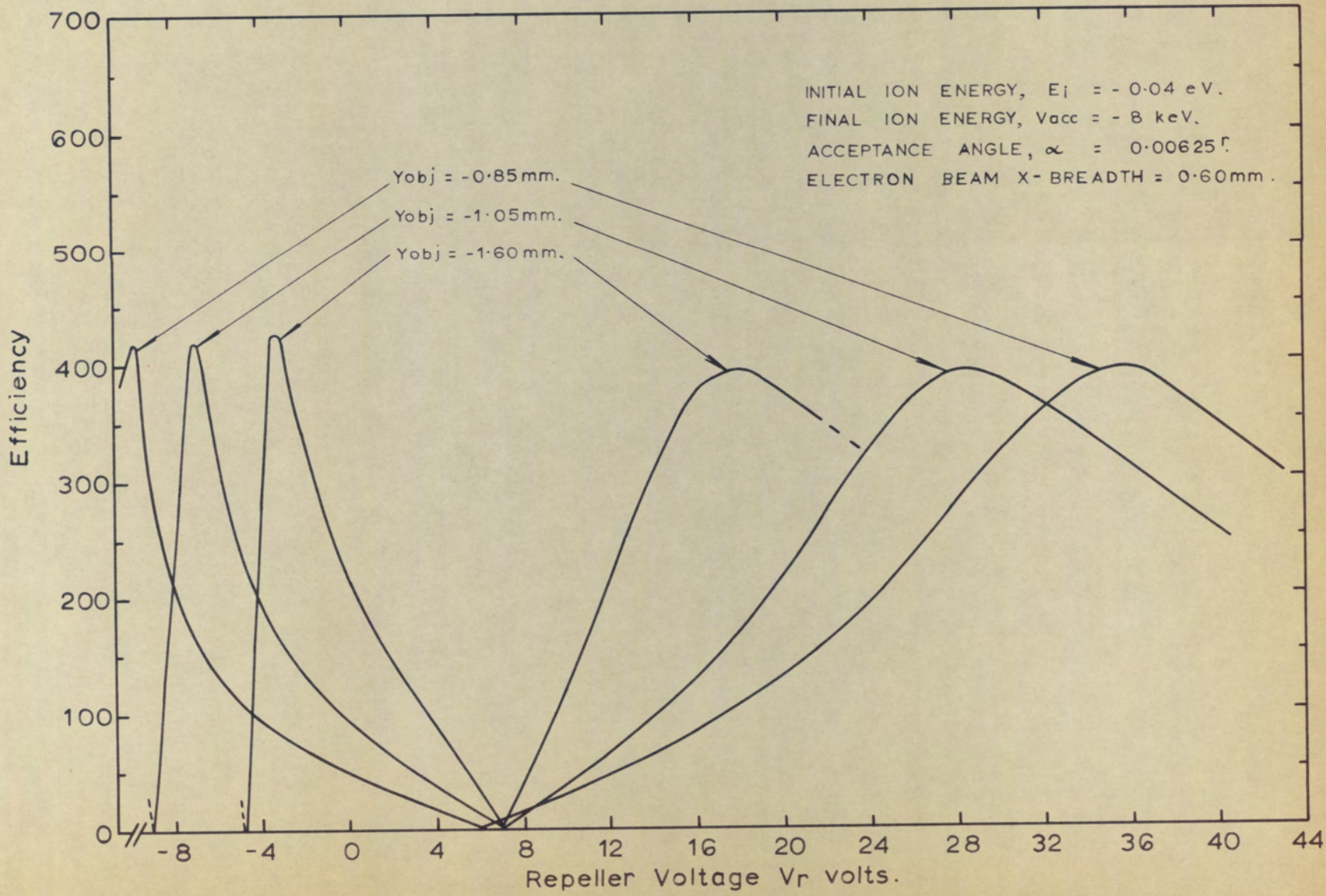

FIGURE 4.11 THEORETICAL REPELLER CURVES FOR VARIOUS OBJECT POSITIONS Yobj, FOR THE MS902 E.B. ION SOURCE.

at least twenty volts, while the shift in the first maxima is a factor of three smaller. Such a variation from source to source is well known, as is exemplified by the curves in figure 4.7. For each object position, the source efficiency at the optimum repeller voltage is substantially the same. This is an agreement with the experimental analysis of electron guns carried out by Haine and Einstein (1952), in which gun brightness was shown to be independent of filament position, provided that the bias voltage was optimised.

The effect of a finite y-width of the electron beam, would be to broaden the repeller peaks, but would not cause any substantial shift of the peaks.

4.2.2 Ion Initial Energy

When an ion is generated from a gas molecule, it will have the velocity and direction of that molecule. Each ion will thus have an initial volt energy, and the assembly of ions will have a distribution of initial energies corresponding to the Maxwell-Boltzmann energy distribution curve. In the calculations and results presented so far, it has been assumed that an ion will have the most probable energy, which for Maxwell-Boltzmann statistics is kT, where k is the Boltzmann constant ($k = 8.617 \times 10^{-5}$ eV. $^{o}K^{-1}$) and T is the absolute temperature. For a source temperature of 190°C, the most probable initial energy of the ion will be -0.04eV. If this is E_{max}, then the number of ions, N, with any given energy E is given by the equation:

$$N = n.E_i \exp(-E_i/E_{max})$$

where n is a constant, dependent on the source pressure and degree of ionisation. From this equation, it may be deduced that $P_{\frac{1}{2}}$, the ratio of the number of ions with energy $(E_{max}/2)$, to the number of ions with energy E_{max}, is given by the equation:

$$P_{\frac{1}{2}} = \tfrac{1}{2} \cdot \frac{\exp(-\frac{1}{2})}{\exp(-1)} = 82.5\%$$

Similarly, for ions with an energy of $2E_{max}$,

$$P_2 = 2 \cdot \frac{\exp(-2)}{\exp(-1)} = 67.5\%$$

The theoretical repeller curves for ions of initial energies -0.02eV, -0.04eV and -0.08eV, shown in figure 4.12, should therefore give a representative set of curves for the system. The efficiency maxima increase with decreasing initial energy, and this agrees with the predictions from the Lagrange-Helmholtz expression, equation (3.12). The quantitative change will be dealt with in more detail in the next section.

As the initial ion energy increases, the repeller voltage required for each efficiency maximum decreases. However the effect is relatively small, and the repeller curve derived for an initial energy of -0.04eV will be representative of the true repeller curve. Finite energy spread

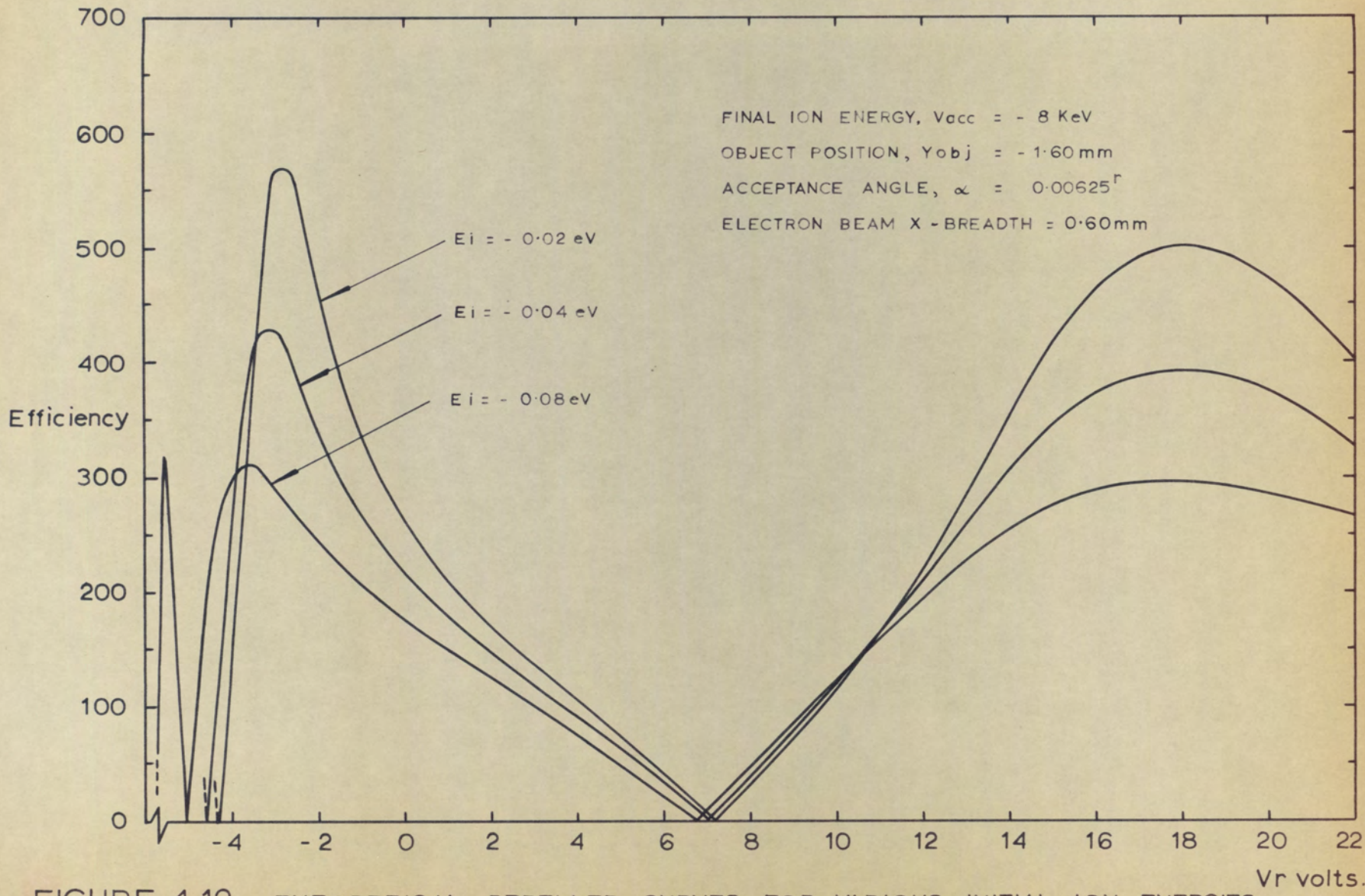

FIGURE 4.12 THEORETICAL REPELLER CURVES FOR VARIOUS INITIAL ION ENERGIES Ei, FOR THE MS902 E.B. ION SOURCE.

of the ions, will result in a first repeller maximum which has substantially the same height as the -0.04eV peak, but which has broader flanks. The second repeller maximum will also be substantially the same as the one calculated for E_i = -0.04eV.

4.2.3 Ion Accelerating Voltage

The theoretical ion repeller curves for three accelerating voltages 8, 4 and 2kV, are shown in figure 4.13. The set of curves display the same characteristics as the previous set of curves for initial ion energy, except that the efficiencies at the ion repeller maxima, increase with increasing accelerating voltage, compared with an efficiency decrease for increasing initial ion energy. This again is in agreement with the Lagrange-Helmholtz equation.

The repeller voltage and beam-centring voltage have been scaled in proportion to the accelerating voltage. The ratio (V_r/V_{acc}) for each repeller maximum changes with changing accelerating voltage. The following table may be compiled from the results of section 4.2.2 and this section:

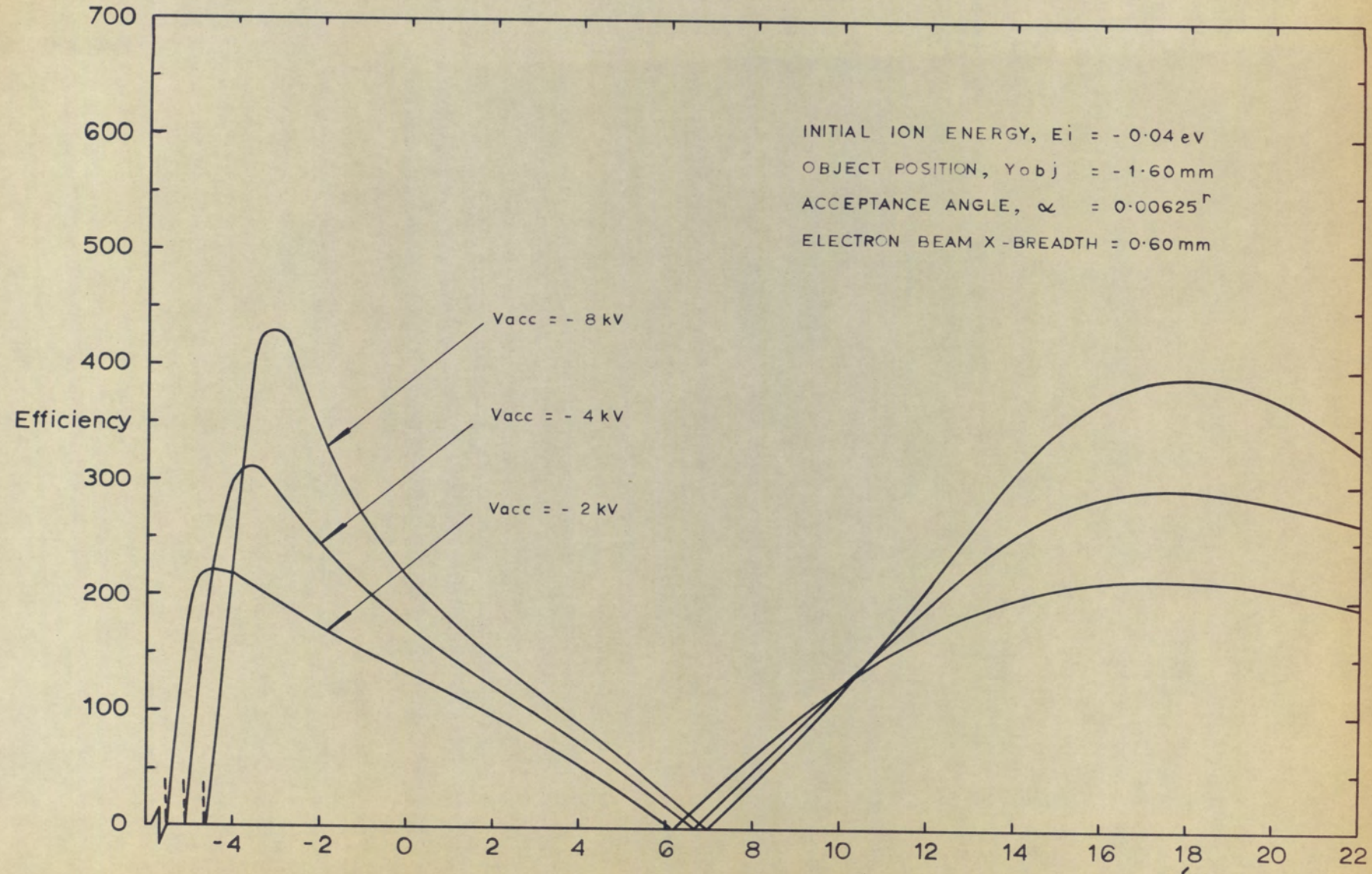

FIGURE 4.13 THEORETICAL REPELLER CURVES FOR VARIOUS ION ACCELERATING VOLTAGES Vacc FOR THE MS902 E.B. ION SOURCE.

	$-V_{acc}$ (eV)	$-E_i$ (eV)	$(V_{acc}/E_i)^{\frac{1}{2}}$	EFFICIENCY (1)	EFFICIENCY (2)	$(V_r)_1$	$(V_r)_2$
	8000	0.02	633	580	490	-2.75	17.57
	8000	0.04	446	430	390	-3.12	17.40
(1)	8000	0.08	316	310	295	-3.64	17.17
	8000	0.04	446	430	390	-3.12	17.40
(2)	4000	0.04	316	310	295	-3.64*	17.17*
	2000	0.04	224	220	220	-4.40*	16.80*

* Voltages scaled by a factor $(8000/-V_{acc})$

Comparing the two arrowed entries, it can be seen that the efficiencies and repeller voltages at the two maxima for the first entry (1) are each exactly the same as their respective values in the second entry (2). Therefore, when all the electrode voltages are scaled in the same proportion, the focal properties of the source are unchanged. This is in agreement with the fundamental paraxial law for electron and ion optical systems operating in the absence of electron and ion space-charge (Maloff and Epstein, 1938, p.80).

The above results are shown graphically in figure 4.14; the efficiency for each maximum, together with the theoretical maximum in efficiency $1/(\epsilon M)$, are each plotted as a function of the ratio $(V_{acc}/E_i)^{\frac{1}{2}}$.

It can be seen that as long as the source is operated at the repeller maximum, the source efficiency is very close to the theoretical limit. For a given accelerating voltage, the source should be operated at as low a temperature as possible, so that the most probable ion energy is as small as possible. In practice, little can be done toward this end, since the source temperature is usually set near to the vaporisation temperature of the compound under analysis. When operating the source at constant temperature, and at the first repeller maximum, the source efficiency is almost exactly proportional to the square-root of the accelerating voltage. The transmission efficiency of the mass spectrometer (see section 1) does not obey this square-root law, and this will be discussed in section 5.

4.2.4 Beam-Centring plate Voltage

The characteristic repeller curves, derived for the MS902 source, for each of three mean beam-centring voltages, are shown in figure 4.15. If this voltage is decreased from its normal value of 7440V, a more negative repeller voltage is required to obtain the first efficiency maximum.

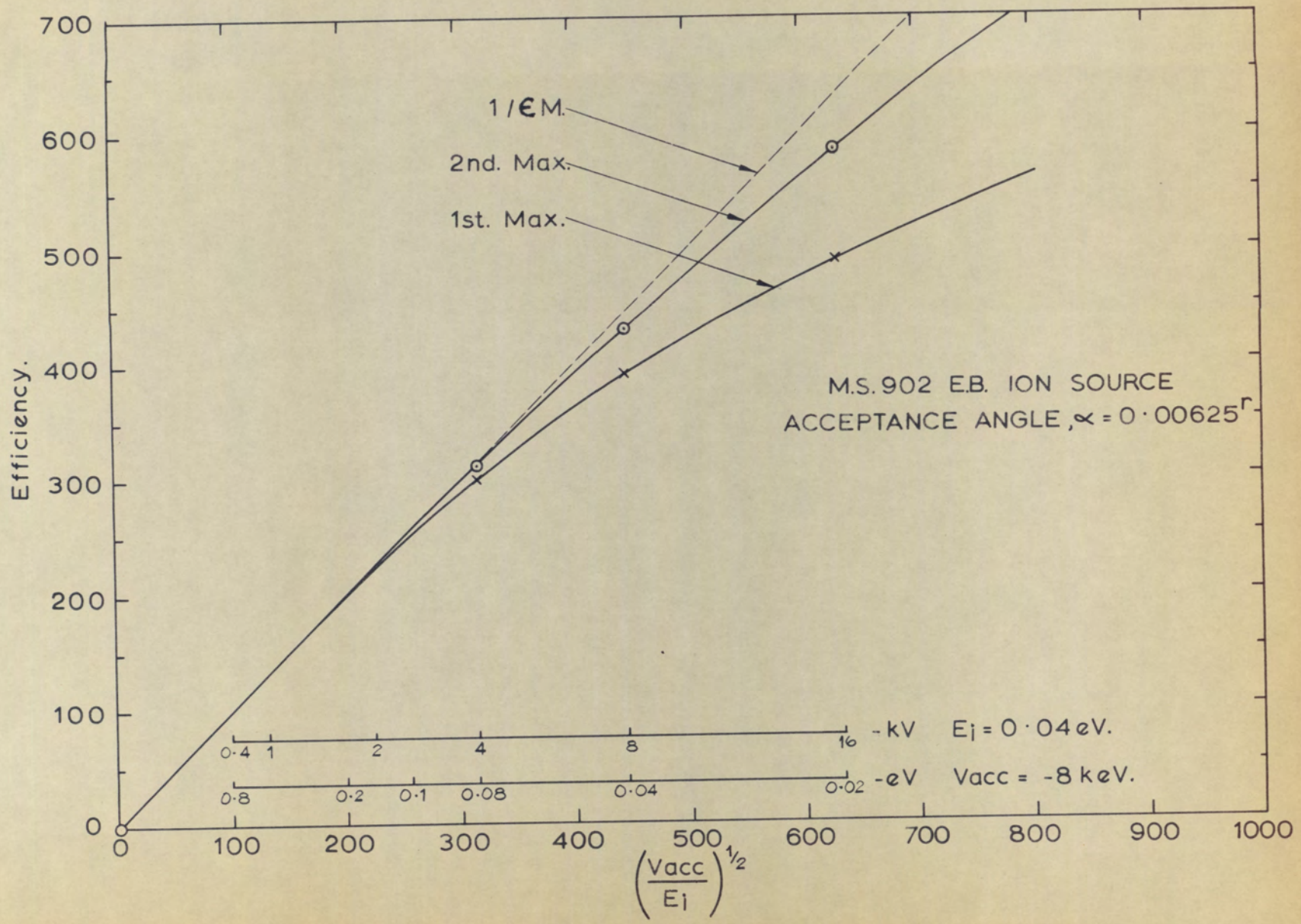

FIGURE 4.14 EFFICIENCIES AT REPELLER MAXIMA AS A FUNCTION OF THE PARAMETER $[V(Acc)/E(INT)]^{\frac{1}{2}}$

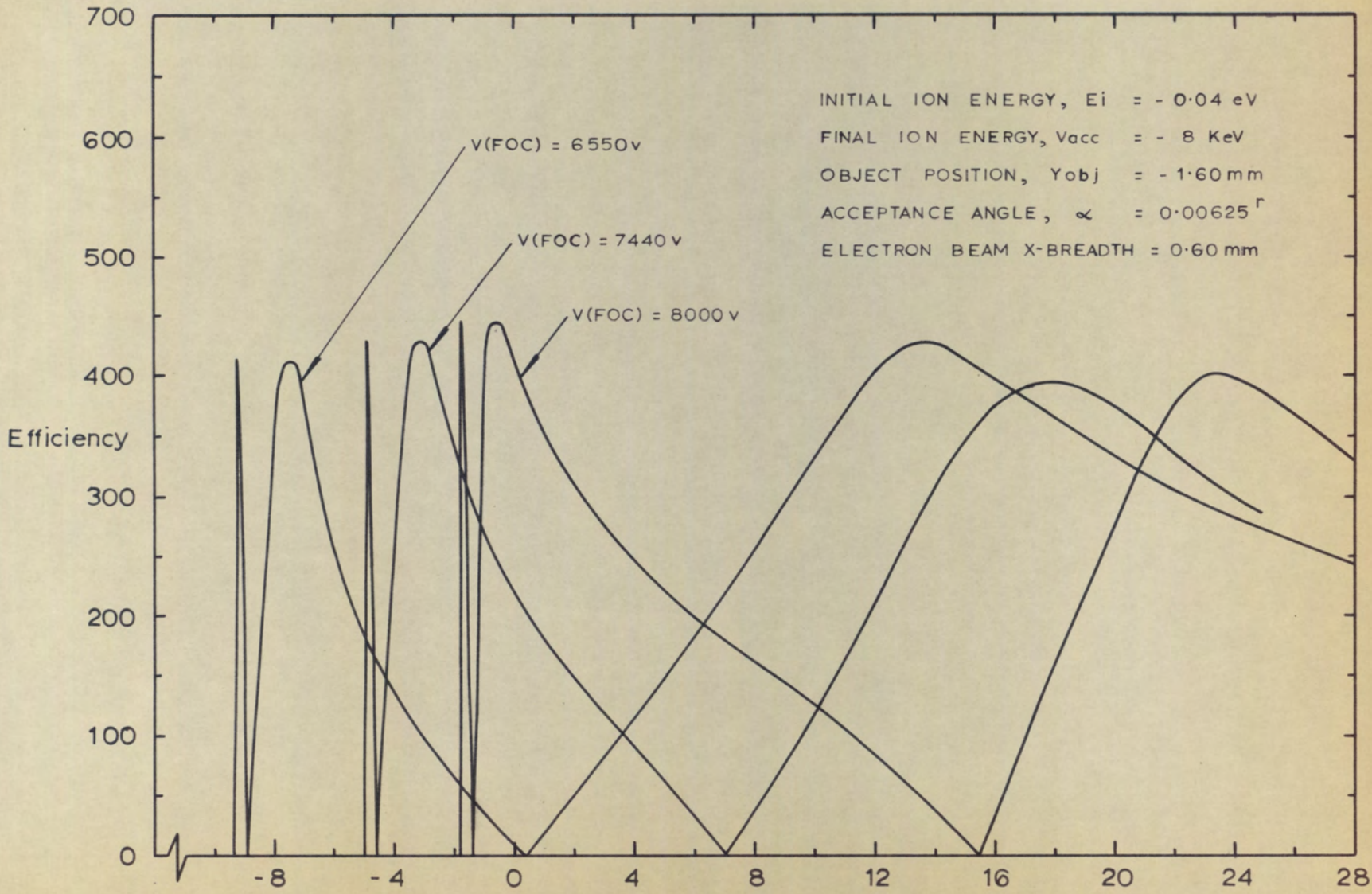

FIGURE 4.15 THEORETICAL REPELLER CURVES FOR VARIOUS MEAN BEAM Vr volts.

CENTRING HALF-PLATE VOLTAGES V(FOC) FOR THE MS902 EB ION SOURCE.

Qualitatively, the increased negative repeller field is required to counteract the increase in extraction field which occurs when the mean beam-centring voltage is decreased.

As with change of object position, there is little change in the efficiency at the repeller maximum when the beam-centring plate voltages are changed.

4.2.5 Ion Exit Slit Thickness

For the simulated MS902 electron bombardment source there are ten geometry parameters and to avoid a lengthy section in which the variation of each one is considered, the ion exit slit thickness has been chosen as a representative parameter. Figure 4.16 shows a set of repeller curves for ion exit thicknesses of 0.4, 0.8 and 1.6 mm. For the MS902 electron bombardment source, the thickness is 0.8 mm.

The effect of making the slit thinner is to shift the first repeller maximum more negative. As with the case of a reduced half-plate voltage, this occurs as a result of the increased penetration of the main accelerating field into the ionization region. The more negative repeller field compensates for this. The opposite effect occurs when the ion exit slit is made thicker.

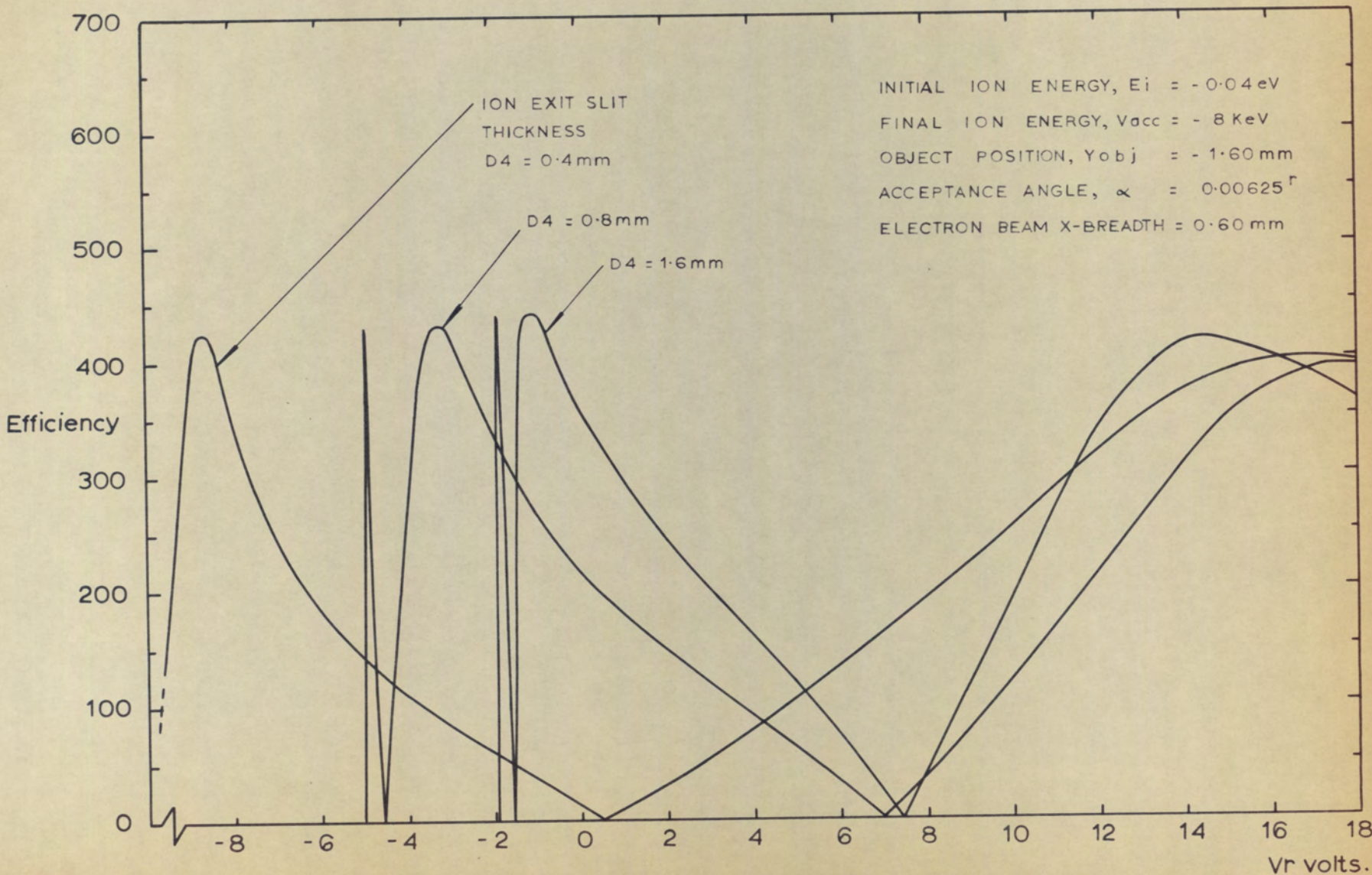

FIGURE 4.16 THEORETICAL REPELLER CURVES FOR VARIOUS ION EXIT SLIT THICKNESSES FOR THE MS902 E.B. ION SOURCE.

It is seen that the optimum source efficiency is the same for different source geometries. Again, this is in agreement with the experimental results of Haine and Einstein (1952), who showed that change in electron gun geometry had little effect on optimum brightness.

The image demagnification, as seen from a plane at plus infinity, is different for different ion exit slit thicknesses. The dependence is shown in figure 4.17, where the demagnifications for first and second repeller maxima are plotted as a function of the ion exit slit thickness. If it is required to obtain a highly demagnified image, then a source with a thick ion exit slit could be used. Such a source could be used to advantage in mass spectrometers where there is no source resolution-slit. However, for a given accelerating voltage, the maximum efficiency of this source is no larger, because the larger linear demagnification is gained at the expense of the angular demagnification.

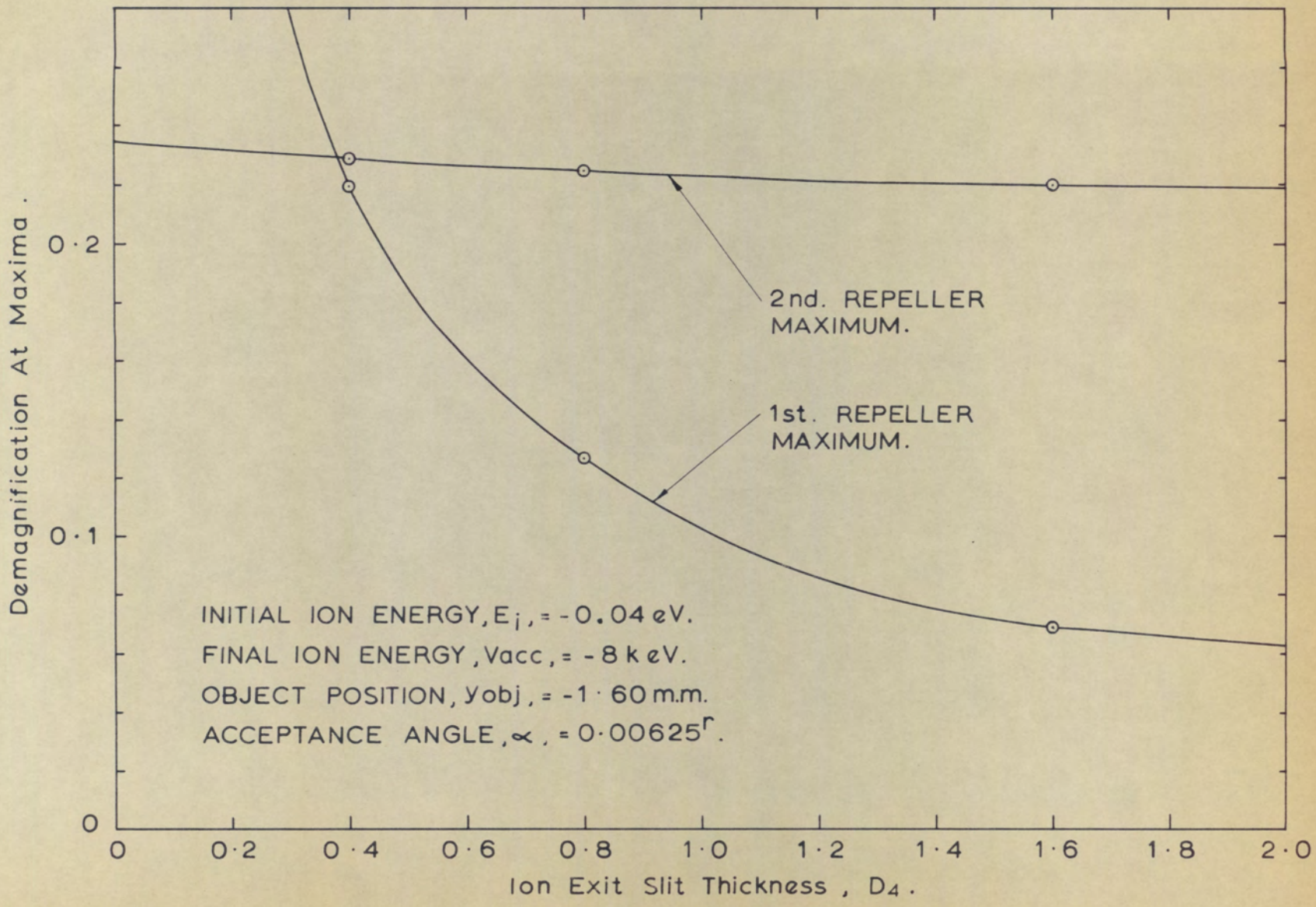

FIGURE 4.17 APPARENT DEMAGNIFICATION, Ma, AT REPELLER MAXIMA AS A FUNCTION OF ION EXIT SLIT THICKNESS, D4, FOR THE M.S.902 E.B. ION SOURCE.

4.3 SOME VARIABLES NOT INCLUDED IN THE COMPUTER ANALYSIS

The computer analysis, as presented so far, has included a number of the more important variables which govern the source performance. In the following sections, some of the variables not included in the computer analysis are considered; thereby, it is possible to determine the way in which they might modify the conclusions already obtained.

4.3.1 Backward-Moving Ions

The ray-tracing part of the program has been particularised for forward moving ions only. Since an ion, at its point of production, may have a velocity in any direction, there will be as many ions initially moving towards the repeller plate ('backward' moving ions), as moving away from the repeller plate ('forward' moving ions). The fate of backward-moving ions in an electron bombardment source may be considered by an approximate analytical method.

It is assumed that the ion of energy E_i, initially starts out from a point A, in a uniform, retarding electric field X, and at an angle α_i to the backward horizontal (figure 4.18 (a)). Since the field is assumed to be uniform, the ion will describe a parabolic path; elementary theory shows that it will cross the point B with the same

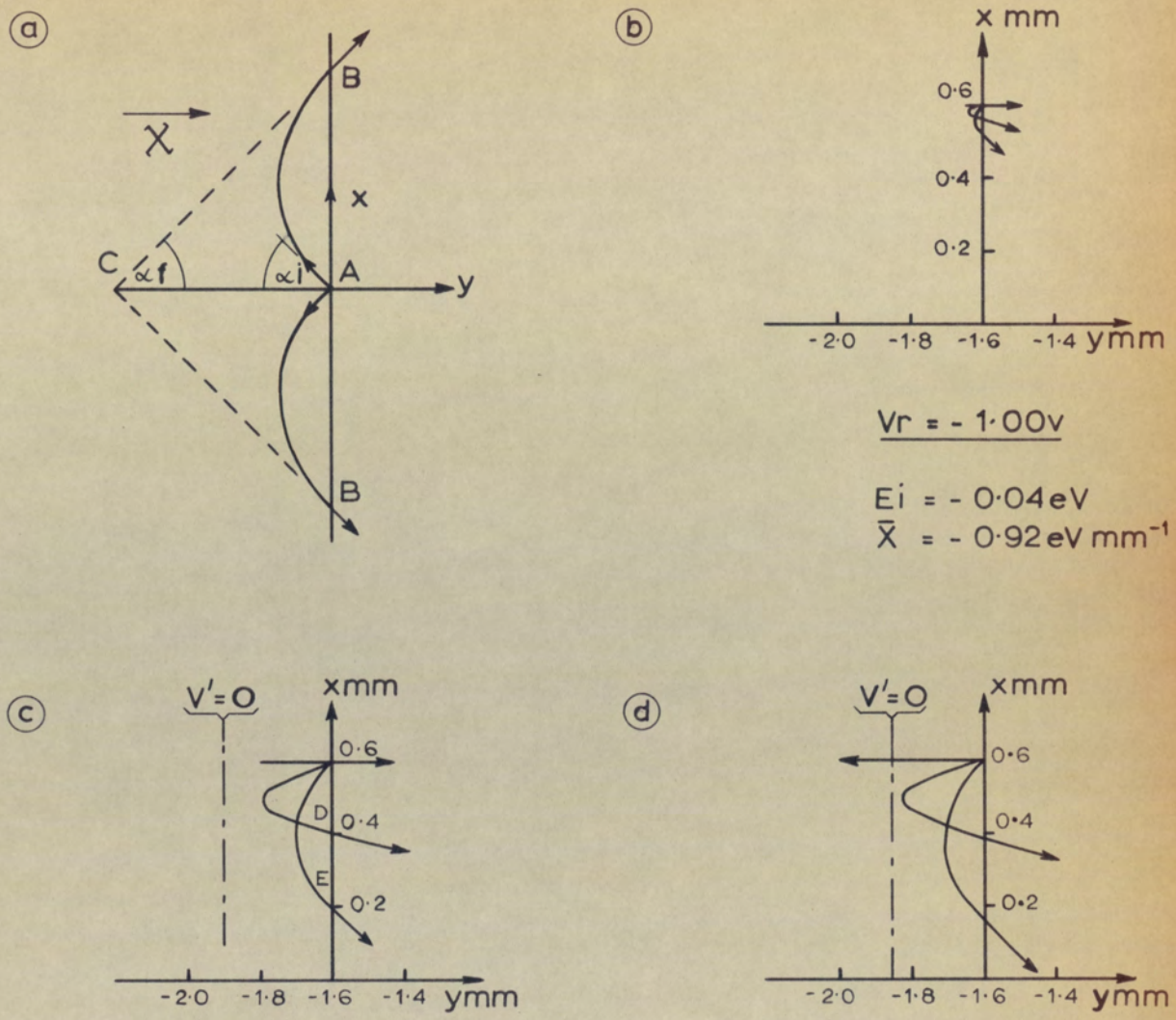

FIGURE 4.18 APPROXIMATE TRAJECTORIES FOR BACKWARD MOVING IONS IN DIFFERENT REPELLER FIELDS.

energy as it had at A, but will be travelling in direction making an angle α_f to the forward horizontal where

$$\alpha_f = \alpha_i$$

It can also be shown that the maximum displacements S_x and S_y in the x and y directions are given, respectively, by the equations:

$$S_x = \frac{2E_i}{X} \sin 2\alpha$$

$$S_y = \frac{E_i}{X} \sin^2\alpha$$

S_x has a maximum when $\alpha = \pi/4$, and S_y has a maximum when $\alpha = \pi/2$.

With this information it is possible to sketch in the approximate paths of ions of initial energy -0.04eV. Figures 4.18 (b), (c) and (d) show such sketches for repeller voltages of -1.00V, -3.12V and -3.20V. In each case ions starting out with initial directions of 45°, 76° and 90° have been given. The fields X have been obtained from the computer print-outs of potential and its derivatives for the appropriate repeller voltage. A field $\bar{X}$ indicates that the field is the mean value over the ion path.

For repeller voltages greater than -1.00V, a wedge of backward-moving ions, with a semi-angle α_i, behaves in exactly the same manner as a similar wedge of forward moving ions, except that the effective starting point of the cone is displaced a small distance back from the real starting point.

For more negative repeller voltages, down to about Vr = -3.12V, the backward-moving ions may still all be withdrawn from the ionization region, although the effective starting point of an ion, D and E, for example, in figure 4.18 (c), is further removed from the true starting point. An ion starting at E will cross the object plane two-thirds of the way down from the top of the object. Thus the effect of the backward-moving ions will be to make the object, and subsequent images, more diffuse. The effect is negligible for $V_r > -1V$, but significant for $V_r \simeq -3V$.

When the repeller voltage is reduced still further to $Vr \leqslant -3.2V$ (figure 4.18 (d)) some backward-moving ions have sufficient energy to surmount the potential barrier, which has its peak at V' = 0 (see broken lines in figures 4.18 (c) and 4.18 (d)). This results in a reduction in the number of ions extracted, and the source efficiency drops.

When $V_r \simeq -4V$ all the backward moving ions are collected by the repeller plate.

Quantitatively, inclusion of the effect of the backward moving ions, results in a repeller curve for which the left-hand side of the peak falls-off more rapidly than in those curves which have been given hitherto. The basic characteristics of the curves are unaltered.

4.3.2 Source Magnetic Field

The electron beam of an electron bombardment source is confined by a magnetic field, whose lines of force are parallel to the path of the electron beam (see figure 2.2). For conventional electron bombardment sources, this field may be between 300 and 500 gauss. Although an ion of mass 100 is almost 200,000 times heavier than an electron, the source magnetic field could be expected to have some effect on the ion trajectory.

Naidu and Westphal (1966 II, p.656) have considered such an effect, and found that even for a magnetic field of 10^4 gauss and a hydrogen ion (M = 1 a.m.u.), the effect is small. Similar conclusions were reached by Reinders, Zilverschoon and Kistemaker (1952) in their analysis of an isotope separator ion source, and also by Ryan and Terry (1965).

It would therefore appear justifiable to ignore the interference of the ion beam by the source magnetic field.

4.3.3 Ion Space-charge

The ion currents emitted from an electron bombardment source do not generally exceed 10^{-9} amps. Typically the ion beam cross-sectional area is 3×10^{-4} cm^2, so that the charge density of the ion beam is usually no more than 3×10^{-6} $A.cm^{-2}$. For electron guns, emission current densities of 5 $A.cm^{-2}$ are often used (Haine, 1961, p.116), but with such beam densities, electron space-charge plays an important part in any subsequent focusing of the beam. For ion guns, where the current densities are a factor of 10^6 smaller, it is unlikely that space charge within the ion beam will cause significant beam spreading.

4.3.4 Electron Space-charge

Since lines of electric force may terminate on the electrons in the electron beam, the presence of the electron beam will alter the potential distribution generated by the slit-aperture system. This problem will be acute when the perveance of the electron beam is close to the maximum perveance, since then the electron beam can be considered to form an electrostatic screen between the main extraction field and the repeller field. The theoretical calculations are difficult, and for this reason the next section considers the problem on an experimental basis.

4.4 Conclusions

Numerical ray tracing through an electron bombardment source analogue can be used to calculate the real and virtual image positions, linear and angular demagnifications and ion residence-time. An approximate analysis yields a theoretical repeller curve displaying the main characteristics of the well-known two-maxima experimental curve. The maxima are shown to result from the presence of one, two or three real images of the ion object, the number present depending on the repeller voltage chosen.

Further ray tracing demonstrates that the source efficiency for any geometry or object plane position, but with a carefully chosen set of voltages on the electrodes is approximately the same, for given initial and final energies. Conversely, it can be concluded that for given voltages on the electrodes, there are relatively few geometries for which this optimum efficiency would be obtained. In each case the optimum efficiency has a value determined principally by the initial and final ion energies. There is therefore no 'optimum' source geometry, which gives higher efficiency than any other source geometry. These are exactly the same conclusions reached by Haine and Einstein (1952) in an experimental study of electron guns, in which brightness was shown to be invariant to filament position and gun geometry, provided that the optimum bias was chosen.

5 - EXPERIMENTAL ANALYSIS OF E.B. ION SOURCES

The theoretical analysis presented so far gives a detailed understanding of the focusing action taking place within the source. In the following sections the overall sensitivity for the mass spectrometer in amps per torr, is calculated and then compared with the experimental value. It is shown that while agreement is good at low electron ionising currents, much higher ion currents and completely different source characteristics, are obtained at high electron currents. Using as a basis the ideas developed in the previous sections, it is shown that this effect is due to the electron space-charge, a factor omitted in the theoretical analysis of sections 2, 3 and 4. Although most of the experimental investigation was carried out with an AEI electron bombardment source on the MS902 mass spectrometer (see photograph opposite), the conclusions obtained will be valid for any Nier-type ion source.

5.1 ION PRODUCTION, AND ION TRANSMISSION AT LOW ELECTRON CURRENTS

In the introductory chapter to this thesis, it was stated that the ion production efficiency of the source and the ion transmission efficiency of the mass spectrometer were each approximately 0.1%. To derive these figures it is necessary to consider the details of the sample inlet system and the ion collector device used in the experimental analysis.

5.1.1 Ionisation Gauge Calibration

Before the sensitivity of the source can be determined, it is necessary to have some means of accurately measuring the pressure in the source ionisation chamber. The Bayard-Alpert (1950) ionisation gauge provided on the mass spectrometer is sited in a flange positioned above the nitrogen cold-trap of the source oil-diffusion pump (see figure 5.1A); the pressure at this point is substantially less than that in the source ionisation chamber. However, the pressure recorded on the gauge will always be a fixed proportion of the true pressure in the source. The simplest way to determine the conversion factor is to calculate first, the pressure rise in the source ionisation region resulting from a measured quantity of sample admitted through an inlet system. This is then compared with the pressure rise noted on the source gauge.

The sample system most used by the organic chemist is the direct insertion probe. To use this, the sample powder under analysis is placed on the quartz or pyrophilite tip of the probe. A system of rough and fine vacuum locks then enables the probe to be easily inserted into the ionisation chamber, where evaporation of the sample can be controlled by the source chamber heaters. However, because the rate of evaporation of the sample is unknown, this method of ion production is unsuitable for the detailed analysis of the source sensitivity. Use was therefore made of the cold inlet system - one of the alternative

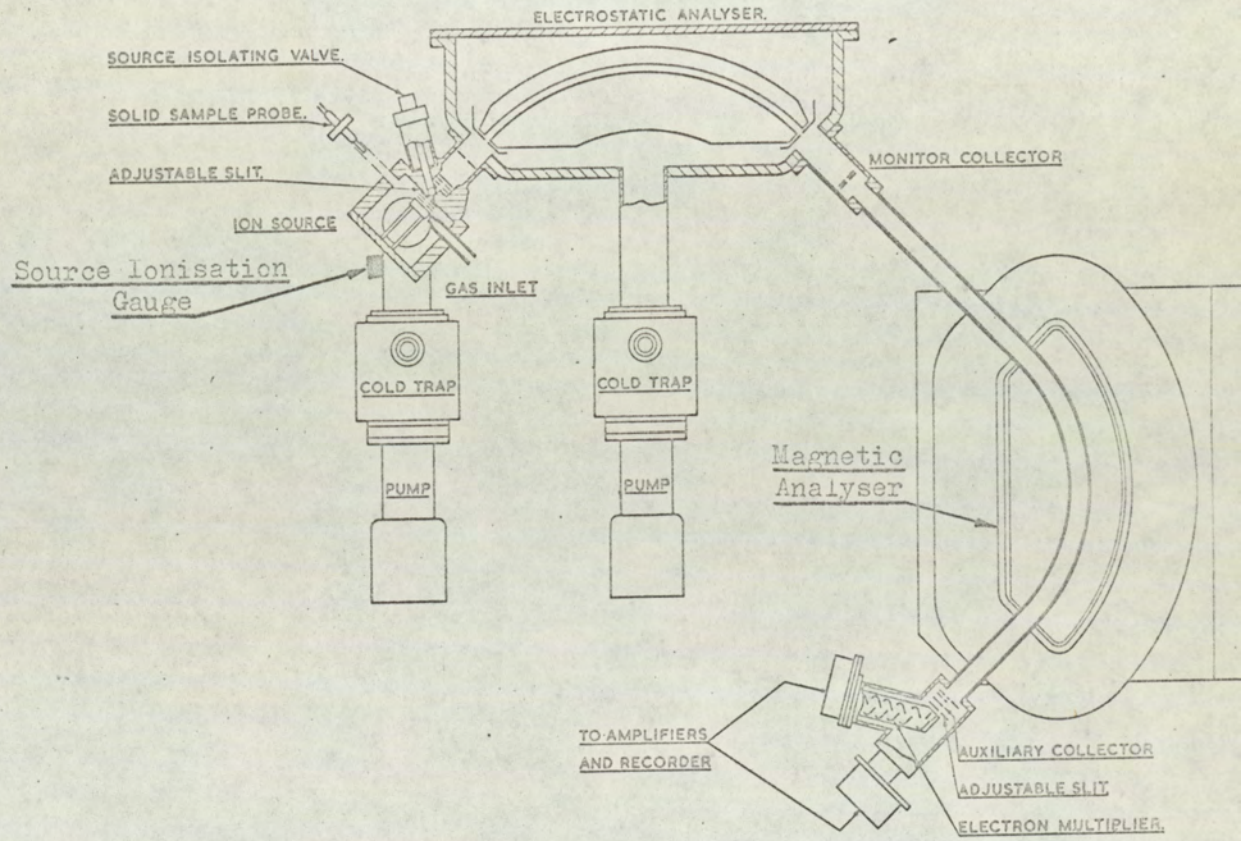

FIGURE 5.1A OVERALL SCHEMATIC OF THE MS902

systems provided on most mass spectrometers. This system, used for samples which are gaseous at room temperature, introduces the sample at a constant rate to the ion source, thereby producing an ion current constant with time. The MS902 cold inlet system is shown diagrammatically in figure 5.1B. It consists of a three-way manifold assembly, a mercury doser, a 2-litre reservoir flask, a standard sintered-glass leak and a two inch oil-diffusion pump.

Therefore, to determine the calibration factor for the ionisation gauge, the sequence of operations required to pass a sample to the source by way of the cold inlet system will be considered. With valve V23 closed and all other valves open, the inlet system is allowed to pump down; valves V22 and V24 are then closed and V23 opened slowly until just over 8 cm of air are registered on the mercury manometer. (This is usually termed 'one dose of air'). When V23 is closed, air will be pumped out through the sinter in the doser until the mercury reservoir level rises to seal it. V43 and V44 are now closed, and V22 opened to allow the 10 cc of air at 80 torr mercury pressure to expand into the two-litre reservoir flask. The pressure, P_F, of the air in the flask will thus be:-

$$P_F = \frac{80 \times 10}{2000} = 0.40 \text{ torr}$$

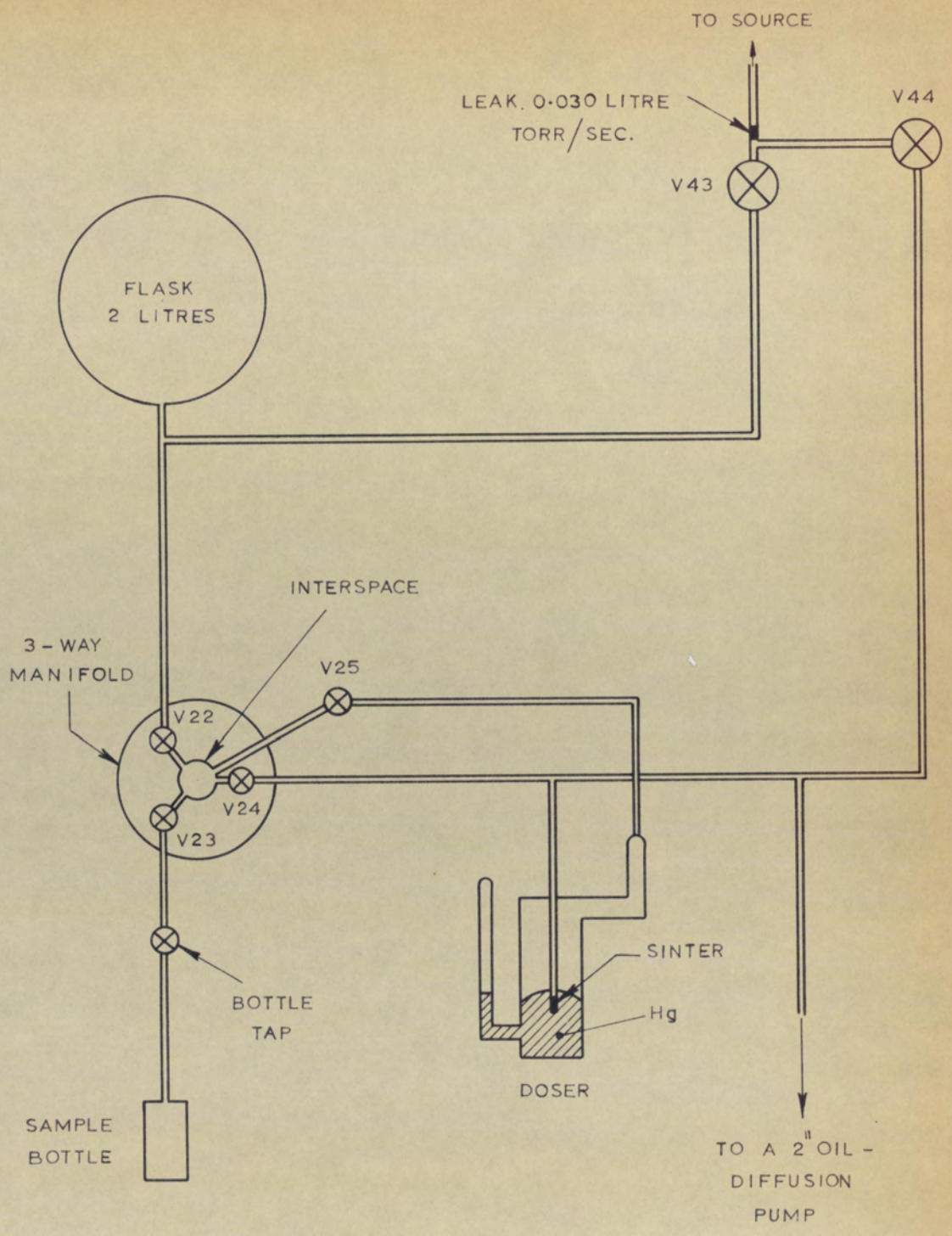

FIGURE 5.1B SCHEMATIC DIAGRAM OF THE COLD INLET SYSTEM.

Valve V43 is opened, and the reservoir gas is allowed to pass to the source through a sintered-glass leak which has a leak-rate of 0.030 litre torr sec^{-1} measured against atmosphere (760 torr). For such a pressure difference, there will be approximately equal portions of viscous flow and molecular flow through the leak. In the cold inlet system, where there is only 0.40 torr pressure difference across the leak, there will only be molecular flow. Thus the quantity of gas per second, Q, passing through the leak will be approximately

$$Q \doteq \frac{0.030 \times 0.40}{2 \times 760} \text{ litre.torr.sec}^{-1}$$

$$\therefore \quad Q \doteq 7.9 \times 10^{-6} \text{ litre.torr.sec.}^{-1}$$

From the leak, the sample gas passes through glass pipework, to the sample inlet port of the ionisation chamber block (see figure 1.6). There is a small gap of about 0".020 between the end of gas inlet-line and the source ionisation chamber, to allow easy removal of the source flange (see figure 5.1A). Merren (private communication), using a retractable inlet-line, has shown that approximately 45% of the sample is lost through this gap. Therefore, the quantity of gas per second flowing into ionisation region is 4.3×10^{-6} litre.torr.sec.$^{-1}$ The volume of gas per second flowing out is 1.4 litre.sec.$^{-1}$ (Banner, private communication), and therefore, from equation (1.3) of section 1,

the resultant gas pressure p in the ionisation chamber is given by:

$$p \approx 4.3 \times 10^{-6}/1.4$$
$$= \underline{3.0\ \mu\tau}$$

The recorded pressure rise on the source ionisation gauge for the same amount of sample (1 dose) is $0.30\mu\tau$, and hence there is a pressure differential of approximately a factor of ten between the source ionisation chamber, and the source ionisation gauge.

5.1.2 Ion Production Efficiency

The ion production efficiency is defined as the ratio of the number of ions per sec, I^+, generated in the source, to the number of molecules per second, Q, flowing into the source ionisation chamber. To calculate Q for a given rate of sample usuage, use is made of the gas equation written in the following form:

$$PV = 1.04 \times 10^{-19}\ nT$$

where P is the pressure in torr exerted by n molecules contained in an enclosure volume Vcc, at a temperature T degrees absolute. Thus at ~~27°C~~ 273°K,

1 litre torr/second ≡ 3.52×10^{19} molecules/second

Now a pressure of 3.0μτ in the source ionisation region is created by a gas flow-rate Q, of 4.3×10^{-6} litre torr/second (section 5.1.1) which, with the use of above equality, can be written as

$$\underline{Q \equiv 1.5 \times 10^{14} \text{ molecules/second}} \qquad \ldots\ldots \qquad (5.1)$$

The number of ions produced from this gas influx may be calculated from the Compton and Van Voorhis equation (1.2) given in section 1. For a 70eV, 500μA electron beam travelling a distance of 1.9 cm through nitrogen ($N = 9.0\ \text{cm}^{-1}\ \tau^{-1}$), the number of ions produced per second will be

$$I^+ = \frac{9.0 \times 500 \times 10^{-6} \times 1.90 \times 3 \times 10^{-6}}{1.60 \times 10^{-19}}$$

$$\therefore \quad \underline{I^+ = 1.6 \times 10^{11} \text{ ions/second}}$$

Thus the ion production efficiency I^+/Q, of the ion source, operating under these conditions, is approximately 0.1%. The ion production efficiency is proportional to the electron ionising current.

5.1.3 Measurement of Ion Current

A plate collector and an electron multiplier collector are usually provided to record the ion current at a given mass. The plate collector is used for calibration of the electron multiplier gain, and for

quantitative ion current measurement. The electron multiplier, placed at a slightly different magnetic analyser radius, is used for high resolving power (H.R.P.) operation in which narrow slits must be used. Gains of up to one million may be used to detect the ion current arriving at the first dynode.

For the present work, wide slits and low resolving powers are quite adequate and so the plate collector has been used, avoiding the necessity of calibrating the multiplier gain. A schematic diagram of the plate collector and its associated amplifier is shown in figure 5.2. Ions reach the plate collector after passing through the collector slit and electron suppressor slit. The latter is at a potential of -85V with respect to the collector slit to repel back to the collector any secondary electrons escaping from it. The collected ion current passes to earth through a 40 kilomegohm resistance, developing across it a voltage which can be amplified by one, to one thousand times in the steps shown in the figure. The output voltage is displayed on a 40V F.S.D. moving-coil meter. With an amplifier gain of times one, a full scale deflection on the meter corresponds to 10^{-9} amp of collected ion current. The smallest current that can be measured on the plate collector system is therefore approximately 10^{-14}A. This is equivalent to the arrival of singly-charged ions at a rate of approximately 10^{5} ions per second.

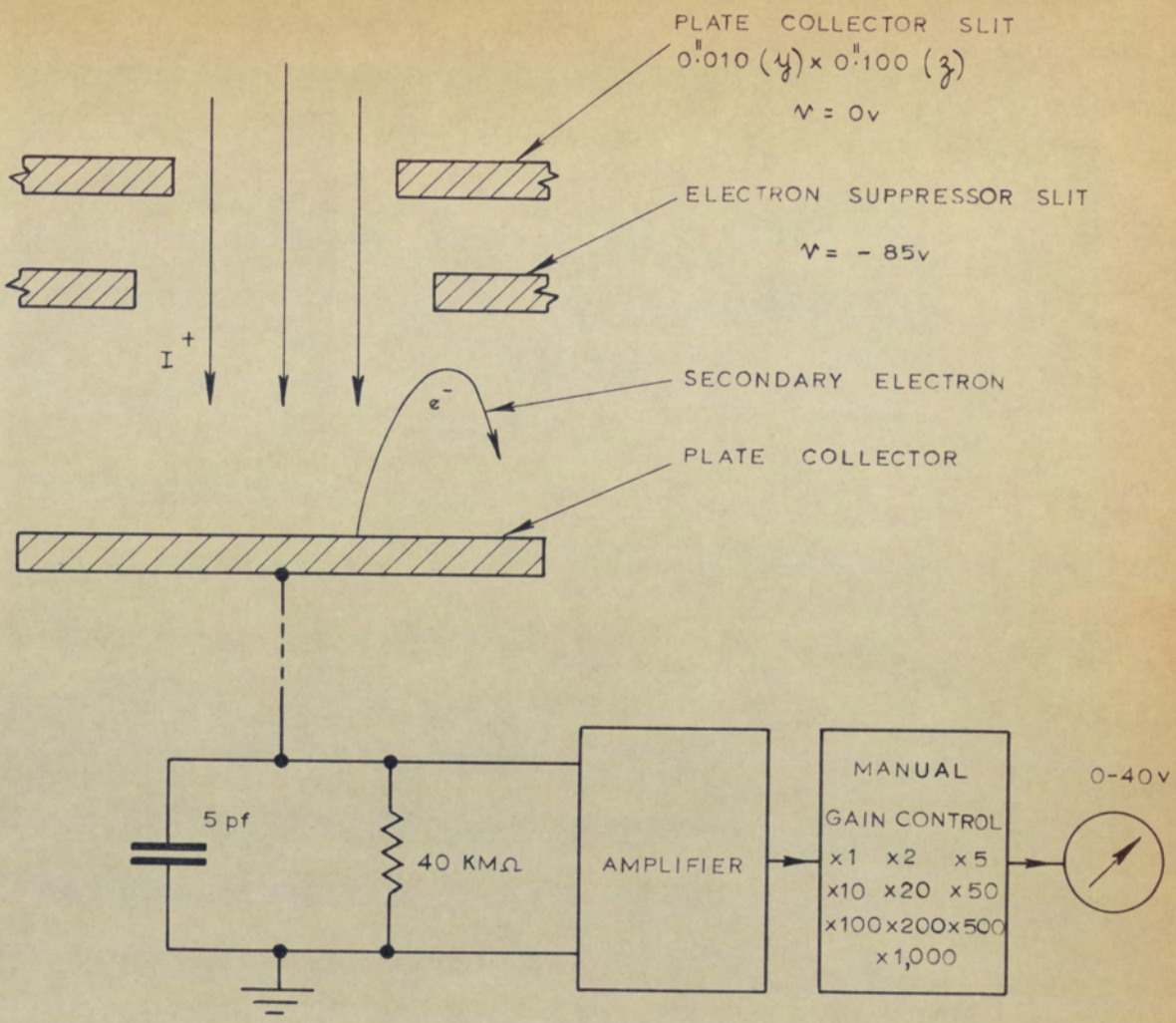

GAIN	COLLECTED ION CURRENT (METER F.S.D.)
x1	10^{-9} A
x 10	10^{-10} A
x100	10^{-11} A
x1000	10^{-12} A

1 'UNIT' = 1/10 F.S.D. ON x 1,000

$\therefore$ 1 UNIT $\equiv 10^{-13}$ A

FIGURE 5.2. ARRANGEMENT FOR DETECTING IONS AT THE LOW RESOLVING POWER ('L.R.P') OR PLATE COLLECTOR.

5.1.4 Ion Transmission Efficiency (Experimental)

The ion transmission efficiency is defined as the ratio of ion current collected at the mass spectrometer collector, to the total ion current produced in the source. Consider an MS902 mass spectrometer with an electron bombardment source operating under the following conditions:

Accelerating Voltage	Vacc	= 8kV
Source temperature	T	= 150°C
Source slit width	Ws	= 0".001
Electron energy	Ve	= 70eV
Source Z-restrictor	Zs	= 0".050
Electron trap current	I_T	= 20μA

First repeller maximum.

For a sample of air introduced to the source, through the cold inlet system, and which causes a pressure rise of 3.0μt in the ionisation region (0.30μt source pressure gauge), the collected molecular nitrogen (m/e = 28) ion current at the plate collector is typically of the order of

$$6.0 \times 10^{-13} A$$

Therefore, the collected ion current per unit pressure rise in the source (the 'sensitivity'), I^+/p is given by the expression:

$$\underline{I^+/p = 2.0 \times 10^{-7} \text{ Amp. Torr}^{-1}} \quad \ldots\ldots \quad (5.2)$$

The ion current I^+, per unit pressure rise p, produced at the electron beam may easily be determined from the Compton and Van Voorhis equation (1.2). For a 70eV, 20μA electron beam travelling a distance of 1.9 cm through nitrogen ($N = 9.0 \text{ cm}^{-1} \text{ T}^{-1}$), I^+/p is given by the equation:

$$I^+/p = 9.0 \times 20 \times 10^{-6} \times 1.9 \text{ Amp. Torr}^{-1}$$

$$\text{or } \underline{I^+/p = 3.4 \times 10^{-4} \text{ Amp. Torr}^{-1}} \quad \ldots\ldots \quad (5.3)$$

From equations (5.2) and (5.3) it may be deduced that the transmission efficiency E_x, of the mass spectrometer from the point of ion production to the plate collector is:

$$\underline{E_x = 0.06\%} \quad \ldots\ldots \quad (5.4)$$

In the next section a comparable figure will be calculated. Use will be made of the ion-optical theory developed in the earlier sections of this thesis.

5.1.5 Ion Transmission Efficiency (Theoretical)

With the MS902 operating under the above conditions, the ion current produced at the electron beam is reduced significantly by loss at three apertures before it reaches the plate collector. Figure 5.3 illustrates the three situations.

When the source operates with 20μA electron current, experiment shows that the ion beam is 0".0079 broad (y) at the source resolution-slit (see figure 5.16). For a 0".001 wide resolution-slit, only 12.6% of the ion beam would be allowed through, as shown in figure 5.3 (A). From figure 4.17 it is seen that the demagnification of the ion optical system at 8kV accelerating voltage is 0.126, and hence the x length of the electron beam, which is also the ion 'object height', is 1.6 mm. This will be termed the 'hot-length' of the filament wire, which physically is 3 mm long.

The angular aperture loss at the point of ion production has already been described in section 4.1.4. Operating at the first repeller maximum, and at 8kV accelerating voltage, the acceptance wedge is 39° for forward-moving ions and has a value of between 20° and 39° for backward-moving ions (see figure 5.3 (B)). To estimate the acceptance wedge for backward-moving ions, use has been made of the calculations in section 4.3.1., and in addition it has been assumed that all of the

(A) Loss by Resolution Slit.

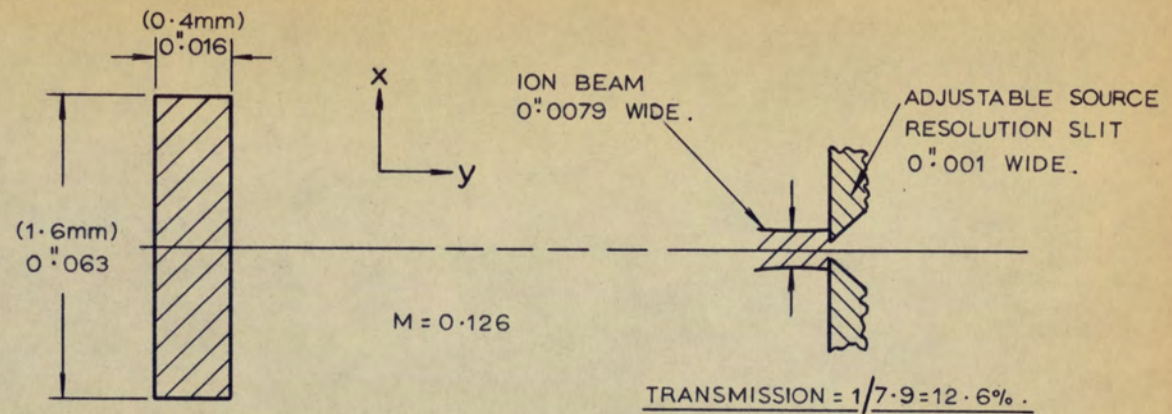

TRANSMISSION = 1/7·9 = 12·6%.

(B) Loss by Angular Aperture.

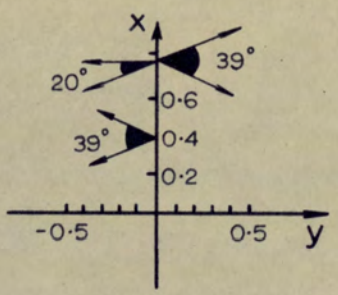

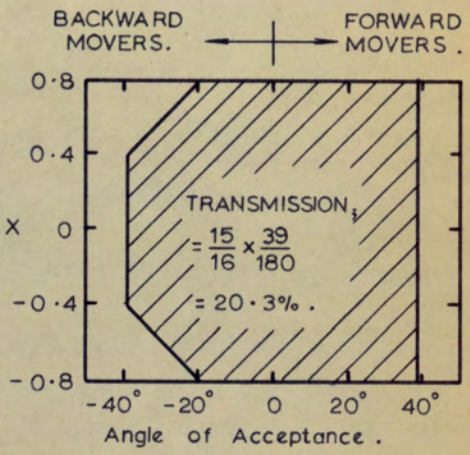

(C) Loss by Z Collimation.

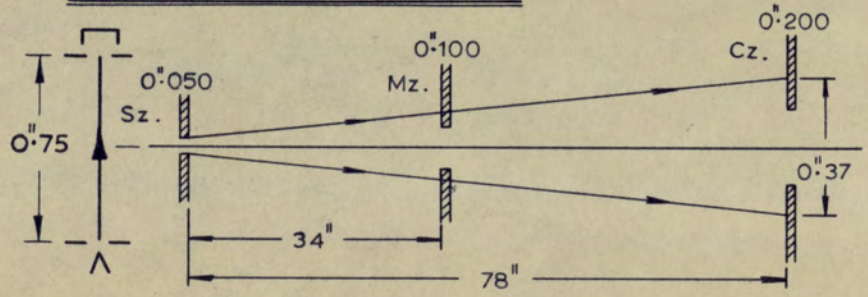

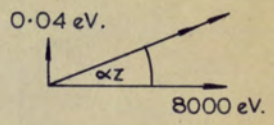

$$\alpha_z = \sqrt{\frac{0.04}{8000}}$$

$$= 0.00224^{r}.$$

TRANSMISSION = 0·2/0·37 = 54%.

FIGURE 5.3. THREE FACTORS CAUSING LOSS IN TRANSMISSION IN THE MS 902 MASS SPECTROMETER AT LOW TRAP CURRENTS (0–20μA.).

transmitted backward-moving ions cross the x-axis within the limits $x = \pm 0.8$ mm; this corresponds to the length of the hot part of the filament. Since an ion is assumed to have an equal probability of moving off in any direction (see section 3.3) the angular transmission is 20.3% (figure 5.3 (B).

A further consequence of random initial direction of the ions is that a large number of ions will have a significant Z velocity. As there is no Z-focusing in the mass spectrometer system, the problem is to consider the drift path of an ion with 0.04eV Z-energy. Figure 5.3 (C) shows the relevant Z apertures in the MS902 mass spectrometer. Half an inch away from the electron beam is the source z-restrictor, Sz, of aperture 0".050. The other Z-apertures are the monitor aperture (0".100) 34" from the source, and the collector aperture (0".200) 78" from the source. For an ion with 8kV forward energy, the angle of deviation between its path and the axis is $(0.04/8000)^{\frac{1}{2}} = 0.00224^{r}$. This results in a 0".37 beam spread at the collector and 54% transmission through the collector slit. A more significant loss of ions occurs at the source Z-restrictor; of the ions produced along the 0".750 long electron beam, no more than a 0".050 long segment of ions passes through the restrictor (figure 5.3C). Thus the overall transmission through the Z-apertures of the mass spectrometer is 54/15 = 3.6%.

A small amount of ion loss occurs as a result of the finite width of the electron beam; at a given repeller voltage, the acceptance wedge for ions leaving the centre of the electron beam is larger than that for ions leaving the front or the back of the electron beam. This is examplified by the repeller curves shown in figure 4.11. The ion loss resulting from this cause is approximately $7\frac{1}{2}\%$.

The overall ion transmission for the mass spectrometer E_{TH}, is the product of these individual ion transmissions. Thus:

$$E_{TH} = 0.126 \times 0.203 \times 0.036 \times 0.925 \times 100$$

or $\underline{E_{TH} = 0.085\%}$

This is in good agreement with the experimental value of efficiency of 0.06%. The difference between the two estimates is probably the result of the combined effects of the experimental error in E_x, and the approximations made in the theoretical treatment for deriving E_{TH}.

At high ionising electron currents ($\gtrsim 500\mu A$), the ion transmission efficiency increases by at least a factor of ten. The details of this phenomenon will be described in section 5.2.

5.1.6 Summary and Conclusions

The true pressure in the ionisation chamber of the MS902 electron bombardment source is approximately ten times that recorded on the source ionisation gauge.

At 500μA electron current, the ion production efficiency - defined as the ratio of the number of ions per sec generated in the source to the number of molecules per second flowing into the ionisation chamber - is approximately 0.1%. Ion production efficiency is proportional to the ionising electron current.

At low ionising electron currents ($\leq$ 20μA), the ion transmission efficiency - defined as the ratio of the ion current collected at the mass spectrometer collector to the total ion current produced in the source - has an experimentally determined value of 0.06%. The theoretical value is 0.085%. The agreement between the two is good; the difference probably results from the combined effects of experimental error, and the approximations made in the theoretical treatment. The theoretical analysis shows that the overall ion loss results from losses at the apertures listed below:

	Transmission
(a) y-aperture (resolution slit)	12.6%
(b) y-angular aperture (alpha slit)	20.3%

	Transmission
(c) Z-angular aperture	54.0%
(d) Z-aperture (source Z-restrictor)	3.6%
(e) Finite width of the electron beam	92.5%

Although the ion transmission is constant at low electron currents, it increases by more than a factor of ten at high electron currents ($\gtrsim$ 500uA). The details of this phenomenon will be described in the next sections.

5.2 EFFECTS OF ELECTRON SPACE-CHARGE

5.2.1 Introduction

As the ionising electron current in an electron bombardment source is increased from 20 to 500μA, the ion current arriving at the mass spectrometer collector (hereafter called 'collected ion current'), frequently increases at a far greater rate than expected. A typical experimental curve is given in Figure 5.4, where the collected ion current is given as a function of electron trap current. The initial rise in collected current is 3.0×10^{-13}A per 10μA of electron current, but after a transition region situated between 20 and 500μA, the rise is 30×10^{-13}A per 10μA of electron current, and this increase continues to at least 2 m.a. electron trap current (the largest current obtainable from the filament power supply used by the author).

The Compton and Van Voorhis equation (1.2) indicates that the number of ions produced in the ionisation region is proportional to the electron current. Now, since the ion transmission efficiency should be independent of electron current, the collected ion current should also be proportional to the ionising electron current. However, in practice, this is not the case, and in the following analysis it will be shown that the effect is attributable to the properties of electron space-charge. Overall ion transmission, and collected ion current increase, because a greater

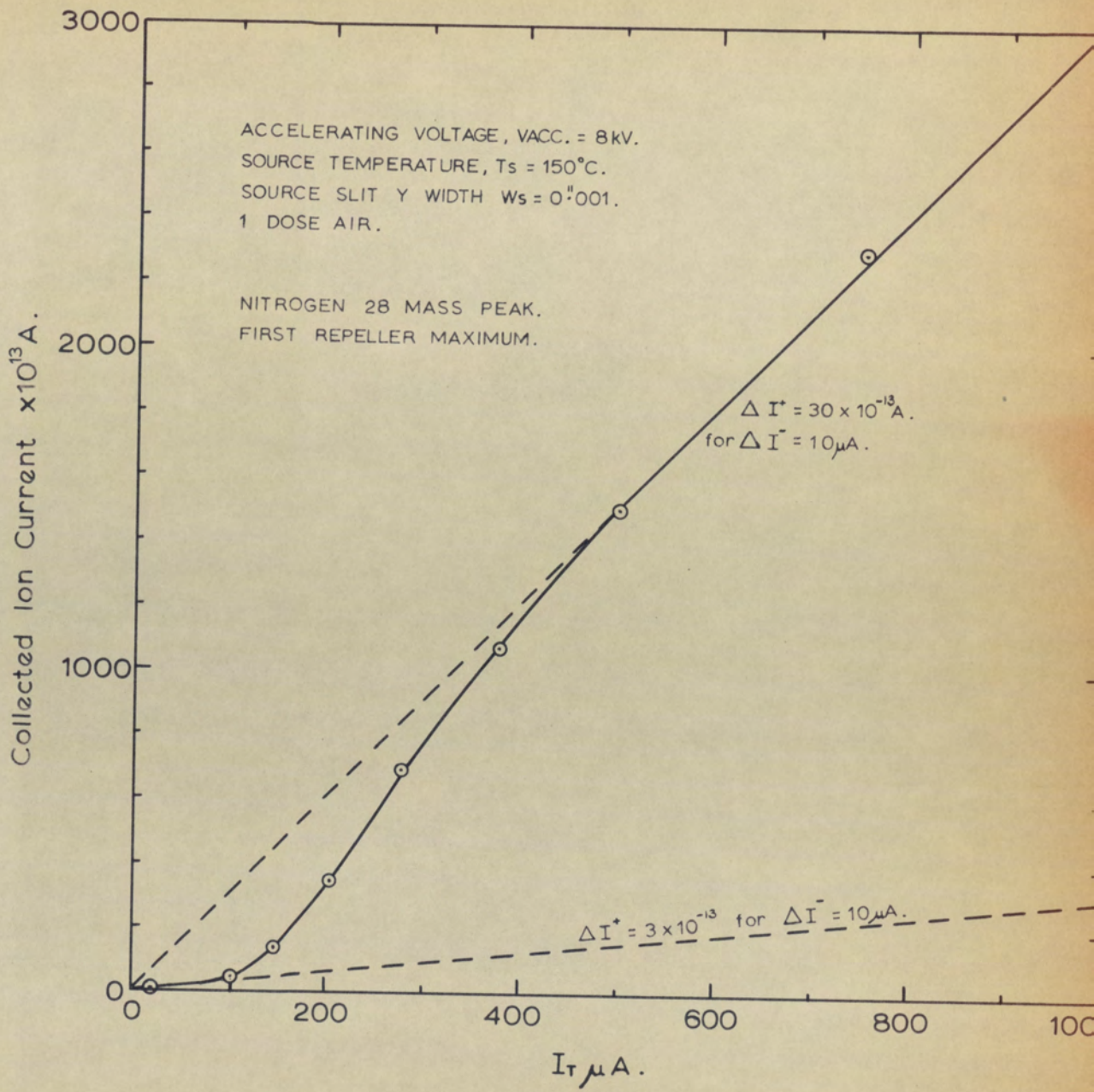

FIGURE 5.4 COLLECTED ION CURRENT AS A FUNCTION OF ELECTRON TRAP CURRENT FOR THE MS 902 e.b. ION SOURCE.

proportion of the ions produced is able to pass through each of the limiting apertures of the mass spectrometer.

Many other characteristics of the source also change with increasing electron current. Figure 5.5 shows the change which occurs in the shape and position of the conventional repeller curve, when the electron trap current is changed from 20μA to 500μA.

For the purposes of comparison, the collected ion currents given in the following sections have been normalised; under the following conditions:

(a) Accelerating Voltage, Vacc = 8kV
(b) Source Temperature, Ts = 150°C
(c) Source Slit Y-width, Ws = 0".001
(d) A sample of air giving a pressure rise of 0.3μτ on the source pressure gauge (1 dose),

and all other controls optimised, the collected nitrogen 28 ion current has been normalised to 1500 x 10^{-13}A, for an electron trap current of 500μA. In practice this figure varied between 1200 and 1800 x 10^{-13}A, the variation resulting mainly from the imprecision in setting up the width of the adjustable source-slit, and in obtaining a given pressure of Nitrogen in the ion chamber. Similarly, the collected Nitrogen 28

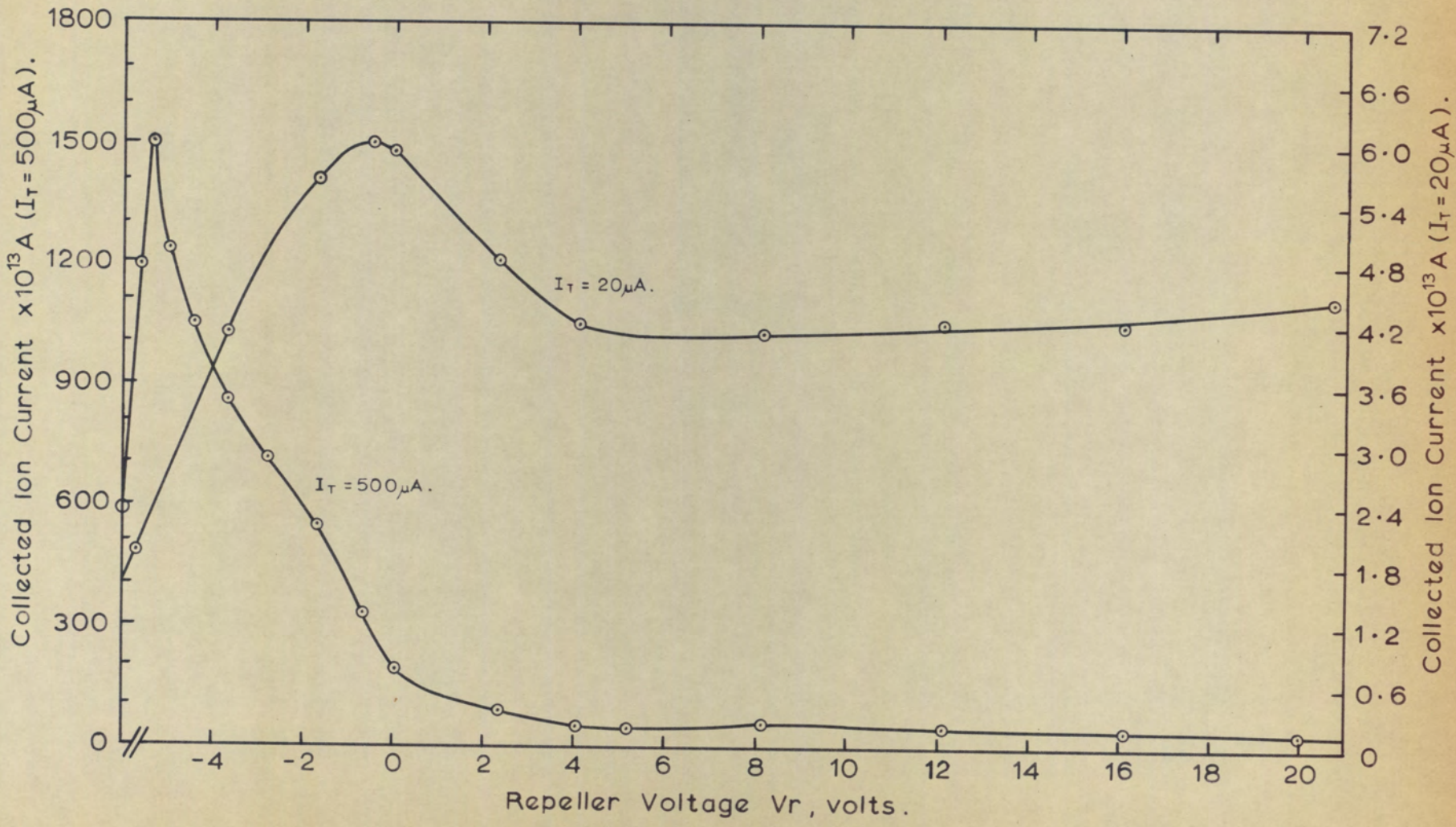

FIGURE 5.5

REPELLER CURVES AT LOW AND HIGH ELECTRON TRAP CURRENT OPERATION.

ion current at 10μA electron current and 70eV electron energy under the above conditions is normalised to 3.0×10^{-13}A, although the actual value was usually in the range 2.4 to 3.6×10^{-13}A.

In the following sections, the origins of the greatly increased collected ion current are deduced by comparing and contrasting the characteristics of the source at high and low electron currents.

5.2.2 Electron-node Formation

The electron beam of an electron bombardment ion source is confined by a magnetic field created by permanent magnets, placed at either end of the source ionisation chamber (see figure 2.2). The magnetic field embraces the accelerating region, drift region and collection region of the electron beam, and so the system is of the "immersed flow" type (Brewer, 1967, p.81). For this type of flow, each electron will rotate about a particular line of magnetic flux, rather than about the axis of symmetry of the gun, as happens in the case of "Brillouin flow". In the study of electron beams in ion sources, the real interest is in the overall shape of the electron beam rather than in the trajectories of individual electrons. The electron beam will be "scalloped", the amount of scalloping depending on the initial electron velocities perpendicular to the magnetic field, and also on the strength of the field (Herrmann, 1958). Figure 5.6a shows a diagram of the beam scalloping which would

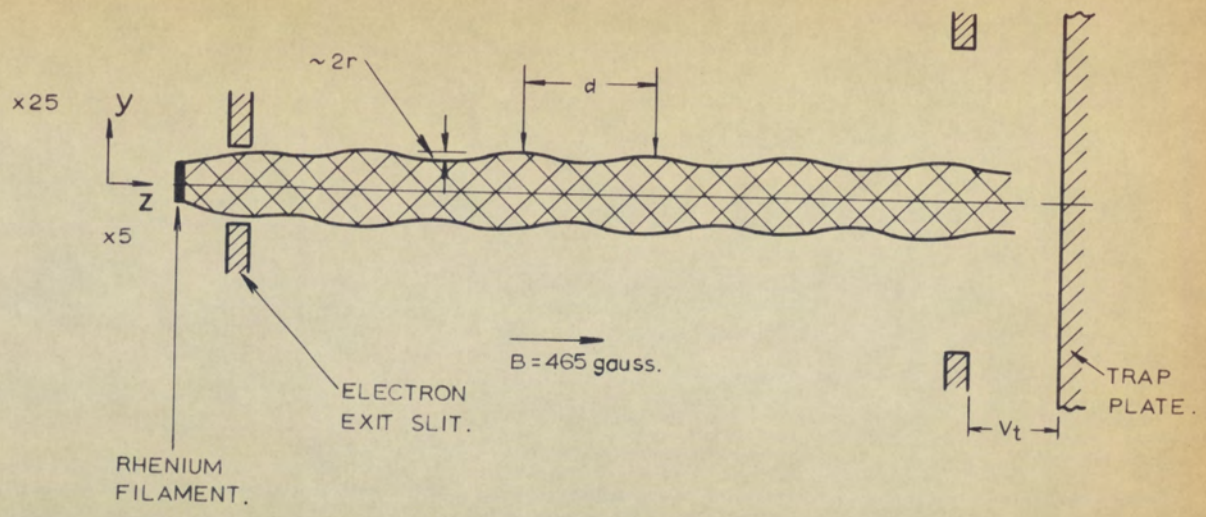

FIGURE 5.6 a). SCALLOPPING OF THE ELECTRON BEAM UNDER IMMERSED FLOW CONDITIONS.

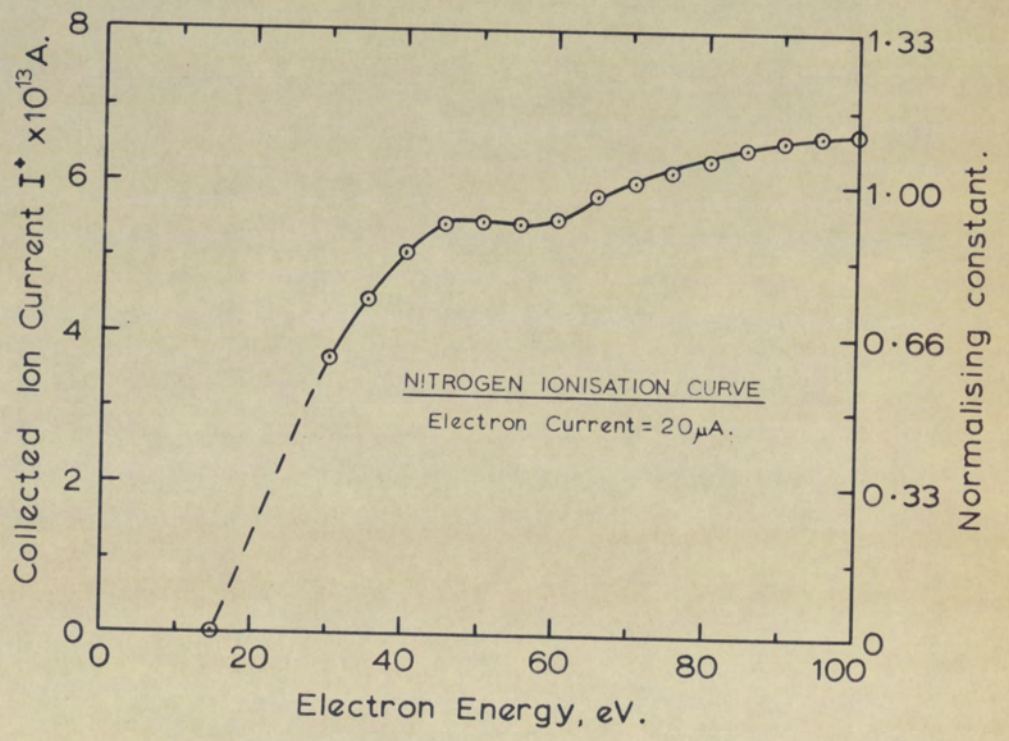

FIGURE 5.6 b). COLLECTED ION CURRENT AS A FUNCTION OF ELECTRON ENERGY FOR AN ELECTRON CURRENT OF 20μA.

be expected to occur in the MS902 electron bombardment source for a 70eV (= Ve) energy beam with a 465 gauss confining field (= B). Nodes are separated by a distance d where

$$d = 21.19 \frac{(V)^{\frac{1}{2}}}{B} \text{ cms.} \qquad \ldots\ldots \qquad (5.5)$$

and therefore, $d = 0.38$ cm.

Each electron with an energy $V_\perp$ (eV) perpendicular to the lines of force will perform a circular motion about a line of force with circle radius, r, given by the expression

$$r = 3.37 \frac{(V_\perp)^{\frac{1}{2}}}{B} \text{ cm.} \qquad \ldots\ldots \qquad (5.6)$$

For $V_\perp = 0.20$eV (2048°C), r = 0.034 mm. The depth of the scallops in the electron beam therefore will be approximately 0.07 mm as shown in figure 5.6A. (Note: equations 5.5 and 5.6 are derived in Appendix V).

It is conventional to electronically stabilise the filament current supply in such a way that a constant electron trap-current is obtained. However, because the cross-sectional area of the electron beam is not constant, the percentage of electron current passing through the trap restricting-plate (T_p in figure 1.5), varies as the electron energy varies. Therefore, if electron trap-current is to be maintained constant, a change of electron energy will result in a small change in the total current passing across the ionisation region. This causes fine structure on 'ionisation curves' - curves of collected ion current as a function of electron bombarding energy - as has been demonstrated by Flesch and Svec (1966) and by Henderson, Riley and Sedgwick (1966).

Figure 5.6B shows the ionisation curve obtained on the MS902 electron bombardment source with an electron trap-current of 20μA. This should be compared with the correct ionisation curve for nitrogen obtained by Compton and Van Voorhis (1925, 1926), as shown in figure 1.4. The ripple occuring at 50eV on the curve obtained on the mass spectrometer (figure 5.6B) is caused by the afore-mentioned effect. The curve will not be examined in more detail, as it has been adequately treated in the literature cited above.

5.2.3 Ionisation Curve at High Electron Currents

At high electron trap-currents ($\gtrsim 500\mu A$), the ionisation curve is considerably different to that at low electron trap currents ($\lesssim 20\mu A$). To examine the fine structure of a $500\mu A$ curve, for example, it is convenient to first eliminate the voltage-dependent ionisation efficiency and the ripples apparent on the $20\mu A$ curve. This is achieved by dividing each point on the $500\mu A$ curve by the value of the "normalising constant" for the corresponding electron energy on the $20\mu A$ curve. The normalising constant, shown on the right-hand ordinate of figure 5.6B, is itself derived by normalising the ion current values to the value at 70eV.

Figure 5.7 shows a Nitrogen ionisation curve at $500\mu A$ electron trap-current normalised in such a manner. The corresponding $20\mu A$ curve, taken on the same source and mass spectrometer immediately after the $500\mu A$ curve, is that already shown in figure 5.6B. From the $500\mu A$ electron current curve, it is seen that the normalised ion current exhibits a strong dependence on the electron energy. The periodicity suggests that the structure is, in some way, connected with the scalloped structure of the electron beam.

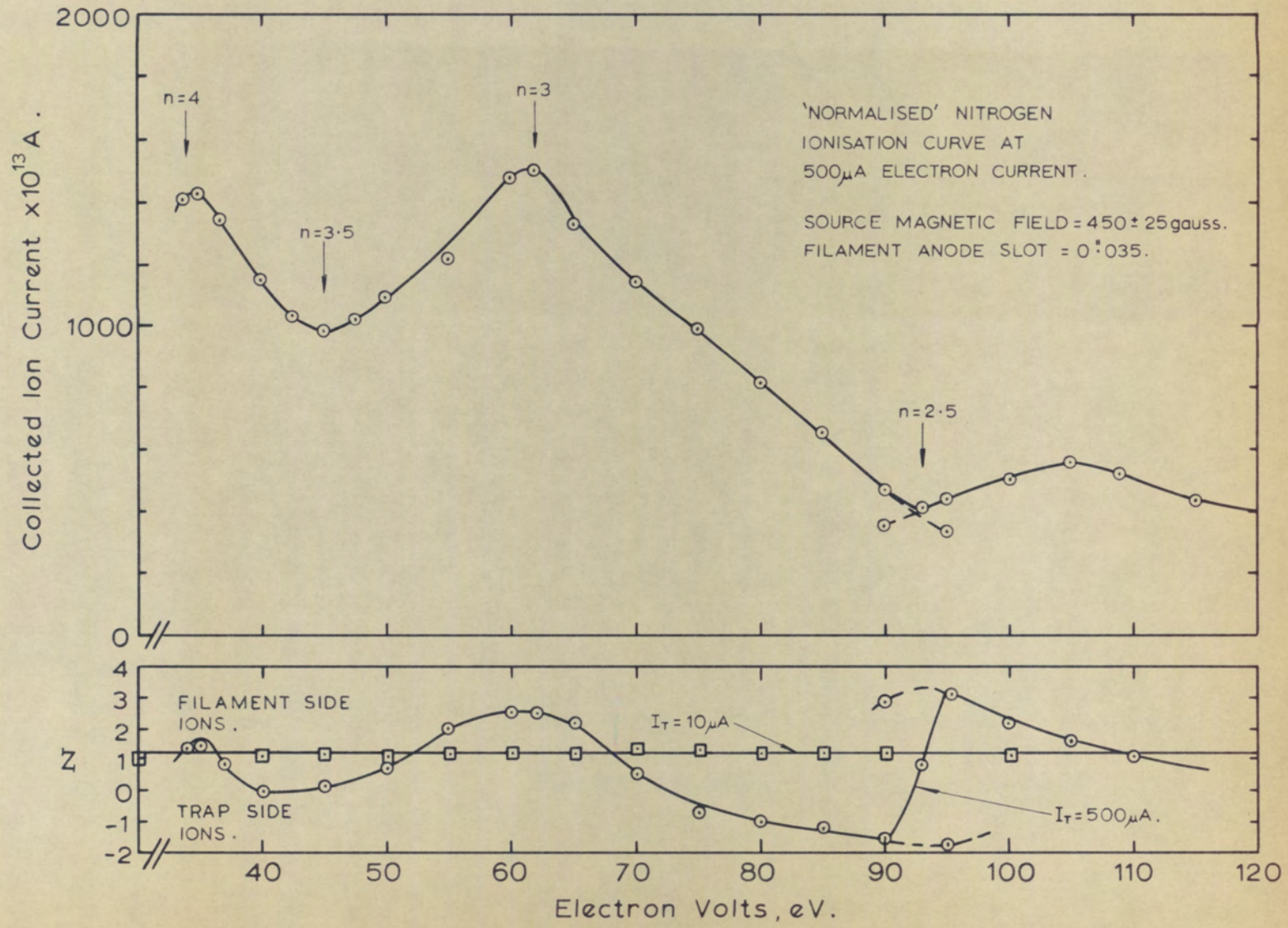

FIGURE 5.7 'NORMALISED' ION CURRENT AND CORRESPONDING Z DEFLECTOR VALUES AS A FUNCTION OF ELECTRON ENERGY, eV, FOR THE MS902 e.b. ION SOURCE.

An approximate analysis of the electron gun, using the computer program described in section 2 and 3, has shown that the apparent image of the filament is formed at between 0.1 to 0.2 mm in front of the filament, for all accelerating voltages between 30 and 100eV. The distance between this first image, and the centre-line of the source, is therefore (11.2 ± 0.5) mms, allowing for the imprecision in setting up the filament.

Assuming that electron image-formation is responsible for the maxima and minima of the 500μA curve, then by using equation 5.5 it can be shown that for each turning-point of the curve in figure 5.7, there are a complete number of half-nodes $2n_t$, formed between the first image and the centre-line of the source. The results are presented below in tabular form,

Ve (±1V)	d mm	n_{calc}	n_t
93.0	4.54	2.46	2.5
62.5	3.72	3.01	3.0
45.0	3.16	3.54	3.5
34.0	2.74	4.09	4.0

where $n_{calc} = 11.2/d$. There is a random error of 1 v. in each voltage measurement, while every 'n' value may have the same systematic

error of up to 8%, resulting from the uncertainties in the values of the magnetic field, and the distance between the first image and the centre-line of the source. There is good agreement between n_{calc} and n_t. Figure 5.8 gives diagrammatically the nodal patterns for the four voltages in question. The nodes ('images') are represented by the dark circles; the first node is situated on the left-hand side, just in front of the filament, and the last node just to the left of the trap collector-plate.

A control which requires adjustment when the electron current is changed, is the one provided to correct for misalignments of the mass spectrometer system in the non-focusing Z-direction. Correction is achieved by applying a potential difference between a pair of deflecting plates situated between the source resolution-slit and the electrostatic analyser (e.s.a.) plates (see figure 1.3A). This Z-deflecting system ~~could~~ can also be used to re-align ion beams which have a Z-component of velocity. The lower graph on figure 5.7 shows the Z-deflecting field (in arbitrary units) required for maximum ion current, as a function of the electron accelerating voltage; curves for 10μA and 500μA electron trap current are shown. It is seen that the Z-deflecting field for the low electron current is at a fixed value of +1.2 and is independent of the electron energy. It is reasonable to suppose that this is the field required to overcome the permanent Z-misalignment of the mass spectrometer system.

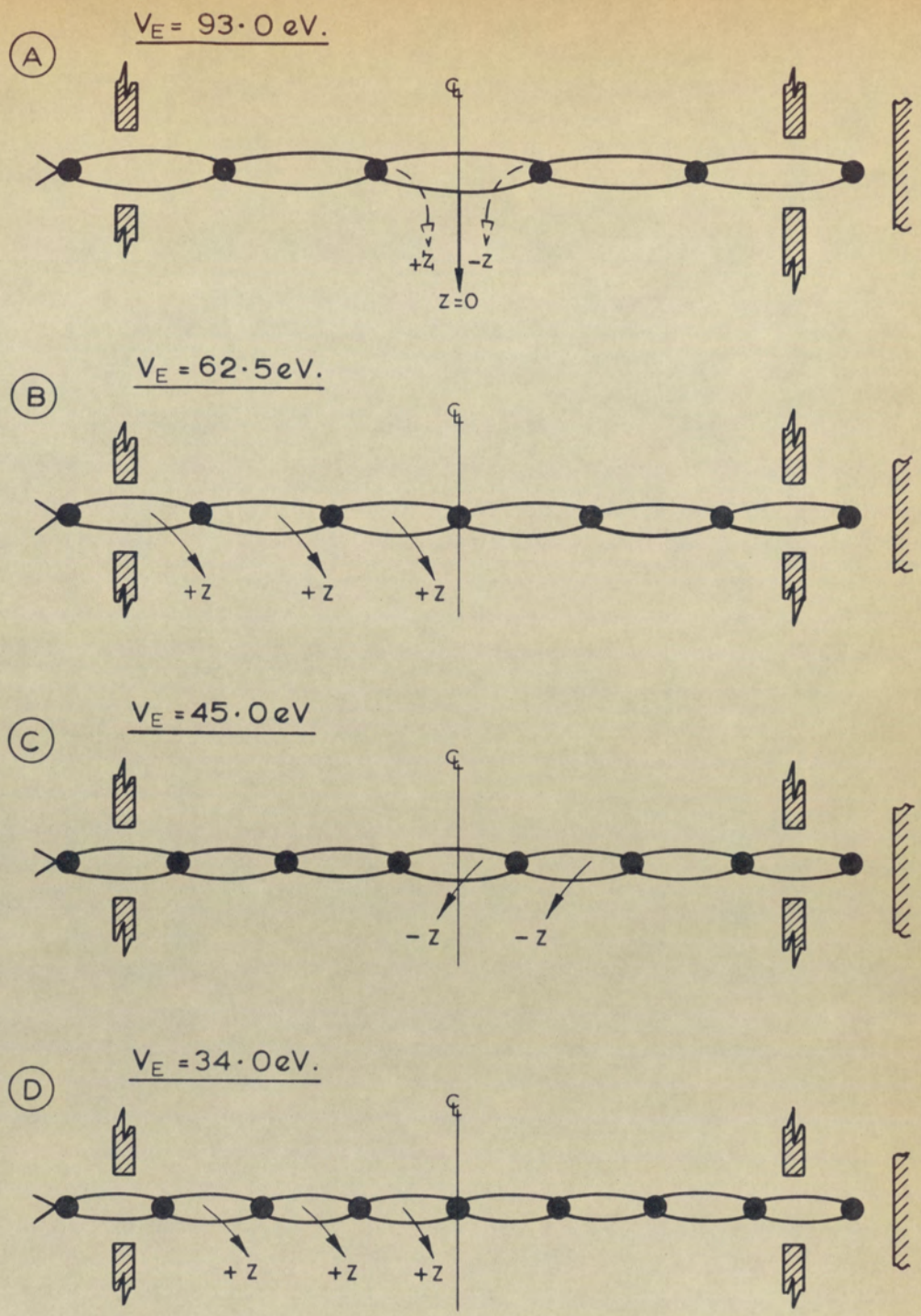

FIGURE 5.8 ELECTRON BEAM NODE DIAGRAMS FOR ION CURRENT MAXIMA AND MINIMA.

However, the 500μA optimum Z-curve shows considerable variation in sympathy with the variations in the ion current curve shown just above it. Furthermore, this Z-curve oscillates about the 20μA Z-curve, indicating that at high trap currents the total field required across the Z-deflecting plates is the sum of the cross-field required to correct system Z-misalignment, and that needed to correct for Z-velocity. For the mass spectrometer used in these experiments, a positive field corrects for ions with a Z-velocity in the filament-to-trap direction; a negative field corrects for ions with velocities in the opposite direction. Thus at the maxima in ion current, the ions emerge from the electron beam with a velocity in a direction from the filament to trap. Since the electron space-charge forces will be weakest at the electron beam antinodes, the ions will emerge at these points. The 62.5 and 34eV diagrams in figure 5.8 show possible paths (diagrammatic only) for ions emerging from the electron beam.

At the 45eV minimum, the ions emerge with the opposite Z velocity, and the possible ion paths are shown in (C) of figure 5.8. The minimum at 93eV is a special case, for it is to be noted that two maxima in ion current occur at opposite polarity Z-fields (see figure 5.7). For voltages less than 93eV, the ions are more easily extracted from the trap-side, while for voltages more than 93eV, filament-side ions escape more easily. When the true minimum is reached, an antinode is exactly on the centre-line of the system and ions emerge with zero Z-velocity (Z = +1.2). The appropriate paths are shown in figure 5.8 (A). A similar 'cross-over' situation was not observed for the 45eV minimum.

It is logical to correlate the ion currents obtained at maxima and minima to the number of antinodes, N, from which ions emerge. Thus, if it is postulated that the ion current per antinode is 500×10^{-13}A, then the 93eV minimum in ion current results from ions emerging from one antinode; the 62.5eV maximum, the sum from three antinodes; the 45eV minimum from two antinodes, and the 34eV maximum from three antinodes. The experimental and theoretical values are compared in the table below. The agreement is good.

Ve	N	I_+ (Theor)	I_+ (Expt)
93.0	1	500	400
62.5	3	1500	1500
45.0	2	1000	980
34.0	3	1500	1400

5.2.4 Space-Charge Barrier

The presence of electron space-charge in an electron beam reduces the potential at the centre of the beam relative to the potential at the perimeter, and a potential well is formed. For magnetically-confined electron beams, larger electron current-densities will cause larger

potential depressions in the electron beam, until the point of space-charge collapse is reached (Brewer, 1967). If ions created near the centre of the electron beam are to be extracted, it is necessary to distort the potential well with external electrostatic fields; use of larger electron current-densities will require greater extraction fields.

Figure 5.9 shows the collected ion current as a function of the mean beam-centring voltage ratio, $R = V_{foc}/V_{acc}$, for low (10μA) and high (500μA) electron currents. For each value of R the repeller voltage has been set for maximum ion current. It is seen that to maintain maximum sensitivity, when changing from low to high electron current, a decrease of the mean beam-centring voltage ratio is required. This has the effect of increasing the proportion of accelerating field leaking into the ionisation chamber, thereby giving an increased extraction field at the electron beam.

To obtain more precise information on the magnitude of the space-charge potential depression, the results presented in figure 5.10 were experimentally obtained. The mean beam-centring voltage required for maximum sensitivity, is plotted as a function of the reciprocal of the accelerating voltage, for several values of electron ionising current. For a given electron current, it was found that the repeller voltage could be kept constant without loøsing more than a few percent of the ion current.

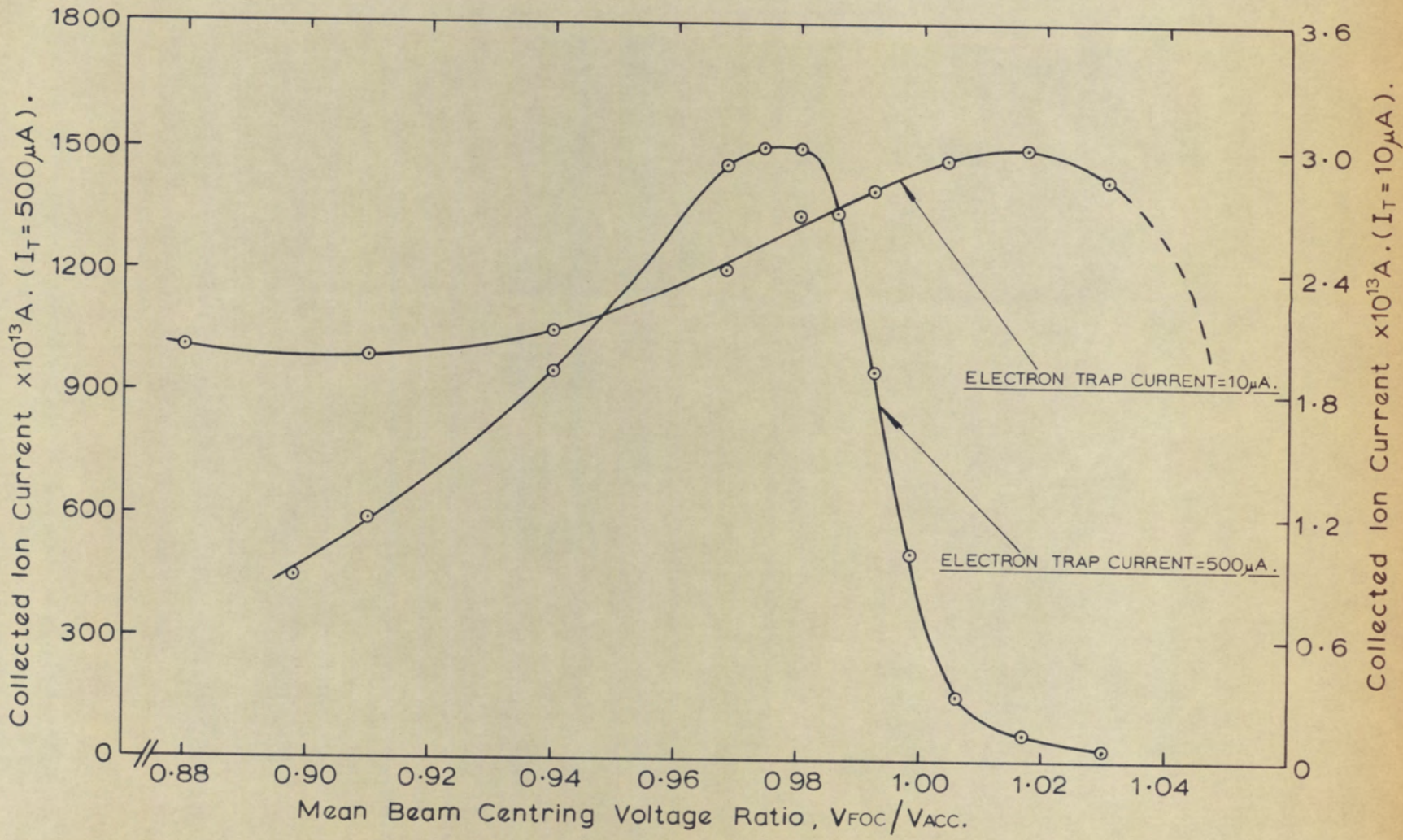

FIGURE 5.9 ION CURRENT AS A FUNCTION OF MEAN BEAM CENTRING VOLTAGE RATIO FOR LOW AND HIGH ELECTRON TRAP CURRENTS.

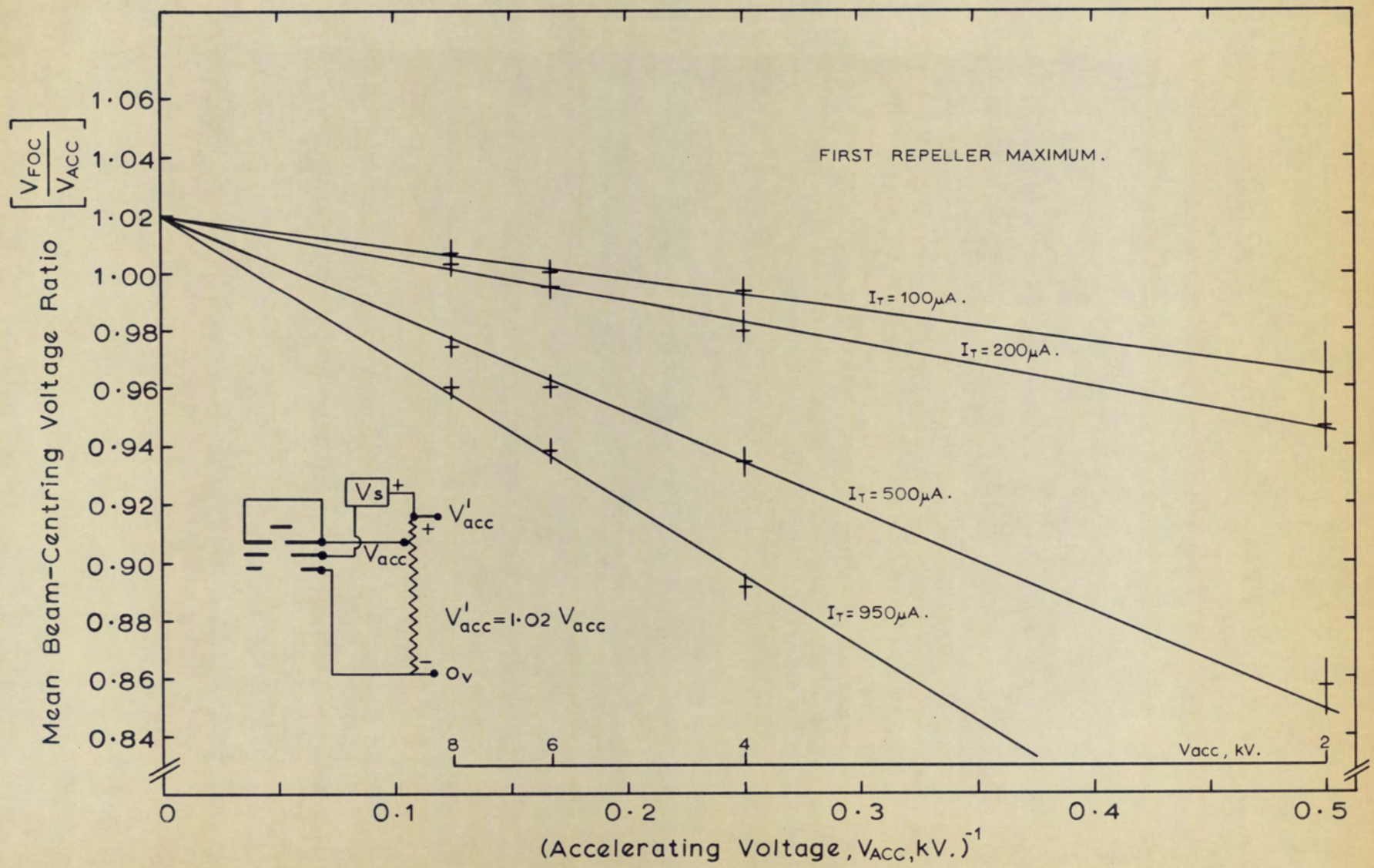

FIGURE 5.10 MEAN BEAM-CENTRING VOLTAGE FOR MAXIMUM SENSITIVITY AS A FUNCTION OF THE RECIPROCAL OF THE ACCELERATING VOLTAGE.

Each curve is, to within the experimental error, a straight line, with each line passing through the same point R = 1.02 of the ordinate axis. Therefore, each line obeys an equation of the form:

$$R = \frac{V_{foc}}{V_{acc}} = \frac{V_s}{V_{acc}} + 1.02$$

where V_s is a constant, dependent on the electron current and having the dimension of voltage; it is independent of accelerating voltage. Therefore, the source will operate at optimum sensitivity provided that the mean of the voltages provided on the beam-centring plates has a value given by the above equation. This can be achieved by supplying the voltages to the source electrodes in the manner shown in the inset to figure 5.10. The accelerating voltage V_{acc} is taken from a tapping-point on a high resistance chain connected across the accelerating voltage supply, which has an output of V'_{acc} volts; V'_{acc} is equal to 1.02 V_{acc}. A further fixed voltage supply V_s (344 ν for 500μA electron current) is connected between V'_{acc} and the beam-centring plates. The circuitry required to apply a field across the beam-centring plates has not been shown. The tapping-point on the high resistance chain, and the value of V_s will be different for different source geometries.

From the graphs of figure 5.10 and that of figure 5.11, it is possible to determine quantitatively the potential depression in the electron beam. Figure 5.11 gives the repeller voltage at maximum sensitivity, as a function of the mean beam-centring voltage, for 20μA electron current. From this graph, it is possible to determine the change in repeller voltage ΔV_r, required to maintain a given field at the electron beam, when the mean beam-centring voltage, B, is changed by a given amount. It is:

$$\frac{\Delta V_r}{\Delta B} = 0.0114$$

If the repeller voltage is changed by ΔV_r, the field at the electron beam, V_i', will change by $\Delta V_r/3.2$. Thus:

$$V_i' = \Delta V_r/3.2$$

Eliminating ΔV_r from these two equations gives:

$$V_i' = 0.0036\ \Delta B$$

This is the change in field occuring at the electron beam, when the mean beam-centring voltage is changed by ΔB, the repeller voltage being kept constant. Figure 5.12 shows the field required (right-hand ordinate) at the electron beam to overcome the space-charge barrier, as

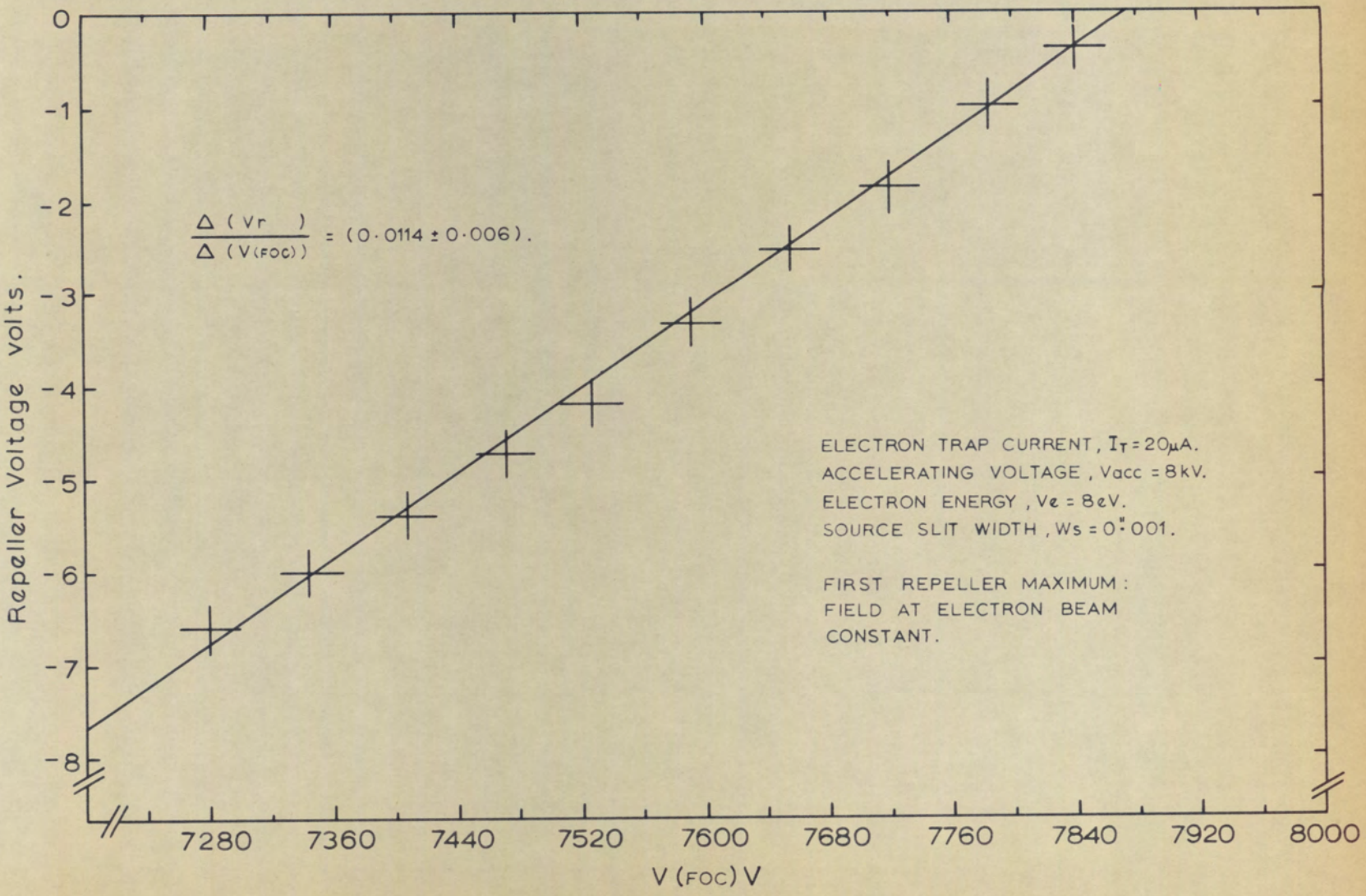

FIGURE 5.11 REPELLER VOLTAGE AT MAXIMUM SENSITIVITY AS A FUNCTION OF THE MEAN BEAM CENTRING VOLTAGE, V (FOC).

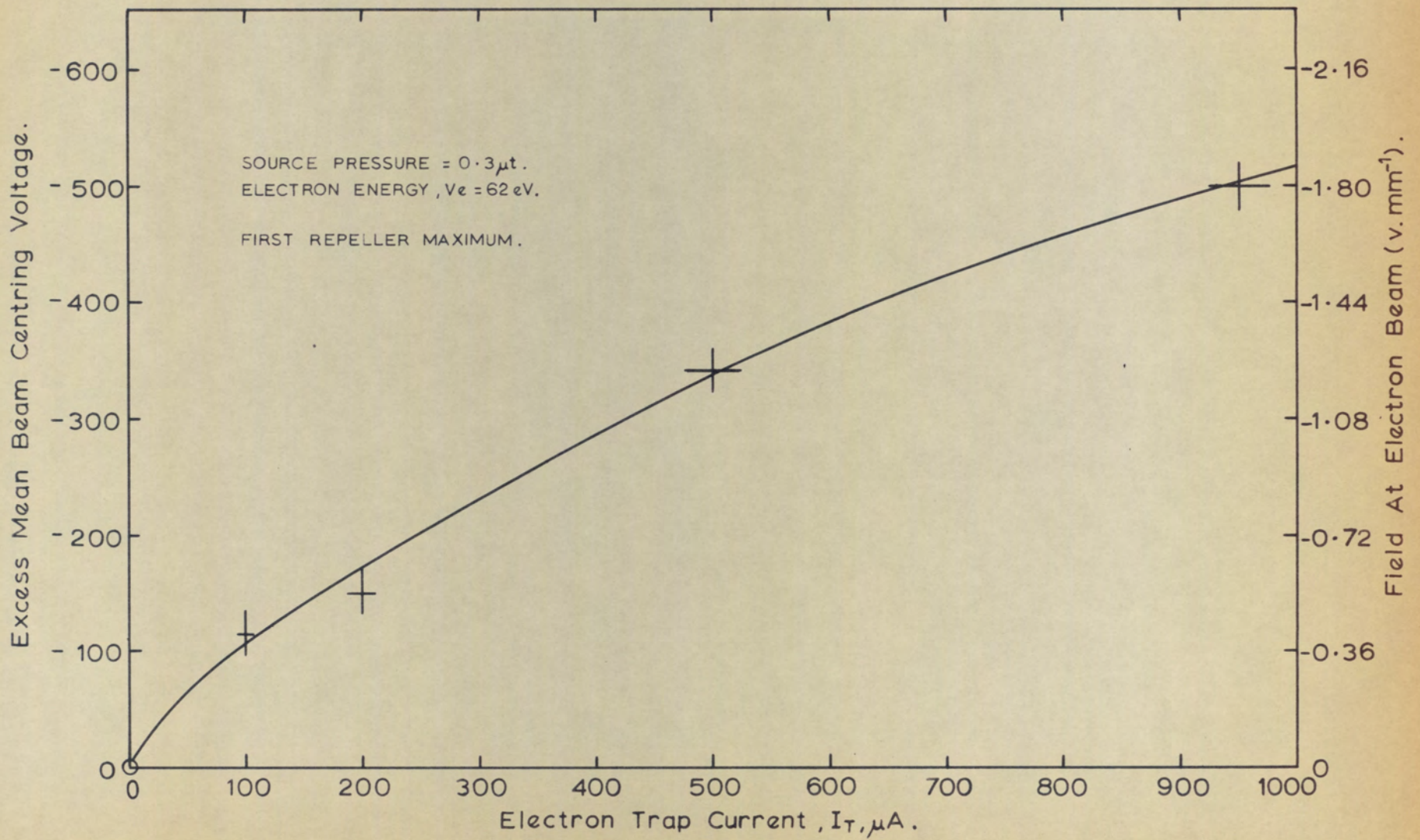

FIGURE 5.12 EXCESS MEAN BEAM CENTRING VOLTAGE REQUIRED TO OVERCOME SPACE CHARGE AS A FUNCTION OF ELECTRON TRAP CURRENT.

a function of electron trap current. The left-hand ordinate shows the corresponding value of the excess voltage required on each beam-centring plate to produce this field. The form of the curve at low trap currents is similar to that observed by Brubaker (1955) and Clampitt (1966).

The theoretical space-charge density which exists in a magnetically-confined, cylindrical electron beam, completely filling an equipotential tube, has been given by Haeff (1939) and by Smith and Hartmann (1940). (See Pierce, 1949, p. 161). Baker and Hasted (1966) have extended this analysis, and have given an approximate expression for the potential depression ΔV volts, at a radius r of a beam of radius a.

$$V = \frac{Ie}{V_o^{1/2}} \cdot \frac{1}{4\pi\epsilon_o\sqrt{2\eta}} \cdot \frac{r^2}{a^2} \text{ volts} \qquad \ldots\ldots \qquad (5.7)$$

where Ie is the electron beam current (Amps)

Vo is the electron beam energy (Volts)

ϵ_o is the permittivity of free space (farad. m^{-1})

η is the charge-to-mass ratio of the electron (coul. kg^{-1})

Inserting the explicit values of the constants into equation 5.7, gives the following expression for the potential depression at the centre of the electron beam:-

$$V = 15{,}100 \cdot \frac{Ie}{Vo^{\frac{3}{2}}} \text{ volts} \qquad \ldots\ldots \qquad (5.8)$$

The electron beam of the MS902 source is a rectangle approximately 0.4mm wide by 2mm broad. Suppose this may be divided into five cylindrical tubes, each carrying one fifth of the total current; then for a 500μA, 62eV electron beam, the potential depression at the centre of each of the 0.2mm radius tubes is

$$V = 15{,}100 . \frac{10^{-4}}{\sqrt{62}} = 0.19 \text{ volts}$$

Therefore, the field required to overcome this potential depression will be approximately

$$(V_s')_{TH} \approx 0.19/0.2 = 0.95 \text{ v. mm}^{-1} \qquad \ldots\ldots \qquad (5.9)$$

From figure 5.12, the experimental value of the field required to overcome space charge in a 500μA, 62eV electron beam is

$$(V_s')_{EX} = 1.2_2 \pm 0.1 \text{ volts. mm}^{-1} \qquad \ldots\ldots \qquad (5.10)$$

The agreement is good, and it may be deduced that the field which overcomes the space-charge barrier, is mainly that produced by the leakage of the main accelerating field into the ion chamber. The ion repeller voltage plays a relatively minor rôle in this process; the

reduced repeller voltage required at high electron currents (see figure 5.5), probably has the effect of compensating for the physical displacement of the electron beam caused by the increased extraction field. Alternatively, the repeller voltage change may serve to enhance the shape of the electron beam antinodes, so that larger ion currents can emerge from the ionisation region.

5.2.5 Relationship between ion current and pressure

The ion current emitted from the ion source does not always increase linearly with pressure in the way specified by equation 5.2. A study of this was first given by Baker and Hasted (1966). In their work on the production of multiply-charged ions in the space-charge well of the electron beam, they showed that the ion current/pressure relationship was complex, obeying different laws for different conditions. Of relevance to this work is their concept of 'trap-area' and 'free area' (p.36). The former term refers to the zone in the electron beam in which the potential barrier is sufficient to trap ions moving with their thermal velocity. The 'free-area' zone is that in which ions have sufficient thermal energy to escape any potential barrier. The trap area will form the core of the electron beam and the free area the perimeter of the electron beam.

The ideas of trap-area and free-area ions may be extended, and they are of particular help in explaining the pressure-dependent characteristics of the electron bombardment ion source in the range 1 to 10$\mu\tau$ nitrogen pressure in the ionisation chamber (hereafter termed 'source pressure'). Figure 5.13 shows the collected ion current as a function of source pressure for low and high electron currents. For 20μA electron current, the ion current is proportional to the pressure and thus obeys equation 5.2. This is not so for 500μA electron current, for after an initial rise in ion current of 1.80×10^{-10}A. dose^{-1} (1 dose $\equiv 3\mu\tau$ source pressure), the rate of increase in ion current approaches a value of 0.22×10^{-10}A. dose^{-1} at a source pressure of 10$\mu\tau$. This curve may be divided into two parts, as shown by the broken lines on figure 5.13. The first part may be attributed to ions which emerge from the well in the direction of the source resolution-slit. These will be termed the 'trap-area' ions, since they have emerged from one small exit point in the electron beam antinode. The second part of the curve may be attributed to the 'free-area' ions, which originate from those parts of the electron beam surrounding the trap area. It is seen that the free-ion current ~~intensity~~ increases linearly with pressure, while the trapped-ion current reaches a maximum value, and stays constant whatever the source pressure thereafter.

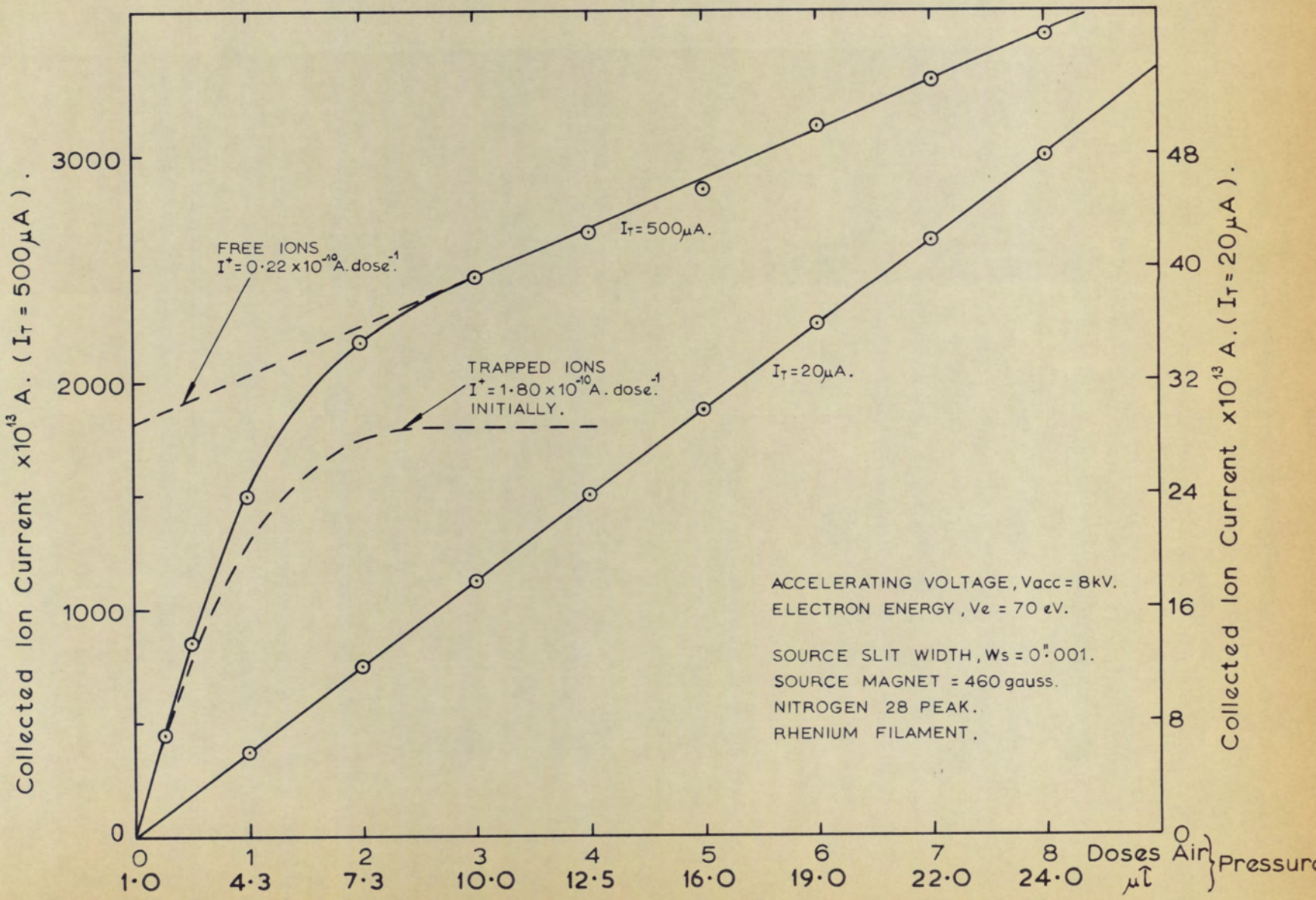

FIGURE 5.13 ION CURRENT AS A FUNCTION OF SOURCE PRESSURE FOR LOW AND HIGH ELECTRON CURRENTS.

The breakdown of the 500μA curve into two portions as described above, is substantiated further by the results given in figure 5.14, and which were taken on the same source and soon after the results given in figure 5.13. The curves show the collected nitrogen 28 ion current, for 1 dose of air, as an increasing amount of the chemical compound heptacosa is added, at 20μA and 500μA electron current. At 20μA electron current, the collected nitrogen 28 current is independent of the heptacosa pressure. However, at 500μA electron current, the collected nitrogen 28 ion current decreases from 1.5×10^{-10}A to a constant value of 0.22×10^{-10}A.

The 500μA curve can again be broken into two sections, one part due to 'trapped' nitrogen ions and one due to 'free' nitrogen ions. Now, above a certain pressure, the trap-area will not yield more than a certain ion current. Therefore, if heptacosa is present in the ionisation region, the ion current flowing out of the trapped region must be shared between nitrogen and heptacosa ions; the greater the heptacosa pressure, the smaller will be the proportion of nitrogen ions emerging from the trapped region. This mechanism is responsible for the fall-off in the 500μA curve shown in figure 5.14. When the nitrogen-equivalent source pressure of the heptacosa is 9.0μτ, the majority of ions emerging from the trapped area are heptacosa ions. The asymptote at 0.22×10^{-10}A corresponds to the nitrogen current from the free area and this is the same value as that determined from figure 5.13.

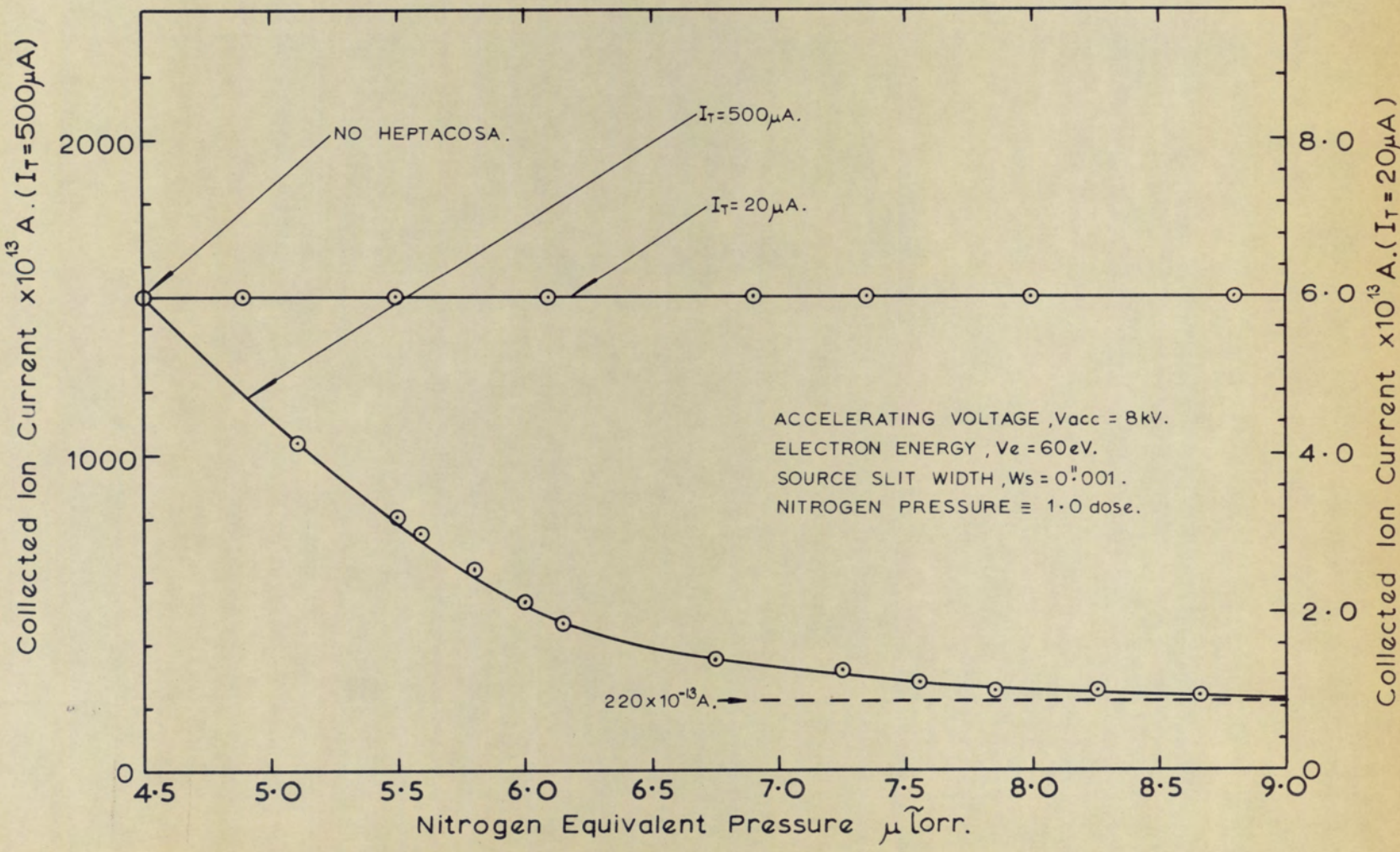

FIGURE 5.14

SUPPRESSION OF THE NITROGEN 28 PEAK ON ADDING HEPTACOSA.

In the above analysis, further evidence has been given in support of the notions of 'trap-area' and 'free-area' zones in an electron beam - ideas first proposed by Baker and Hasted (1966). In addition, for source pressures of less than $1\mu\tau$, the sensitivity of the electron bombardment source to trapped ions, at 500μA trap current, is

$$(20/500).(1.80/0.006) = \underline{12.0} \qquad \ldots\ldots \qquad (5.11)$$

times as sensitive as would be expected when the sensitivity at 20μA is linearly extrapolated to 500μA electron current. Similarly the sensitivity to free ions at 500μA electron current is

$$(20/500)\ (0.22/0.006) = \underline{1.5} \qquad \ldots\ldots \qquad (5.12)$$

times as sensitive as would be expected from low electron current sensitivity.

These factors, not given by Baker and Hasted, are important in the determination of the mechanism of the ion extraction at high electron currents. A description of the phenomena which cause the saturation in emitted ion current will be given in section 5.2.8.

5.2.6 Some Further Properties of the 'Trap-area'

Figure 5.15 shows the collected ion current as a function of the ion accelerating voltage, for 500μA and 10μA electron current. Curves for rhenium wire and tungsten ribbon filaments are given.

At low electron ionising currents, the observed linear relationship is readily explainable in terms of ideas developed in previous sections. In section 4.2.3 it was shown that the ion withdrawal angle, and hence the theoretical source efficiency, was approximately proportional to the square root of the ion accelerating voltage. Similarly, in section 5.1.4, it was seen that the existence of ions with a Z-component of velocity resulted in the ion transmission, through the Z-apertures, being proportional to the square root of the accelerating voltage. Therefore, at the ion collector the ion current will vary directly in proportion to the accelerating voltage - the product of two square root laws.

However, for the high electron current, the ion current rises approximately linearly with accelerating voltage, but above about 4kV, ~~asymptotes to~~ attains a constant value. It is concluded that above this accelerating voltage, all trap-area ions have initial angles within the ion withdrawal wedge, and all pass through the Z-apertures. Now, in section 5.1, it was seen that at low electron ionising currents,

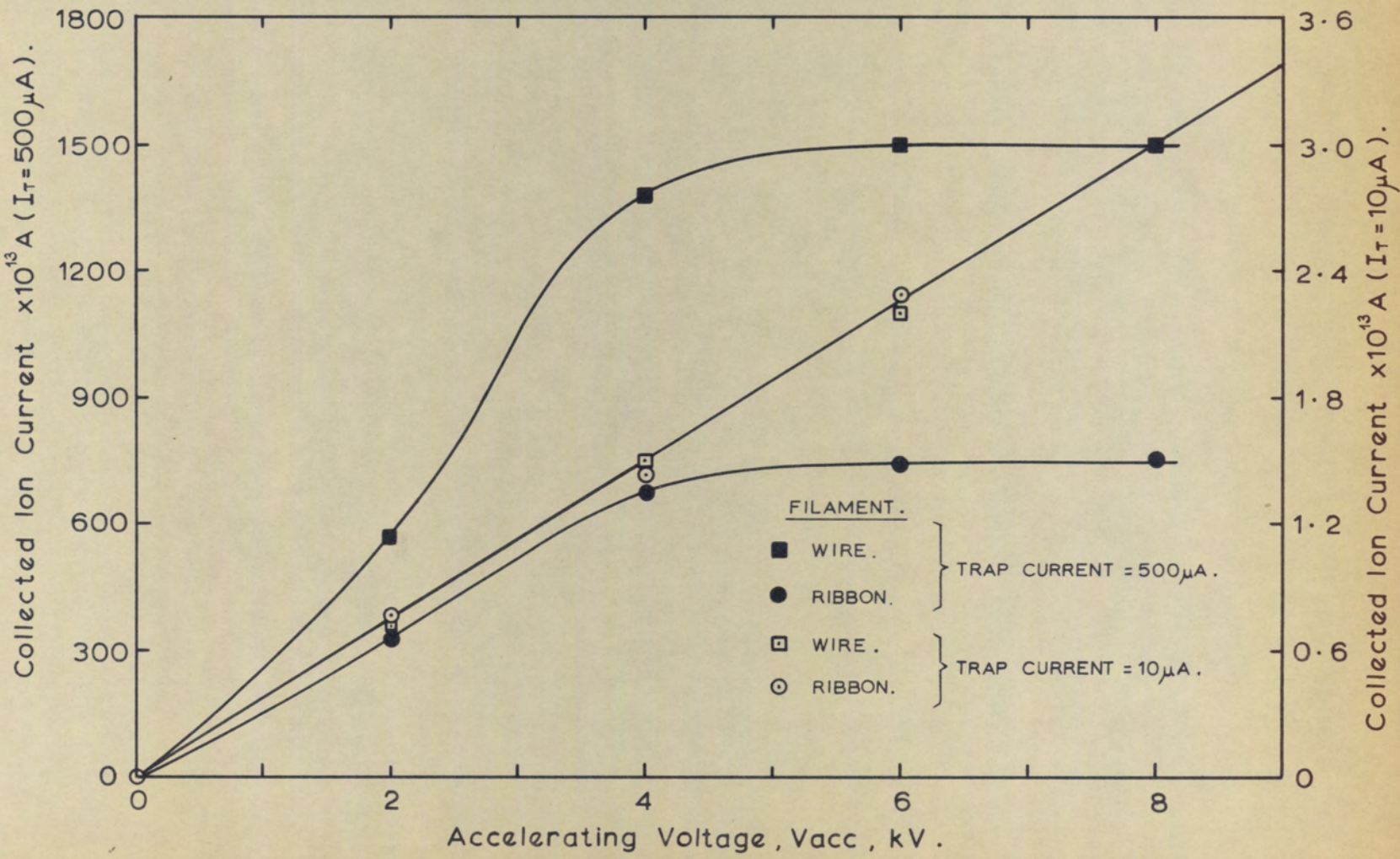

FIGURE 5.15 ION CURRENT AS A FUNCTION OF ACCELERATING VOLTAGE FOR HIGH AND LOW TRAP CURRENTS.

the ion transmission through y and z angular apertures was 20.3% and 54%, respectively. Therefore, at high electron current, for which there is no loss of ions at these apertures, the transmission efficiency of the mass spectrometer to the trap-area ions will be increased by a factor of ten. The effect can be explained by postulating that ions can escape only from relatively small apertures in the antinodes of the electron beam. After the ions are formed in the trap-area, they will oscillate back and forth in the potential well, until they are moving in the correct direction to escape. In this way, a large proportion of the ions produced in the trap-area will eventually reach the mass spectrometer collector, although the average residence-time of the ions in the source will be increased.

Further evidence that ions emerge from a small zone of the electron beam, can be deduced figure 5.16. In this figure, the ion current is given as a function of the width of the source resolution-slit; curves for low and high electron currents are shown. As the slit is opened, the point at which the ion current ceases to increase gives an indication of the overall y-width of the ion beam. For low electron currents the ion beam width is approximately 0".008 compared with a width of 0".003 at high electron currents. The demagnification of the ion source is 0.126 (see section 4.1.4) at 8kV accelerating voltage; therefore, the width of that part of the electron beam which emits ions decreases from 0".063 to 0".024, on changing from low to high electron current.

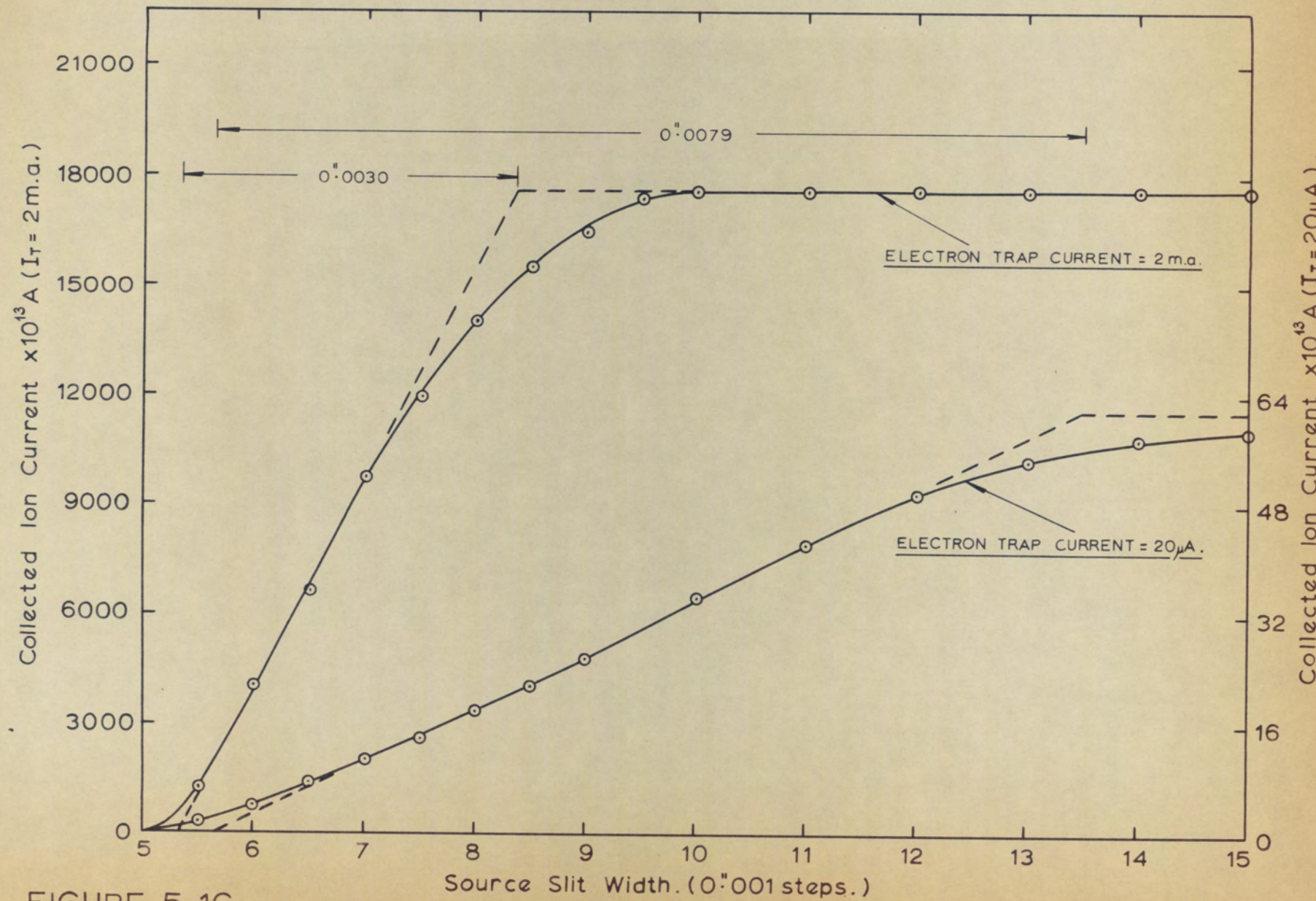

FIGURE 5.16 ION CURRENT AS A FUNCTION OF SOURCE SLIT WIDTH FOR LOW AND HIGH ELECTRON CURRENTS

With the above data, and with the use of equation 5.7, it is possible to construct a diagram of the equipotentials in a 500μA electron beam. This is shown in figure 5.17. The majority of ions emerge from the central 0.4mm zone and the initial angles are all less than 14° to the horizontal. The 'Penumbra' region extends for about 0.1mm on either side of this. Ions extracted from the 0.6mm zone of umbra and penumbra originate from close to the 0.00 volt equipotential line, which extends over a distance of 1.6mm in the X-direction. It follows that another effect of electron space-charge is to reduce the ion 'object' height by a factor of 2.7 (=1.6/0.6). This has the effect of increasing the transmission efficiency of the mass spectrometer by a factor of 2.7.

5.2.7 Proportion of Electron current in the trap-area

It is apparent from figure 5.17 that the ion current observed at high electron current is comprised of all the gas molecules ionised in the central core of electrons. To determine the proportion of electrons in this central core, the first step is to calculate the ion current which is produced in the central core.

With the following conditions:

A source pressure,	$P_s = 3\mu\tau$,
Width of source resolution-slit	$W_s = 0.001$,
A source Z-restrictor,	$Z_s = 0.050$,
The measured ion current,	$I^+ = 1.80 \times 10^{-10}$A.
$\therefore$ for $W_s = 0.003$	$I^+ = 5.40 \times 10^{-10}$A.

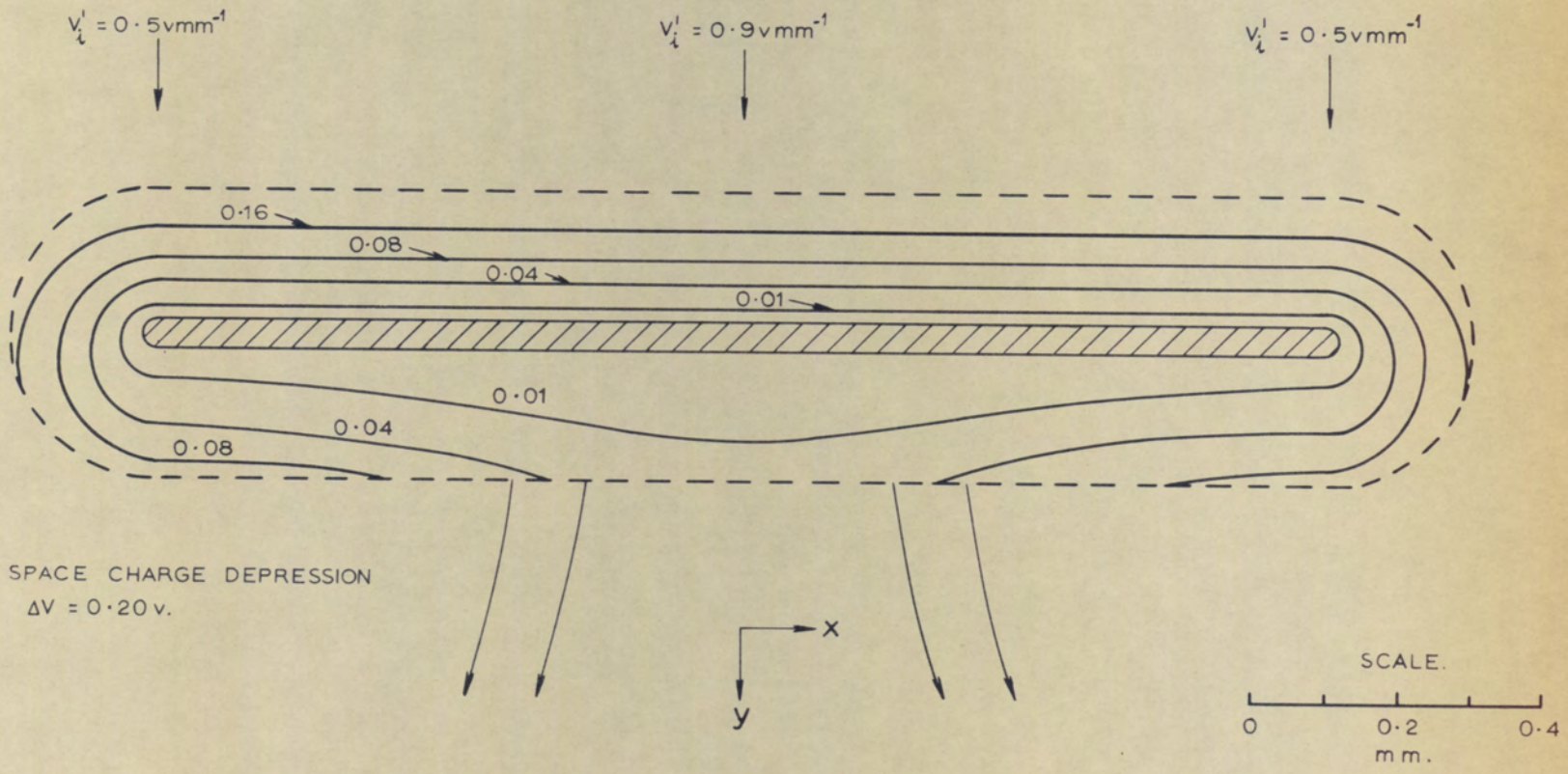

FIGURE 5.17 APPROXIMATE EQUIPOTENTIALS IN AN ELECTRON BEAM SUBJECT TO AN APPLIED CROSS FIELD.

Now with a 0".050 Z-restrictor, the ion current is extracted from three 0".050 zones (see section 5.2.3) and the total ion current generated in the central core of the 0".750 long electron beam is

$$I^+ = \frac{0.750}{3 \times 0.050} \times 5.40 \times 10^{-10}$$

$$\therefore \quad \underline{I^+ = 2.70 \times 10^{-9} A} \qquad \ldots\ldots \qquad (5.13)$$

From equation (5.2) the total ion current produced in a 500μA electron beam is

$$I^+ = 9 \times 500 \times 10^{-6} \times 2.0 \times 3.0 \times 10^{-6}$$

$$\therefore \quad \underline{I^+ = 2.70 \times 10^{-8} A} \qquad \ldots\ldots \qquad (5.14)$$

From equations (5.13) and (5.14), the proportion of electron current, I_{cz}, in the central zone is given by

$$I_{cz} = \frac{2.7}{27} \times 500 = \frac{500}{10} = \underline{50\mu A} \qquad \ldots\ldots \qquad (5.15)$$

The remaining 450μA of electron current surrounding this zone is the 'free-zone' of the electron beam. The results of the above analysis show that the ion current produced in the central zone of the electron beam is one-tenth of the total ion current produced. Now, it is

experimentally observed that the ion current collected from this region is twelve times that collected from the rest of the electron beam (section 5.2.5). From this data, it is deduced that the ions originating in the trap-area are 120 times more likely to reach the mass spectrometer collector. Most of the contributory factors have already been detailed, but for completeness they are summarised below:

(a)	α angular spread reduction	x5
(b)	Z angular spread reduction	x2
(c)	Ion object height reduction	x2.7
(d)	Ions from three antinodes	x3
(e)	Other factors	x1.5
(f)	Trap-area ions, one-tenth of total	x0.1
	Overall Gain	x12

'Other factors' is obtained by the elimination of other small losses which occur at low electron currents (see section 5.1).

5.2.8 Theoretical Saturation Ion Current

In section 5.2.5 it was shown that an electron bombardment source exhibits saturation at 4.3$\mu\tau$ nitrogen equivalent pressure in the ion chamber. Equation 5.13 is valid for a source pressure of 3.0$\mu\tau$, and

hence for 4.3μτ pressure the ion current will be approximately 3.9×10^{-9}A. This is the total ion current that may be withdrawn from the trap-area, for all pressures above 4.3μτ . The theoretical value may easily be calculated.

The calculation is based on ideas first presented by Langmuir (1929). The phenomenon so far called saturation is in fact, complete neutralisation of the electron space-charge by the ions produced. Langmuir considered the effect of ions generated in an accelerating electron beam such as would be encountered in a thermionic vacuum tube. For the present analysis, it will be assumed that the electrons encounter zero field in their direction of travel. The ions produced will move initially with thermal energy. There will be a small field leaking into the electron beam, which will extract the ions, but for purposes of the following analysis this field will be neglected.

Let the electrons of mass m_e, velocity v_e, have a volt energy V_e. Similarly let the ions produced have a mass m_p, a velocity v_p, and a volt energy V_p, then

$$V_e = k\, m_e\, v_e^2 \qquad \ldots\ldots \qquad (5.16)$$

$$\text{and } V_p = k\, m_p\, v_p^2 \qquad \ldots\ldots \qquad (5.17)$$

Where k is a constant. By dividing equation (5.16) by equation (5.17) and taking the square root, the following expression relating the electron velocity to ion velocity is obtained:

$$\frac{v_e}{v_p} = \left[\frac{V_e}{V_p} \cdot \frac{m_p}{m_e}\right]^{\frac{1}{2}} \qquad \ldots\ldots \qquad (5.18)$$

If there is a charge density of n_e electrons per cc, and n_p protons per cc, then the ratio of electron current, I_e, to proton current I_p is given by

$$\frac{I_e}{I_p} = \frac{n_e}{n_p} \cdot \frac{v_e}{v_p} \qquad \ldots\ldots \qquad (5.19)$$

For space-charge neutralisation of the electrons in the central zone the ion density must equal the electron density, or $n_p = n_e$. Therefore, from equations (5.18) and (5.19):

$$\frac{I_e}{I_p} = \left[\frac{V_e}{V_p} \cdot \frac{m_p}{m_e}\right]^{\frac{1}{2}}$$

For an ion of atomic mass M a.m.u., the ion current I_p, will be given by:-

$$I_p = \left[\frac{V_p}{V_e \cdot 1835M}\right]^{\frac{1}{2}} \cdot I_e \qquad \ldots\ldots \qquad (5.20)$$

For example, with a 70eV electron beam, which produces 0.04eV ions from nitrogen gas (M = 28 a.m.u.), the maximum ion current that can be produced is given by the equation:

$$I_p = \left[\frac{0.04}{70 \times 1835 \times 28}\right]^{\frac{1}{2}} I_e$$

$$= I_e/9482$$

With an electron current in the central zone of 50μA, the maximum ion current is:

$$\underline{I_p = 5.3 \times 10^{-9} A} \qquad \ldots\ldots \qquad (5.21)$$

The experimental value of the maximum ion current, $I^+ = 3.9 \times 10^{-9}$A (equation 5.13), is 30% lower than this theoretical value. Considering the experimental errors involved and the approximations made in the theoretical treatment, the agreement is very good.

From a practical point of view the agreement between the theoretical and experimental results means that the saturation in emitted ion current is indeed space-charge neutralisation of the electrons by the ions produced. Thus, it is not possible, using a conventional electron bombardment source, to obtain high sensitivity if the source chamber pressure is greater than approximately 4.3μτ (0.43μτ gauge pressure). In this context, sensitivity is taken to mean the ion current rise per unit of sample added.

Conversely, it may be stated that to obtain high sensitivity, the source must be operated with a background pressure of less than about $0.1\mu\tau$ (source gauge) and on introduction of the sample the source gauge pressure must not rise above $0.5\mu\tau$. Above this pressure the sensitivity, or the increase in ion current per given sample size, is 12% of its value below this pressure.

5.3 SUMMARY AND CONCLUSIONS

For electron ionising currents less than about 20μA, the ion transmission of the mass spectrometer system under low resolving power operating conditions is about one tenth of a percent. Theoretical analysis shows that ion loss occurs mainly at the alpha, z, and beam-defining apertures, increase of which would cause loss in resolution.

For electron currents above about 500μA, it is well known that the space-charge forces in the electron beam create a potential well in which the ions are trapped. The experimental evidence presented in this thesis suggests that under these conditions the ions emerge in a preferential direction from the electron beam antinodes, so that above 4000 volts accelerating voltage all ions pass through the alpha and z apertures of the MS902. The ion object size is reduced, and in addition collected ions emerge from three of the electron beam antinodes.

However, as one-tenth of the total number of ions produced is trapped in this way, the overall sensitivity increase is only a factor of 12. This is derived by forming the product of the following factors.

(a)	α-angular spread reduction	x5
(b)	z-angular spread reduction	x2
(c)	Ion object height reduction	x2.7
(d)	Ions from three antinodes	x3
(e)	Other factors	x1.5
(f)	Trap-area, one-tenth of total	x0.1
	Overall Gain	x12

This agrees with the experimentally observed increase in sensitivity.

When a source operates under these conditions, no further increases in sensitivity would be obtained by increasing the accelerating voltage or by employing Z-focusing. Conversely the mass spectrometer may be voltage scanned without change of sensitivity, and accurate isotope ratio measurements may be made.

The biggest ~~single~~ disadvantage of the source is that the features described above only hold good below source pressures of 5×10^{-6} torr (a gauge pressure of 5×10^{-7} torr). Above this pressure, space-charge neutralisation of the electrons by the ions, prevents further ions from being produced. This phenomenon causes 'suppression' of sample fragment ions by reference compound ions, which effectively reduces the sensitivity of the source to the sample ions. Any improved source design should incorporate means for minimising the pressure saturation and suppression effects. The possibility of achieving this will be discussed in the final section.

6 - WAYS OF IMPROVING SOURCE DESIGN

In previous sections the detailed workings and characteristics of the electron bombardment source at low and high electron currents have been considered. In the course of these experiments the properties of a number of source assemblies were investigated. Although the sources were nominally identical to one another, it was found that the ion current delivered by some sources was a factor of twenty smaller than that given by others. In the first part of this section this effect is analysed in more detail, and constructional modifications are described which enable every source to deliver high ion currents. The second part discusses the feasibility of attaining still better source efficiencies, and describes some preliminary results obtained with a source incorporating a partitioned ionisation chamber for minimising peak suppression effects.

6.1 Ways of Maintaining High Sensitivity

6.1.1 Slit Tolerances

In section 5, it was seen that when the source was operated at high electron currents, the total field required at the ionisation region to extract ions was the sum of the field required to overcome the potential barrier created by the electron space-charge, together with that needed

to maintain the optimum ion optical properties of the extraction lens system. Therefore, to obtain high sensitivity it would seem sufficient to provide the correct extraction field at the electron beam. However, this is not the case and if, for example, the gap between the beam-centring plates is reduced by 20%, the maximum ion current obtainable from the source typically drops by a factor of twenty, even though all the voltage controls are optimised. A geometry change such as this will alter the way in which the electrostatic field varies along the ion path. It was found experimentally that to obtain the highest sensitivities the gap between the beam-centring plates should be reduced from 0".062 to 0".058 with a tolerance on the dimension of ± 0".002. A similar tolerance is required on the 0".040 distance separating the ion exit slit and the beam-centring plates (dimension 'd_3' on figure 2.4).

To maintain constancy of extraction field, an additional requirement is to have reproducible manufacture of the ion exit slit. Previously, the slot in the exit slit was produced by punching, and as wear developed on the punching tool, the outer slit edges became more deformed in the manner shown in the sketch in figure 6.1 (a). For the improved source, the exit slit has been punched out of thicker material and then lapped down to the correct thickness. This procedure produces slits with square edges as shown in figure 6.1 (b), regardless of the age of the punching tool.

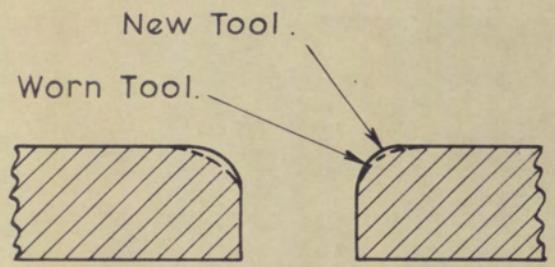

(a) Previous Manufacture
Of Ion Exit Slit.

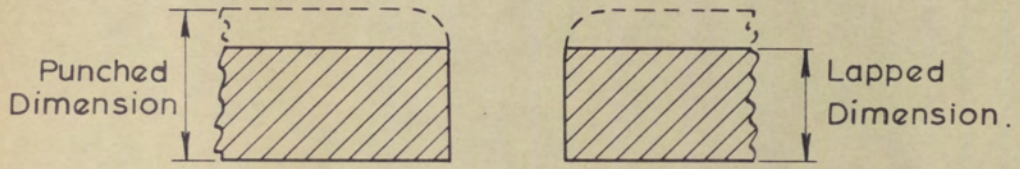

(b) New Manufacture
Of Ion Exit Slit.

FIGURE 6.1 ION EXIT PLATE MANUFACTURE.

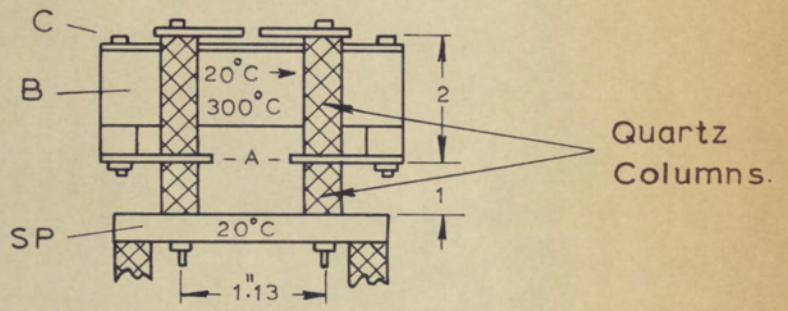

(a) Previous Mounting.

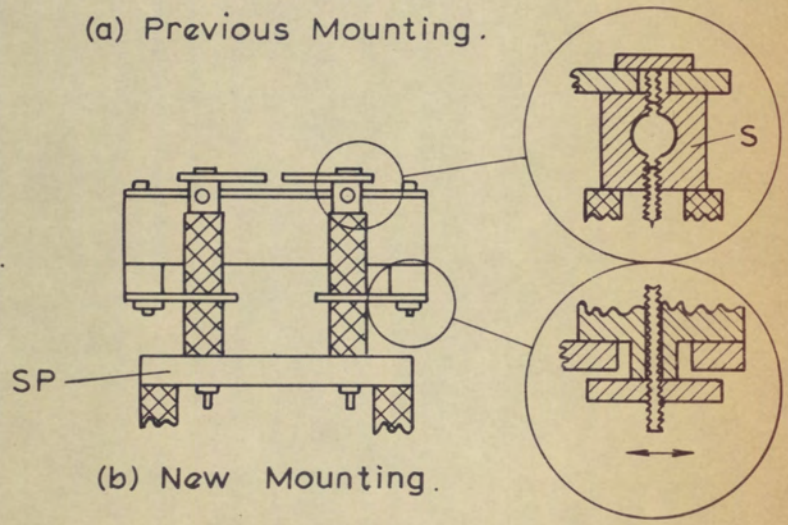

(b) New Mounting.

FIGURE 6.2 BEAM CENTRING PLATE MOUNTING.

Obtaining a constant gap between the beam-centring plates was more difficult. The first of the two problems to be tackled was the springing apart of the half-plates which occurred when the alignment dowels were removed. This has been corrected by modifying the columns supporting the plates as shown diagrammatically in figure 6.2 (a) and (b). The ion chamber block B_9 is clamped to the support plate, SP_9 by means of the threaded metal spacer S. Only when the block is secure and aligned are the beam-centring plates fixed in position. With this constructional change it is possible to ensure that the gap between the beam-centring plates can be set to an accuracy of better than $\pm$ 0.002.

When using the direct insertion probe (see section 5), it is usual to heat the ionisation chamber to a temperature in the range of 20°C to 300°C, so that the optimum evaporation rate of the sample under investigation can be selected. It is therefore important that the source characteristics remain constant over this temperature range. However, in the experiments detailed in section 5, it was noted that the ion current was not constant with temperature variation, and in some cases the ion current fell by a factor of two, for a change in temperature of 50°C. It was found that this was caused by a change in the gap between the beam-centring plates. The way in which this occurs is explained with reference to figure 6.2 (a). The support plate SP_9 is thermally isolated from the ionisation block B_9 and any expansion of the latter

will force apart the quartz supporting columns at levels A and C. One way of curing this fault is to securely fix the ionisation chamber to one pair of supporting columns, and to allow a sliding fit at the other pair as shown in figure 6.2 (b).

Note: Although all of the above improvements were suggested by the author, the detailed constructional changes were carried out by the Division's Mechanical Engineering Department.

6.1.2 Mean Beam-Centring Voltage

It was seen in section 5.2.4 that the ion current obtained from the source is extremely dependent on the mean beam-centring voltage. In addition, the optimum voltage required was a function of the accelerating voltage and the electron current. Therefore to obtain high sensitivity the source controls should include a mean beam-centring voltage control, which will vary this voltage between approximately 85% and 95% of the accelerating voltage.

6.1.3 Electron Beam Position

In the course of the experiments detailed in section 5, it was initially found that the filament wire and magnet positions needed very accurate alignment, to allow a large proportion of the electron current to reach

the electron trap. If this was not done the filament emission was typically in excess of 2 m.a. for 500μa trap current, and the rhenium filament burnt out within an hour.

Two simple modifications are required to avoid the tedious trial and error alignment of the electron beam. These changes are explained with reference to the diagrams in figure 6.3 In the original filament assembly the 0".016 wide slot in the anode was punched in 0".032 thick material, with the filament placed 0".100 away, as shown in figure 6.3 (a). This geometry was originally designed for the 0".030 wide, 0".001 thick filament which was used in sources up to the end of 1966. After this date, a 0".007 diameter rhenium wire filament was fitted for its improved chemical inertness (see section 6.2.1). However because the latter emits a beam one quarter of the width of that from the tungsten filament, alignment of the wire is critical. To reduce this effect the slot size has been increased to 0".025 as shown in figure 6.3 (b).

In a Nier source the beam of ionising electrons follows the path of the field-lines of the confining magnetic field. In a correctly-aligned system, the line joining the electron gun and trap will be coincident with the line joining the geometrical centres of the magnet pole-pieces as shown in figure 6.3 (c). However, should there be any small misalignment of the magnet poles, the electron beam path will be considerably curved, since it is common practice to use magnet pole

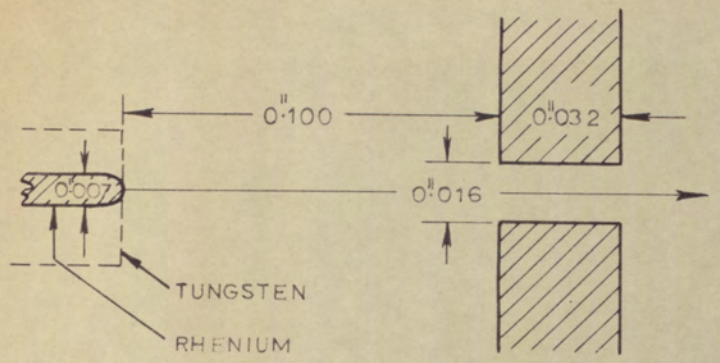

(a) Filament Assembly Before Modification.

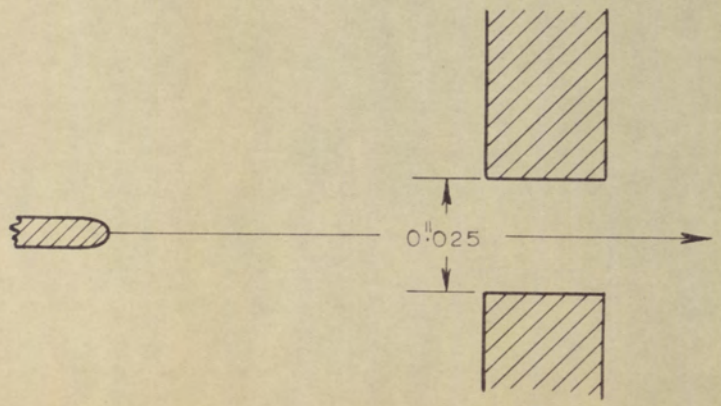

(b) Filament Assembly After Modification.

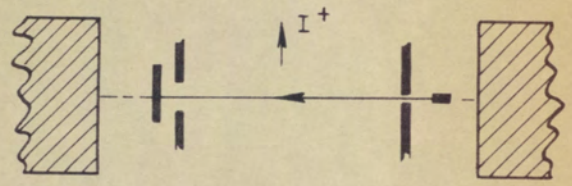

(c) Correct Alignment.

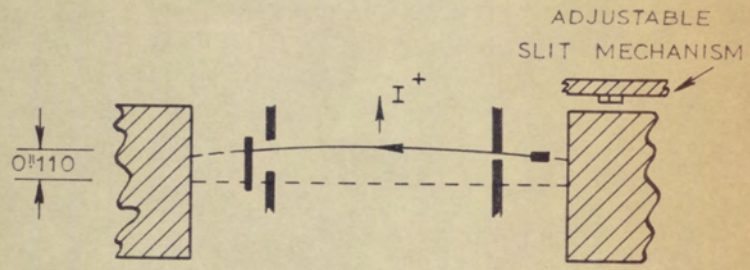

(d) Actual Alignment.

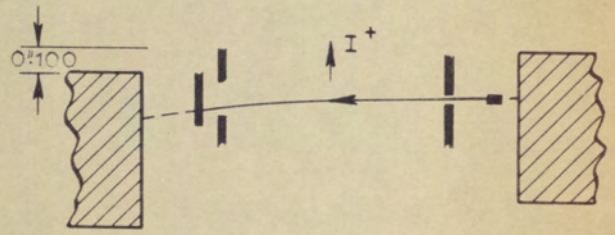

(e) Improvement on (d).

FIGURE 6.3 ALIGNMENT OF THE ELECTRON BEAM.

pieces whose separation is two or three times the diameter of the pole face. In the MS902 mass spectrometer the proximity of the adjustable slit mechanism makes such a misalignment unavoidable, and the two centre lines are 0".110 apart as shown in figure 6.3 (d). With this arrangement, the electron beam follows a curved path, with the result that only a small part of it is able to travel through the electron slit. As before, this leads to high emission and reduced filament life. It has been found experimentally that this may be prevented by displacing the pole-piece on the trap-side by approximately 0".100 in the direction shown in figure 6.3 (e). This modifies the electron beam path, so that nearly all the electrons pass through the defining apertures. Further experiments indicated that the position of the pole-pieces should be set to an accuracy of better than ± 0".020.

With the two modifications detailed above, it is possible to obtain 500μA electron trap current for as little as 550μA emission current.

6.1.4 Cleanliness

The sources must be chemically clean to obtain high sensitivity. Any residual hydrocarbons, mineral oil or finger grease, for example, on the ionisation chamber surfaces will cause a background pressure, and a background ion current will be produced. If this ion current exceeds the ion current produced when complete neutralisation of the electron

space-charge occurs (the 'saturation' ion current), the source sensitivity to sample ions will be reduced. An acceptable background ion current is one which is less than 20% of the saturation ion current. For most source impurities this background ion current is given by a residual pressure in the source of 10^{-6} torr. Baking the ionisation chamber at 200°C for several hours should be sufficient to achieve this.

6.1.5 Summary

The changes required to the electron bombardment source to ensure that it will operate at high sensitivity are tabulated overleaf. Although items (2), (4) and (8) are required to correct constructional faults in the source assembly used by the author, the other items are applicable to all Nier-type electron bombardment sources.

ITEM	CHANGE	MOTIVATION
(1) Ion Exit Slit	Square edges	Reproducibility
(2) Beam-Centring Plates	Modified mounting	To allow precise alignment of gap.
(3) Beam-Centring Plates	Gap dimension (MS902: old 0".062 new 0".058)	Optimisation of ion current
(4) Ionisation Chamber	Modified mounting	To prevent Beam-Centring gap change with ionisation chamber temperature change.
(5) Assembled Source	Jig aligned	Alignment of source with respect to mass spectrometer.
(6) Beam-Centring Voltage	Mean value variable	To optimise for high Sensitivity
(7) Electron Exit Slit	Enlarge width of slot for rhenium wire fil. (MS902: old 0".016 new 0".025)	Relaxation of tolerance on emitting wire position.
(8) Magnet Poles	Left-hand pole piece withdrawn by 0".100	Alignment of electron beam.
(9) Cleanliness	Background ion current $\not>$ 20% x Saturation ion current (MS902: $I^+ \not> 3 \times 10^{-11}$A.)	To obtain high sensitivity

6.2 Ways of Improving Source Sensitivity

6.2.1 Ion Production

As shown in section one, ion production can be increased by increasing the electron path length, increasing the electron ionising current or by reducing the flow rate of gas out of the ion chamber.

If increased sensitivity is to be obtained by increasing the electron path length, then the latter must be increased without altering the distance between the electron gun and trap. Arranging the magnetic field so that the electrons perform trochoidal trajectories achieves this, but as shown by Barnard (see section 1.4) no significant gains in sensitivity are obtained.

Increasing electron current is certainly feasible. For the 0.007 diameter rhenium wire, the upper limit is probably 1.2 m.a. emission current, or 1 m.a. electron trap current. A rhenium filament has been operated under these conditions for about 40 hours, but inspection of the wire after use revealed that it was heavily pitted. This indicates that the filament lifetime will not be much in excess of 40 hours, the shortest life that is normally acceptable. The ion current produced was double that obtained with 500μa electron trap current.

At present, a rhenium filament is favoured by the organic chemist, for in comparison with a tungsten one, it gives a reduction in the CO^+ line in the background spectrum of approximately a factor of five. In addition, it has a smaller 'memory' effect - that is, a smaller capacity for the retention of a previous sample. (Zandberg and Tontegode, 1966). However if sensitivity is more important, tungsten filaments with their higher emissivity for a given life may be used with advantage. A tungsten filament of 0.006 diameter has been run at 2 m.a. trap current with 2.5 m.a. emission current for times in excess of 100 hours, with the wire showing no sign of pitting or thinning. The ion current was four times that obtained with 500μa trap current (see, for example, figure 5.16). The 2 m.a. trap current is the largest that can be obtained with the present filament power supply, but there is no reason to suppose that a 0.006 tungsten filament should not have a useful life with 3 m.a. or perhaps as much as 4 m.a. electron trap current. With these operating conditions, ion currents respectively six times and eight times larger than that obtained at 500μa could be expected.

The third way of increasing ion production is by reducing gas flow rate out of the ionisation chamber. For the MS902 source the total pumping speed of 1.4 litre/second is controlled mainly by the ion exit slit, with a pumping speed of 0.7 litre/second, and the electron-trap aperture with a pumping speed of approximately 0.5 litre/second (A.E. Banner, private communication). The ion exit slit aperture cannot be reduced

without adversely affecting the ion optics of the source, and any reduction in the trap aperture would not reduce the total pumping speed by more than 30%.

It is concluded that the only way to significantly improve ion production efficiency is to increase the electron current. A tungsten wire filament will give at least 2.5 m.a. emission current, although the more chemically-inert rhenium filament will yield up to 1.2 m.a. emission current with a lifetime of more than 40 hours.

6.2.2 Ion Transmission

Ion transmission can be increased by producing an ion beam with smaller angular spreads in the focusing (y) and non-focusing (z) directions, smaller ion object width, or smaller energy spread.

However, as shown in section 5, under high sensitivity conditions, the beam emerging from the ion-trap zones just fills the beam-defining angular apertures of the mass spectrometer and there would be little point in aiming for improvement in these properties.

The energy spread of the ion beam emerging from the source contributes a relatively small amount to the total aberration of the mass spectrometer, and again there would be little to gain by improvement of this aberration.

At high resolution, the most significant loss of ions is at the adjustable source slit and there would be considerable gain in reducing the overall beam width at this point. This beam width is determined by the filament aperture length. To obtain a reduced beam width, a suitable modification would be to reduce the length of the aperture from 0".125 to 0".032. In practice, this may be conveniently done by using a 0".032 diameter round aperture (see figure 6.4). At present, the hot part of the filament extends over about 0".080 and such a change, while reducing the ion object size by a factor of two, would require the filament to produce a higher-density electron beam, for a given electron trap current. Therefore, as far as overall mass spectrometer efficiency and filament life are concerned, this modification is equivalent to increasing the electron ionising current passing through the standard filament aperture. Although there is little difference between the two methods, it is probably easier to increase electron ionising current since all this requires is the change of a resistor in the source supply circuit.

As with ion production, it is seen that the maximum ion transmission is limited almost exclusively by the maximum emissivity of the filament. Further increases in overall mass spectrometer efficiency are dependent on obtaining electron guns emitting higher-density electron beams.

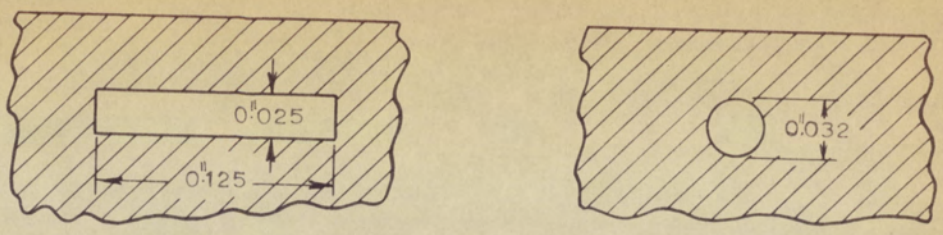

(a) Present Electron Aperture.

(b) Alternative Aperture.

FIGURE 6.4 ELECTRON BEAM APERTURE.

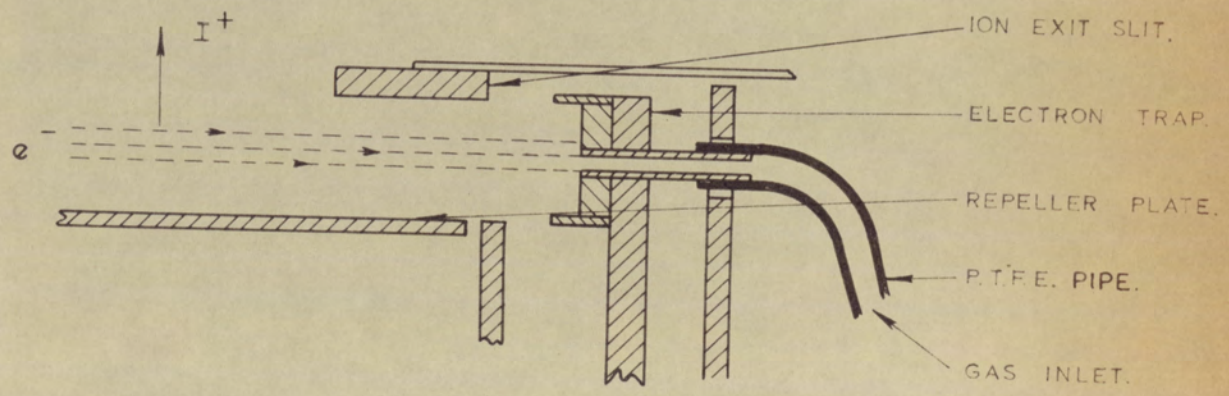

FIGURE 6.5 GAS ENTRY THROUGH ELECTRON TRAP.

6.2.3 Saturation Pressure

In section 5.2.8 it was shown that the saturation pressure was the pressure at which there was neutralisation of the electron space-charge, by the ions produced. For given values of the electron current, electron accelerating voltage and ion mass, the only way to increase the pressure at which this occurs would be to increase the initial ion energy (equation 5.20). However, initial ion energy is controlled by the sample temperature, which is usually set to give a satisfactory sample-evaporation rate. Thus initial ion energy cannot be changed. Nevertheless, it was reasoned that the threshold of pressure saturation might be raised if the ion spent less time within the confines of the electron beam. Under normal conditions, ions are formed with random initial direction, so that it would be possible for a newly-created ion to move-off perpendicular to the direction of motion of the electron beam. Such an ion will oscillate backwards and forwards many times in the potential well created by the electron space-charge, before it eventually escapes from an antinode. If, on the other hand, gas molecules were fired along the direction of the electron beam, the ions formed would be moving in preferential direction and should quickly escape from the potential well. To test this theory, a standard source was modified so that the nitrogen gas sample could be routed, either through a normal inlet port, or through a new inlet pipe emerging through the electron trap as shown in figure 6.5. However, contrary to expectation no significant difference was

noted between the sensitivity/pressure curves for the two methods of entry. Such a result indicates that for either method of sample entry, any ions produced make few oscillations before escaping from the potential well.

As an alternative approach to the problem, the source design sketched in figure 6.6 (a) was constructed. The aim of this is to separate the ionisation region of the reference compound from that of the sample compound, so that however much reference compound is used, there will be no suppression of the sample peaks in the manner described in section 5.2.5. The conventional ionisation chamber is divided into two parts by means of a central partition. Each chamber has its own electron beam and repeller plate, but ions from the two chambers are extracted by common ion exit slit, beam-centring plates and earth slit, in the expectation that the two ion beams will merge and travel as one through the mass spectrometer. The two electron beams were generated by a single filament wire constructed in manner shown in figure 6.6 (b). To ensure that the two tips were the hottest parts of the filament, a short tungsten rod was welded to the centre of the wire. With the arrangement (a) two small ion beams were observed, but each required a different beam-centring voltage (+250V and -250V) to line up the beam with the adjustable source slit. The design therefore fails to combine the two emerging beams. In an effort to improve this, the centre partition was modified as shown in design (c). For this geometry,

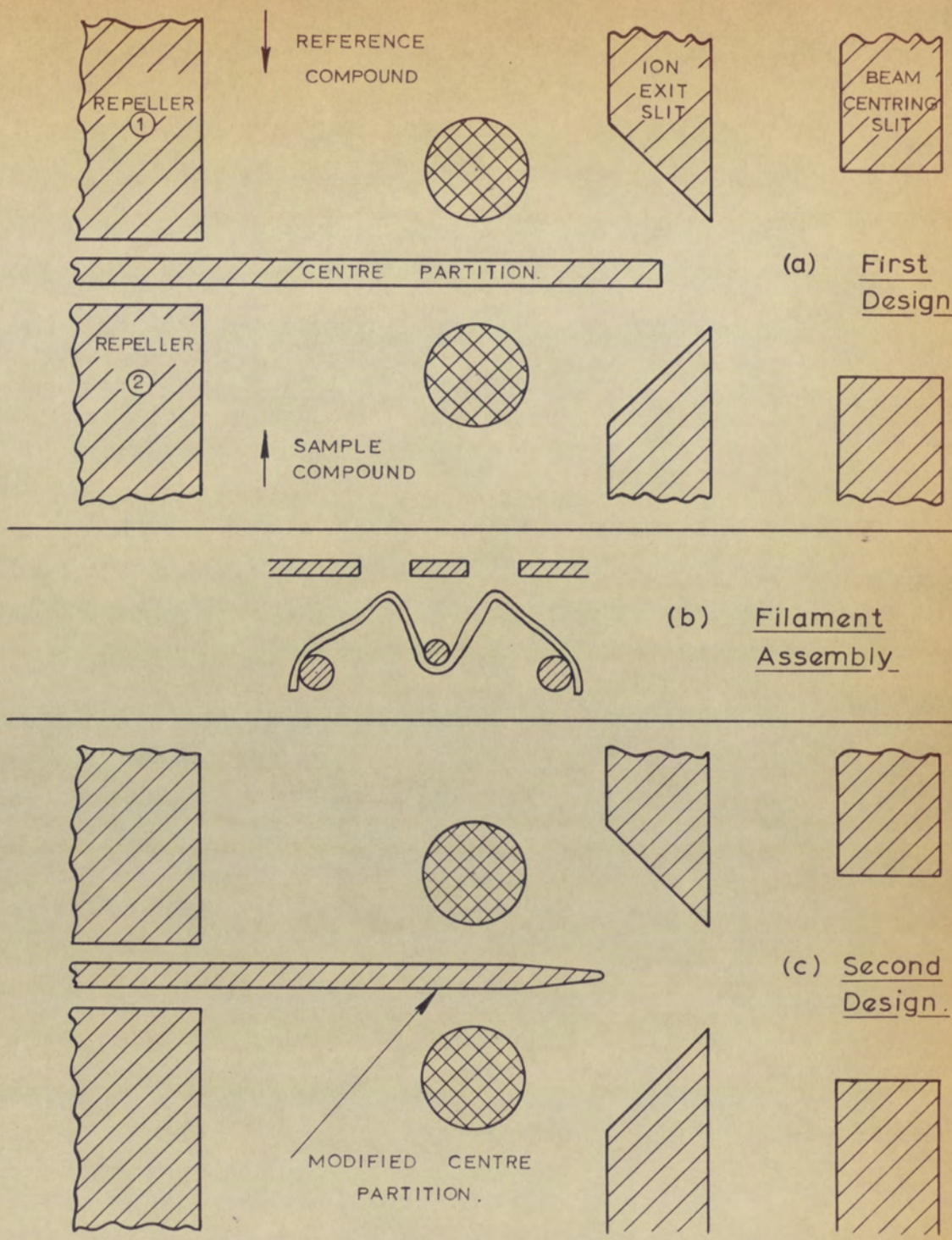

FIGURE 6.6 PARTITIONED SOURCE DESIGN.

there was a high ion current from each chamber. Furthermore, it was found that only 12% of the gas in one chamber leaked into the other chamber; thus the partitioning is adequate for typical operating conditions, when for example, there will be a 10^{-7} torr contribution in the sample chamber for a reference compound pressure of 8×10^{-7} torr. The optimum beam-centring voltages (+50V and -250V) were found to be nearer to each other; however, this is still not close enough for the source to be of immediate application. Possible design changes to improve this might include shaped source electrodes, and a smaller distance between the electron beams.

From the above results, it is seen that the partitioned source promises to be of use in organic mass spectrometry, although further development is required for the source to produce merged ion beams.

6.2.4 Summary and Conclusions

The sensitivity of the MS902 electron bombardment source can be increased again by at least a factor of four, by using a 0.006 diameter tungsten wire filament operating with a 2 m.a. electron ionising current. The present rhenium wire filament, favoured by the organic chemist for its chemical inertness, could operate at 1 m.a. with lifetimes in excess of 40 hours. Any further increase in mass spectrometer efficiency is dependent on obtaining electron beams with higher electron densities.

Suppression of sample ion peaks by reference ion peaks can be avoided by using a partitioned ion source. However, the original design needs modifying so that the sample and reference ion beams merge together at the adjustable source slit.

7 - CONCLUSIONS

By making use of new iterative procedures, developed in this thesis, the paraxial focal properties of an ion source can be computed at least ten times faster than has hitherto been possible. This permits an extensive study of the source to be made, without incurring prohibitively high computer costs. The axial potential distribution in the source is determined by using a conformal transformation method, and the characteristic trajectories are plotted by use of the Liebmann (1949) and Archard (1954) ray tracing recurrence relations. Comparison with results obtained by numerical relaxation and resistor network analysis shows that the absolute accuracy of the potentials in the main focussing region is better than 3%, while relative accuracy of the potential values, one to another, is better than one part in 10^5. The iterative process can be used for slit systems with gap-to-separation asymmetry ratios of between 1:5 and 5:1, which is quite adequate for most practical slit systems.

The results of the theoretical analysis show that there can be one, two or three ion-optical images in the zone between the ionisation region and the resolution slit of the mass spectrometer; for a given source geometry, the number of images present is determined by the voltage on the repeller plate. If initial ion energies are small ($\lesssim$ 0.1eV), fine interval sizes are required at the beginning of each trajectory.

The results of the paraxial analysis are approximately valid for an ion object which has a height equal to the width of the aperture in the ion exit slit; for example, the true demagnification of an object of this size is no more than 15% larger than that calculated by paraxial theory. This accuracy is adequate for the derivation of a theoretical repeller curve displaying the main characteristics of the well-known experimental curve. Further ray-tracing demonstrates that a source of a given geometry will produce the same emitted ion current as a source of any other geometry, provided that the voltages used for focussing the ion beam are optimised.

At high electron ionising currents, the presence of electron space-charge completely alters the characteristics of an electron bombardment source. Under certain circumstances the electron space-charge can cause the ion current emitted from the source to increase appreciably. Theoretical and experimental evidence suggests that this arises because the space-charge forces in the electron beam restrict emergence of ions from the source, to within a small angular wedge. To obtain the increased ion current requires careful choice of the relative dimensions and positions of the slit-aperture electrodes. Determination of the dependence of high sensitivity on geometry, would require a more complete theoretical investigation in which the effects of electron space-charge were included. A computer program which when modified, could be used in this study is the 'electron or ion gun analysis program' written by Hamza (1966).

A limitation of the high ion current source is that the ion current increases with pressure at a much reduced rate when the pressure in the source is increased above a certain critical value. At this critical pressure, there is complete neutralisation of the electron space-charge by the ions produced. In organic mass spectrometry the effect becomes noticeable when the partial pressure of the reference compound in the source exceeds the critical pressure. When a sample compound is subsequently added to the source, the total ion current obtained from the sample is much less than it would have been in the absence of the reference compound. The effect can be reduced substantially by using a source in which there are separate ionisation regions for reference and sample compounds. However, preliminary experimentation with this type of source, shows that it may be difficult to make it fulfil the important requirement of merged sample and reference ion beams at the resolution slit of the mass spectrometer.

Further study of the electron bombardment source might include an investigation of electron gun design. Larger ion currents can be obtained by using higher-density electron beams. A possible way of achieving this would be to include an electrostatic lens to focus the electron beam, after acceleration but prior to magnetic confinement.

Present electron densities are still approximately a factor of ten below the point at which space-charge collapse of a magnetically-confined electron beam occurs (Brewer, 1967). There is, therefore, ample room for improvement before this fundamental limit is reached.

APPENDIX I

TRANSFORM FOR TWO SLITS AND A PLANE

The application of conformal transformation to the study of three-electrode electrostatic slit-lenses was detailed simultaneously by Laudet (1953) and Archard (1954). In both treatments however, in order to derive the transformation constants without too much difficulty, certain conditions were made regarding the symmetry of the system. This work was extended by Boerboom (1959, 1960 a, b), as mentioned in the text.

Descriptions of the Schwarz-Christoffel method together with worked examples are given in Gibbs (1958), Green (1962), Binns and Lawrenson (1963), Morse and Feshback (p. 443, 1953) and Walker (1933). Of these, the books by Gibbs and Green give the simplest introduction to the method.

(NOTE: the references are given with Section 2 references).

1.1 TRANSFORMATION EQUATION

The potential boundaries in the z-plane and the corresponding w-plane are shown in figures Ia and Ib respectively. The real boundary to be mapped is the contour PABCDED'C'B'A'P', which transforms to a straight line in the transformed plane. If the origin in the w-plane is chosen at E, then by symmetry, the labelled points may be assigned values in the w-plane of ∞, a, b, c, d, o, -d, -c, -b, -a, $-\infty$ respectively, where the a, b, c and d are real constants, which are uniquely specified by a given lens geometry.

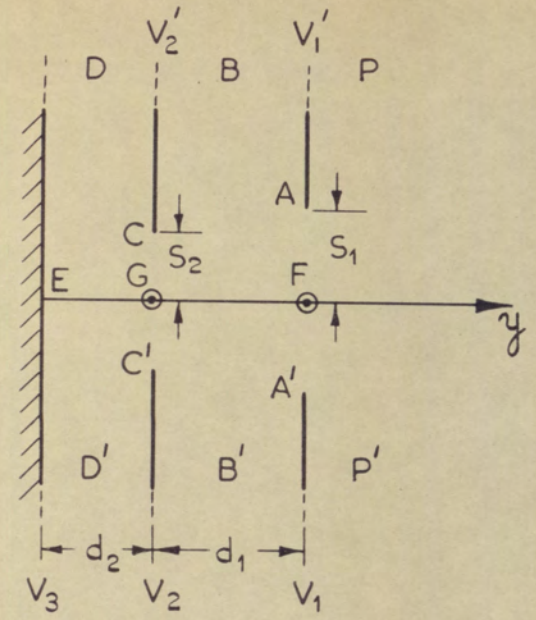

FIG. Ia Z—plane

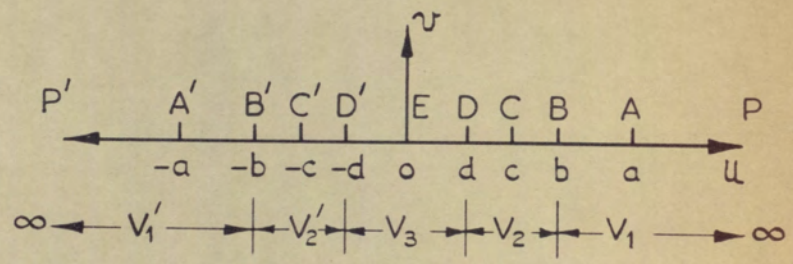

FIG. Ib ω —plane

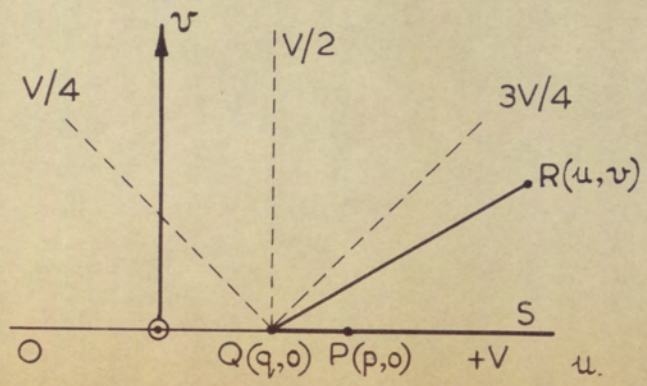

FIG. Ic

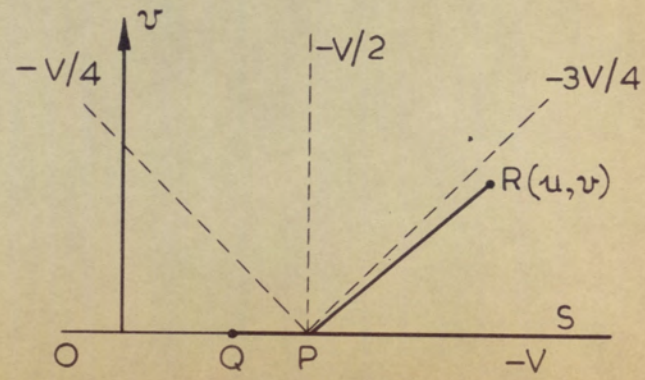

FIG. Id

FIGURE I. MAPPING IN THE COMPLEX PLANE.

The Schwarz-Christoffel differential equation (After Gibbs, 1958) relating co-ordinate points in the z- and w-planes can be given by the expression:-

$$\frac{dz}{dw} = N\,(w-1)^{-\alpha}(w-m)^{-\beta}(w-n)^{-\gamma}\ldots\ldots(w-t)^{-\kappa} \qquad \ldots\ldots \text{(1a)}$$

where $\alpha\pi, \beta\pi \ldots\ldots \kappa\pi$ are the exterior angles of the polyogonal contour to be transformed, and N is an arbitrary constant. The interior angles are $(1-\alpha)\pi$, $(1-\beta)\pi \ldots\ldots (1-\kappa)\pi$, respectively. Since it is permissible to set the values of two of the arbitrary constants, it is convenient to set N=1 and to set w=o at E.

For the above problem the values of $\alpha, \beta, \gamma, \delta$ and ϵ (corresponding to the points A to E) are given below:-

At A:- $(1-\alpha)\pi = 2\pi \quad \therefore \quad \alpha = -1$

At B:- $(1-\beta)\pi = 0 \quad \therefore \quad \beta = 1$

At C:- $(1-\gamma)\pi = 2\pi \quad \therefore \quad \gamma = -1$

At D:- $(1-\delta)\pi = 0 \quad \therefore \quad \delta = 1$

At E:- $(1-\epsilon)\pi = \pi \quad \therefore \quad \epsilon = 0$

The factor corresponding to the vertex F is infinite, and must therefore be omitted. Vertices A', B', C' and D' have angles the same as vertices A to D. Substituting the factors into equation (1a), the Schwarz-Christoffel equation for the geometry under consideration becomes:-

$$\frac{dz}{dw} = \frac{(w^2-a^2)(w^2-c^2)}{(w^2-b^2)(w^2-d^2)} \qquad \ldots\ldots \text{(1b)}$$

1.2 INTEGRATION OF THE SCHWARZ-CHRISTOFFEL EQUATION

Equation (1b) may be re-written as:-

$$z = \int_0^w \frac{(s^2-a^2)(s^2-c^2)}{(s^2-b^2)(s^2-d^2)}\,ds \qquad \ldots\ldots \quad (2)$$

which is easily integrated after partial fractionization. First consider the partial fractionization of:-

$$S = \frac{(s-a)(s-c)}{(s-b)(s-d)} \quad \ldots\ldots (3a) \qquad \text{into the form:} \quad S = A + \frac{B}{s-b} + \frac{C}{s-d} \quad \ldots\ldots (3b)$$

where A, B and C are to be determined. Comparing the two forms 3a, 3b gives the identity:-

$$(s-a)\ (s-c) \equiv A(s-b)(s-d) + B(s-d) + C(s-b)$$

Equating terms in s^2:- $\quad 1 = A$

" " " s :- $\quad -a-c = -b-d + B+C \quad \ldots\ldots \quad (3c)$

" " non-s :- $\quad ac = bd - Bd - Cb \quad \ldots\ldots \quad (3d)$

Eliminating B from equations (3c) and (3d) gives:-

$$ac = bd - d\,(b + d - a - c) + C(d-b)$$

$$\therefore\ C\,(d-b) = d^2 - (a+c)d + ac$$

$$\therefore \qquad C = \frac{-(a-d)\ (c-d)}{(b-d)} \qquad \ldots\ldots \quad (5)$$

and substituting C from (5) into (3c) gives:-

$$B = \frac{-(a-b)\ (b-c)}{(b-d)} \qquad \ldots\ldots \quad (6)$$

The integral (2) may thus be re-written in the form:-

$$z = \int_o^w \left[1 + \frac{B'}{(s^2-b^2)} + \frac{C'}{(s^2-d^2)} \right] ds$$

Where B' and C' respectively have the same form as B and C, but with each letter squared (compare Equations (2) and (3a)).

$$\therefore \quad z = w + L \ln \frac{(w-b)}{(w+b)} + M \ln \frac{(w-d)}{(w+d)} + P \quad \ldots\ldots \quad (7)$$

where:

$$L = -\frac{(a^2-b^2)(b^2-c^2)}{2b(b^2-d^2)} \quad , \quad M = -\frac{(a^2-d^2)(c^2-d^2)}{2d(b^2-d^2)}$$

and P is the constant of integration, which in general may be complex. Suppose the x, y co-ordinate system in the complex z-plane is that shown in figure Ia, where the origin is placed midway between the edges of the second slit-aperture. The value of the constant may be found by applying equation (7) to the points w = a and w = o. Let z = x + iy and P = p + iq ($i = \sqrt{-1}$). When w = a, the terms in (7) with coefficients L and M are real since $a > b > c > d > o$. In addition, y = o by definition of the co-ordinate system, and therefore q = o.

For w = o, x = o which makes z and the terms in equation (7) with coefficients L and M, purely imaginary. Hence the real part of P, p, must equal zero.

Thus, for the above-defined co-ordinate system in the z-plane the transformation equation becomes:-

$$z = w + L \ln \left[\frac{w-b}{w+b} \right] + M \ln \left[\frac{w-d}{w+d} \right] \quad \ldots\ldots \quad (8)$$

1.3 SPECIFICATION OF THE TRANSFORMATION CONSTANTS

The four unknown constants a, b, c and d may be expressed in terms of $2s_1$ and $2s_2$ the slit widths, d_1 the spacing between the first and second slits and d_2, the spacing between the second slit and the plane.

(i) From equation (8), the slit width $2s_1$ is given by:-

$$\begin{aligned} 2s_1 &= Re\left[z_{(w=a)}\right] - Re\left[z_{(w=-a)}\right] \\ &= Re\left[z_{(w=a)} - z_{(w=-a)}\right] \\ &= 2\left[a + L\ln\frac{a-b}{a+b} + M\ln\frac{a-d}{a+d}\right] \end{aligned}$$

$$\therefore \quad s_1 = a + L\ln\frac{a-b}{a+b} + M\ln\frac{a-d}{a+d}$$

(ii) Similarly, $2s_2 = Re\left[z_{(w=c)} - z_{(w=-c)}\right]$

$$= c + Re\left[L\ln\frac{b-c}{b+c} + Li\pi + M\ln\frac{c-d}{c+d}\right] - Re\left[z_{(w=-c)}\right]$$

where the principal value of the logarithm has been assumed.

$$\therefore \quad s_2 = c + L\ln\frac{b-c}{b+c} + M\ln\frac{c-d}{c+d}$$

(iii) The residue at w = -b is L and so the discontinuity at B in the z-plane, $-id_1$, is given by:-

$$-id_1 = Li\pi$$

$$\therefore L = -d_1/\pi$$

(iv) Similarly, by considering the discontinuity at c, $M = -d_2/\pi$ is obtained.

Putting $r_1 = d_1/\pi$ and $r_2 = d_2/\pi$ gives the following set of four simultaneous equations required for the determination of a, b, c and d

$$s_1 = a + r_1 \ln \frac{a+b}{a-b} + r_2 \ln \frac{a+d}{a-d} \qquad \ldots\ldots (9)$$

$$s_2 = c + r_1 \ln \frac{b+c}{b-c} + r_2 \ln \frac{c+d}{c-d} \qquad \ldots\ldots (10)$$

$$r_1 = \frac{(a^2-b^2)(b^2-c^2)}{2b(b^2-d^2)} \qquad \ldots\ldots (11)$$

$$r_2 = \frac{(a^2-d^2)(c^2-d^2)}{2d(b^2-d^2)} \qquad \ldots\ldots (12)$$

s_1, s_2, r_1 and r_2 are known from the geometry of the problem. The new method derived for solving the equations (9), (10), (11) and (12) is given in Appendix II.

1.4 SOLUTION OF LAPLACE'S EQUATION IN THE w-PLANE

So far, there is the equation (8) relating a co-ordinate point in the slit system cross-sectional plane (z) to a corresponding unique point in the transformed plane (w). The constants of the transformation, a to d, are obtained from the solution of the above set of equations (9) to (12). Since Laplace's equation remains invariant in the transformation, the problem now reduces to solving Laplace's equation in the transformed plane. The potential at a given point in the transformed plane is then exactly equal to the potential at the corresponding point, specified by equation (8), in the slit system cross-sectional plane.

The potential-defining electrodes map as straight lines along the u-axis of the w-plane, as shown in figure Ib. The potential in the w-plane may be derived by a further transformation, but it is preferred to use the method of Boerboom (1959) which illustrates the principles involved. Consider, at first, the system in figure 1c; along the u-axis of the w-plane let the potential be +V to the left of Q (q,o), and zero to the right of Q. The broken lines are along equipotentials, and the potential at a point R (u,v) is given by $(V/\pi)\ \hat{RQS}$. Similarly the potential at the point R, in the arrangement of figured 1d, equals $(-V/\pi)\ \hat{RPS}$. If now a further system has a potential distribution along the u-axis given by:

Potential = 0 for $p > u > q$

Potential = V for $p < u < q$

the potential at R may be found by linear superposition of the above cases.

$$\therefore\ V(u,v) = \frac{V}{\pi}\left\{\arctan\frac{v}{u-q} - \arctan\frac{v}{u-p}\right\} \quad \ldots\ldots \quad (13)$$

In practice, interest centres on the potential distribution along the axis of the slit-aperture cross-sectional plane i.e. along the y-axis of figure Ia. In this case, z is imaginary and from equation (8) it follows that w is too. Thus, w = iv and the y-axis of the z-plane maps onto the v-axis of the w-plane. Changing the origin in the z-plane to G, the form of equation (8) relevant to the y-axis, reduces to:-

$$iy = iv - \frac{d_1}{\pi}\ln\frac{(iv-b)}{(iv+b)}\ \frac{-d_2}{\pi}\ln\frac{(iv-d)}{(iv+d)}\ +id_1$$

and using the identity $\log_e\frac{(iv-r)}{(iv+r)} \equiv 2i\arctan\left(\frac{r}{v}\right)$ gives the equation

$$y = v - \frac{2d_1}{\pi}\arctan\left(\frac{b}{v}\right) - \frac{2d_2}{\pi}\arctan\left(\frac{d}{v}\right) + d_1 \quad \ldots\ldots \quad (14)$$

The potential along the v-axis is obtained from equation (13) by placing $u = o$

$$\therefore V(u,v) = \frac{V}{\pi}\left(\arctan\frac{v}{p} - \arctan\frac{v}{q}\right) \quad \ldots\ldots \quad (15)$$

The area to the right of the plane electrode DED' in the z-plane maps onto the upper half of the w-plane, and hence the angles RQS and RPS of figures Ic and Id will be in the range 0 to π. This fact is important when determining the value of the arctan function (a many-valued function).

Equation (15) gives the potential along the v-axis of the w-plane resulting from an electrode, at potential V, along the u-axis between the abscissae $u = p$ and $u = q$. For the series of electrodes shown in figure Ia, at potentials V_1', V_2', V_3, V_2 and V_1, the resultant potential along the v-axis is again found by the principle of superposition:-

$$V(o,v) = \frac{V_1'}{\pi}\left\{\arctan\frac{(-v)}{(\infty)} - \arctan\frac{(-v)}{(\overline{b})}\right\} + \frac{V_2'}{\pi}\left\{\arctan\frac{(-v)}{(\overline{b})} - \arctan\frac{(-v)}{(\overline{d})}\right\}$$

$$+ \frac{V_3}{\pi}\left\{\arctan\frac{(-v)}{(\overline{d})} - \arctan\frac{(v)}{(\overline{d})}\right\} + \frac{V_2}{\pi}\left\{\arctan\frac{(v)}{(\overline{d})} - \arctan\frac{(v)}{(\overline{b})}\right\}$$

$$+ \frac{V_1}{\pi}\left\{\arctan\frac{(v)}{(\overline{b})} - \arctan\frac{(v)}{(\infty)}\right\} + \frac{V_3}{\pi}\left\{\arctan\left(\frac{v}{o}\right) - \arctan\left(\frac{-v}{o}\right)\right\}$$

If it is assumed that there are no cross-fields in the slit system, then

$V_1 = V_1'$ and $V_2 = V_2'$

and $$V(o,v) = \frac{2}{\pi}(V_1 - V_2)\arctan\frac{(v)}{(b)} + \frac{2}{\pi}(V_2 - V_3)\arctan\frac{(v)}{(d)} + V_3 \ldots \quad (16)$$

Equations (14) and (16) thus form a pair of parametric equations giving the potential V at a point y, along the y-axis of the slit system cross-sectional plane, by way of the auxiliary parameter v. Since it is not possible to eliminate v between (14) and (16), the computational method is to set up a table of v values and to then compute the appropriate values of y and V.

1.5 DERIVATIVES OF POTENTIAL

The ray-tracing part of the computer program requires the first and second derivatives of the axial potential distribution, the analytical parametic expressions for which, may be derived from equations (1b) and (16)

(a) $$V'(o,y) = \frac{\partial V}{\partial y} = \left(\frac{\partial V}{\partial v}\right)\left(\frac{\partial v}{\partial y}\right)$$

---

where $\frac{\partial V}{\partial v} = \frac{2}{\pi}(V_1 - V_2)\frac{b}{b^2 + v^2} + \frac{2}{\pi}(V_2 - V_3)\frac{d}{d^2 + v^2}$; and $\frac{\partial v}{\partial y} = \frac{(v^2+b^2)(v^2+d^2)}{(v^2+a^2)(v^2+c^2)}$

(b) $$V'' = \frac{\partial}{\partial y}\left[\left(\frac{\partial V}{\partial v}\right).\left(\frac{\partial v}{\partial y}\right)\right] = \frac{\partial v}{\partial y}.\frac{\partial}{\partial y}.\left(\frac{\partial V}{\partial v}\right) + \frac{\partial V}{\partial v}.\frac{\partial}{\partial y}\left(\frac{1}{(\partial y/\partial v)}\right)$$

$$\therefore \quad V'' = \left(\frac{\partial v}{\partial y}\right)^2\left[\frac{\partial^2 V}{\partial v^2} - \frac{\partial^2 y}{\partial v^2}\,.\,V'\right]$$

---

where $\partial v/\partial y$ is given above, and :-

$$\frac{\partial^2 V}{\partial v^2} = \frac{-4.b.v}{\pi(b^2 + v^2)^2}.(V_1 - V_2) - \frac{4.d.v}{\pi(d^2 + v^2)^2}.(V_2 - V_3)$$

$$\frac{\partial^2 y}{\partial v^2} = -\frac{4.b.v.d1}{\pi(b^2 + v^2)^2} - \frac{4.d.v.d2}{\pi(d^2 + v^2)^2}$$

[Differentiate equation (14) twice w.r.t. v]

APPENDIX II

ITERATIVE SCHEME FOR DERIVING THE TRANSFORMATION CONSTANTS

2.1 APPROXIMATE EQUATIONS FOR INITIAL VALUES

The general scheme for the solution of equations (9) to (12) in the text is similar to that given by Boerboom (1959). The equations are first approximated to a simpler form so that initial values of the constants a, b, c and d may be found.

The improved method differs in the way of approximating the equations. Boerboom's approximations fail when the slit apertures become greater than the slit separation, because the initial values of a, b, c and d formed violate the fundamental transformation condition that:-

$$a > b > c > d$$

The effect of using $b > a$, for example, is to make the term $\ln (a + b)/(a - b)$ imaginary, which corresponds to no practical case. To avoid such mishaps logarithmic terms have been included in the approximate equations in the following manner:-

(i) For equation (9) of the text it is noted that $a > b > c > d$, and hence the logarithmic term in a and b will be more significant than the term in a and d. Thus a suitable approximation will be:-

$$s_1 = Kr_1 \ln \frac{a + b}{a - b} \qquad \ldots\ldots \quad (1)$$

where the constant K is a correction factor to allow for the neglected terms.

(ii) For equation (10) of the text, it is likely that both the logarithmic terms will be of the same order since $b/c \approx c/d$ (Archard, 1954). A suitable approximation is therefore

$$s_2 = 2K' r_1 \ln \frac{b + c}{b - c} \qquad \ldots\ldots \qquad (2)$$

where the constant K' is a second correction factor which could be expected to be of the same order as K.

(iii) For equation (11) of the text, $b^2 \gg d^2$, giving as a suitable approximation

$$2r_1/b \doteqdot [(a/b)^2 - 1][1 - (c/b)^2] \qquad \ldots\ldots \qquad (3)$$

(iv) Similarly for equation (12) of the text, $a^2 \gg d^2$, $b^2 \gg d^2$ and hence

$$2r_2/d \doteqdot [(c/d)^2 - 1] (a/b)^2 \qquad \ldots\ldots \qquad (4)$$

Before equations (1) to (4) can be solved to generate the initial values of a to d, the constants K and K' must be determined. There are two supplementary conditions which may be used. The value of the first constant 'a' is always very close to $0.5s_1$ (See Table of values for different configurations in Boerboom, 1960a), and so an initial value for 'a' was arbitrarily chosen to be $0.52s_1$. The further condition is that K is likely to be similar in magnitude to K'.

The quantities K and K' have therefore been generated using an additional iteration as follows:-

(i) Set K' equal to one.

(ii) Hence (c/b) = than $(s_2/4K'r_1)$ from equation (2).

(iii) Set 'a' equal to $0.52s_1$.

(iv) From equation (3):

$$b = \frac{r_1}{Q}\left\{\sqrt{1 + \left(\frac{Qa}{r_1}\right)^2} - 1\right\} \quad \text{where } Q = 1 - (c/b)^2$$

(v) Thus from equation (1), K may be found.

(vi) K is then compared with K': If K is greater than K' (as it will be initially), K' is increased by 0.05 and the process from (ii) onwards is repeated. If K is just less than or equal to K' the iteration has fulfilled the condition of determining a K approximately equal to K', and the next iteration process may be commenced.

For a system of five slit apertures and a plane, where the slit apertures have the same width as the slit separation the constants K and K' are of the order of 2.

2.2 ITERATIVE METHOD FOR OBTAINING ACCURATE SOLUTION

Starting from the initial values of a, b, c, d it is possible to construct an iterative scheme to obtain these values to any degree of precision required.

Following Boerboom (1959) the method is to add the dropped terms to the approximate equations, so that they revert back to a mathematically exact form.

Thus equation (1) would become:-

$$Kr_1 \ln \frac{a+b}{a-b} = s_1 + \left[-a + (K-1).r_1.\ln \frac{a+b}{a-b} - r_2.\ln \frac{a+d}{a-d} \right] \ldots\ldots \quad (5)$$

where the term in the square brackets is a term added to equation (1) to convert it back to the original form, equation (9) of the text.

The iterative procedure is to use the latest values of a, b, c and d to compute the square bracket terms in the set of corrected equations, of which equation (5) is an example. There are then a set of equations which may easily be solved for new values of a, b, c and d. This process is repeated until the values of a to d are of sufficient accuracy, (but see the next section on the question of convergence). It is to be noted that the values of K and K', computed as in section 1.2, are constant throughout this iteration.

2.3 EXTENSION TO A SYSTEM OF A PLANE AND FIVE SLIT APERTURES

The methods outlined in Appendix I and in the previous two sections are all applicable to the system comprising a plane and any number of parallel slit apertures, and the equations are derived in an exactly analogous manner.

As an additional precaution against the possibility of the successive values of each transformation constant oscillating with increasing divergence about the respective true value, the following sequence has been embodied in the iterative procedure. The modified procedure is to carry out the first two iterations in the normal way, and for the third iteration to use the mean values of each constant generated in the previous two iterations. The fourth iteration is as before, but the fifth uses the mean values of the third and fourth iterations. In this way convergence is achieved, subject to the conditions discussed in section 1.6 of the text.

To obtain the same accuracy of solution for well-behaved geometries, the modified method requires a few more iterations than the original method, but the extra time involved is insignificant.

A P P E N D I X III

3.1 DERIVATION OF THE GENERAL RAY EQUATION

The generaly ray equation is derived by eliminating the time variable from the equations of motion of a charged particle in an electric field

$$m \frac{d^2y}{dt^2} = -eE_y; \quad m \frac{d^2x}{dt^2} = -eE_x , \qquad \ldots\ldots \quad (1)$$

and the energy equation

$$\frac{m}{2} \left[\left(\frac{dx}{dt}\right)^2 + \left(\frac{dy}{dt}\right)^2 \right] = -eV . \qquad \ldots\ldots \quad (2)$$

To achieve this it is noted that

$$dx/dy = \frac{dx/dt}{dy/dt}$$

and therefore

$$\frac{d^2x}{dy^2} = \frac{1}{dy/dt} \frac{d}{dy}\left(\frac{dx}{dt}\right) - \frac{dx}{dt} \frac{d/dy \ (dy/dt)}{(dy/dt)^2}$$

or

$$\frac{d^2x}{dy^2} = \frac{d^2x/dt^2}{(dy/dt)^2} - \frac{dx/dt}{dy/dt} \frac{d^2y/dt^2}{(dy/dt)^2} \qquad \ldots\ldots \quad (3)$$

Eliminating e/m between equations (1) and (2) gives

$$\left.\begin{aligned} \frac{d^2y}{dt^2} &= \left[\frac{(dx)^2}{(dt)} + \frac{(dy)^2}{(dt)}\right]\frac{E_y}{2V} \\ \text{and} \quad \frac{d^2x}{dt^2} &= \left[\frac{(dx)^2}{(dt)} + \frac{(dy)^2}{(dt)}\right]\frac{E_x}{2V} \end{aligned}\right\} \quad \ldots\ldots \quad (4)$$

which substituted into equation (3) yields

$$2V \cdot \frac{d^2x}{dy^2} = \left[\frac{(dx)^2}{(dt)} + \frac{(dy)^2}{(dt)}\right]\left[E_x - \frac{dx}{dy}\,E_y\right]\left(\frac{dy}{dt}\right)^{-2}$$

$$\therefore \quad 2Vx'' = (1+x'^2)\,(E_x - x'E_y)$$

where $x' = dx/dy$ and $x'' = d^2x/dy^2$

$$\therefore \quad \frac{2Vx''}{1+(x')^2} + \frac{\partial V}{\partial y}\cdot x' - \frac{\partial V}{\partial x} = 0. \quad \ldots\ldots \quad (5)$$

---

which is equation (3.3) of the text.

3.2 DERIVATION OF THE LIEBMANN/ARCHARD EQUATIONS

These equations are for paraxial rays and it is therefore justifiable to assume that $x' \ll 1$.

Equation (5) then reduces to its paraxial form:-

$$x'' = \frac{1}{2V}\left[x \cdot \frac{E_x}{x} - E_y \cdot x'\right] \quad \ldots\ldots \quad (6)$$

It is then assumed that the continuous curves representing the field terms $V, (E_x/x)$ and E_y are each replaced by stepped lines, each step of constant field value coinciding with the interval, Δy, of the numerical integration.

$$\therefore \quad x''' = \frac{1}{2V} \cdot \left[x' \cdot \frac{E_x}{x} - E_y \cdot x'' \right]$$

$$\text{or} \qquad x''' = \left(\frac{1}{2V}\right)^2 \left[2V\, x' \frac{E_x}{x} - E_x E_y + x' E_y^2 \right] \qquad \ldots\ldots \qquad (7)$$

To derive the recurrence relations, use is made of the Taylor series expansions of x and x' in ascending powers of Δy, the distance between the n^{th} and $(n + 1)^{th}$ step along the y axis. These are

$$\left.\begin{aligned} x_{n+1} &= x_n + x_n' \Delta y + x_n'' \frac{\Delta y^2}{2} + x_n''' \frac{\Delta y^3}{6} + \ldots\ldots \\ x'_{n+1} &= x'_n + x_n'' \Delta y + x_n''' \frac{\Delta y^2}{2} + \ldots\ldots \end{aligned}\right\} \qquad \ldots\ldots \qquad (8)$$

In addition, use is made of the following Taylor expansion of the potential function $V(x, y)$ in ascending powers of x.

$$V(x, y) = V(y) + \left(\frac{\partial V}{\partial x}\right)_y \cdot x + \frac{1}{2} \left(\frac{\partial^2 V}{\partial x^2}\right)_y \cdot x^2 + \ldots\ldots$$

For the case under consideration the system is symmetrical about the y axis, and hence all the odd order derivatives are zero. Further, from Laplace's equation $\frac{\partial^2 V}{\partial x^2} = -\frac{\partial^2 V}{\partial y^2}$

$$\therefore \quad V(x, y) = V(y) - \frac{1}{2} \left(\frac{\partial^2 V}{\partial y^2}\right)_y \cdot x^2 + \ldots\ldots \qquad \ldots\ldots \qquad (9)$$

Thus the potential at an off-axis point (x, y) may be expressed in terms of the potential V(y) and its derivatives along the axis.

By differentiating equation (9) first with respect to x and then with respect to y it may be deduced that

$$E_x = -V''x; \quad E_y = +V'$$

including derivatives up to second order in potential.

Hence equations (6) and (7) become

$$x'' = \frac{1}{2V} \quad (-xV'' - V'x')$$

$$x''' = \frac{1}{4V^2} \left[(V'^2 - 2VV'')\, x' - V'V''\, x \right]$$

Substituting these in equations (8) gives the expressions:-

$$x_{n+1} = x_n \left[1 - 1/4 \quad (V''/V)\,\Delta y^2 + 1/24 \quad (V'V''/V^2)\,\Delta y^3 \right]$$
$$+ x'_n \left[\Delta y - 1/4\ (V'/V)\,\Delta y^2 + 1/24 \left\{ (V'/V)^2 - 2(V''/V) \right\} \Delta y^3 \right]$$

and $$x'_{n+1} = x'_n \cdot \left[1 - 1/2\ (V'/V)\ \Delta y + 1/8 \quad \left\{ (V'/V)^2 - 2\ (V''/V) \right\} \Delta y^2 \right]$$
$$+ x_n \left[-1/2\ (V''/V)\,\Delta y + 1/8 \quad (V'V''/V^2)\ \Delta y^2 \right]$$

which are the Liebmann/Archard recurrence relations given in the text.

3.3 MAXIMUM OF OFF-AXIS EFFICIENCY

The problem is to find the relative values of δ_+ and δ_- for the maximum value of $|\delta_+ - \delta_-|$ subject to the condition that $(\tan \delta_+ - \tan \delta_-)$ is a constant.

The same values of δ_+ and δ_- will be found at the maximum of the function:

$$f = (\delta_+ - \delta_-) + \lambda(\tan \delta_+ - \tan \delta_-) \qquad \ldots\ldots (10)$$

where λ is a constant. For clarity let $A = \delta_+$ and $B = \delta_-$. At the turning values of the function f, the following equations must hold simultaneously:

$$\frac{\partial f}{\partial A} = 1 + \lambda \sec^2 A = 0$$

$$\frac{\partial f}{\partial B} = -1 - \lambda \sec^2 B = 0$$

Eliminating λ from these two equations gives

$$\sec^2 A = \sec^2 B$$

or $\cos A = \pm \cos B$

which gives $A = \pm B$ for the quadrant $-\pi/2 < A < \pi/2$

$$-\pi/2 < B < \pi/2$$

Now when $A = B$, $|A - B|$ is a minimum, and hence $|A - B|$ has a maximum when $A = -B$ or when $\underline{\delta_+ = -\delta_-}$.

A P P E N D I X IV

PREPARING A DATA TAPE FOR THE COMPUTER PROGRAM KSA67

A flow diagram for KSA67 showing the data controlled options is shown overleaf. The data tape contains three distinct blocks of numbers. These blocks specify respectively, the data for the calculation of the transformation constants, data for the potential distributions and the initial conditions for the computed trajectories.

The data is presented in the following order:-

T

S_1 S_2 S_3 S_4 S_5

D_0 D_1 D_2 D_3 D_4 D_5

V_0 V_1 V_2 V_3 V_4 V_5 V_6

S' I ΔV_I J $\Delta V_J \ldots K$ ΔV_K P

R

either $\begin{cases} M & Y_1 \quad Y_2 \ldots Y_M \\ E_i \end{cases}$ or $\begin{cases} -M & E_1 \quad E_2 \ldots E_M \\ YOBJ \end{cases}$

---

further data

0

→*

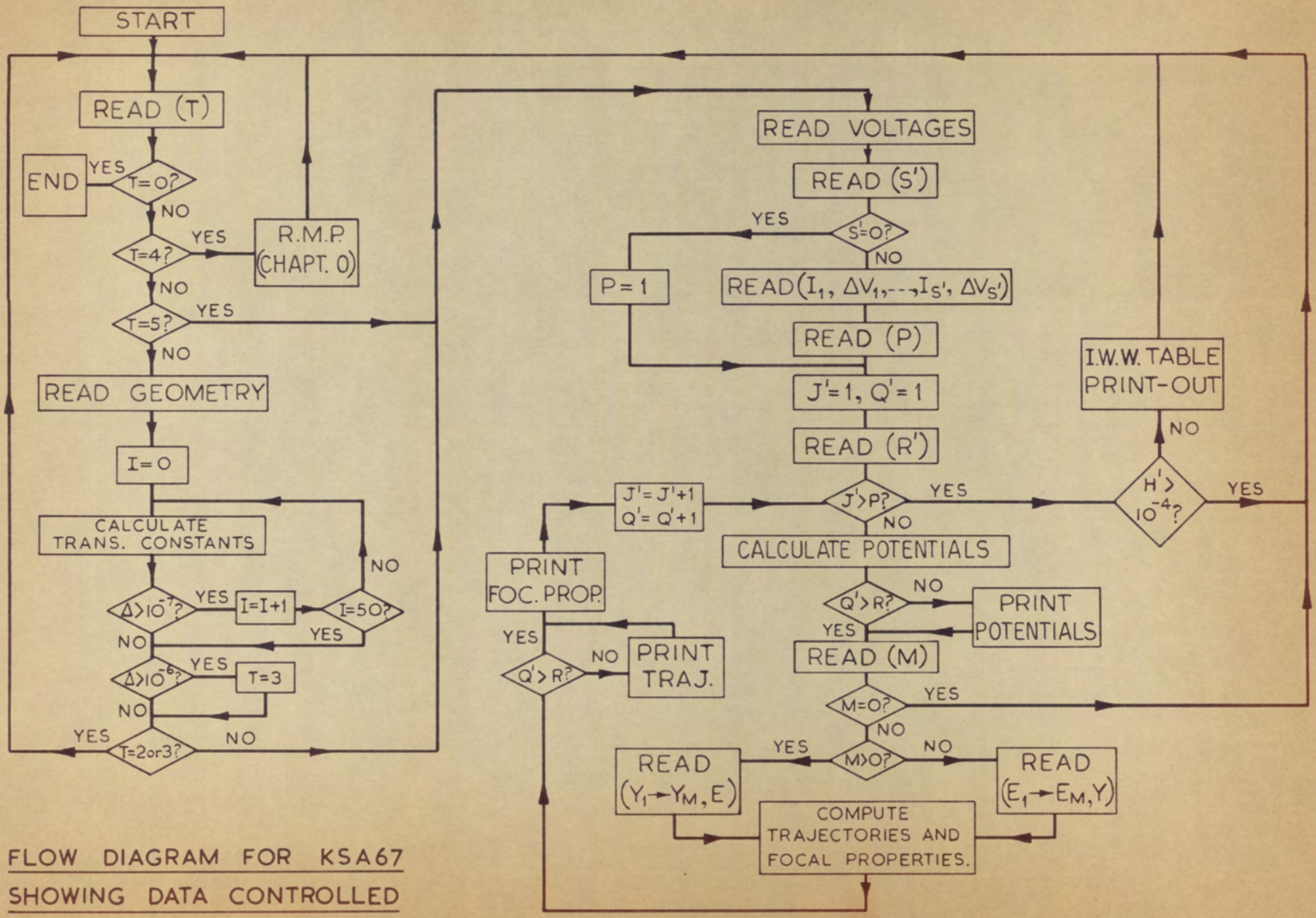

FLOW DIAGRAM FOR KSA67 SHOWING DATA CONTROLLED OPTIONS.

(a) CONTROL NUMBERS

The integer T heading each set of data is a control number and defines the operations to be carried out. The permissible values of T and their functions are given below:

T	FUNCTIONS
0	Terminate Execution
1	Execute complete calculation
2	Calculate Transformation Constants only
(3)	Internal use only
4	Read more program (RMP)
5	Commence at Voltage calculation

If any other value of T is set, the execution will be the same as if T = 1 were set. If T = 3 is mistakenly used, the transformation constants will be calculated and then the caption 'Transform solution not accurate enough after 51 iterations' will appear, and a further value of T will be sought.

A typical calculation will have a data tape starting with a T value of 1 and ending always with a T value of 0.

(b) GEOMETRY CONSTANTS

The geometry constants S_1 to S_5 and D_0 to D_5 must be specified in the order shown above. D_0 is the distance between the ion exit slit and the adjustable source slit, and is used in the time-of-flight calculation (Section 3.8). If T has been set equal to 2, a further value of T is sought after the output of the calculated transformation constants.

(c) VOLTAGE CONSTANTS

The row of voltages V_0 to V_6 give the initial voltages on the system electrodes, which are assigned to successive electrodes such that V_6 is the voltage of the plane electrode. The following row of data specifies the way in which it is required to vary the voltage of selected (or all) electrodes. S'is the total number of electrodes for which it is required to increment the voltage. Then follows a pair of data values for each of the voltage-change electrodes. I, J, K... are the positional numbers of the voltage electrodes, and $\Delta V_I \ldots \Delta V_K$ are the voltage increments required on the specified electrodes I, J, K. For example ...3 5... would mean that it was required to increment the voltage V_2 (not V_3) in steps of 5v.

P, positioned at the end of this data row specifies the total number of times the electrode voltage configuration will be incremented. P may be any integer greater than or equal to one. If S' is equal to zero (i.e. no voltage changes wish to be considered) nothing further need be put on this data row.

(d) TRAJECTORY INITIAL CONDITIONS

This data set is preceded by 'R', an integer greater than or equal to zero which specifies the number of computed voltage distributions and trajectory plots that are to be ~~computed~~ printed out. For example, if P is set equal to 6 and R equal to 1, then twelve tables will be computed - six each of voltage distributions and trajectory plots. Since R = 1, only the first set will be printed out for inspection. In this data set there is the choice of specifying a fixed ion initial energy (E_i) combined with up to seven different object positions (Y_1 to Y_M), or alternatively have a fixed object position with up to seven different initial energies. The former is allowed when M is positive and the latter when M is negative. If M is zero, control passes to Chapter 1, and another value of T is sought.

(e) FURTHER DATA SETS

After the completion of a complete lens calculation (a 'data set',) control passes to Chapter 1 and a further value of T is sought. Thus if the next value on the data tape is 1 the data for the next geometry can be read in.

If this next value is 5, the next line of data will be a new electrode voltage line-up, it being understood that the same geometry as for the previous calculation is required. The first data set of a run will never start with a T value of 5.

A zero terminates the run, and the last data set will always end with

0
→*

(f) CHAPTER 0

In KSA67, chapter 0 is used to set the values of four variables. Normally each one takes a pre-assigned value but one or more may be altered if desired.

The variables are given below:-

i. B' is the α-slit half-width in radians. This is usually set to $B' = 0.00625$.

ii. G' is the initial slope of the 'paraxial' rays which may be computed. This is normally set to $G' = 0.1$. The starting off-axis distance is always zero and this is specified in the body of the program.

iii. H is the starting off-axis distance of the 'off-axis' ray, which is set to 1.20. The ion withdrawal wedge table will thus give the efficiencies for H = 0.3, 0.6, 0.9 and 1.20.

iv. H' is the starting off-axis slope of the off-axis ray, which is set to zero. If H' is set to a non-zero value ($|H'| > 0.0001$), the efficiency calculation has no meaning and the program outputs up to and including the focal property table, and then returns control to Chapter 1 to ask for a new T value.

Chapter 0 therefore takes the following form:-

KSA67

CHAPTER 0

$B' = 0.00625$

$G' = 0.1$

$H = 1.20$

$H' = 0$

ACROSS (1,1)

CLOSE

Data

The appropriate Chapter 0 is followed by the data in the form detailed above.

(g) READ MORE PROGRAM (RMP)

The variables set in Chapter 0 have been chosen to be those variables which rarely require alteration. Should the need arise to change these between data sets the RMP facility has been incorporated in the program. If the data set commences with a T number of 4 the RMP instruction is executed and the next thing that follows on the data tape must be a Chapter 0. This in turn will be followed by a new value of T and the rest of the data in the normal way.

Chapter 0 may also be used to transfer control to a point in the middle of the program, in the same way that T = 5 transfers control straight to the voltage calculation. However, the programmer should study the program carefully before doing this as the values of the primed integer constants are not preserved in an RMP operation.

(h) EXAMPLE

As an example of a data set for KSA67, the following gives the data required to obtain the output shown in Figures 2.7, 3.1, 3.5, 3.6 (1st data set) and Figure 2.8 (2nd data set).

```
→*
AUTOJOB
JOB (S, 5, 2/30, P)
LIBRARY (KSA67)
CHAPTER 0
B' = 0.00625
G' = 1.0
H  = 0.60
H' = 0
ACROSS (1,1)
CLOSE
```

```
1
 3.2   1.6   1.6   0.8   0.8
11.4   2.8   0.8   1.0   0.8   3.2
0      0     7440  7440  8000  8000  7995.3
1      7     1.7   8
1
3    -1.50  -1.60 -1.70
-0.04
5
0     0     7440  7440  8000  8000  7997
0
1
0
0
→*
```

The instructions immediately preceding Chapter 0 call the program KSA67 from the magnetic disc K-code library.

(i) TIME ALLOWANCE

The approximate time taken for program execution can be calculated in the following way.

(i) Allow two minutes for compilation and calculation of the transformation constants.

(ii) Allow 40 seconds for each calculation involving a determination of a voltage and its derivatives. The total number is given by the data value (P).

Thus the estimated time taken for the example in section (h) would be

$$(2 + 2P/3) + 2/3 = 8 \text{ minutes.}$$

compared with an actual time of 6.50 minutes.

APPENDIX V

ELECTRON MOTION IN A STATIC MAGNETIC FIELD

(a) IMPLICIT EQUATIONS

Suppose the electron, charge e, mass m, has a velocity v_p, energy, V_p, perpendicular to the magnetic field, and velocity v_o, energy, V_o, parallel to the magnetic field of strength B.

The force equation perpendicular to the field is

$$\frac{m v_p^2}{r} = \frac{e v_p B}{c}$$

where r is the radius of the circular motion

$$\therefore \quad r = \left(\frac{c}{e}\right) \cdot m \frac{v_p}{B} \qquad \ldots\ldots \quad (1)$$

$$\text{or} \quad r = \frac{(2m)^{1/2}}{e/c} \cdot \left[\frac{V_p^{1/2}}{B}\right] \qquad \ldots\ldots \quad (2)$$

The period of the motion T, is given by the equation

$$T = \frac{2\pi r}{v_p} = \frac{2\pi mc}{eB} \quad \text{from equation (1)}$$

Suppose that in the period T the electron travels a distance d in the direction of the field, then d is defined by the equation

$$d = v_0 T = \frac{2\pi mc}{e B} \cdot v_0$$

$$\text{or} \quad d = 2\pi \cdot \frac{(2m)^{\frac{1}{2}}}{e/c} \cdot \left[\frac{V_0^{\frac{1}{2}}}{B}\right] \qquad \ldots\ldots \qquad (3)$$

(b) Explicit forms of d and r

The values of the atomic constants used are:-

$$m = 9.1083 \times 10^{-28} \text{ gm.}$$

$$\frac{e}{c} = 1.602 \times 10^{-20} \text{ e.m.u.}$$

$$1eV = 1.602 \times 10^{-12} \text{ ergs}$$

Thus equation (2) becomes:

$$r = \frac{(2 \times 9.1083 \times 10^{-28} \times 1.602 \times 10^{-12})^{\frac{1}{2}}}{1.602 \times 10^{-20}} \left[\frac{V_p^{\frac{1}{2}}}{B}\right]$$

$$= \left[\frac{18.2166}{1.602}\right]^{\frac{1}{2}} \cdot \left[\frac{V_p^{\frac{1}{2}}}{B}\right]$$

$$\therefore \quad r = 3.37 \cdot \frac{V_p^{\frac{1}{2}}}{B} \text{ cm}$$

B in gauss
V_p in electron volts

which is equation 5.6 of Section 5.

From equation (3) the value of d is given by:

$$d = 6.2832 \times 3.372 . \frac{V_o^{\frac{1}{2}}}{B}$$

$$\therefore \quad d = 21.19 \ \frac{V_o^{\frac{1}{2}}}{B} \quad \text{cm}$$

B in gauss
V_p in electron volts

---

which is equation 5.5 of Section 5.

REFERENCES

NOTES:

(a) The References to the literature are classified by Section.

(b) In the following references, 'ASTM' refers to the annual conference on mass spectrometry, organised by the American Society for the Testing of Materials, E14 Committee.

SECTION 1 - INTRODUCTION

ARCHARD, G.D. (1954) "Some properties of symmetrical slit ("cylindrical") electron lenses", Brit. J. App. Phys., 5, pp. 395-399 (1954).

ASTON, F.W. (1919) "Positive-ray spectrograph", Phil. Mag. 38, pp. 707-714 (1919)

ASTON, F.W. (1920) "Mass Spectra of chemical elements", Phil. Mag. 39, pp. 611-625 (1920)

BAKER, F.A.
HASTED, J.B. (1966) "Electron collision studies with trapped positive ions", Phil. Trans. Roy. Soc. A261, pp. 33-65 (1966)

BARBER, M.
POWERS, P.
WALLINGTON, M.J.
WOLSTENHOLME, W.A. (1966) "Computer interpretation of high resolution mass spectra", Nature, 212, No. 5064, pp. 784-787 (1966)

BARNARD, G.P. (1949) "A new ion source for mass spectrometry", Nature 164, pp. 283-285 (1949)

BARNARD, G.P. (1956) "Mass Spectrometer Researches" DSIR, HMSO, 1965

BERRY, C.E. (1956) "Image curvature in magnetic sector mass spectrometers", Rev. Sci. Inst. 27 pp. 849-853 (1956)

BEYNON, J.H. (1960) "Mass Spectrometry and its applications to Organic Chemistry", Elsevier, 1960

CAMPBELL, A.J. (1965)
HALLIDAY, J.S. "Mass measurement from low intensity ion beams", pp. 200-203 Proc. 13th Ann. Conf. on Mass Spectrometry, A.S.T.M. 1965

COMPTON, K.T.
VAN VOORHIS, C.C. (1925, 1926) "Probability of ionisation of gas molecules by electron impacts".
Phys. Rev. 26, pp. 436-453 (1925)
Phys. Rev. 27, pp. 724-731 (1926)

DEMPSTER, A.J. (1916) "Ionisation and Dissociation of Hydrogen Molecules and the formation of H_3" Phil. Mag. 31, pp. 438-443 (1916)

DEMPSTER, A.J. (1918) "New method of positive-ray analysis" Phys. Rev. 11, pp. 316-325 (1918)

DOCTOROFF, M.
GROSSEL, S.S. (1962) "A high sensitivity mass spectrometer ion source", pp. 261-262. "Proc. 10th Ann. Conf. on Mass Spectrometry. ASTM, 1962.

DUCKWORTH, H.E.
GHOSHAL, S.N. (1963) "Mass Spectrometry", pp. 201-274 C.A. McDowell, Ed. McGraw Hill, 1963.

EWALD, H.
SAUERMANN, G.
LIEBL, H. (1959) "The performance and image error correction of the new stigmatic focusing mass spectrograph", pp. 10-15 in 'Advances in Mass Spectrometry' Vol. 1; J.D. Waldron, Ed. Pergamon, 1959.

FARMER, J.B. (1963) "Types of Mass Spectrometers", pp. 7-44 in 'Mass Spectrometers'; C.A. McDowell, Ed. McGraw Hill, 1963

FINKELSTEIN, A.T.
SMITH, L.P. (1940) "A high efficiency ion source", Rev. Sci. Inst. 11, pp. 94-97 (1940)

GREEN, B.N.
MERREN, T.O.
MURRAY, J.G. (1965) "Fast Scanning of Mass Spectra at High Resolution", pp. 204-211, Proc. 13th Ann. Conf. on Mass Spectrometry ASTM, 1965

HAINE, M.E.
EINSTEIN, P.A. (1952) "Characteristics of the hot cathode electron microscope gun", Brit. J. App. Phys. 3, pp. 40-46, 1952

JOHNSON, J.G.
NIER, O. (1953) "Angular aberrations in sector shaped electromagnetic lenses for focusing beams of charged particles" , Phys. Rev., 91, pp. 10-17 (1953)

LIEBMANN, G. (1949) "An improved method of numerical ray tracing through electron lenses", Proc. Phys. Soc. 62, pp. 753-772 (1949)

MATSUDA, H.
FUKUMOTO, S. (1966) "A new mass spectrograph with very large dispersion", Z. Naturforsh. 21A, pp. 25-33, 1966

MATTAUCH, J.
HERZOG, R. (1934) "On a new mass spectrograph" Z. Physik, 89, pp. 786-795, 1934.

MATTAUCH, J. (1936) "A double focusing mass spectrograph and the masses of N^{15} and O^{18}", Phys. Rev. 50, pp. 617-623, 1936

NIER, A.O. (1947) "A mass spectrometer for isotope and gas analysis", Rev. Sci. Inst. 18, pp. 398-411 (1947)

NIER, A.O.
ROBERTS, T.R. (1951) "The determination of atomic mass doublets by means of a mass spectrometer", Phys. Rev. 81, pp. 507-510 (1951)

OKAMOTO, J.
MITANI, E. (1967) "A bright ion source for mass spectrometer", Proc. 15th Ann. Conf. on Mass Spectrometry, ASTM, pp. 526-528 (1967)

REDHEAD, P.A. (1966) "Multiple-impact ionization in neon and argon using a trapped-ion source", Proc. 14th Ann. Conf. on Mass Spectrometry, ASTM, pp. 661-667 (1966)

REDHEAD, P.A. (1967) "Multiple ionisation in rare gases by successive electron impacts (0-250eV)", Can. Jour. Phys., 45, pp. 1791-1812, (1967)

THOMSON, J.J. (1911) "Rays of positive electricity", Phil. Mag. 21, pp. 225-249 (1911)

TSUYAMA, H.
HIROSE, H.
NAKAJIMA, Y. (1967) "An advanced ion source with coaxial electron/ion beam acceleration", Proc. 15th Ann. Conf. on Mass Spectrometry, ASTM, pp. 532-536 (1967)

WIEN, W (1898) "Discharge in rarefied gases", Annal. Phys. Chem. 65, pp. 440-452 (1898)

SECTION 2 - COMPUTATION OF THE POTENTIAL DISTRIBUTION

ARCHARD, G.D. (1954) "Potential distribution of symmetrical cylindrical electron lenses", Brit. J. App. Phys., 5, pp. 179-181 (1954)

BINNS, K.J.
LAWRENSON, P.J. (1963) "Analysis and Computation of Electric and Magnetic field problems", Pergammon Press, 1963

BOERBOOM, A.J.H. (1957) "De ionenoptiek van de Massaspectrometer", unpublished Ph. D. thesis Rijksuniversiteit, Leiden (1957)

BOERBOOM, A.J.H. (1959) "Numerical calculation of the potential distribution in ion slit lens systems Pt.I", Z. Naturforschg, 14a, pp. 809-816 (1959)

BOERBOOM, A.J.H. (1960a) "Numerical calculation of the potential distribution in ion slit lens systems - II", Z. Naturforschg, 15a, pp. 244-252 (1960)

BOERBOOM, A.J.H. (1960b) "Numerical calculation of the potential distribution in ion slit lens systems - III", Z. Naturforschg, 15a, pp. 253-259 (1960)

BRÜCHE, E.
SCHERZER, O. (1934) "Geometrische Electronenoptik ", p. 69, J. Springer, Berlin (1934)

BULLOUGH, R.
HEATH, A.C.
VINE, J. (1963) "A general purpose digital computer program for the evaluation of electron lens parameters", AEI Engineering Supplement, pp. 42-46, October, 1963.

DIETZ, L.A. (1959) "Ion optics for the V-type surface ionisation filament used in mass spectrometry" Rev. Sci. Inst., 30, pp. 235-241 (1959)

GIBBS, W.J. (1958) "Conformal Transformation in Electrical Engineering", Chapman and Hall, 1958

GLASER, A.
HENNEBERG, W. (1935) "Die potentialverteilung in Schlitzblende und Lochblende", Zeitschr. F. Techn. Physik, 16, pp. 222-230 (1935)

GREEN, S.L. (1962) "The theory and use of the complex variable", Pitman, 1962

HAMZA, V. (1966) "A computer program for electron or ion gun analysis - operations manual", N66-15367 Stanford University, California, Microwave Laboratory (1966)

HENNEBERG, W. (1935) "Das potential von Schlitzblende und Lochblende", Z. Phys., 94, pp. 22-27 (1935)

KIRSTEIN, P.T.
HORNSBY, J.S. (1964) "An investigation into the use of iteration methods for the analysis of axially symmetric and sheet beam electrode shapes with an emitting surface". I.E.E.E. Trans. Elect. Dev. ED-11, pp. 196-204 (1964)

LAUDET, M. (1953) "Potential et Champ d'une Lentille Electrostatique cylindrique à trois fentes", Cahiers de Phys. 41, pp. 72-80 (1953)

LIEBMANN, G. (1950) "Solution of partial differential equations with a resistance network analogue", Brit. J. App. Phys., 1, pp. 92-103 (1950)

MOCH, R.
ROTH, E.
SALMON, J. (1950) "Etude à la cuve Rheographique de sources d'ions utilisées en spectrometre de masse. Determination des trajectoires". J. Phys. Radium Fr., 11, pp. 524-528, (1950)

MORSE, P.M.
FESHBACK, N. (1953) "Methods of Theoretical Physics", Vol. 1 New York, McGraw Hill, 1953.

STRASCHKEWITCH (1940) "Elektrische Elektronenzylinderlinsen" Journ. of Physics U.R.S.S., 3, pp. 507- (1940)

WALKER, M. (1933) "The Schwarz-Christoffel Transformation and its applications - a simple exposition", Dover, 1933.

ZWORYKIN, V.K.
MORTON, G.A.
RAMBERG, E.G.
HILLIER, J.
VANCE, A.W. (1945) "Electron Optics and the Electron Microscope", Wiley, 1945.

SECTION 3 - CALCULATION OF THE PARAXIAL FOCAL PROPERTIES

ALLARD, J.L.
RUSSELL, R.D. (1963) "The electric potential in the region of a thin slit", Brit. J. App. Phys., 14, pp. 800-804 (1963)

ARCHARD, G.D. (1954) "Some properties of symmetrical slit ("cylindrical") electron lenses", Brit. J. App. Phys. 5, pp. 395-399 (1954)

BERTEIN, F. (1950a) "Convergence transversale créeé par les fentes des instruments d'optique ionique", C.R. Acad. Sci. Fr., 231, pp. 766-767 (1950)

BERTEIN, F. (1950b) "Sur la suppression de la fente de sortie dans une source d'ions", C.R. Acad. Sci. Fr., 231 pp. 1134-1136 (1950)

BERTEIN, F. (1950c) "Sur les aberrations des lentilles ioniques dans les sources d'ions", C.R. Acad. Sci. Fr., 231 pp. 1448-1449 (1950)

BORN, M.
WOLF (1959) "Principles of Optics", Pergammon Press, 1959

CLAUSIUS, R. (1864) Pogg. Ann. t. CXXI, pp. 1-44 (1864). "Ueber die Concentration von Wärme und Lichtstrahlen und die Gränzen ihrer Wirkung".

GANS, R. (1937) "Strahlengang in elektronenoptischen systemen" Ziets. techn. Physik, 18, pp. 41-48 (1937)

GRIVET, P. (1965) "Electron Optics" English translation Pergammon Press, 1965.

HAINE, M.E.
EINSTEIN, P.A. (1952) "Characteristics of the hot cathode electron microscope gun", Brit. J. App. Phys. 3, pp. 40-46, (1952)

HAINE, M.E. (1961) "The Electron Microscope", Spon, 1961.

HAMZA, V. (1966) "A computer program for electron or ion gun analysis-operations manual", N66-15367 Stanford University, California, Microwave Laboratory, 1966

HANSZEN, K.J.
LAUER, R. (1967) "Electrostatic Lenses" p. 257 of "Focusing of Charged Particles, I", Ed. A. Septier Acad. Press, 1967.

HECHTEL, J.R. (1962) "Electron ray tracing by means of resistor network and digital computer", I.R.E. Trans. on Elect. Dev. ED-9 pp. 62-68 (1962)

Von HELMHOLTZ (1874) Pogg. Ann., Jubelband, p. 566 (1874)

JACOB, L. (1951) "An introduction to Electron Optics", Methuen Monograph, 1951.

KIRCHHOFF, G. (1860) "Ueber das Verhältmiss zwischen dem Emissionsvermögen und dem Absorptionsvermögen der Körper für Wärme und Licht"., Pogg. Ann. T. CIX, pp. 275-301 (1860)

LAGRANGE (1803) "Sur une loi generale d'optique" Memoire de l'Academie de Berlin , 1803

LIEBMANN, G. (1949) "An improved method of numerical ray tracing through electron lenses", Proc. Phys. Soc. 62, (B) pp. 753-772 (1949)

MALOFF, I.G.
EPSTEIN, D.W. (1938) "Electron Optics in Television", New York, McGraw Hill, 1938.

NAIDU, P.S.
WESTPHAL, K.O. (1966) "Some theoretical considerations of ion optics of the mass spectrometer ion source" Pt. I and II, Brit. J. App. Phys. 17, pp. 645-656 (1966)

PIERCE, J.R. (1949) "Theory and design of electron beams". Van Nostrand, New York, (1949)

LORD RAYLEIGH (1886) "Notes, chiefly historical, on some fundamental propositions in optics", Phil. Mag. (5) 21, pp. 466-476 (1886)

REINDERS, M.E.
ZILVERSCHOON, C.J.
KISTEMAKER, J. (1952) "Determination of ion paths in crossed electric and magnetic fields", App. Sci. Res. (B) Netherland 2, pp. 264-268 (1952)

SMITH (1738) "Compleat system of Opticks", Cambridge Press (1738)

STRASCHKEWITCH (1940) "Elektrische Elektronenzylinderlinsen", Journ. of Physics U.R.S.S., 3, pp. 507-(1940)

VAUTHIER, R. (1950a) "Optique ionique de la source d'ions des spectrometres de masse", C.R. Acad. Sci.Fr. 231, pp. 764-765 (1950)

VAUTHIER, R. (1950b) "Optique ionique de la source d'ions des spectrometres de masse", C.R. Acad. Sci. Fr. 231, pp. 1218-1220 (1950)

VAUTHIER, R. (1955a) "Applications of the optics of electric charges to mass spectrometry", Ann. Phys. (Paris) 10, pp. 968-1025 (1955)

VAUTHIER, R. (1955b) "A study of the electron beam of mass spectrometer ion sources". C.R. Acad. Sci. Paris, 241, pp. 1033-1036 (1955)

VINE, J. (1959) "Application of a combination of analogue and digital computers to electron ray tracing". Comp. Jour. 2, pp. 134-144 (1959)

ZWORYKIN, V.K.
MORTON, G.A.
RAMBERG, E.G.
HILLIER, J.
VANCE, A.W. (1945) "Electron Optics and the Electron Microscope", Wiley, 1945.

SECTION 4 - RESULTS OF THE THEORETICAL ANALYSIS

HAINE, M.E. (1961) "The Electron Microscope", Spon, 1961

HAINE, M.E.
EINSTEIN, P.A. (1952) "Characteristics of the hot cathode electron microscope gun". Brit. J. App. Phys. 3, pp. 40-46, 1952.

MALOFF, I.G.
EPSTEIN, D.W. (1938) "Electron Optics in Television", New York, McGraw Hill, 1938.

NAIDU, P.S.
WESTPHAL, K.O. (1966) "Some theoretical considerations of ion optics of the mass spectrometer ion source", Pt. I and II, Brit. J. App. Phys. 17, pp. 645-656 (1966)

REINDERS, M.E.
ZILVERSCHOON, C.J.
KISTEMAKER, J. (1952) "Determination of ion paths in crossed electric and magnetic fields", App. Sci. Res. (B) Netherland 2, pp. 264-268 (1952)

RYAN, K.R.
TERRY, J.O. (1965) "The application of calculation of Ion source systems and ion energy spread to some of the problems of Ion-Molecule Interactions". Aerospace Research Laboratories report No. 65-170, August, 1965. Catalogue No. AD-626978.

SECTION 5 - EXPERIMENTAL ANALYSIS OF E.B. ION SOURCES

BAKER, F.A.
HASTED, J.B. (1966) "Electron Collision Studies with Trapped Positive Ions" Phil. Trans. Roy. Soc. A261 pp. 33-65 (1966)

BAYARD, R.T.
ALPERT, D. (1950) "Extension of the low pressure range of the ionisation gauge", Rev. Sci. Inst. 21, pp. 571-572 (1950)

BREWER , G.R. (1967) "Focusing of high density electron beams", pp. 73-121 of "Focusing of Charged Particles" Vol. II Ed. A. Septier. Academic Press, 1967.

BRUBAKER, W.M. (1955) "Influence of Space Charge on the Potential Distribution in Mass Spectrometer Ion Sources", Jour. App. Phys. 26, No. 8, pp. 1007-1012 (1955)

CLAMPITT, R. (1966) "Some characteristics of electron impact ion sources", Proc. 14th Ann. Mass Spectrometry Conf., pp. 658-660 A.S.T.M., Dallas, 1966

COMPTON, K.T.
VAN VOORHIS, C.C.
(1925, 1926) "Probability of ionisation of gas molecules by electron impact". Part I - Phys. Rev. 26, 436-453 (1925) Part II - Critique - Phys. Rev. 27, 724-731 (1926)

FLESCH, G.D.
SVEC, H.H. (1966) "A more efficient electron gun for sector mass spectrometers", Proc. 14th Ann. Mass Spectrometry Conf., pp. 651-657, A.S.T.M. Dallas, 1966

HAEFF, A.V. (1939) "Space charge effects in electron beams", Proc. I.R.E. 27, pp. 586-602 (1939)

HENDERSON, E.
RILEY, P.N.K.
SEDGWICK, R.D. (1966) "The effect of the source magnetic field on the determination of ionisation efficiency curves using a sector mass spectrometer". J. Sci. Inst. 43, pp. 726-727 (1966)

HERRMANN, G. (1958) "Optical theory of thermal velocity effects in cylindrical electron beams". J. Appl. Phys. 29, pp. 127-128 (1958)

LANGMUIR, I. (1929) "The interaction of electron and positive ion space charges in cathode sheaths", Phys. Rev. 33, pp. 954-989 (1929)

PIERCE, J.R. (1949) "Theory and Design of electron beams", Van Nostrand, New York, 1949.

SMITH, L.P.
HARTMANN, P.L. (1940) "The formation and maintenance of electron and ion beams". Jour. App. Phys. 11, pp. 220-229 (1940)

SECTION 6 - WAYS OF IMPROVING SOURCE DESIGN

ZANDBERG, É. YA — "Thermionic Emission from Rhenium (Review)"

TONTEGODE, A. YA (1966) — Sov. Phys. - Tech. Phys. 11, 6, pp. 713-725 (1966)

SECTION 7 - CONCLUSIONS

BREWER, G.R. (1967) — "Focusing of high-density electron beams", pp. 73-121 of 'Focusing of Charged Particles" Vol. II, A. Septier (Ed.), Academic Press, 1967.

HAMZA, V. (1966) — "A computer program for electron or ion gun analysis - operations manual", N66-15367, Stanford University, California, Microwave Laboratory, (1966).

Computer interpretation of high resolution mass spectra

By M. Barber, P. Powers, M. J. Wallington and W. A. Wolstenholme

Reprinted from *Nature*, Vol. 212, No. 5064, pp 784-787

AEI

COMPUTER INTERPRETATION OF HIGH RESOLUTION MASS SPECTRA*

By M. BARBER, P. POWERS, M. J. WALLINGTON and W. A. WOLSTENHOLME
Consultant Laboratory, Associated Electrical Industries, Ltd., Manchester

At the 1965 meeting of Committee *E*-14 of the American Society for Testing Materials, results were presented[1,2] which showed that complete high resolution mass spectra could be recorded electrically in 10 sec and the data then processed using computing techniques to give, if desired, an element map[3]. The sensitivity of the system is such that a useful spectrum can be obtained from 0·2 μg.

Fig. 1 shows diagrammatically the arrangement of such a system. A reference sample, usually perfluorokerosene, is admitted to the mass spectrometer together with the unknown sample which may be a single organic compound or the effluent coming directly from a gas–liquid chromatography column.

The element map is now a well known way of tabulating in a digestible form the large amount of precise data which is obtained from a complete high resolution mass spectrum. For many compounds, however, the size of such a map becomes unwieldy. For example, for a compound containing four nitrogen atoms and six oxygen atoms, the map would contain thirty-five columns. Moreover, the interpretation of such maps can become time consuming and tedious. The next logical step would, therefore, seem to be to programme the computer to carry out at least a partial interpretation of the data.

Two possible approaches to this task are (*a*) to get the computer to generate all possible structures for a given molecular formula and to check each structure against the mass spectrum, and (*b*) knowing the compound type, to programme the computer to look for specific fragmentation processes for structure determination. This article describes some of the results which we have obtained using the second method. For the initial study we have chosen peptides which, because they are built up from relatively simple units, lend themselves readily to this type of approach. Examples of linear, cyclic and *cyclo*depsipeptides have been considered. All spectra were obtained using a high resolution, fast scanning mass spectrometer.

The basic logic and operations in the programme are shown in Fig. 2. The programme has been written so that it can be connected directly to the element map programme and so that an interpretation can be made before or instead of the mapping process. The peaks in the mass spectrum are stored as atomic compositions and the first operation of the computer is to find the molecular formula of the compound. Once this has been done there are, in the case of peptides, several deductions which the computer can make by consideration of the molecular formula alone.

(*a*) If mono-amino mono-carboxylic acids only are considered, by analysis of the numbers of nitrogen and oxygen atoms and the number of double bond equivalents in the molecular formula, the type of peptide can be determined. For example, for a cyclic peptide the number of nitrogens is equal to the number of oxygens, and if the number of double bond equivalents is equal to the number of oxygens minus one, the peptide is linear. In this part of the programme it is necessary to consider the presence of phenylalanine which, although mono-amino mono-carboxylic, does contain four "extra" double bond equivalents. The computer, therefore, is programmed during this operation to determine the number of phenylalanine units present.

(*b*) It is also possible for the computer to carry out an amino-acid analysis, again by consideration of the number

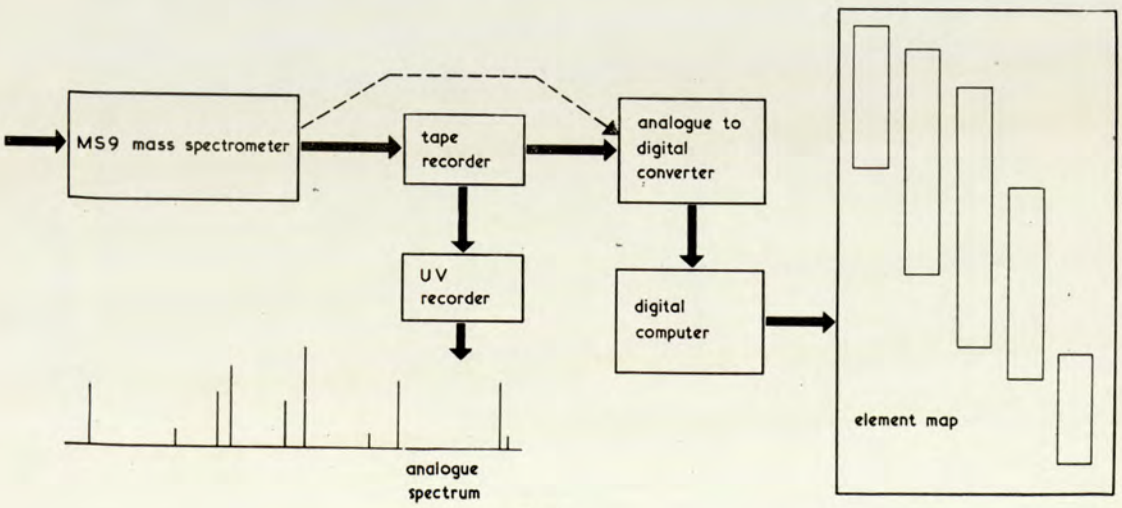

Fig. 1.

* This paper was presented at the fourteenth annual meeting of the ASTM Committee *E*-14 on Mass Spectrometry and Allied Topics in Dallas, May 1966.

amino-acids and hydroxy acids, or the arrangement may be irregular. The computer is programmed, therefore, to look for amino-acids and hydroxy acids alternately, but if a hydroxy acid cannot be found, another amino-acid unit is searched for. The hydroxy acid units are recognized as $C_nH_{2n-2}O_2$, because only mono-hydroxy acids have been considered at this stage. If the computer can find neither acid type unit, it will say so and try an alternative initial loss. The end of a complete sequence is recognized if the residue contains no nitrogen, that is, after the final amino-acid unit has been found, as this will be the part of the hydroxy acid involved in the initial ring opening. For completeness of print-out, OH is added to this residue and the unit is then printed out as it occurs in the ring.

Fig. 3 shows the computer output obtained when the high resolution spectrum of $(Gly\text{-}Ala\text{-}Phe)_2$ was read into the computer. In this case, an incorrect amino-acid analysis was deliberately fed in. It can be seen that the computer first finds the molecular formula. The amino-acid analysis was read in incorrectly as one unit of glycine, two units of alanine and three units of phenylalanine. The computer, of course, finds that this does not add up to the molecular formula and prints "amino acid analysis incorrect". It then proceeds to correct it by subtracting one unit of glycine, alanine and phenylalanine from the molecular formula and at this stage it prints the residue as "new molecular formula". All possible combinations of amino-acids which could add up to this formula are then found—in this example only one, namely, one unit each of glycine, alanine and phenylalanine. This is printed and the amino-acid analysis is now corrected, that is two units each of glycine, alanine and phenylalanine. Only these three amino-acids are now used for sequencing. The initial losses found are alanine and phenylalanine. The sequencing is then completed using the initial loss of alanine—the amino-acids are in this case listed vertically, and "*cyclo*" is printed when the sequence is complete. The initial loss of phenylalanine is next taken and in this case only a partial sequence is found—Phe. Since no other initial losses are available, the sequencing using fragmentation type *A* is completed.

Fig. 4 shows the output obtained using the complete high resolution spectrum (containing about a hundred peaks) of the regular *cyclo*hexadepsipeptide enniatin A[7]. The first amino-acid unit lost was methyl leucine (MLU) and in this case any other initial losses are stored but not printed at this stage. A C5 hydroxy acid is next found and then another methyl leucine unit, etc. The sequence is complete when the final hydroxy acid unit is found.

Fig. 5 shows an example of an irregular *cyclo*hexadepsipeptide, isariin[8,9], which contains five amino-acids and one hydroxy acid. This figure shows an example of the determination of the peptide type after the molecular formula has been found. In this case no phenylalanine units are found to be present. The first amino-acid unit

```
DATE 27.4.66
TIME 18.00
COMPUTER ANALYSIS OF MASS SPECTRA MB/A/SA/5A7
C28 H34 N6 O6
MOLECULAR WEIGHT = 550
KNOWN AMINO ACIDS
 1  GLY
 2  ALA
 3  PHE
AMINO ACID ANALYSIS INCORRECT
COMPLETE ANALYSIS USING KNOWN AMINO ACIDS
NEW MOLECULAR FORMULA C14 H17 N3 O3

 0
 0
 0
 0
 0
 1  GLY
 1  ALA
 1  PHE

 2  GLY
 2  ALA
 2  PHE

AMINO ACID ANALYSIS NOW CORRECTED
SEQUENCING ON ABOVE BASIS
FRAGMENTATION TYPE A
INITIAL LOSS AFTER RING OPENING
ALA
PHE
END OF SPECTRA REACHED FOR INITIAL LOSSES
SEQUENCING NOW CARRIED OUT FROM INITIAL LOSSES
SEQUENCE
ALA
GLY
PHE
ALA
GLY
PHE
CYCLO
SEQUENCE
PHE
PARTIAL SEQUENCING ONLY
INTERPRETATION USING FRAGMENTATION A COMPLETED
```

Fig. 3.

lost is valine and the sequence is completed when the one hydroxy acid unit present at the end is found, that is $C_{12}H_{22}O_2$.

It should be pointed out here that in these two cases of *cyclo*depsipeptides, it was found that the computer could fail to complete the sequence, or even give an incorrect sequence, mainly as a result of peaks being present in the spectrum, particularly at low mass, which corresponded to the loss of $C_nH_{2n-2}O_2$ after the previous loss of an amino-acid. An incorrect hydroxy acid was thus found. To overcome this, we found it necessary, in the case of

```
DATE 12.5.66
TIME 15.33

COMPUTER ANALYSIS OF MASS SPECTRA-CYCLODEPSIPEPTIDES    A/SA/57

C 36  H 63  N  3  O  9
MOLECULAR WEIGHT =  681
FIRST AMINO ACID UNIT LOSS

MLU-C  5  H  8  O  2 -MLU-C  5  H  8  O  2 -MLU-C  5  H  8  O  2

HYDROXY ACID END NOW FOUND
SEQUENCE IS COMPLETE FOR A CYCLODEPSIPEPTIDE
```

Fig. 4

of nitrogens, oxygens and double bond equivalents in the molecular formula. The computer has been programmed to consider nineteen amino-acids and to print all possible combinations of these which will give the molecular formula. This can be done directly for cyclic peptides, but for linear peptides the N-acyl group and the C-terminal group, usually OCH_3, must first be subtracted. With *cyclo*depsipeptides a knowledge of the hydroxy acids present would be necessary.

Another important point in connexion with the amino-acid analysis is that the computer will accept any known chemical evidence; for example, any qualitative and/or quantitative analysis of the amino-acids present. This information, if any, can be read in and the computer will

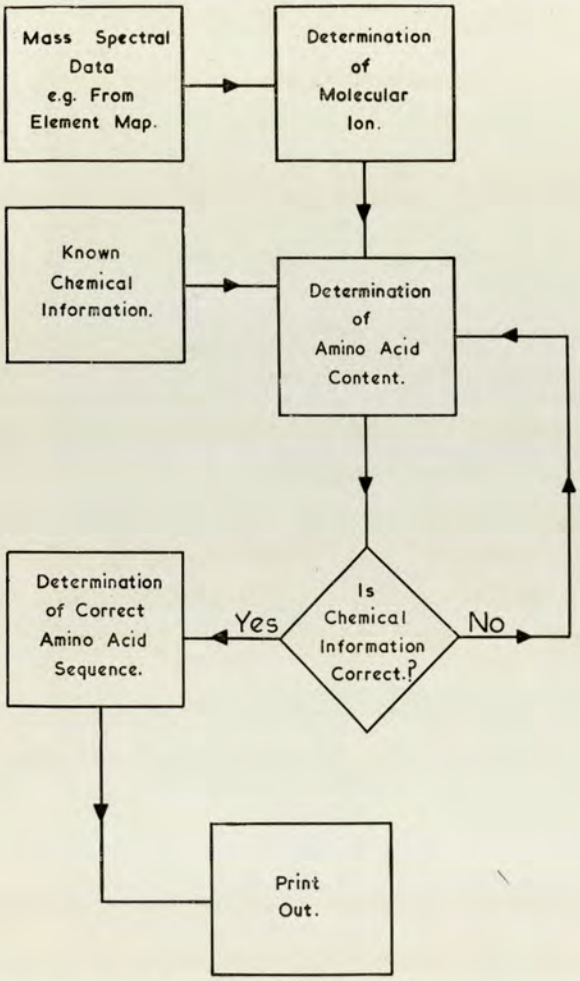

Fig. 2. Peptide analysis programme.

check it against the molecular formula determined by the mass spectrometer and, if necessary, correct it. An example of this type will be given.

When an amino-acid analysis has been performed, the computer will then only consider those acids for subsequent sequence determination.

The sequencing part of the programme varies slightly depending on the type of peptide being analysed. The main features in each case are as follows:

(i) *Linear peptides.* One of the main fragmentations in linear peptides is simple cleavage of the peptide bonds[4] which results in the successive loss of amino-acid units. This type of fragmentation also occurs after ring opening in cyclic and *cyclo*depsipeptides. The amino-acids are, therefore, stored in the computer as peptide units; for example, valine is stored as C_5H_9NO VAL.

With linear peptides, the computer is programmed so that after the molecular ion has been found, the C-terminal group (OCH_3 for peptide methyl esters) is subtracted from it and the residue is stored. Each peak in the mass spectrum (stored as an atomic composition) is then subtracted from the molecular ion minus OCH_3 and the residue is compared with the amino-acid units in the store. When an amino-acid unit loss is found this unit is subtracted from the molecular ion minus OCH_3 and the new residue is stored. Each peak in the spectrum is then subtracted from this residue and the result compared with the amino-acid units as before. Each acid unit loss found is, of course, printed out. For the reason that a peak is not always observed in the spectrum which corresponds to the acyl ion itself the computer is programmed to print out the residue containing the N-terminal amino-acid if the acyl ion (containing no nitrogen) is not observed.

(ii) *Cyclic peptides.* Two types of fragmentation[5], differing in the mode of initial ring opening, have been considered for cyclic peptides. The first, which we have called type *A*, occurs when the peptide ring opens by way of a McLafferty type rearrangement. The simple cleavage of a peptide bond following this then involves the loss of an amino-acid unit $+NH_2$. In this case, therefore, the computer is programmed to find the initial amino-acid loss by testing each peak in the mass spectrum to see if it is deficient with respect to the molecular ion by NH_2 plus an amino-acid unit. All such "initial losses" are looked for and stored because the peptide ring can open at more than one place. These residues (M^+-NH_2-amino-acid unit) are then taken in turn and used for further sequencing in the same way as for linear peptides. In this case, the completion of sequencing is recognized when the total amino-acid units found equal the molecular formula. If the sequencing is incomplete using one initial loss, that is, the computer cannot find a peak corresponding to the further loss of an amino-acid unit, the residue at that stage is printed out and the next initial loss in the store is considered.

The second fragmentation (type *B*) we have considered for cyclic peptides is that involving ring opening by loss of an amine fragment (that is, an amino-acid unit minus CO). In this case, therefore, the initial losses are found by subtracting CO from the molecular formula and then testing every peak against the residue as before. Further sequencing is carried out as for type *A* fragmentation.

(iii) *Cyclodepsipeptides.* These peptides contain hydroxy acid as well as amino-acid units. There are present, therefore, ester bonds as well as the usual amide or peptide bonds. The fragmentation of these peptides has been studied in some detail[6], and three types are predominant. The type we have used so far for this work is that in which the ring opens at the ester bond and involves the loss of CO_2. The resultant ion can then lose a hydrogen atom and further fragmentation proceeds by simple cleavage of the amide and ester bonds, successive units of amino and hydroxy acids thus being lost. The first step in the sequencing is for the computer to find all initial losses by looking for a peak deficient with respect to the molecular ion by an amino-acid unit plus OH (the first loss after ring opening will always be an amino-acid unit). *Cyclo*depsipeptides may contain regularly alternating units of

```
DATE 90.81.72
TIME 63.54

COMPUTER ANALYSIS OF MASS SPECTRA. GENERAL      A/SA/57

C 33  H 59  N  5  O  7
MOLECULAR WEIGHT =  637

PEPTIDE IS CYCLO-DEPSI.

NO. OF PHE.=  0
FIRST AMINO ACID UNIT LOSS

VAL-ALA-LEU-VAL-GLY-C 12  H 22  O  2

HYDROXY ACID END NOW FOUND
SEQUENCE IS COMPLETE FOR A CYCLODEPSIPEPTIDE
```

Fig. 5.

these depsipeptides only, to read into the computer a qualitative acid analysis, for example, that which would be obtained after hydrolysis of the peptide.

Fig. 6 shows an example of a linear N-acyl tetrapeptide methyl ester. Here the acyl ion itself was present and the complete sequence together with the acyl group is printed. It is worth noting that in our first programme for linear peptides the technique which we adopted was to make the computer start with the acyl ion and work upwards in mass. When this was done, the computer printed the acid sequence Ala-Val-Gly-Gly. A second unit of glycine not present in the peptide had been found by the computer because the peak in the spectrum corresponding to loss of the leucine side chain by way of a McLafferty rearrangement had the atomic composition corresponding to this sequence[4]. This anomaly is avoided if our present technique of starting at high mass is adopted.

```
DATE 10.5.66.
TIME 21.20

COMPUTER ANALYSIS OF MASS SPECTRA 1      A/SA/51  P.P.

LINEAR PEPTIDES

PARENT PEAK IS C 27  H 50  N 4  O 6

AMINO ACID ARRANGEMENT IS

C 10  H 19  O 1  -ALA-VAL-GLY-LEU-OCH3
```

Fig. 6.

Conclusions

The results we have obtained with these peptides show great promise. Computer interpretation of the complete high resolution mass spectrum can completely remove the necessity for a quantitative amino-acid analysis. Further, for linear peptides the use of the complete high resolution scan obviates the necessity to acylate with a long chain fatty acid. An acetyl group is sufficient since the computer identifies all peaks by their atomic compositions.

This type of work will be continued with other types of compound using specific fragmentation processes where the compound type is known and also using the "structure generation" method for the more general case.

Senn and McLafferty[10] and Biemann *et al.*[11] have also investigated the computer interpretation of the mass spectra of peptides; however, they have considered only linear peptides and have not used the computer to perform any amino-acid analysis or "peptide type" determination.

[1] Green, B. N., Merren, T. O., and Murray, J. G., *Proc. Thirteenth Amer. Soc. Test. Materials E-14 Meeting, St. Louis* (1965).

[2] Campbell, A. J., and Halliday, J. S., *Proc. Thirteenth Amer. Soc. Test. Materials E-14 Meeting, St. Louis* (1965).

[3] Biemann, K., Bommer, P., and Desiderio, D., *Tetrahedron Lett.*, **26**, 172 (1964).

[4] Bricas, E., van Heijenoort, J., Barber, M., Wolstenholme, W. A., Das, B. C., and Lederer, E., *Biochemistry*, **4**, 2254 (1965).

[5] Millard, B. J., *Tetrahedron Lett.*, **34**, 3041 (1965).

[6] Wulfson *et al.*, *Tetrahedron Lett.*, **42**, 2793 (1965).

[7] Shemyakin, M. M., *Russian Chem. Rev.* (March 1962).

[8] Vining, L. C., and Taber, W. A., *Canad. J. Chem.*, **40**, 1579 (1962).

[9] Wolstenholme, W. A., and Vining, L. C. *Tetrahedron Lett.*, **24**, 2785 (1966).

[10] Senn, M., and McLafferty, F. W., *Biochem. Biophys. Res. Commun.*, 23 4 (1966).

[11] Biemann, K., Cone, C., and Webster, B. R., *J. Amer. Chem. Soc.*, 2597 1966).

AEI

Associated Electrical Industries Ltd
Electronics Group
Scientific Apparatus Dept
Barton Dock Road, Urmston, Manchester
Telephone: (061) LONgford 4466

Publication 2500–73 EdA 1000 0167 Printed in England

Reprinted from *Nature*, Vol. 212, No. 5064 November 19th, 1966